MORPHOLOGICAL VARIATION IN THE DISTAL HUMERUS OF EXTANT HOMINIDS AND FOSSIL HOMININS

by

Kaya G. Zelazny

A dissertation submitted to Johns Hopkins University in conformity with the requirements for the degree of Doctor of Philosophy

Baltimore, MD

Submission Date: 1/4/2019

ABSTRACT

Relative to most other postcranial regions, the distal humerus is commonly preserved in the fossil hominin record. It is also integral to upper limb function, and therefore potentially useful in reconstructing locomotion. However, variability within species and overlapping morphological ranges has made identifying functionally or phylogenetically discriminating features difficult. This project uses 3D morphometrics with sliding semilandmarks in an attempt to overcome these difficulties. It also explores the impacts of distal humeral allometry and developmental plasticity in order to clarify interpretations.

A total of 250 modern (Holocene) humans, 125 extant great apes, and 10 fossil hominin specimens were included in the study. Results show that articular, periarticular, and shaft morphology differs between modern humans and *Pan, Gorilla*, and *Pongo*. The relationship of fossil hominins to extant species varies by region. Articular morphology is human-like, characterized by low to moderate articular relief. However, both periarticular and shaft morphology are more ape-like, driven by anteroposteriorly compressed periarticular surfaces, proximally positioned epicondyles, and robust diaphyses.

Allometry of these characteristics was tested by regressing principal component scores against body mass, distal humeral centroid size, and biepicondylar breadth. This also tested the influence of choice of size measure. Body mass and centroid size were highly correlated but uncovered different relationships between small fossil hominins

(A.L. 288-1, SKX 10924, SK 24600) and extant taxa. With respect to centroid sizes, small fossils appear unique. However, they are similar to small extant nonhuman hominoids with respect to body mass. This is caused by differences in the relationship of mass to centroid size among extant taxa.

To determine the responsiveness of the distal humerus to mechanical loading, bilateral asymmetry of cross-sectional properties and centroid sizes of regions across the distal humerus were calculated and compared within modern humans. Asymmetry was significant for all properties, but declined distally from 40% through the periarticular region. Asymmetries were correlated with ZP asymmetry at midshaft, but correlations declined with distance.

In total, these results suggest that fossil hominin distal humeri have more similarities to extant apes than previously reported, in regions particularly responsive to loading, which may support claims of retained arboreal behaviors.

Dissertation Advisors:

Christopher B. Ruff, Johns Hopkins University

Adam D. Sylvester, Johns Hopkins University

Dissertation Committee:

Carol V. Ward, University of Missouri

Melissa Tallman, Grand Valley State University

PREFACE

Acknowledgments

I would like to thank the many people who aided and supported me throughout my graduate school career. First I would like to thank my committee. Drs. Carol Ward and Melissa Tallman provided invaluable advice looking forward. I am indebted to Dr. Adam Sylvester for inspiring and nurturing my newfound love of coding. In particular, I am hugely grateful to Dr. Christopher Ruff. His scientific insights and expectations of rigor were invaluable, and I will spend a lifetime attempting to live up to his example. However I am especially grateful for his dedication, dependability and professionalism as a mentor, and for always making me feel like someone who could be taken seriously. Without him, I couldn't have done it.

I also thank the many people who provided access to materials that made this dissertation possible. Thank you to Drs. Carol Ward, J. Michael Plavcan, Fredrick Kyalo, Di Vincenzo, Piperno, and Manzi, as well as the National Museums of Kenya and NSF grant BCS-0647557 for providing access to fossil scans. I thank the many curators and museum professionals who graciously allowed me access to osteological materials available at their institutions, including Dr. Patrick Semal and the Institut royal des Sciences Naturelles de Belgique, Darrin Lunde and Dr. David Hunt at the Smithsonian Institution National Museum of Natural History, Mark Omura at the Harvard Museum of Comparative Zoology, and Véronique Laborde at the Musée de l'Homme.

There are many others I am personally grateful to. My cohort Ellen Fricano was unwavering in her support, and her friendship and good example were invaluable. I also

thank the rest of the Johns Hopkins faculty, past and present, Drs. Johnathan Perry, Valerie DeLeon, Dave Weishampel, Gabriel Bever, Siobhán Cooke, and especially Dr. Ken Rose, who always believed in me. Thank you as well to the FAE students for their friendship and support, especially my labmate Christine Harper.

Finally, thank you to my family, Max Pinz, and my friends for their boundless love and support during this process. I particularly thank my parents, who always kept me grounded and reminded me that I was in this for the joy of the work. And, as always, to Ian.

Table of Contents

List of Figures

List of Tables

1 Introduction

Evolution of the human upper limb is of clear importance in understanding the behavioral trajectory of our species. Human locomotion is unique among primates, characterized by obligate bipedalism. This strongly affects nearly all aspects of modern human life and provides a tantalizing clue to the driving factors behind our evolution. Our closest relatives, the chimpanzees and other great apes, spend a significant amount of time in the trees. How and why humans diverged from this pattern of behavior is unclear.

The earliest work on human evolution suggested that bipedalism evolved as a means of freeing the hands for carrying and tool use (Darwin, 1871), suggesting that the changes to upper limb behavior were coincident with bipedalism, and were a causal factor in its development. Alternative theories are also inextricably linked to changes in use of the upper limb. These include a variety of environmentally-based selection pressures, including among others an increase in more open habitats that required compromises to arboreal adaptations in favor of bipedal ones either for travel across an open landscape (Lamarck, 1809), for visual surveillance (Dart, 1925), or for foraging (Jolly, 1970; Hunt, 1994), perhaps occurring as an extension of bipedal arboreal behaviors (Thorpe et al., 2007). Determining the functional capabilities of the upper limb across the transition to obligate bipedality is crucial to assessing the probability of such hypotheses.

Upper limb function may also help to explain and contextualize the apparent diversity of the early hominin tree. The partial disjunction of upper and lower limb evolutionary changes (Young et al., 2010) means that there is potential variability in the trajectories characterizing upper and lower limb use in different lineages. Despite evidence of bipedal locomotion in all hominin taxa considered in this study (Table 1-1 below), disparate selective pressures may have resulted in taxa that shared bipedal adaptations, but differed in their upper limb use. Although there has been extensive debate over possible evidence for fossil hominin arboreality (see section 1.3 for full discussion), given the abundance of contemporaneous hominin species, heterogeneity in the locomotor repertoire of these taxa should not be discounted and might provide key insights into factors driving the radiation of early hominins. The mosaic morphological features of recently discovered hominins present new evidence of possible locomotor diversity in the fossil record and support claims of extended retention of arboreal behaviors in both *Australopithecus sediba* (Kivell et al., 2011, 2015; Churchill et al., 2013; Rein et al., 2017a) and *Homo naledi* (Kivell et al., 2015; Feuerriegel et al., 2017), partly on the basis of upper limb morphology. Understanding differences in both the capability of hominin species to exploit arboreal resources, and the frequency of these behaviors, may provide insights into the niches occupied by different hominin species, and could provide clues as to how contemporaneous species interacted.

While arboreality can be examined through the study of many postcranial traits (Drapeau, 2008; Zipfel et al., 2011; Green, 2013), the relative prevalence of the distal

humerus in the fossil record and the confluence of forces acting on the elbow make this region promising for investigation of habitual use of the upper limb (Lague, 2015). Yet understanding the interaction between form and function of the distal humerus is particularly complicated because of the dual role the humerus plays in controlling flexion-extension and pronation-supination. The elbow joint is made up of three subsidiary articulations, two of which (the humeroulnar and humeroradial) involve the distal humerus. The functions of these two subsidiary joints are distinct, though their articular surfaces are adjacent and continuous. Broad conclusions about the functional significance of specific regions and features can be drawn through consideration of anatomy and relevant mechanical factors.

1.1 General Distal Humeral Morphology

Humeral features vary among extant catarrhines and among hominids (the genera *Homo, Pan, Gorilla* and *Pongo*; Fleagle, 2013). Key features are demonstrated on a human, chimpanzee, and an orangutan in Figure 1-1 in order to orient the reader. The relative size, shape, and position of the homologous features labeled in Figure 1-1 constitute the basis for both functional and phylogenetic inferences discussed in the remainder of this chapter.

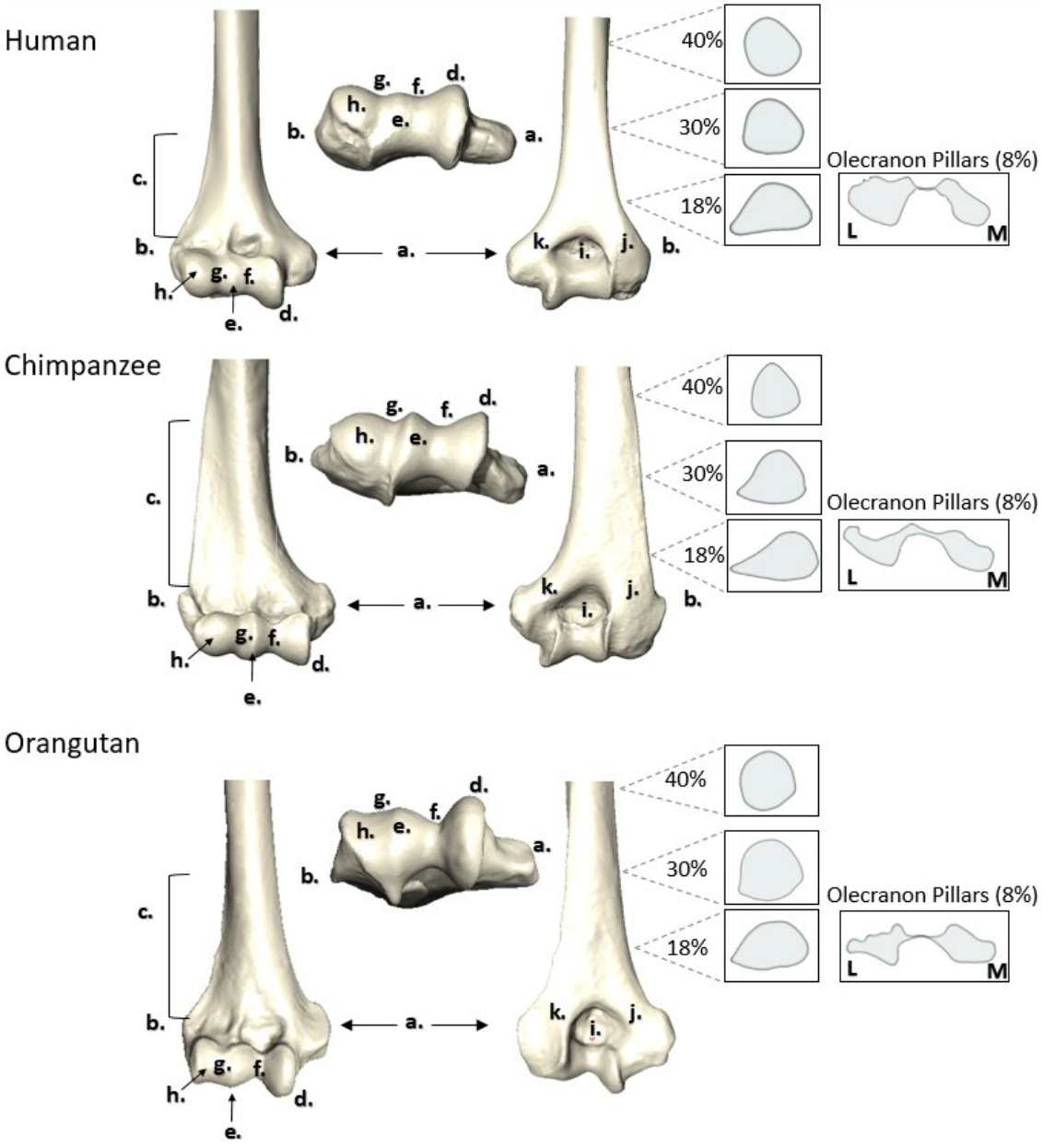

Figure 1-1 Comparison of important features of the human, chimpanzee, and orang distal humerus. From left to right: Anterior, inferior, posterior view. Cross-sectional contours for 40, 30, 18%, and 8% are depicted. Images not to scale.

Articular morphology affects stability of the elbow joint, independence of the subsidiary joints, and range of motion (Hamrick, 1996). The humeroulnar joint is a uniaxial hinge joint active in flexion and extension, formed by the articulation of the humeral trochlea (Figure 1-1 d,e,f) with the ulna. The ulna transmits force both when compressive forces are applied to the hand (Birkbeck et al., 1997; Pfaeffle et al., 2000), as in knuckle-walking, palmigrady, and suspension (Napier and Davis, 1959). Therefore, trochlear morphology affects both range of flexion and extension (Rose, 1988) via features such as size and extent of the trochlea adjacent to the olecranon fossa (Knussman, 1967; Aiello and Dean, 1990), as well as stability, through the medial and lateral trochlear crests (Figure 1-1 d and e, respectively), keeling, the trochlear groove (f), and overall breadth (Jenkins, 1973; Rose, 1988, 1993; Aiello and Dean, 1990).

The humeroradial joint (Figure 1-1, g) occurs at the point of contact between the capitulum (h) and the radius (Gray and Standring, 2008) (see Figure 1-1). It controls rotational motions necessary for pronation and supination. The radius bears most of the load from the hand during quadrupedal behaviors such as knuckle-walking (Napier and Davis, 1959), although the interosseous membrane transfers a part of these loads to the proximal ulna (Birkbeck et al., 1997; Pfaeffle et al., 2000; Ruff et al., 2013). Stability at this joint is created by capitular curvature and size and depth of the adjacent zona conoidea (Rose, 1988, 1993), which prevent displacement, while its sphericity determines range of motion (Rose, 1993; Nakatsukasa, 1994). The extent to which the

capitulum extends posteriorly determines how far the radius is able to extend (Rose, 1993), influencing its supportive capacity in extended postures.

The periarticular region and distal humeral shaft are chiefly influenced by muscular insertions and load bearing (Jones et al., 1977; Ibáñez-Gimeno et al., 2013a). The periarticular region is here defined as the area of the metaphysis adjacent to the olecranon fossa, bracketed proximally by the superiormost point on the rim of the olecranon fossa and distally by the proximal edge of the articular surface. It bears prominent processes for muscles of wrist flexion (medial epicondyle, Figure 1-1 a) and extension (lateral epicondyle, b; supracondylar crest, c), but is also an origin for muscles controlling pronation and supination of the forearm (superior medial epicondyle and lateral epicondyle, respectively) (Gray and Standring, 2008). The periarticular region also bears fossae (coronoid, radial, olecranon) that expand range of motion, though the extent of this effect has been debated (Straus, 1948; Kubicka et al., 2015). The overall contours of this region, specifically the olecranon pillars on either side of the olecranon fossa (Figure 1-1 k and j), may be linked to support during different types of locomotion (Senut, 1981a, but see McHenry, 1976).

The distal humeral shaft includes insertion sites for muscles involved in elbow flexion and extension. The anterior surface is the attachment site for the brachialis muscle, a forearm flexor, while the medial head of the triceps attaches to the posterior surface of the bone and acts as an elbow/forearm extensor (Gray and Standring, 2008). The brachioradialis, originating along the lateral supracondylar ridge of the humerus,

also flexes the elbow. The positioning of these muscles and their attachment sites varies among taxa (Miller, 1932; Knussman, 1967; Zihlman et al., 2011). In combination with the forces from m. biceps brachii, this changes the moment arm of the forces exerted, affecting both speed and power of the resultant motions. This is particularly notable in the flexors (Miller, 1932; Ibáñez-Gimeno et al., 2013b). The humeral shaft is additionally affected by bending moments exerted during arboreal and terrestrial weight-bearing behaviors, as well as non-locomotor activities such as throwing, carrying, and other manipulative behaviors. These affect the cross-sectional geometry of the shaft (Shaw and Stock, 2009; see insets in Figure 1-1 for depictions, for discussion see below).

The overall effect is a functionally crucial bone that is also geometrically complex and difficult to characterize quantitatively (Straus, 1948; Lague and Jungers, 1996). Previous analyses of the distal humerus have relied almost entirely on linear measurements or geometric morphometric techniques applied to points in two dimensions (Knussman, 1967; Patterson and Howells, 1967; McHenry, 1976; Bacon, 2000; Lague, 2014, but see Tallman, 2010, 2013; Holliday and Friedl, 2013). However, the complex of forces acting on the elbow do not act in two dimensions, and the relative position of features in three dimensions is critical to understanding the function of the elbow joint as a cohesive whole. Therefore, both linear measurements and modern geometric morphometric techniques based on fixed landmarks omit meaningful variation. Defining reliably homologous points from a functional perspective is so difficult that structures of clear functional and taxonomic importance, like the lateral

epicondyle, have sometimes been omitted due to their "irregular and frequently ill-defined form and contour" (Straus, 1948). Because the articular surface is formed of a series of continuous curves without clearly defined demarcations (Gunz et al., 2005), other authors have relied on extremal points and constructed landmarks that are dependent upon perspective and orientation (e.g., Bacon, 2000; Lague, 2014). However, these landmarks cannot capture subtle differences in curvature that may be key to understanding *in vivo* function, and because they cannot be placed independently, they are deficient in information (Gunz et al., 2005). This dissertation addresses these issues by using sliding semi-landmarks to quantify morphology of the distal humerus in three dimensions and place it into functional context. It also assesses two factors that may partially explain variation in these features: developmental plasticity and body size.

1.2 Comparative Morphology and Function in Catarrhines

Features of the hominid and fossil hominin elbow complex have been the subject of a number of functional interpretations (Day, 1978; Senut, 1981b; Senut and Tardieu, 1985; Stern, 2000), despite doubts that humeral features differ sufficiently to justify such conclusions (McHenry, 1976; Feldesman, 1982; Hill and Ward, 1988; Lague and Jungers, 1996; Bacon, 2000; Ward, 2002; Lague, 2014). All assessments of humeral traits with regard to function, regardless of the resulting conclusion, rely on morphological comparison within and between extant species. Morphological features of hominids are therefore reviewed below, with a focus on common hominoid traits (which are therefore present in all hominids) and traits that have been linked to locomotor

behavior through "…'common sense' interpretations based on the visual inspection of skeletal or dissected material" (Rose, 1993).

Distal humeral morphological distinctions between Old World monkeys and apes have been linked to differences in the mobility and habitual positioning of the upper limb. While old world monkeys are typically pronograde quadrupeds (Gebo, 1996; Arias-Martorell et al., 2015), apes exhibit habitually orthograde postures, engaging in vertical climbing and below branch suspension in addition to specialized terrestrial behaviors (i.e., knuckle-walking and bipedalism) (Tuttle and Watts, 1985; Cant, 1987; Hunt, 1992; Doran, 1996). Limb posture between these groups differs accordingly. Hominoids have a higher degree of mobility in the forelimb in both flexion-extension and pronation-supination. They maintain full rotational ability throughout flexion and extension, and are able to hyperextend the elbow (Rose, 1988). In cercopithecoids, these motions are restricted in favor of stability in pronograde postures. These differences in behavior are reflected in the morphology of the distal humerus.

While the elbow of cercopithecoids is primarily stable during full pronation due to close-packing of the joint (Rose, 1988), in the hominids (humans, *Pan, Gorilla, Pongo*) that are the focus of this study as well as other hominoids (including lesser apes), both the humeroulnar and humeroradial joints possesses characteristics that maintain stability in a variety of limb positions (Rose, 1993). The hominid humeroulnar joint is resistant to mediolateral forces during flexion and extension due to a wide trochlea with medial and lateral keeling that peak in prominent medial and lateral crests (Rose, 1993).

The lateral crest in particular is extended and pronounced posteriorly, and contact between the ulna and the lateral wall of the olecranon fossa is thought to resist loads exerted on the joint during hyperextension (Tuttle and Basmajian, 1974; Aiello and Dean, 1990; Ward et al., 2001) (Figure 1-1). The lateral trochlear crest in combination with a prominent zona conoidea creates independent stabilization for the humeroulnar and humeroradial articulations, and creates in some individuals the appearance of a doubled spool (see chimpanzee in Figure 1-1) (Senut, 1981a). The humeroradial articulation is stabilized by a pseudo-socket, composed of the pronounced zona conoidea and globular capitulum, providing increased humeroradial surface contact especially in flexion. These stabilizing features are absent in old world monkeys, which tend to have a mediolaterally (ML) narrower, anteroposteriorly (AP) deeper cylindrical trochlea that is relatively continuous with the capitulum owing to lack of a prominent lateral trochlear crest and zona conoidea (Rose, 1988, 1993; Aiello and Dean, 1990).

These traits are, however, variable among hominids, and previous workers have sought to link this variation to differences in behavior (Napier and Davis, 1959; McHenry and Corruccini, 1975; McHenry, 1976; Senut and Tardieu, 1985). Both in the literature and in the present study, impact on hominid distal humeral morphology of three main types of locomotor behavior are considered: climbing/suspension, knuckle-walking, and manually unsupported locomotion (i.e., bipedalism). Functional interpretations of morphology are linked to locomotor differences between genera (Knussman, 1967; Senut, 1981b; Ruff, 2002; Carlson, 2005): arboreal traits are expected to be emphasized

in highly arboreal orangutans and present to a lesser degree in chimpanzees and gorillas. Features shared by African apes, but not other hominid taxa, are expected to be adaptive for terrestrial load bearing during knuckle-walking, and traits specific to humans are interpreted as either a release from locomotor selection or as adaptation to tool use (e.g., digging, throwing).

The high frequency of suspensory behaviors in *Pongo* (Cant, 1987; Thorpe and Crompton, 2006) has been posited to result in an increase in supportive traits to stabilize loads traveling across the elbow during varied degrees of joint excursion. This is principally noted at the humeroulnar articulation. Orangutans have an exaggerated trochlea, bearing a deep trochlear groove and a large medial trochlea with marked lipping (see Figure 1-1 d and f) that contacts the medial portion of the ulnar trochlear notch (Rose, 1993). These traits are thought to help resist mediolateral deviation, providing stability during flexion and extension with a wide range of suspensory hand postures (Rose, 1993). A particularly deep coronoid fossa proximal to the trochlear groove and high incidence of the supratrochlear foramen are likely to increase range of flexion (Rose, 1993). Orangutans, like other great apes, have cross-sectionally triangular medial and lateral pillars thought to be linked to the forces traveling across this region during suspension, but the medial pillar is said to be uniquely flattened anteroposteriorly (Figure 1-1, olecranon pillar inset) (Senut, 1981b). This feature is unexplained. While all great apes share a more rounded diaphyseal cross section at 18% compared to humans, humans are statistically more similar to orangutans at this section

than to any other species (Figure 1-1, cross section insets) (Lague, 2015). Such commonalities between humans and orangutans are particularly useful when considering whether traits present in *Pan* and *Gorilla* are indicative of convergent quadrupedal terrestrial locomotion, or reflective of arboreal behaviors shared by hominoids more broadly. When traits are shared by the two knuckle-walking genera but not humans or orangutans, it is particularly important to consider the possibility of convergence, though such a pattern may have other explanations.

During knuckle-walking, the forearm is fully pronated and loaded in compression, rather than tension (Sarmiento, 1988; Swartz, 1990; though suspensory locomotion can also create compressive forces), and features unique to African ape articular surfaces have been interpreted as improving stability in this position. They therefore both differ in some ways from purported stabilizing traits in *Pongo* (Rose, 1993). This is particularly visible in morphology of the humeroradial articulation (see Figure 1-1). The posteriodistal surface of the capitulum is expanded to allow the radius to support weight bearing with the elbow in hyperextension (Patterson and Howells, 1967; Aiello and Dean, 1990; Rose, 1993). The zona conoidea is particularly deep, mitigating the potential for radial displacement and providing increased surface contact during compressive load transfer (Rose, 1988). On the humeroulnar articulation, the lateral trochlear crest is likewise especially prominent (see Figure 1-1 e), both preventing dislocation during climbing (Senut and Tardieu, 1985) and stabilizing in hyperextension due to its posterior extension along the olecranon fossa (Aiello and Dean, 1990). This

feature is especially typical of gorillas (Aiello and Dean, 1990), though in Figure 1-1 it is best demonstrated in the orangutan.

Human humeri differ substantially from those of other great apes (Patterson and Howells, 1967; McHenry, 1976; Senut, 1980; Bacon, 2000; Susman et al., 2001; Lague, 2014, 2015), despite early assertions that "the lower end of the humerus is basically so similar in man and the anthropoid apes that it is of extremely limited value in taxonomic and phylogenetic studies" (Straus, 1948). These differences are attributed to the freeing of the upper limb from the demands of weight support, and affect all distal humeral regions. In humans, there is little extension of the trochlea into the olecranon fossa, which itself is shallow (Knussman, 1967; Senut, 1981a), has neither the steep walls that are especially prominent in African apes nor ulnar contact along its lateral wall. These features reflect the lesser importance of loaded extension in humans and contrast with the deep, steep-walled olecranon fossa and high, posteriorly extended lateral trochlear crest seen in other hominids (Aiello and Dean, 1990). The human capitulum lacks the distal expansion seen in apes (Patterson and Howells, 1967; Aiello and Dean, 1990; Susman et al., 2001), and is positioned primarily on the anterior surface, , also reflecting the reduced loading of the radius. Correspondingly, there is less stabilization of the humeroradial articulation, which also has a less distinct zona conoidea than seen in other great apes (Rose, 1988, 1993; Susman et al., 2001).

Muscular processes in the periarticular region also differ between humans and other hominids. The lateral epicondyle is located more proximally in great apes,

especially *Pan* and *Pongo*, and distally in humans relative to the capitulum, which may increase the mechanical advantage of extensors of the hand in apes (Senut and Tardieu, 1985) (Figure 1-1, height of b relative to h). The lateral supracondylar crest is also more developed in great apes, especially chimpanzees, and less developed in humans (Knussman, 1967; Senut, 1980; Aiello and Dean, 1990). This perhaps indicates that wrist movements (m. extensor carpi radialis longus) and elbow flexion (m. brachioradialis) are enhanced in great apes, likely for climbing (Aiello and Dean, 1990). The medial epicondyle differs in form between humans and other hominids. A 'distinct blunt knob' is found in other great apes at the end of the supinator ridge on the medial epicondyle. This is absent in humans (Broom, 1938), who instead have a more proximodistally angled medial epicondyle that creates a greater angle with the shaft (Patterson and Howells, 1967). These differences must alter the lever advantage of a suite of muscles controlling wrist flexion and pronation (Ibáñez-Gimeno et al., 2013b, 2014), but proper quantification of medial epicondylar shape is elusive using fixed landmark techniques. The significance of these effects is therefore so far undetermined.

Differences in loading and muscular control also likely influence the olecranon pillars, which in humans, but not great apes, are asymmetric (Figure 1-1, pillar insets) (Senut, 1980, 1981a). The cross section of the lateral olecranon pillar in humans is quadrangular rather than triangular (Senut, 1981a) because of the extension and trifurcation in the periarticular region of a column-like structure running down the anterior surface of the distal diaphysis (Le Floch, 1982), analogous to the medial swelling

of the distal diaphysis in chimpanzees (Patterson and Howells, 1967; Senut, 1981a). The lateral pillar has been interpreted as an extension of the radius and thumb column, and manipulation may therefore explain its different form in humans.

Cross-sectional shape of the distal shaft also differs between humans and great apes in part because of the anterior swelling of the midline region of the distal diaphysis into a projecting column in humans (Figure 1-1). Together with posterior flattening of the distal diaphysis (Lague, 2015) this creates in humans a triangular diaphyseal cross-sectional shape (Le Floch, 1982; Lague, 2015). The distal diaphysis of great apes instead has a rounded posterior aspect (Lague, 2015) (Figure 1-1), creating an ovoid shape with a mediolateral major axis. This difference has been used for taxonomic assignments of fossils (Susman et al., 2001; Lague, 2015), some of which differ from the human condition (Lague, 2015). The long axis of the distal humeral shaft also differs between humans and great apes. In humans it is generally straight, while in great apes it is anteroposteriorly bowed (Holliday and Friedl, 2013). Based on the near absence of curvature seen in human humeral shafts and the minor curvature seen in hylobatids, it has been suggested that marked humeral bowing is due to terrestrial postures in the African apes and compressive orthograde postures in *Pongo* (Holliday and Friedl, 2013), though other factors might account for the small size of this trait in hylobatids (e.g., smaller body mass).

1.3 Fossil Hominins

Humeri are relatively common in the hominin fossil record compared to other limb bones, and are available for a number of taxa (Yokley and Churchill, 2006; McHenry and Brown, 2008; Lague, 2014). Table 1-1 summarizes the fossils included in this study, including a brief description of humeral regions preserved in each, and the entire sample is illustrated in Fig. 1-2. Images of individual specimens are also included as they are discussed in sections 1.3.1 and 1.3.2.

Table 1-1 List of fossil humeri included in this study

SPECIMEN	SPECIES	AGE (MYA)	REGIONS PRESERVED
KNM-KP 271 KANAPOI, KENYA	*A. anamensis*	4.12-4.07	Articular surface to ~13 mm above the olecranon fossa.
A.L. 288-1 HADAR, ETHIOPIA	*A. afarensis*	3.2	*Right:* Complete humerus, head crushed. *Left*: Articular surface to ~26.5mm above the olecranon fossa.
StW 431 STERKFONTEIN, SA	*A. africanus*	2.8-2.4	Articular surface, portions of periarticular surface and entire distal shaft to approximately midshaft.
KNM-ER 1504 KOOBI FORA, KENYA	*P. boisei (?)*	1.9	Articular surface to ~34 mm above the olecranon fossa.
KNM-ER 6020 KOOBI FORA, KENYA	*P. boisei (?)*	1.8	Articular surface, no medial epicondyle, distal diaphysis to ~63 mm above the olecranon fossa.
KNM-ER 739 KOOBI FORA, KENYA	*P. boisei (?)*	1.5	Articular surface and nearly entire shaft (missing proximal region including tubercles).
TM 1517 KROMDRAAI, SA	*P. robustus*	2	Articular surface to ~18 mm above the olecranon fossa.
SK 24600 SWARTKRANS, SA	*P. robustus / Homo sp.*	1.8-1.6	Articular surface to ~15 mm above the olecranon fossa.
SKX 10924 SWARTKRANS, SA	*P. robustus / Homo sp.*	1.8-1	Articular surface to ~25 mm above the olecranon fossa.
GOMBORE IB-7954 (MK3) MELKA KUNTURE, ETHIOPIA	*H. erectus (?)*	1.5	Articular surface to ~65 mm above the olecranon fossa.

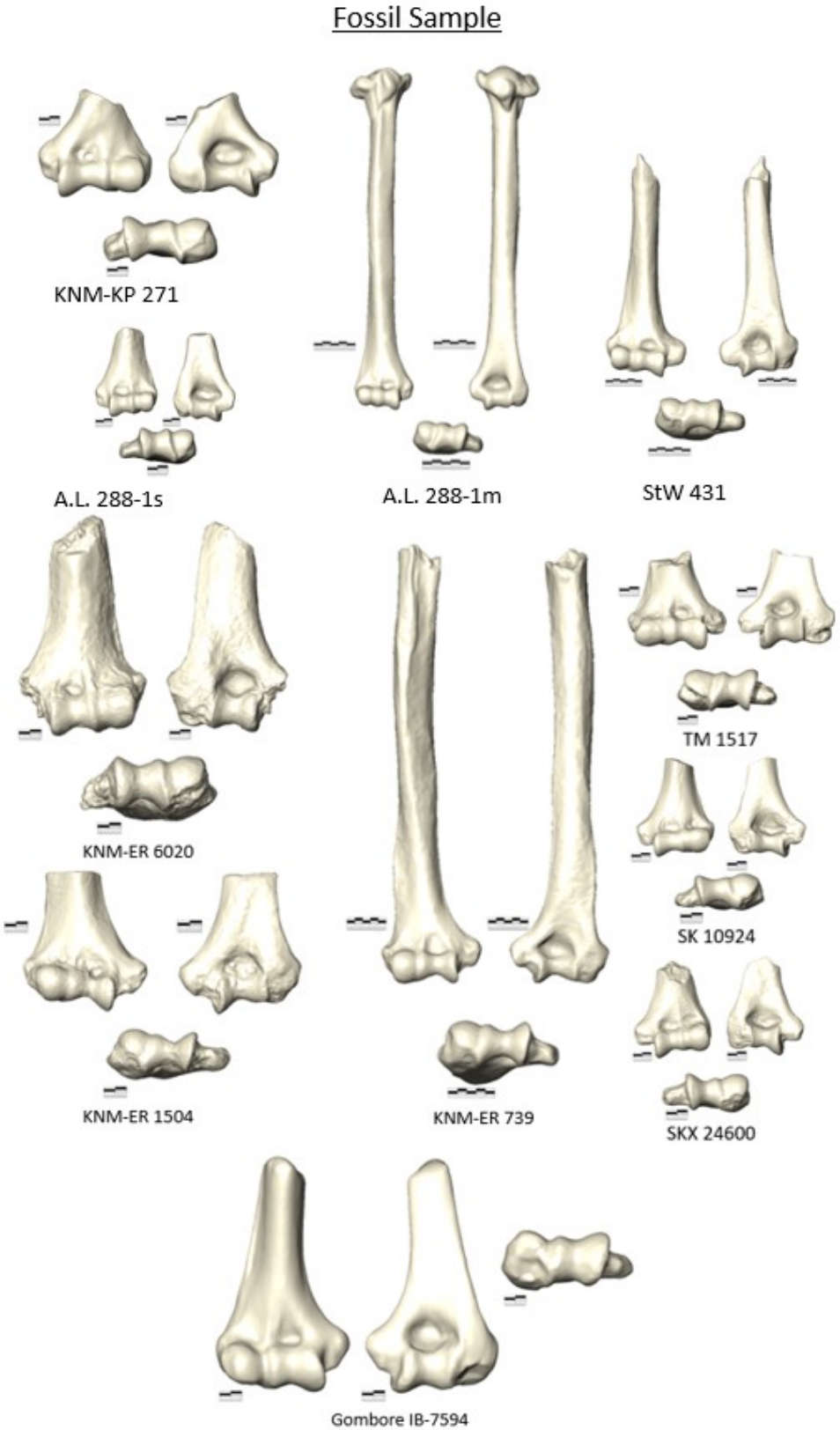

Figure 1-2 Images of the fossils contained in Table 1-1.

Fossil hominin morphology has been assessed in light of differences among extant taxa in an effort to reconstruct behavior. There is ongoing debate about the meaning of postcranial traits in fossil hominins that appear linked to arboreality in extant species (see summaries in Stern, 2000; Ward, 2002). Several features found in early hominins, particularly *Australopithecus*, appear indicative of suspension and climbing, including a number of distal humeral features. A proximal lateral epicondyle, projecting medial epicondyle, and strong brachioradialis crest in many fossils compared to modern humans suggests antebrachial musculature like that of great apes (Senut, 1980; Churchill et al., 2013). Stabilizing traits are observed in the trochlea in *A. afarensis* (Senut, 1980); *A. sediba* has brachial (forearm to arm) proportions more like those of other great apes than like humans (Churchill et al., 2013); and *A. africanus* has large forelimb relative to hind limb joints (McHenry and Berger, 1998b), suggesting ape-like use of the upper limb (i.e., climbing). Other regions of the body also show indications of arboreality in australopiths. A cranially directed glenoid fossa and other characteristics of the shoulder are consistent with adaptations for climbing in great apes (Larson, 2007; Green and Alemseged, 2012; Churchill et al., 2013), as are curved manual phalanges (Stern and Susman, 1983; Kivell et al., 2015) and certain ulnar traits (Drapeau, 2008; Tallman, 2015). While some argue that these features indicate retention of arboreal behaviors (Senut, 1980; Stern and Susman, 1983; Senut and Tardieu, 1985; Lague and Jungers, 1996; Stern, 2000; Churchill et al., 2013; Rein et al., 2017b) , others (Latimer and Lovejoy, 1989; Latimer, 1991; Ohman et al., 1997; Ward, 2002) contend that these

primitive traits were retained either because they conveyed no selective advantage or disadvantage, or because the selective disadvantage had not been present long enough to fully overcome the primitive condition (Gould and Vrba, 1982; Ward, 2002). These latter assertions are based mainly on the hind limb, arguing that the bipedal adaptations compromised climbing abilities, which indicates climbing did not confer a significant selective advantage for fossil hominins (Latimer, 1991; Ward, 2002). However, these two perspectives are not entirely irreconcilable; behaviors need not confer significant selective advantage to be present (Ward, 2002). A brief history of fossil hominin humeral traits and how they have been interpreted is given below, with an emphasis on traits that have contributed to this debate.

1.3.1 Early work

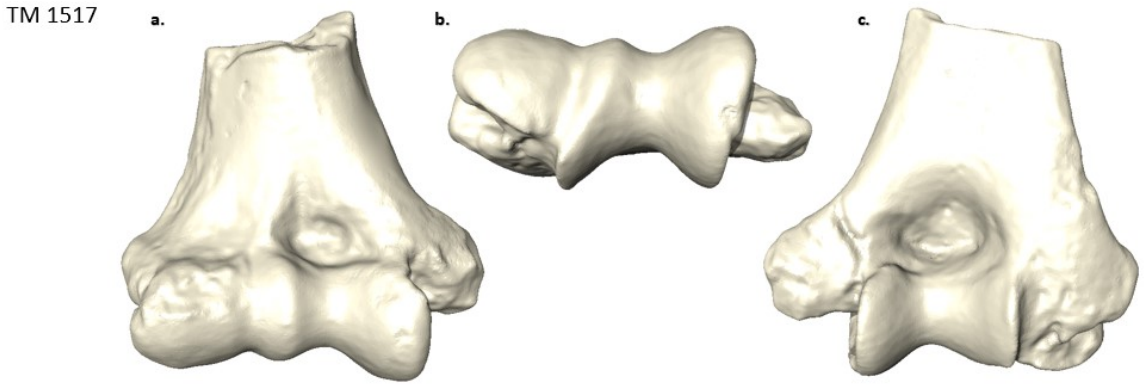

Figure 1-3 Unreconstructed morphology of TM 1517. 3D polygonal model. a. anterior view, b. inferior view, c. posterior view.

The first fossil early hominin humerus was found by Robert Broom at Kromdraai in association with a skull, and is part of the type specimen of *Paranthropus robustus* (TM 1517, Figure 1-3). TM 1517 is worth considering in some detail as it set the stage for subsequent analyses and illustrates some of the difficulties in taxonomic and functional interpretation of this anatomical region. Broom immediately noted its similarity to modern humans (Broom, 1938), e.g., women of the local San people (Schepers and Broom, 1946), despite some subtle differences. He rejected the idea that *Paranthropus* engaged in arboreal behavior on the basis of this humerus, noting its apparent dissimilarity from those of chimpanzees and gorillas (see below). He suggested that *Paranthropus* was therefore likely to have had an upper limb behavioral repertoire similar to that of modern humans, using the upper limb for manipulation of tools and weapons rather than locomotion. On the basis of independent qualitative assessments, subsequent authors concurred with Broom's conclusions about the lack of arboreal behavior and the specimen's human morphological affinities (Le Gros Clark, 1947a; b), but these remarks were shortly called into question by Straus's metric analysis of variation in the distal humerus among modern taxa (Straus, 1948).

Debate over the affinities of TM 1517 centered on two questions. The first was whether distal humeri were taxonomically differentiable at all, a necessary prerequisite for answering the second question and the second was; whether the morphology of TM 1517 indicated phylogeny or function. Straus (1948) urged extreme caution regarding the first question, finding only a limited number of measurements that varied

significantly between humans and great apes. Broom (1938) and Le Gros Clark's (1947) observations about the human-like morphology of TM 1517 mainly focused on muscular attachments, observing that the origins of extensor and pronator muscles were proportioned as in humans, the lateral supracondylar crest was moderate, curving anteriorly as it extended distally, and surface attachments for the triceps and brachialis were similar to those of humans in shape, size, and rugosity. These were not the properties that Straus found to differentiate humans and great apes – rather, he found that the width of the capitulum, distance of the medial epicondyle from the trochlea, and breadth of the olecranon fossa were the most taxonomically significant differences, while muscular ridges were exceedingly variable within taxa and therefore useless as discriminators.

While the olecranon fossa of TM 1517 had been described as shallow and human-like, assessment confirmed by Straus's metric analysis, the second two features Straus found to discriminate between humans and great apes, the capitulum and medial epicondyle, had been noted by both Broom and Le Gros Clark as points of difference between humans and TM 1517. In these early descriptions, they noted that TM 1517 had a large, irregular, and flattened capitulum compared to the 'marble-like' human one (Schepers and Broom, 1946) and was positioned less anteriorly than in humans (Le Gros Clark, 1947a; b). It also possessed a deep furrow between the edge of the capitulum and the lateral epicondyle, otherwise found only in male chimpanzees (Schepers and Broom, 1946). Straus's measurements confirmed that the capitulum of *Paranthropus* differed

from that of modern humans. In ratios which attempted to account for overall size, the capitulum of TM 1517 was wider than all but two of the 37 humans measured by Straus, making it more chimpanzee-like, although the average chimpanzee capitulum was larger still. However, Straus disagreed with Le Gros Clark's remarks that the capitulum, and even more so the trochlea, was positioned anteriorly relative to the shaft in humans, but not in TM 1517. Le Gros Clark's assertions were not borne out by Straus's diagraphic tracings. This caused Straus to reject one of the few functional differences proposed for *Paranthropus*, Le Gros Clark's hypothesis that *Paranthropus* had diminished flexor power and increased ability to hyperextend the elbow.

The medial epicondyle was described as narrow and pointed by all early workers (Schepers and Broom, 1946; Le Gros Clark, 1947b; a; Straus, 1948)(note its profile in Figure 1-3 a and c relative to Figure 1-1, especially the proximodistal height of the medial epicondyle relative to its length). Metrically, it differentiated TM 1517 from both humans and chimpanzees – according to Straus, this feature approximated the gorilla condition (Straus, 1948). Straus also noted an additional feature he was unable to measure due to its "irregular and frequently ill-defined form and contour", but which nevertheless appeared significantly different between humans and great apes – the lateral epicondyle. Though its complex shape made reliable and homologous measurement impossible, Straus noted its strangely large size in the fossil. Broom had also noted a distinct blunt point on the superior border of this that was found also in gorillas, orangs, and male chimpanzees, but not humans, though he had concluded that

it was otherwise more human-like than ape-like. Straus disagreed on this point, and indeed with Broom and Le Gros Clark's overall conclusion that the Kromdraai humerus in general was human-like – rather, he considered the fossil to possess a mosaic of clearly hominid features, but to be no more like humans than chimpanzees. He therefore concluded that it was impossible on the basis of this humerus to conclude that TM 1517 could not have knuckle-walked or spent significant time in the trees.

Straus's study set the tone for future analyses of distal humeri, which relied on combinations of ratios and linear measurements (Patterson and Howells, 1967; McHenry and Corruccini, 1975; McHenry, 1976; Lague and Jungers, 1996; Yokley and Churchill, 2006) and subsequently on re-formulating of these dimensions as a configuration of landmarks in two dimensions (Bacon, 2000; Lague, 2014) to compare the growing fossil hominin record to variation within and between extant hominids. Like Straus, later authors also used forms of diagraphic tracings to assess morphology not well suited to landmarks or linear measurements, such as the contours of the periarticular region of the bone (Senut, 1981a; Le Floch, 1982). This work was continued by qualitative (Susman et al., 2001) and quantitative (Lague, 2015) evaluation of distal shaft cross-sectional shape.

1.3.2 Fossil Hominin Functional and Morphological Affinities

There are now humeri associated with at least eight early hominin taxa – *Australopithecus anamensis, A. afarensis, A. africanus, A. sediba, Paranthropus boisei, P. robustus, Homo cf. habilis,* and *Homo cf. erectus*, six of which are included in the present

study (Table 1-1). The distal humerus has been used to group and taxonomically identify individual specimens (Senut, 1981a; Bacon, 2000; Susman et al., 2001; Lague, 2015) and to draw functional conclusions about their behavior (Senut, 1980; Feldesman, 1982; Senut and Tardieu, 1985), though there has at times been continued argument that distal humeri are not sufficiently different between hominid taxa to support such analyses (Feldesman, 1982). The section below summarizes this discussion as pertains to each of the fossils included in this study.

1.3.2.1 A. anamensis

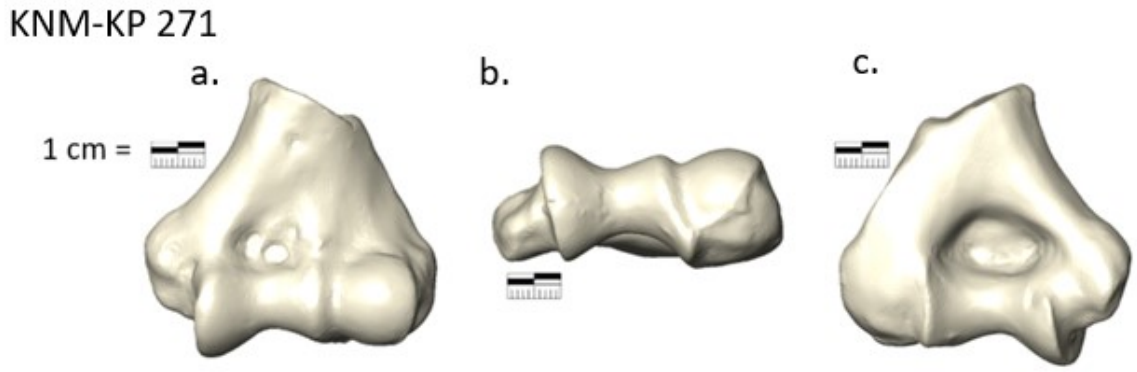

Figure 1-4 Morphology of KNM-KP 271, image taken from 3d polygonal model based on scan of cast. Patent supratrochlear foramen in original specimen has been filled. a. anterior view, b. inferior view, c. posterior view

Australopithecus anamensis, as represented by KNM-KP 271 (Figure 1-4), has historically presented a conundrum. Despite its age (over 4 Mya, McHenry and Brown, 2008), many authors have noted the similarity of KNM-KP 271 to *Homo*, especially in the weak development of the lateral trochlear crest (Patterson and Howells, 1967; McHenry

and Corruccini, 1975; McHenry, 1976; Day, 1978; Senut, 1980; Senut and Tardieu, 1985; McHenry and Brown, 2008), rather than other members of the genus *Australopithecus*. Other *Homo*-like features of KNM-KP 271 include the abbreviated length and mild angulation of the lateral trochlear crest, the low, poorly developed lateral epicondyle, and the small surface area of the capitulum on the distal surface (Senut and Tardieu, 1985). Though *A. anamensis* was a habitual biped (Ward et al., 2001), it has not been suggested that its locomotor behavior was more similar to modern humans than other members of its genus. Rather, primitive features have been noted in the hand and long bones of the upper limb, which may suggest occasional climbing (Ward et al., 2001). Some workers have even suggested knuckle-walking behavior in *A. anamensis* (Richmond and Strait, 2000), but these conclusions have since been discounted due to methodological concerns (Ward et al., 2001). The morphological similarities between KNM-KP 271 and *Homo* have also been questioned; Feldesman (1982) finds KNM-KP 271 to be closest in morphology to *Paranthropus* (KNM-ER 739 and KNM-ER 1504) rather than *Homo* on the basis of olecranon fossa depth, "trochlear guttering" and medial biepicondylar breadth. Other studies confirmed its affinities with other australopiths, finding that it is indistinguishable from *A. afarensis* (Hill and Ward, 1988), However, other authors find that A.L. 288-1 (discussed below) and KNM-KP 271 differ significantly (Lague and Jungers, 1996), with some describing KNM-KP 271 as more "gorilla-like" and A.L. 288-1 as "chimp-like" (Bacon, 2000), though these differences are thought to be largely size-related rather than functional or taxonomic (Bacon, 2000). Several factors

weaken functional or taxonomic arguments based on similarities between *Homo* and KNM-KP 271. The aforementioned underdeveloped lateral trochlear crest is variable in modern human populations (Hill and Ward, 1988; Lague and Jungers, 1996; Lague, 2014), and abrasion of the lateral trochlear crest in the fossil may significantly affect assessment of this feature (Ward et al., 2001). KNM-KP 271 is large compared to most humans, and it is possible that allometric effects account for some of the observed similarities. When these are accounted for KNM-KP 271 shows no special affinity with *Homo* (Lague, 2014).

1.3.2.2 A. afarensis

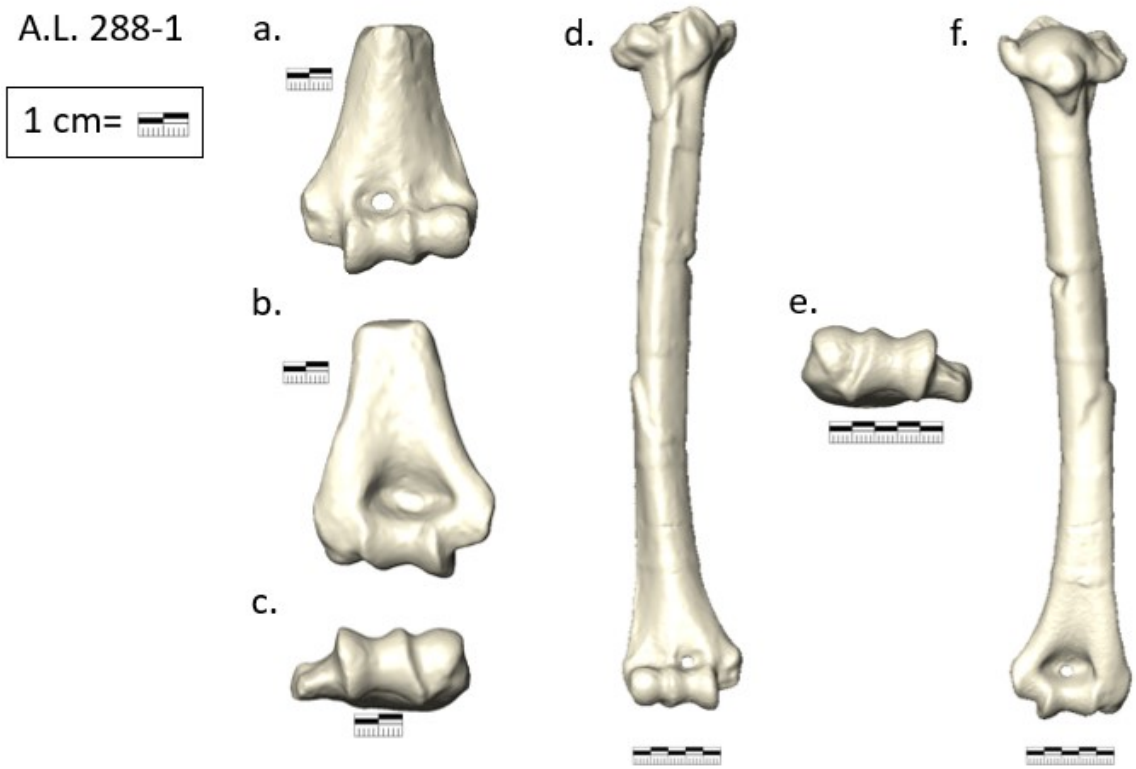

Figure 1-5 Morphology of A.L. 288-1 (*A. afarensis*), image from 3d polygonal model. Left humerus (A.L. 288-1s): a. anterior view, b. inferior view, c. posterior view. Right humerus (A.L. 288-1m): d. anterior view, e. inferior view, f. posterior view.

Australopithecus afarensis is the best-known early hominin species, and therefore particularly important for understanding early hominin locomotion. It is generally accepted that *A. afarensis* was bipedal, but considerable debate remains over the importance of arboreality to the species (Stern and Susman, 1983; Susman et al., 1984; Stern, 2000; Ward, 2002; Ruff et al., 2016). Compared to modern humans, the forelimb is long relative to the hind limb (Jungers, 1982; Susman et al., 1984). A.L. 288-1 also has a particularly strong humerus (Ruff et al., 2016) and phalanges with higher

curvature than modern humans (Stern and Susman, 1983; Susman et al., 1984), consistent with more arboreal behavior than modern humans or *Homo erectus* (Ruff et al., 2016).

A.L. 288-1 is unique among australopiths in that both right and left humeri have been found (Figure 1-5). The two bones are generally similar (Johanson et al., 1982; McHenry and Brown, 2008), though there is some evidence of laterality (Lague, 2015; Ruff et al., 2016). Lucy is smaller than modern humans and many fossil hominins (Ruff et al., 2018b), and her humeri are correspondingly small; allometric affects therefore should be considered when interpreting her morphology (Bacon, 2000; Lague, 2014). Consistent with assertions of potential arboreality in *A. afarensis*, A.L. 288-1 bears a marked lateral trochlear crest with a deep zona conoidea (Johanson et al., 1982; Senut and Tardieu, 1985). The lateral epicondyle is higher than in humans, the capitulum extends posteriorly and is strongly developed on the distal surface (Senut and Tardieu, 1985), and the olecranon fossa is deep, though the lateral trochlear crest does not extend along its border (Johanson et al., 1982). The coronoid and radial fossae are prominent on the anterior surface of the bone (Johanson et al., 1982). The periarticular region of A.L. 288-1 is flattened anteroposteriorly (AP), with olecranon pillars that are ape-like in cross section (Senut, 1981a), traits that have been interpreted as indicating suspension. Cross-sectionally, all members of the genus *Australopithecus* and *Paranthropus robustus* share a similar diaphyseal morphology, characterized by a broad rather than flattened AP diameter, which distinguishes it from *A. sediba* and *H. habilis*,

but a lateral flange and posterior rounding that distinguish it from *Homo sapiens* (Lague, 2015). However, the lateral supratrochlear crest is not particularly well-developed (Johanson et al., 1982). Despite the robust features discussed above, Lucy's overall humeral morphology is more human-like than ape-like (Lague and Jungers, 1996; McHenry and Brown, 2008).

1.3.2.3 A. africanus

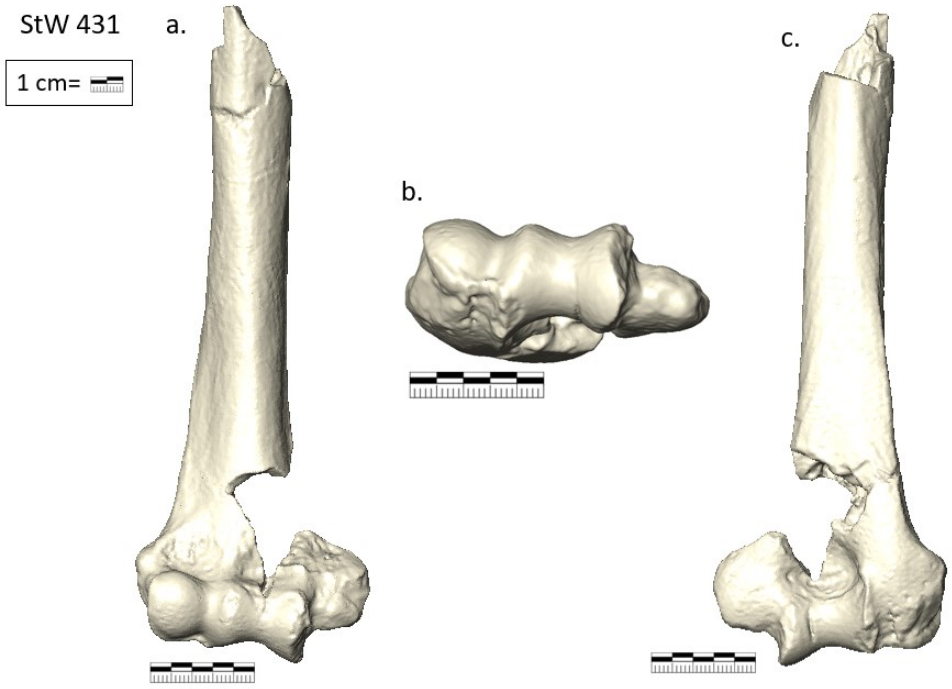

Figure 1-6 Morphology of StW 431. a. anterior view, b. inferior view, c. posterior view.

As in *A. afarensis,* the bipedal adaptations of *Australopithecus africanus* have long been recognized (Dart, 1925). *A. africanus* is generally thought to be human-like in its postcranial morphology, including its hands (Ward, 2002), but other characteristics, including a possibly abductable hallux (Clarke and Tobias, 1995), significantly larger (and

therefore more ape-like) forelimbs (McHenry and Berger, 1998a) that are chimp-like in their strength relative to the hind limb (Ruff et al., 2016), and an ape-like ulna (Tallman, 2015) suggest the possibility that *A. africanus* was at least partially arboreal, potentially more so than other members of the genus (McHenry and Berger, 1998b).

StW 431 (*A. africanus*) (Fig. 1.6) has been noted by some authors to be morphologically enigmatic in its relationship to other fossils (Bacon, 2000; McHenry and Brown, 2008), and to be quite similar to gorillas in overall shape (Lague and Jungers, 1996; McHenry and Brown, 2008), though this relationship with great apes does not appear in all analyses (Rosas et al., 2015). Its closest morphological correlate among fossils appears to be *A. afarensis* (Lague and Jungers, 1996; McHenry and Brown, 2008). Relative to modern humans, the lateral trochlear crest of StW 431 is pronounced, and the lateral epicondyle is well-developed (Toussaint et al., 2003). The periarticular region is anteroposteriorly flattened (Toussaint et al., 2003), as noted for other fossils including *afarensis*, but in StW 431 this appears to affect both olecranon pillars; the medial pillar is flattened and the lateral pillar is subtriangular, compared to the nearly triangular shape of both in *afarensis* (Toussaint et al., 2003).

1.3.2.4 P. boisei

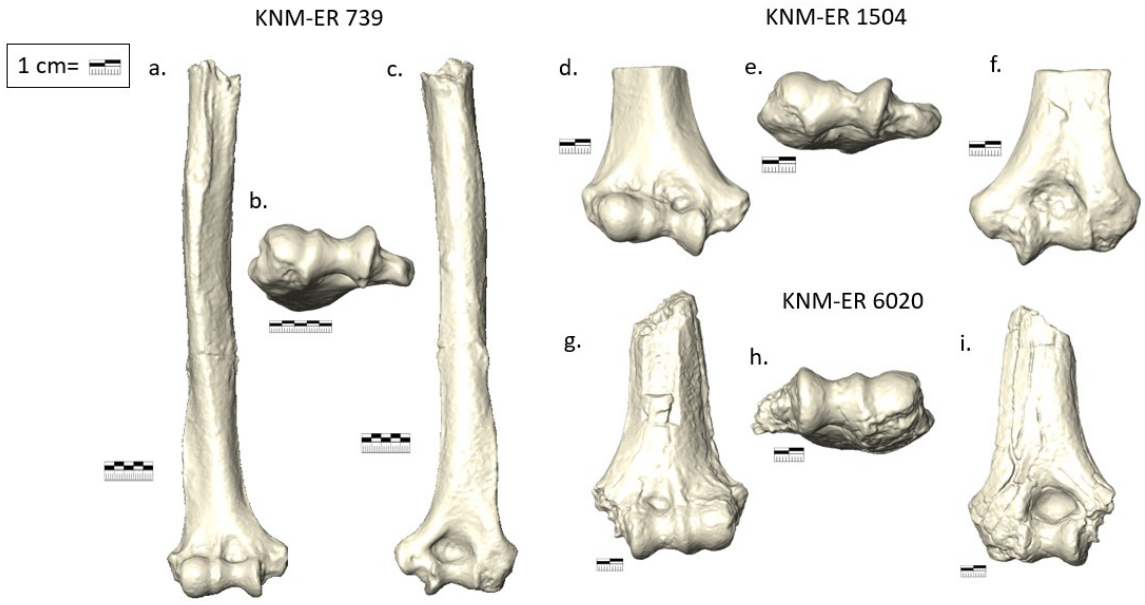

Figure 1-7 Morphology of KNM-ER 739 (a-c), KNM-ER 1504 (d-f), and KNM-ER 6020 (g-i). Anterior views: a, d, g. Inferior views: b, e, h. Posterior views: c, f, i.

Like *A. africanus*, *Paranthropus boisei* (to which this study attributes KNM-ER 739, KNM-ER 1504 and KNM-ER 6020 per Lague (2014) and Leakey (1971, 1973)) has a remarkably strong humeral diaphysis (Ruff et al., 2016). Members of this species appear to share a common humeral morphology distinct from other fossil hominins (Lague and Jungers, 1996; McHenry and Brown, 2008; Lague, 2014), and have been tentatively attributed to *P. boisei* on this basis, in the absence of craniodental remains.

The distal humerus of *P. boisei* has an AP constricted trochlea and large capitulum relative to those of humans (Figure 1-7). These traits are present despite a wide range in humeral size (Leakey, 1973). KNM-ER 739 is large and extremely robust in its dimensions and muscular attachments (Leakey, 1971), which Leakey suggests in his

description may indicate knuckle-walking (Leakey, 1971). This hypothesis is unsupported by later work (McHenry, 1976). Knuckle-walkers have three traits that distinguish them from other groups: a high lateral epicondyle, a thin but projecting medial epicondyle, and a deep olecranon fossa with a steep lateral wall (McHenry, 1976). While *P. boisei* appears to share the first two traits, its olecranon fossa is shallow and human-like (McHenry, 1976; Senut, 1981b; Lague and Jungers, 1996), thought to be a marker of freedom from upper limb locomotor requirements. However, the sides of the olecranon fossa have been noted to be relatively steeper in KNM-ER 739 than in modern humans (Leakey, 1973). *Paranthropus boisei* humeri also havemediolaterally narrow zona conoideae and wide medial and lateral olecranon pillars (Senut, 1981b; Lague and Jungers, 1996).

While the large shaft of KNM-ER 739 bears superficial similarity to that of female gorillas, the articular and periarticular regions show features more similar to modern humans and orangutans (McHenry, 1976). Later authors emphasized this relationship, going as far as to suggest that the human-like characteristics of the Koobi Fora humeri attributed to *P. boisei* might justify attribution to *H. habilis* or *H. rudolphensis* (Lague and Jungers, 1996; Lague, 2014). However, marked anteroposterior flattening of the distal diaphysis in these humeri is atypical of humans, as is the high degree of posterior convexity (Lague, 2015). Their shape is overall intermediate between *Homo erectus* and non-*erectus* early *Homo* rather than matching any known *Homo* specimens. This contour is shared with OH 80 (*P. boisei*, part of a partial skeleton dated to 1.34 Ma, not included

in the present study but the only specimen associated with dental material) (Lague, 2015), reaffirming the original assignment of these specimens to *Paranthropus.* The shared traits of *P. boisei* and *Homo* are suggested to mirror the craniodental synapamorphies of these two genera (Lague, 2014).

1.3.2.5 P. robustus

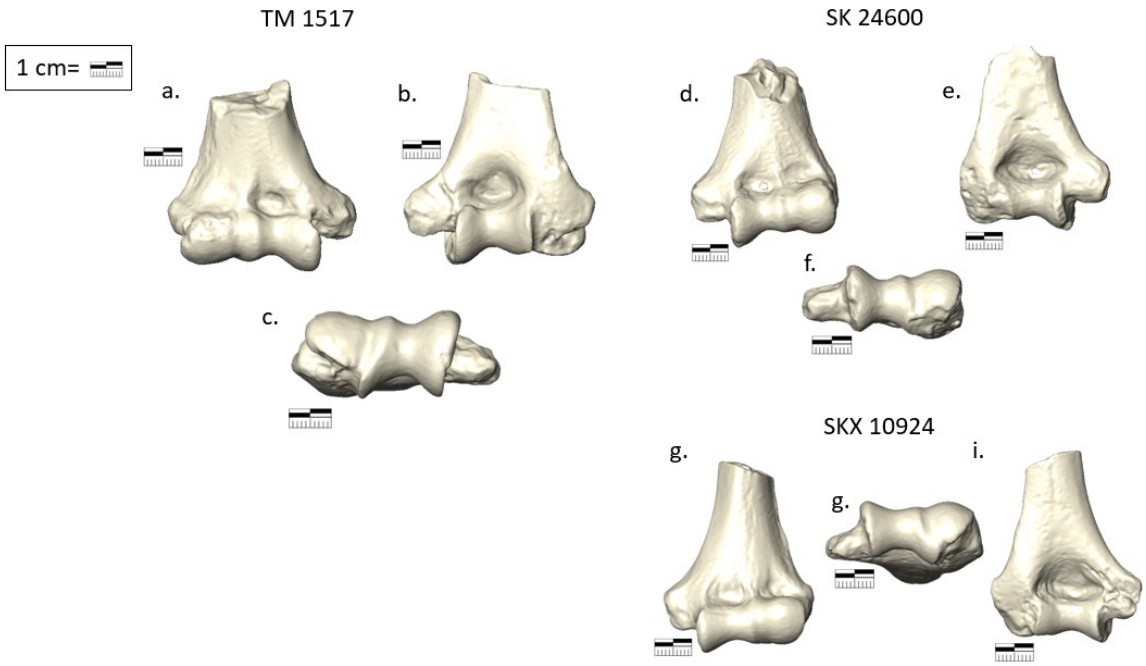

Figure 1-8 Morphology of TM 1517 (a-c), SK 24600 (d-f) and SKX 10924 (g-i).

As with *P. boisei*, a dearth of *P. robustus* postcrania makes locomotor assessments uncertain, but no appreciable differences have been noted in the existing elements (Ward, 2013), and its locomotor repertoire is therefore expected to mirror that of other australopiths. Some authors find that there appears to be a disparity between the elbow morphology of *P. robustus* and *P. boisei* in which *P. robustus* retains *Australopithecus*-like morphology but *P. boisei* is similar to early members of the genus

Homo (Lague, 2014). This is somewhat unexpected. Evidence from the radius suggests that *Paranthropus*, like *Australopithecus*, had a well-supported elbow and may have retained arboreal capabilities (Grine and Susman, 1991; Crompton et al., 2008).However, there is also uncertainty regarding taxonomic assignment of *Paranthropus* humeri, which may explain some of the difficulty in definitively describing the morphology of *P. robustus*. The present study begins with the tentative assumption that either or both SK 24600 and SKX 10924 (depicted in Figure 1-8) may belong to *P. robustus*. SK 24600 is assigned to *P. robustus* by Susman et al. (2001) and SKX 10924 is assigned to *P. robustus* by Lague (2014). Both SK 24600 and SKX 10924 have however also been assigned to *Homo* (Susman et al., 2001; Lague, 2014). These attributions depend on distal diaphyseal cross-sectional shape: Susman et al. (2001) interpret the more flattened specimen (24600) as *P. robustus*, but Lague (2014) notes that markedly flattened distal diaphyses were characteristic of non-erectus early *Homo* rather than *P. robustus*, and therefore comes to an opposite conclusion regarding taxonomy of the two specimens. Due to this uncertainty, definitive description of *P. robustus* humeral traits must rely heavily on TM 1517, discussed in section 1.3.1 and depicted in Figure 1-3. The morphologies of SKX 10924 and SK 24600 are discussed below.

Features aligning *P. robustus* with *Australopithecus* include an AP flattened articular surface that appears mediolaterally elongated, proximal placement of the most projecting point of the medial epicondyle, and the strong development of the lateral epicondyle, characteristics reported by Lague (2014) in describing SKX 10924. However,

Susman et al. (2001) note on this same individual an indistinct zona conoidea, weak trochlear groove, relatively weak supracondylar crest and wide olecranon fossa with sloping borders, traits which, while sometimes present in *Australopithecus*, are features that align fossil hominins with modern humans. Susman et al. (2001) also note of SKX 10924 a relatively large anteroposterior shaft diameter, anteriorly positioned capitulum, and distal lateral epicondyle, all traits that resemble humans. Both SKX 10924 and SK 24600 are much smaller than other *Paranthropus* humeri (Susman et al., 2001), which may affect interpretation of their traits. It is important to note that Lague's analyses (2014) adjust for allometry in humeral morphology, and that SKX 10924 is more similar to average humans than to smaller humans more similar to it in size (Lague, 2014). It is interesting to note that TM 1517 is also much larger in size than both individuals, though not as large as humeri assigned to *P. boisei* (Lague, 2014).

Lague (2014) finds that when size is accounted for, SK 24600 is closer to modern human morphology than both TM 1517 and SKX 10924, and is also more human-like than any *Australopithecus* specimens. Other authors note a mix of traits, both like and unlike modern humans Susman et al. (2001). Like SKX 10924 and modern humans, SK 24600 has an anteriorly positioned capitulum, but unlike SKX 10924, it has a more proximally positioned lateral epicondyle and distinct zona conoidea (Susman et al., 2001). Other notable traits of SK 24600 include a large medial trochlear keel with a well-defined crest and deep trochlear groove.

Much of the disagreement over the taxonomy of SKX 10924 and SK 24600 derives from the shape of the distal shaft. Susman et al. (2001) note that SKX 10924 differs from three other distal humeral fragments found at Swartkrans (SKX 19495, SK 24600, SK 2598). Through comparisons to extant species and TM 1517, Susman et al. state that *Paranthropus robustus* has a flattened, mediolaterally broad distal diaphysis, while *Homo* has a more rounded shape. Since both *Paranthropus robustus* and *Homo* cf *erectus* are found in the assemblages at Swartkrans, Susman et al. (2001) conclude that SK 24600 belongs to the former and SKX 10924 the latter, based on a combination of the human-like cross-sectional contour of SKX 10924 and the pronounced, and therefore ape-like, articular relief of SK 24600.

1.3.2.6 Fossil Homo

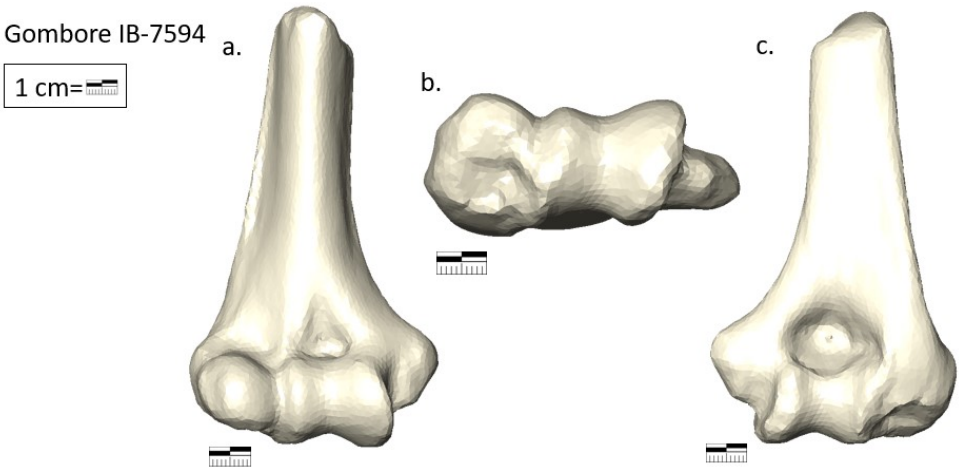

Figure 1-9 Morphology of Gombore-IB 7594. a. anterior view, b. inferior view, c. posterior view.

In this study, fossil *Homo* is represented by Gombore IB 7594, likely *Homo erectus* (Chavaillon et al., 1977; Coppens, 2004; Di Vincenzo et al., 2015; Lague, 2015)

(Figure 1-9). Few definitive *Homo* humeri older than 1 Mya have been studied. Apart from the Gombore humerus, five of the humeri discussed above have at times been considered possible members of the genus *Homo* (KNM-KP 271, early *Homo,* Senut and Tardieu, 1985; KNM-ER 739 and KNM-ER 1504, *H. rudolfensis*, Lague and Jungers, 1996; SKX 10924, *Homo sp.*, Susman et al., 2001; SK 24600, *Homo habilis*, Lague, 2014, 2015), demonstrating the difficulty in finding humeral morphology unique to the genus and the problems posed by using humeral traits to make taxonomic assignments. It has been noted that Gombore IB 7594 itself could belong to *P. boisei* (Lague and Jungers, 1996), but the preponderance of the evidence confirms assignment to *Homo* (Chavaillon et al., 1977; Senut, 1980, 1981a; Senut and Tardieu, 1985; Bacon, 2000; Coppens, 2004; Di Vincenzo et al., 2015). A few early humeri not included in the present study have also been assigned to the genus: KNM-ER 3735, KNM-WT 15000, D 4507. These are not included due to problems with preservation (KNM-ER 3735), developmental age and thus articular development (KNM-WT 15000), and availability (D 4507). Most *Homo* material is unsurprisingly more recent, composed of specimens of *H. heidelbergensis, H. neanderthalensis*, and both archeological and modern *H. sapiens*. Therefore, description of fossil *Homo* has relied substantially on drawing connections with modern populations and by contrast to great apes.

Fossil *Homo* shares with modern humans poor definition between the trochlea and capitulum either due to a poorly developed lateral trochlear crest (Senut and Tardieu, 1985) or indistinct zona conoidea (Di Vincenzo et al., 2015). The small lateral

epicondyle is low, level with the superior portion of the capitulum, which is itself narrow and poorly developed on its inferior aspect (Senut, 1980; Senut and Tardieu, 1985; Aiello and Dean, 1990). The anterior border of the shaft creates an anteriorly projecting (i.e., not posteriorly curved) column (Senut, 1981a; Susman et al., 2001). This strong similarity to modern humans suggests fully human-like upper limb anatomy. However, there appears to be a difference between the diaphyseal shape of *H. erectus* and *H. cf habilis* (Lague, 2015). The distal diaphyses of *Homo cf. habilis* are anteroposteriorly flattened to a degree not seen in any extant hominids. This is not observed in *H. erectus*, which has a profile resembling modern humans and orangutans (Lague, 2015). The anterolateral portion of the diaphysis also differs between species of *Homo*: it is concave in *H. erectus* but convex in *habilis* (Lague, 2015).

1.4 Components of Variability

1.4.1 Size

While quantifying variation in the distal humerus can identify differences among taxa, it does not by itself explain this variation. One potential influence on variation is the effect of size differences on shape of the distal humerus (i.e., allometry). Size-shape interactions are common throughout the locomotor skeleton (e.g., Alexander, 1980; Biewener, 1983; Jungers, 1984). A few studies of the distal humerus suggest that allometric effects explain a substantial portion of the variation previously attributed to functional and taxonomic differences (Bacon, 2000; Lague, 2014). Two measures of size have commonly been used in humeral studies: centroid size of humeral landmarks (Bacon, 2000; Arias-Martorell et al., 2015; Di Vincenzo et al., 2015; Lague, 2015) and biepicondylar breadth (Carretero et al., 2009; De Castro et al., 2012).

Within modern humans, an increase in humeral size is associated with a proximal shift in the position of the epicondyles (Lague, 2014). The medial epicondyle of large humeri projects less, while the lateral epicondyle projects more (Lague, 2014). This finding is particularly notable given the frequent finding that position of the lateral epicondyle distinguishes great apes and hominin fossils from modern humans, and has been interpreted as increasing the leverage of extensor musculature in a way that may be adaptive during climbing (Senut and Tardieu, 1985).

Large size is also linked to changes in the distal articular surface of the humerus. In large individuals the capitulum is mediolaterally wider along the inferior surface of the bone and narrow at its origin on the anterior surface (Lague, 2014). Larger humeri also have more distally placed trochlear crests, which make these crests appear truncated in large specimens (Lague, 2014). The articular surface is also relatively wider in large specimens, through the growth of specific features; the medial half of the trochlea expands, as does the zona conoidea (Lague, 2014). These articular traits also in some ways mirror the difference between humans and great apes (see section 1.2), and therefore may be inappropriately interpreted as functional (at least in terms of locomotor behavior).

Though many early hominin fossils are small relative to those of modern humans (Ruff et al., 2018b), interpretation of temporal patterns in distal humeral morphology can change dramatically depending on whether allometric effects are taken into account (Lague, 2014). Authors generally agree that humeral morphological diversity increased between 1-2 Mya (McHenry and Brown, 2008; Lague, 2014), but without body size correction, early fossil hominins (KNM-KP 271, A.L. 288-1) appear far more similar to modern humans than many fossils of intermediate age (StW 431, KNM-ER 1504, KNM-ER 739) (McHenry and Brown, 2008). When compared to modern humans of equivalent size, a more linear progression emerges because the similarity of early hominins to modern humans relies on comparison to much larger individuals (Lague, 2014). This is important for interpretation of fossil hominin behavior because of the parallel between

allometric effects and apparent functional differences in the distal humerus. Ape-like features (described above) can be partially attributed to size affects in large humans. However in small fossil hominins, they should be interpreted as a possible indication of elbow support and stabilization for locomotor behaviors as seen in great apes instead. Allometric considerations also affect taxonomic designations, as demonstrated in section 1.3.2.5 above. Assignment of SK 24600 to *Homo* rather than *Paranthropus* relies on size-adjusted comparison of features (Lague, 2014), with different relationships emerging if fossils are compared to the modern range of human body sizes.

Understanding the influence of size on fossil hominin humeral morphology is not simple, in part because it is not clear what features in this region constitute an appropriate proxy for size. Recent studies have used centroid size of the distal humerus itself as a proxy for size (Bacon, 2000; Lague, 2014; Di Vincenzo et al., 2015; Rosas et al., 2015), but this is potentially circular, if overall size of this region scales non-isometrically with body size, or varies systematically with locomotor behavior. There is some evidence that this may be the case; articular size (Fleagle, 2013; Perry et al., 2018) in primates and trochlear size (Susman et al., 1984) in hominoids are both positively allometric, and recent studies have shown a complex scaling pattern for the distal humerus within anthropoids that may reflect functional behavior (Perry et al., 2018). Use of humeral biepicondylar breadth as a size measure (De Castro et al., 2012) presents the same concern, with the added question of whether the epicondyles are invariant with respect to factors such as mechanical loading during life.

Body mass has a number of advantages as a scaling variable (Jungers, 1984), but relationships between body mass and distal humeral dimensions have not yet been used to evaluate evolutionary trends in hominins (but see McHenry, 1992; Senturia, 1995; Halenar, 2011; and Di Vincenzo et al., 2015). Body mass cannot be independently calculated (from other areas of the skeleton) for many fossil hominin distal humeral specimens, but the effects of using proxies such as distal humeral centroid size or biepicondylar breadth should be evaluated in a comparative context given indications that relationships between such measures differ taxonomically (McHenry, 1992). Forelimb properties may predict substantially lower body weights for fossil hominins than other measures, depending on whether humans alone or all hominids are used as a reference sample because of different scaling patterns of humeral dimensions to body mass (McHenry, 1992). While this finding has implications for early hominin behavior in its own right, it emphasizes the need for cautious interpretation of apparent allometric relationships in the distal humerus. Results and interpretations must be adjusted accordingly, depending on the proxy, and these findings argue for the development of clear, unbiased proxies for size.

1.4.2 Asymmetry

Another issue in interpreting humeral morphological variation is the extent to which features are affected during life by *in vivo* use, i.e., their developmental plasticity. Variation in the degree of developmental plasticity of different traits has implications for their utility in both reconstructing behavior as well as taxonomic assignments (Ward,

2002; Ruff et al., 2018a). Traits that vary in response to use and environment are preferable for inferring living behavior of fossil hominins (Ward, 2002; Ruff et al., 2018a), while those that are more genetically canalized may be preferable for their evolutionary significance (Ward, 2002).

It is clear from many studies that long bone diaphyses are developmentally plastic, increasing in strength and rigidity under conditions of increased mechanical loading (see summary in Ruff et al., 2006). This has been clearly demonstrated in a number of studies of bilateral asymmetry of the humerus in modern human samples (Jones et al., 1977; Trinkaus et al., 1994; Haapasalo et al., 2000; Bass et al., 2002; Shaw and Stock, 2009; Shaw, 2011; Warden et al., 2014; Nadell and Shaw, 2016; Sládek et al., 2016). Handedness in modern humans results in asymmetric loading of the upper limb (Auerbach and Ruff, 2006; Shaw, 2011), which is reflected in bilateral asymmetry of cross-sectional diaphyseal properties. This appears to occur through both periosteal expansion and increased cortical thickness on the dominant side, and affects multiple elements in the upper limb (Roy et al., 1994; Auerbach and Ruff, 2006; Warden et al., 2014). Evidence that bilateral asymmetry is greatly increased in athletes engaging in unimanual events (see references above), and is not present in neonates (Steele and Mays, 1995; Blackburn, 2011) supports the conclusion that these differences are the result of *in vivo* use. Therefore, bilateral asymmetry in humeral shaft properties can be used as guide to the degree of asymmetry in mechanical loading of the upper limbs, and

thus to set up a kind of natural experiment of the effects of mechanical loading on other regions of the humerus.

This is necessary because while differences in mechanical properties in the middle region of the humeral diaphysis are known to correlate with handedness (Shaw, 2011), to what extent this relationship applies to metaphyseal and periarticular epiphyseal regions is not clear. A study of modern athletes found no evidence of adaptive remodeling of the radius or tibia at 4% of bone length, in the metaphyseal regions (Nadell and Shaw, 2016), but the humerus was not evaluated. However, a site in the distal humeral diaphysis, at 20% of bone length from the distal end, did show effects of mechanical use in another study (Haapasalo et al., 2000). This finding is of particular interest in light of studies by Lague (2015) and Susman et al. (2001), which used the shape of equivalent sections (15%-21% bone length) for taxonomic assignments in early hominins. There is recent evidence that handedness affects the shape of diaphyseal cross sections (Kubicka et al., 2018) in certain populations. If mechanical properties of the distal diaphyseal region studied by Lague (2014) are developmentally plastic, this could indicate that the region is also morphologically plastic, potentially affecting its use as a taxonomically diagnostic tool. Given Senut's (1981a, 1981b) assertions that olecranon pillar shape both varies taxonomically and is indicative of different patterns of loading between taxa, the periarticular region is also of interest. The present study examines mechanical properties of one distal diaphyseal section (18% biomechanical length) and three sections that cross the olecranon pillars – one at their origin at the

proximal rim of the olecranon fossa, one along the biepicondylar line, and one midway between these two sections, roughly bisecting each pillar (see Chapter 2). These are compared in the same individuals to directional asymmetry at 40% of bone length from the distal end, a section that replicates differences in mechanical properties present at midshaft, but which avoids the deltoid tuberosity (Ruff, 2002; Nadell and Shaw, 2016).

Although articulations appear to be much less developmentally plastic than diaphyses (Trinkaus et al., 1994; Lieberman et al., 2001; Ruff et al., 1991; Auerbach and Ruff, 2006), there is some evidence for adaptation to mechanical loading in both articular surface dimensions (Frost, 1979; Hamrick, 1996, 1999; Plochocki, 2004) and periarticular dimensions, particularly the epicondyles (Blackburn and Knüsel, 2006). Mechanical plasticity through the epicondylar region would complicate use of biepicondylar breadth as a scaling variable, and would affect interpretation of interspecies differences in epicondylar form. Whether epicondylar size, shape, and orientation should be interpreted as taxonomically distinct, perhaps as a result of selection, or as a marker of mechanical adaptation of individuals, is dependent upon the degree to which these properties are plastic developmentally.

Bilateral asymmetry is best documented in humans, but there is evidence in great apes of both hand preference (Hopkins et al., 2011) and asymmetry in humeral biomechanical properties (Sarringhaus et al., 2005). It is unclear whether differences in cross-sectional properties reflect preferential use for weight support during locomotion or during manual tasks (Sarringhaus et al., 2005), as lateralization exists in both leading

limb preference and tool use (Hopkins and Morris, 1993). Evidence that hand specialization was present as far back as early *Homo* (Frayer et al., 2016) and may have been present in the last common ancestor of *Homo*, *Pan*, and *Gorilla* (Hopkins et al., 2011) argues for consideration of function-driven asymmetry in humeral properties of fossil hominins, and broadens the potential implications of asymmetry in distal diaphyseal, metaphyseal, and articular properties.

1.5 Overview of the Text

The goal of this dissertation is to create a fuller picture of the morphological diversity, plasticity, and evolution of the distal humerus in order to make functional inferences about locomotor evolution in the human lineage. Chapter 2 details the methods used to examine this question including a description of the extant and fossil samples. It also contains background and justification for the morphometric techniques and body mass and asymmetry calculations used in the analytical chapters, as well as a description of the statistical methods used. Chapters 3 through 5 present results of the analyses. Chapter 3 uses bilateral asymmetry in the cross-sectional properties of modern humans to examine the plasticity of different humeral regions, and seeks to determine to what extent *in vivo* use influences the structure of the shaft, periarticular, and articular regions. Chapter 4 focuses on external morphology. Fixed and sliding semi-landmarks are used to quantify variation in the surface morphology of extant hominids and ten fossil hominins. Chapter 5 addresses the effects of body mass on humeral morphology, which it compares with two measures of size (centroid size, biepicondylar

breadth) in order to determine their validity as scaling variables. Chapter 6 reviews and discusses the results of each analysis, while Chapter 7 synthesizes these findings and considers their broader implications.

2 Materials & Methods

This chapter will describe the samples, data collection process, and analytical methods used for the studies of asymmetry, morphology, and allometry included in Chapters 3-5. A description of the modern human and extant great ape samples will be presented first. While the fossils included in this study have been described in Chapter 1 along with a discussion of the relevant literature, a brief account of the source of scan data for each fossil, its preservation, and any reconstructions performed upon it is presented here. Because some of the geometric morphometric (GM) techniques employed were custom-designed for this study, some more extensive background information on relevant GM techniques is included in that section.

2.1 Materials

The total sample for this work includes both extant and fossil specimens. The extant sample is given in Table 2-1 and described below. Subgroups used for each study are also detailed in Table 2-1. The fossil sample is presented in Table 2-2 and described in section 2.1.2.

2.1.1 Extant Groups

Table 2-1 Total sample

Modern Human Sample	**Institution**	**Chapter 3: Asymmetry**	**Chapter 4: Morphology**	**Chapter 5: Allometry**
Terry (White)	NMNH	33 M, 32 F	33 M, 32 F	31 M, 30 F
Terry (Black)	NMNH	32 M, 30 F	31 M, 33 F	33 M, 2 F
Puye	NMNH	18 M, 15 F	16 M, 13 F	16 M, 13 F
Indian Knoll	NMNH	21 M, 9 F	20 M, 9 F	20 M, 9 F
Illinois	NMNH	17 M, 15 F	17 M, 16 F	17 M, 15 F
Lisht	NMNH	9 M, 12 F, + 1 U	8 M, 12 F	8 M, 11 F, + 1U
Babongo/Babinga †	MdH, IRSNB	--	6 M, 4 F	6 M, 4 F
Great Apes				
Pan troglodytes §	NMNH, MCZ, CMNH	--	14 M, 16 F	11 M, 14 F +2 U
P. t. troglodytes=24				
P. t. verus=4				
P. t. schweinfurthii=1				
Unspecified=2				
Pan paniscus £	MCZ, RMCA	--	12 M, 11 F	12 M, 8 F
Gorilla gorilla €	NMNH, MCZ , CMNH	--	8 M, 13 F	10 M, 11 F+1 U
Gorilla beringei ¥ ϕ	NMNH, MCZ, RMCA	--	17 M, 9 F	14 M, 8 F
G. b. beringei=13				
G. b. graueri=12				
Pongo pygmaeus δ	NMNH, CMNH	--	5 M, 15 F	7 M, 15 F
Pongo abelii	NMNH	--	2 M, 3 F	1M, 2F

Description of the extant comparative sample. Institution codes: CMNH= Cleveland Museum of Natural History, IRSNB = Institut Royal des Sciences Naturelles de Belgique (Brussels), MCZ = Museum of Comparative Zoology (Harvard University, Cambridge), MdH = Musee de l'Homme (Paris), NMNH = Smithsonian National Museum of Natural History (Washington, D.C.), RMCA=Royal Museum for Central Africa (Tervuren). Terry, Puye, Indian Knoll, Illinois, Lisht, and MdH Babongo/Babinga scanned by K. G. Zelazny. † 4 individuals courtesy of P. Semal. § 12 individuals courtesy of C. Ward. £ 9 individuals scanned by C. Ward, 7 courtesy of J. M. Plavcan. € 12 courtesy of C. Ward. ¥ 10 courtesy of J. M. Plavcan. δ 5 courtesy of C. Ward.

2.1.1.1.1 Modern Humans

Seven populations of recent modern humans were used in this study, chosen to encompass a wide range of variation in size, ancestry and activity patterns (see Table 2-1). The sample includes roughly equivalent numbers of males and females, although

certain subsamples (e.g., Indian Knoll) are less sex balanced. Individuals were sexed using a combination of standard sex estimation methods (Ubelaker and Buikstra, 1994), primarily pelvic morphology (Phenice, 1969; Milner, 1992), though cranial traits were also considered (Acsádi and Nemeskéri, 1970). All individuals are adults with no observed pathological conditions. For individuals of known age (Terry Collection), only those under age 55 were included, to minimize the effects of aging (i.e., osteoporosis) on cross-sectional properties. Three Paleoindian populations and one ancient Egyptian population were included in this study in order to provide a contrast to the urban-industrial Terry collection, and include a range of lifestyles and activity patterns. Individuals were selected based on preservation and no obvious bone deficiencies were observed. To maximize potential sample sizes, no attempt was made to eliminate older individuals in these samples. However, less than 15% of the total archaeological sample fell into the oldest age bracket when ages were assessed using pubic symphyseal morphology (Brooks and Suchey, 1990), relative dental wear (Brothwell, 1981) (calibrated by population), and sacroiliac morphology (Lovejoy et al., 1985), and no individuals had ages above 50 recorded in the collection inventory. Specimens from these groups may show slight abrasion; where this affected cross-sectional scans or impeded accurate landmark placement, specimens were excluded from the corresponding analyses. A description of the specific populations sampled follows.

Terry (White and Black)

The Terry Collection is a large 19th and 20th century sample consisting of individuals from a working class population in St. Louis (Missouri, USA), collected by Drs. Robert J. Terry and Mildred Trotter (Hunt and Albanese, 2005). The sample includes individuals of both African and European ancestry; these groups are treated as separate samples here. Individuals are associated with known age, sex, ancestry, and pathological conditions.

African Pygmies

The Pygmy sample includes individuals from a number of groups settled in the Congo Basin of Central Africa, whose skeletal remains are housed in the Musée de l'Homme in Paris (France) and the Institut Royal des Sciences Naturelles de Belgique in Brussels (Belgium). The museums acquired the skeletal materials between 1909 and 1938. Catalog information for these individuals indicates they lived in the Democratic Republic of Congo, French Equatorial Africa, Central Africa and Gabon. These individuals are listed as belonging to the Babongo and Babinga groups, which correspond to the modern Aka, Bakola, Bakoya, and Babongo tribes (Soengas, 2009). They are chiefly included in order to extend the size range of our modern human comparative sample for better comparison to small-bodied fossil hominins.

Indian Knoll

The Indian Knoll sample is a Native American sample from the Archaic period of Kentucky (Johnston and Snow, 1961). This site is pre-agricultural, and individuals in this population supported themselves through foraging and hunting (Webb, 2001). This sample was chosen for inclusion because an active, pre-agriculture lifestyle is likely to increase skeletal robusticity and may amplify bilateral asymmetry in handedness depending upon hunting practices (Sládek et al., 2016).

Illinois

This sample comes from a Native American Middle Woodland Hopewellian population, excavated near the mouth of the Illinois River in Calhoun and Jersey counties, Illinois (Perino, 1968; Blakely, 1971). While the Middle Woodland is regarded as an agricultural period, it is characterized by small-scale cultivation of native crops rather than the later dominance of large-scale production of maize and other crops seen during the Late Woodland period (Bridges et al., 2000), and no direct evidence of domestication is present at this site. Consequently, the sample is considered part of a transitional period, likely incorporating limited agricultural practices.

Puye

The Puye sample is a late prehistoric archeological sample of Native Americans from New Mexico (Hewett, 1953). The Puye relied on agriculture for subsistence and likely had increased activity levels relative to living industrial populations. The size range of the Puye includes individuals that are quite small (Squyres and Ruff, 2015). Inclusion

of this sample increases the number and genetic diversity of small individuals in the overall study.

Lisht

The Lisht sample belongs to an agricultural population dated to the Twelfth Dynasty in Egypt (Mace, 1921; Godde, 2009). Agricultural practices during this period, including irrigation, allowed for a relatively sedentary population within which certain individuals regularly engaged in field labor (Grajetzki, 2012).

2.1.1.1.2 Great Apes

This study includes specimens from each of the three nonhuman hominid genera - *Pan*, *Gorilla*, and *Pongo*. Two species from each genus are represented in order to increase sample sizes, and to examine possible functional effects within great apes on humeral morphology (see below and Chapter 4). All specimens were wild-shot, skeletally mature individuals. Table 2-1 details the composition of each species.

Pan and *Gorilla* species are considered independently in the morphometric analyses in Chapter 4 in an effort to examine the possible effects of different patterns of arboreal behavior on morphology. Species within these genera vary in the amount of time spent in the trees. *Gorilla beringei beringei* (Groves, 2001) is the most terrestrial taxon included, spending only 2.9% of daily activity in the trees (Tuttle and Watts, 1985). *Gorilla gorilla gorilla* is notably more arboreal (Remis, 1995), while the subspecies *Gorilla beringei graueri* (Groves, 2001) may be intermediate in behavior (Yamagiwa, 1994; 1996). Bonobos and chimpanzees are both more arboreal than all subspecies of

gorilla, but species of *Pan* have also been reported to vary in their locomotor repertoire (Doran, 1996); bonobos are thought to be the more arboreal of the two, although see Ramons (2014). Both species of *Pongo* are more arboreal than *Pan* and *Gorilla*, engaging in suspension, brachiation, vertical climbing, tree-swaying, and quadrumanous clambering, with limited time spent engaged in terrestrial quadrupedal locomotion (Thorpe and Crompton, 2006). Sumatran orangutans (*P. abelii*) are almost exclusively arboreal (Sugardjito, 1982; Cant, 1987), though Bornean orangutans (*P. pygmaeus*), especially large males, sometimes travel terrestrially (Cant, 1987; Acrenaz et al., 2014).

While species of *Pan* and *Gorilla* are considered independently in the Chapter 4 analyses of morphology, species are pooled (within genera) in allometric analyses in Chapter 5. In both chapters, *P. abelii* and *P. pygmaeus* are pooled in order to increase sample size. Apes are not included in the asymmetry analysis in Chapter 3, because bilateral cross-sectional scans were unavailable.

2.1.2 Fossil Hominins

Ten fossil hominin specimens were included in this study. All measurements included in the following chapters were measured on three-dimensional surface models. Table 2-2 lists the source of each surface scan, species to which the specimen has been attributed (see Chapter 1 for rationale), and any alterations made during reconstruction beyond minor smoothing, which was performed for all extant and fossil surface models in order to improve sliding and point projection. Surfaces were scanned using a NextEngine desktop 3D laser scanner running ScanStudio (Version 2.0.2) (NextEngine

Inc., Santa Monica, CA) or a Konica-Minolta Vivid 9i (Konica-Minolta, Tokyo, Japan). The surface scanning techniques employed are described in further detail in section 2.3.2 below.

Table 2-2 Fossils included in this study

Specimen	Species Attributions	Reconstructed Regions
A.L. 288-1£	*A. afarensis*	Shaft (right) - alignment of shaft, chipping, tape marks
KP 271£	*A. anamensis*	Shaft – dent on anterior surface Trochlea – concretion
Gombore IB-7594€	*Homo erectus*	Triangles subdivided and remeshed to improve scan quality
KNM-ER 739§	*P. boisei (?)*	Shaft – chipping Medial epicondyle – posterior pitting Medial trochlea – chipping
KNM-ER 1504§	*P. boisei (?)*	Shaft – posterior chipping Trochlea – anterolateral pitting
KNM-ER 6020§	*P. boisei (?)*	Shaft – anterior chipping , cracks (all surfaces) Trochlea – lateral pitting Capitulum - dents
SKX 10924¥	*Homo sp.,* *P. robustus*	Medial epicondyle – chip, posterior pitting
SK 24600¥	*Homo sp.,* *P. robustus*	Lateral posterior surface – pitting Trochlea – abrasion of medial crest Capitulum – chip on margin
StW 431¥	*A. africanus*	Shaft – large lateral portion missing Medial epicondyle – chipping Olecranon fossa – superior segment Trochlea – posteromedial crack, anterior crack, abrasion of medial crest
TM 1517¥	*P. robustus*	Medial epicondyle – cracks Capitulum – abrasion (superior)

£ Right and left scanned from cast by author
€ Provided by Fabio Di Vincenzo courtesy of Drs. Piperno and Manzi, Sapienza University, Rome authorized by the National Museum of Ethiopia
§ Provided by J. Michael Plavcan, courtesy of Dr. Fredrick Kyalo Manthi and the National Museums of Kenya
¥ Provided by Carol Ward

Reconstruction was performed on surface models in Geomagic (3D Systems, Cary, NC). For small deformities, the aberrant area was manually selected and deleted; these areas were then filled using a built-in feature of Geomagic that allows the user to fill holes using patches that follow the curvature of the surrounding area. For fossils with large segments missing, the surrounding curvature did not predict realistic morphology for the missing areas. Therefore, the initial filling procedure was followed by digital resculpting of the estimated area to create morphology that is more realistic. Images of the original and reconstructed scans are presented in Figures 1-10 with a brief history of each specimen and any remarks on the effect of state of preservation on use of the methods included in this study.

A.L. 288-1

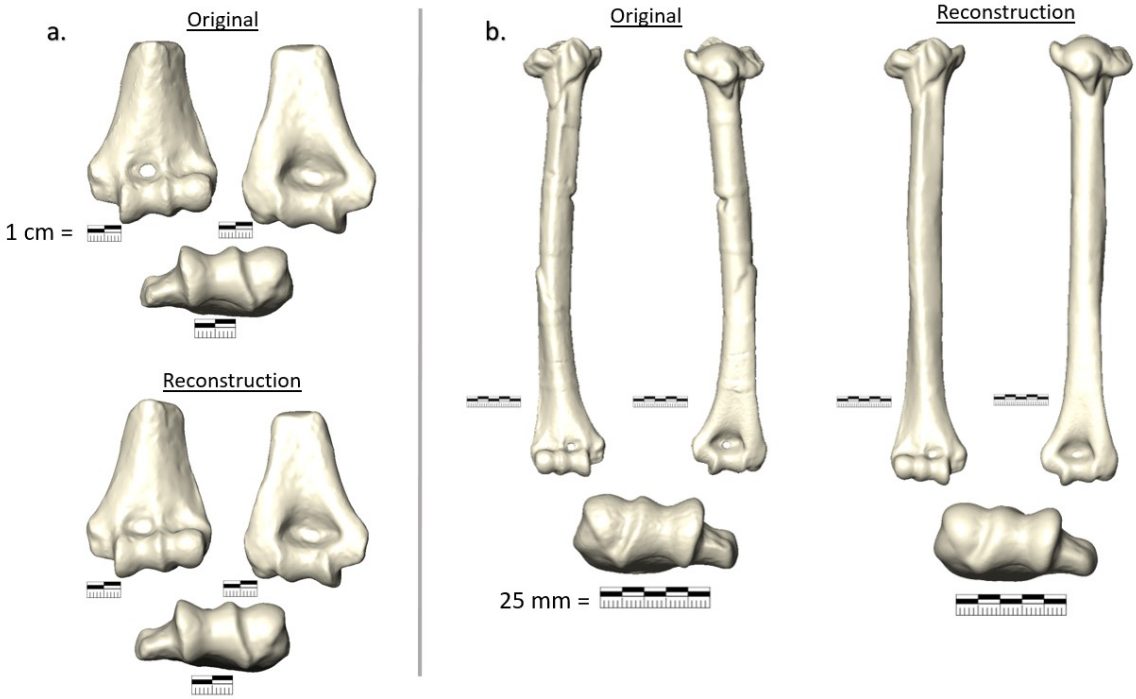

Figure 2-1 Anterior, posterior, and inferior views of A.L. 288-1s (a) and A.L. 288-1m (b).

Discovered in Hadar, Ethiopia in 1974, A.L. 288-1 ("Lucy") is a partial skeleton of a female member of the species *Australopithecus afarensis*, dated to 3.2 Mya (Johanson and Taieb, 1976). The complete right humerus (A.L. 288-1m) is preserved as well as the distal portion of the left humerus (A.L. 288-1s). The proximal articular surface of the right humerus is crushed, and the shaft is preserved in two large pieces and associated fragments (Johanson et al., 1982). Right and left humeri were scanned from 3D printed models derived from micro-CT scans of the specimens (Ruff et al., 2016). The posterior portion of the capitular border of A.L. 288-1 is somewhat indeterminate on the casts scanned, possibly due to slight abrasion on the original (Johanson et al., 1982).

KNM-KP 271

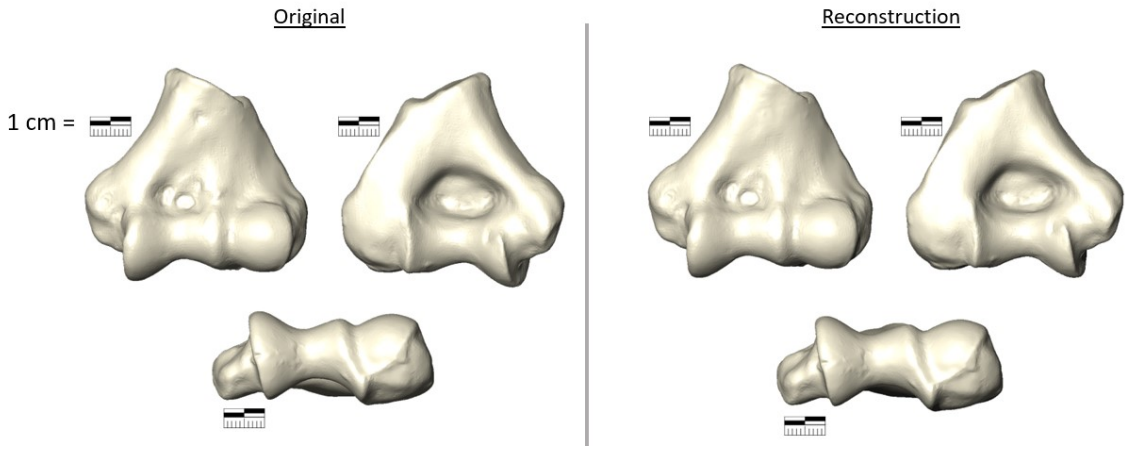

Figure 2-2 Anterior, inferior, and posterior views of original and minimally retouched models of KNM-KP 271.

KNM-KP 271, found in 1966 at Kanapoi, Kenya, is a left distal humerus attributed to *Australopithecus anamensis*, dated to between 3.5 and 4.1 Mya (Patterson and Howells, 1967; Leakey et al., 1995). This specimen was scanned from a scientific cast provided by the National Museums of Kenya to Dr. Christopher B. Ruff. Minimal surface retouching was performed.

Gombore IB-7594

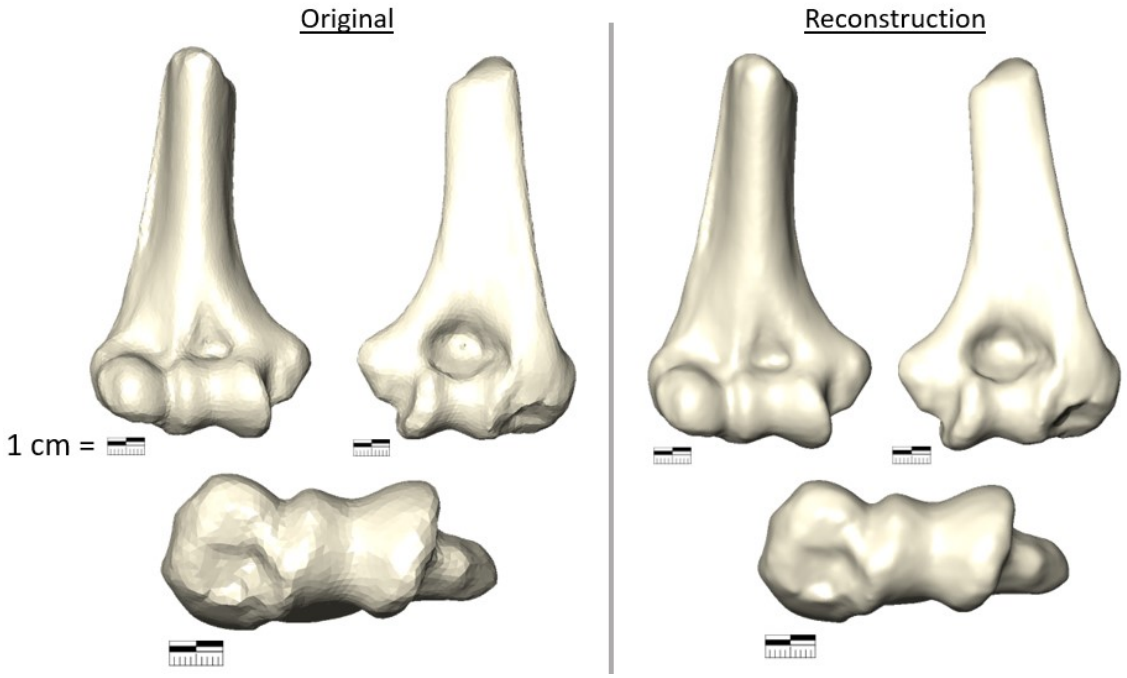

Figure 2-3 Original (left) and retouched (right) surface models of IB-7594.

Gombore IB-7594, also known as MK3, is an exceptionally large distal right humerus found in the Gombore I formation at Melka Kunture, Ethiopia in 1976,. It has been dated to approximately 1.5 Mya, and most likely belongs to *H. erectus* on the basis of age, size, and associated lithics (Coppens, 2004). This scan was provided by Dr. Fabio Di Vincenzo, courtesy of Drs. Piperno and Manzi. IB 7594 has significant abrasion on the distal portion of the capitulum, creating some uncertainty as to full extent of the capitulum. Damage to the area directly posterior to the capitulum was not reconstructed due to inability to assess the original morphology.

KNM-ER 1504

Figure 2-4 Anterior, posterior, and inferior views of KNM-ER 1504 original (left) and reconstruction (right).

KNM-ER 1504 is a right distal humerus found in association with two femoral fragments, 1503 and 1505, collected from the Koobi Fora formation in East Turkana, Kenya in 1972 and dated to 1.9 Mya (Leakey, 1973; McHenry and Brown, 2008). The original scan was provided by Dr. J. Michael Plavcan, courtesy of Dr. Fredrick Kyalo Manthi and the National Museums of Kenya; minimal reconstruction was performed to fill chipping on the posterior distal shaft.

KNM-ER 739

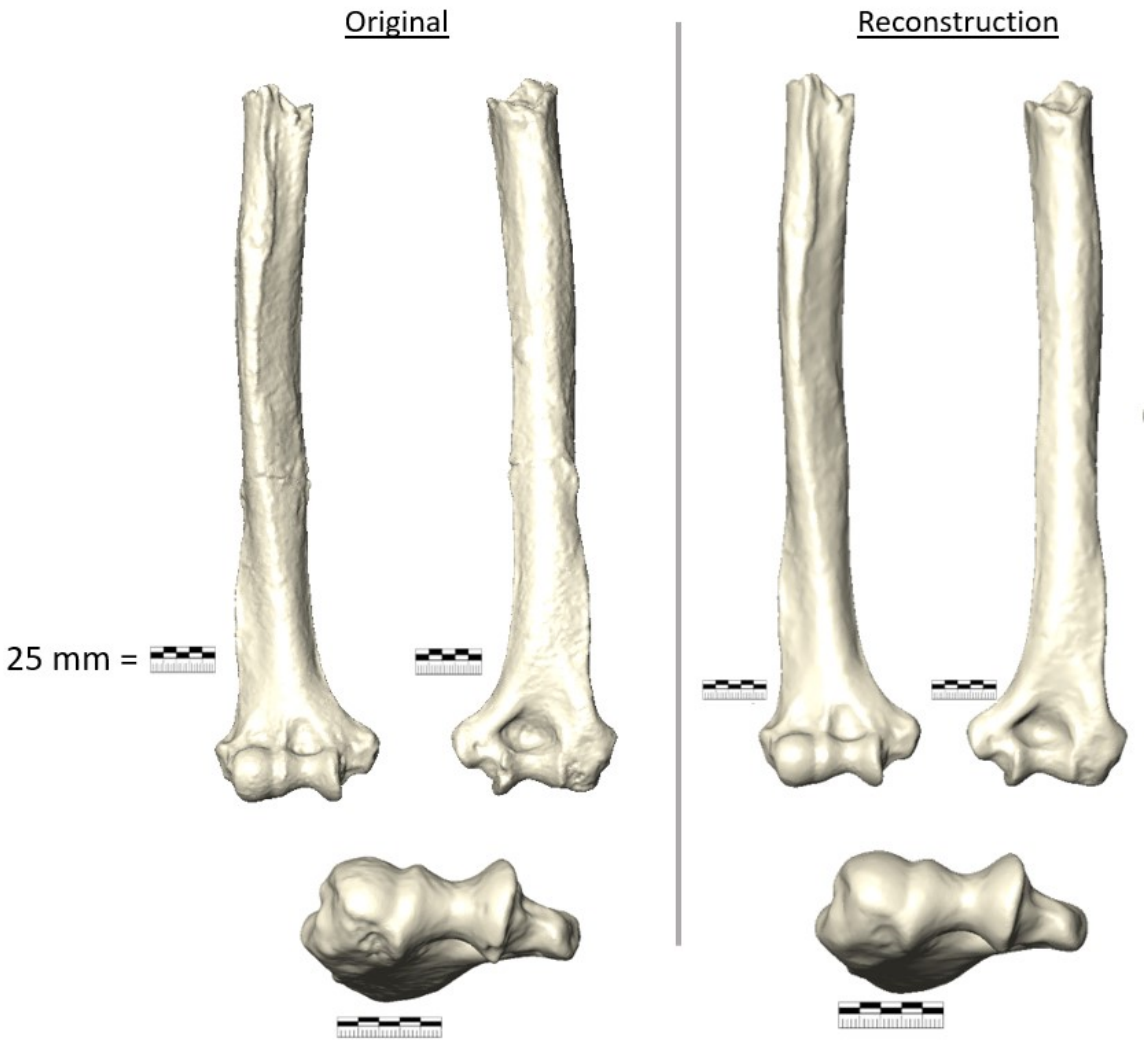

Figure 2-5 KNM-ER 739 original (left) and reconstruction (right).

KNM-ER 739 is a right humerus found from Ileret, Kenya, that preserves an almost complete shaft as well as the distal articular surface. It is dated to 1.5 Mya, and has been tentatively assigned to *Paranthropus boisei* (Leakey, 1971). It is large and remarkably robust.

KNM-ER 6020

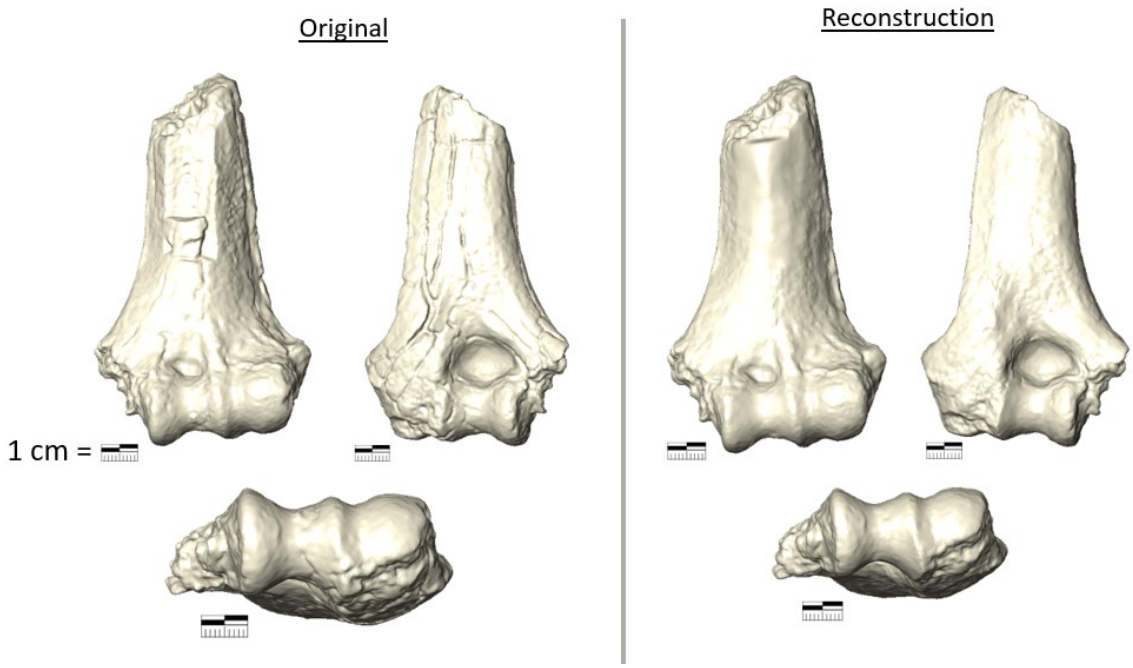

Figure 2-6 SKX 6020 original (left) and reconstruction (right).

KNM-ER 6020 is a partial left distal humerus from the Koobi Fora Formation, Kenya, dated at 1.8 Mya and tentatively assigned to *Paranthropus* boisei (Leakey and Walker, 1985; McHenry and Brown, 2008). This humerus exhibits severe weathering, including chipping and large longitudinal cracks. The medial epicondyle is absent, but the full articular surface is preserved in this specimen; it is therefore included in a limited number of analyses, many but not all of which require presence of the medial epicondyle. Chipping and cracks have been reconstructed, but the medial epicondyle has not.

SKX 10924

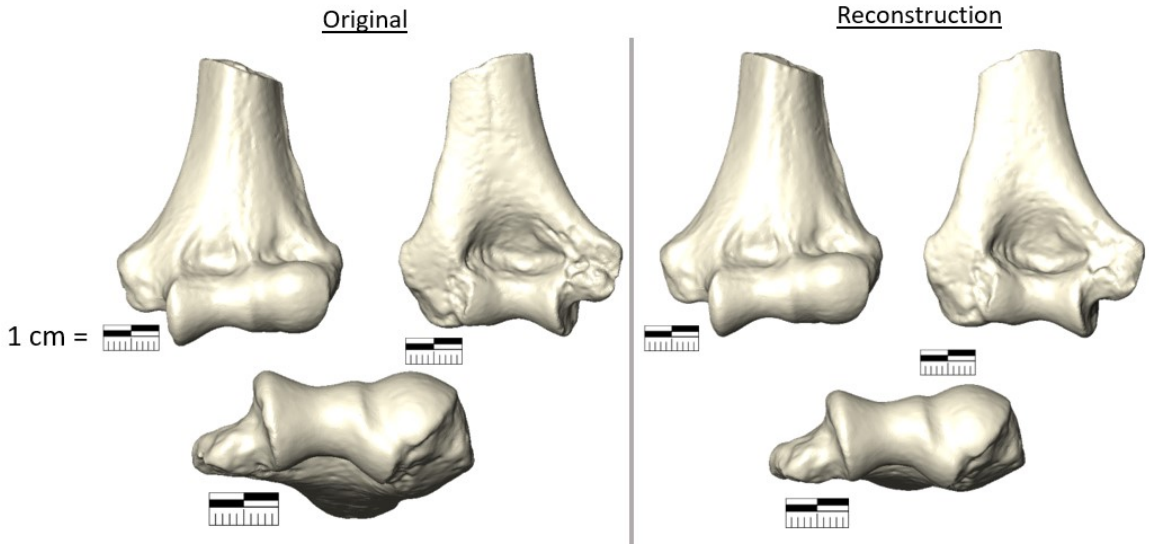

Figure 2-7 SKX 10924 original (left) and reconstruction (right).

SKX 10924 is a left distal humerus from Swartkrans, South Africa, attributed to either *Homo sp.* or *Paranthropus robustus* and dated to 1.8-1 Mya (Susman et al., 2001; McHenry and Brown, 2008; Lague, 2015). It preserves the distal portion of the bone with some pitting and damage to the posterior portion of the bone, especially on the posterior portion of the medial epicondyle. This damage has been conservatively filled in the reconstructed model.

SK 24600

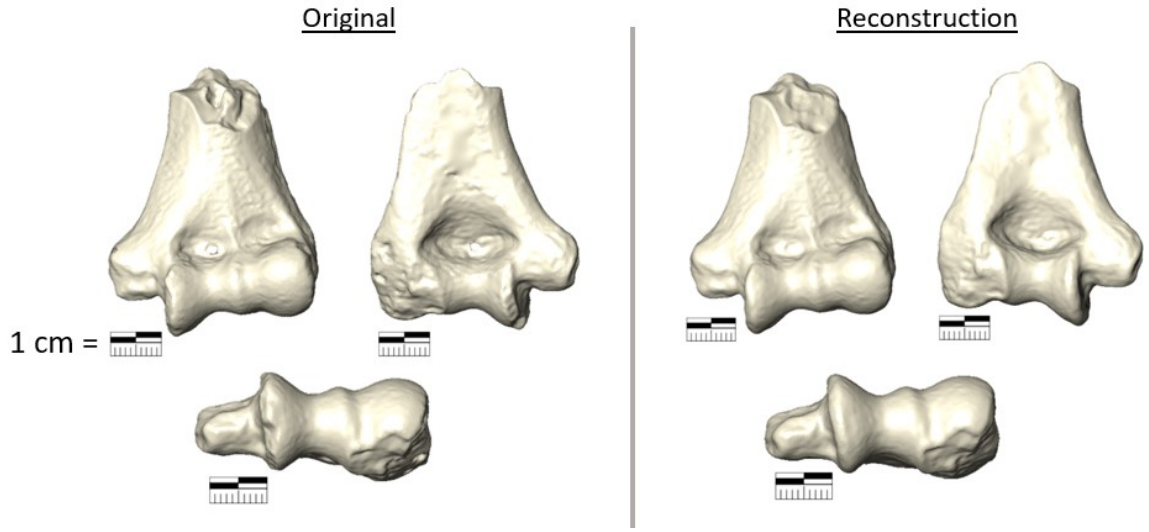

Figure 2-8 SK 24600 original (left) and reconstruction (right).

SK 24600 is a left distal humerus from Swartkrans, South Africa dated to 1.6-1.8 Mya and alternately attributed to *Paranthropus robustus* or non-erectus early *Homo* (Susman et al., 2001; Lague, 2015). There is erosion along both the medial and lateral portions of the bone, affecting the lateral epicondyle as well as the capitular and trochlear margins. Trochlear damage was repaired, but minimal reconstruction of the capitulum was performed, due to inability to ascertain its original extent.

StW 431

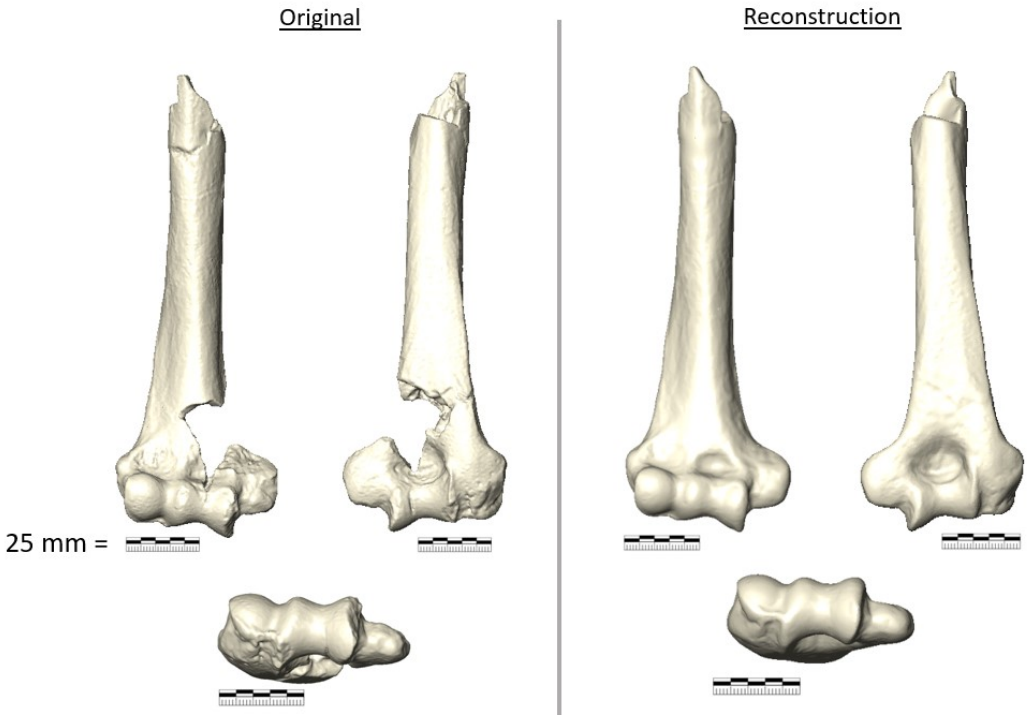

Figure 2-9 StW 431 original (left) and reconstruction (right).

StW 431 is partial right humerus attributed to *Australopithecus africanus*, found in the deposits at Sterkfontein in 1987 (Toussaint et al., 2003). The fossil lacks the medial olecranon pillar and medial supracondylar ridge, but large portions of the shaft and the entirety of the articular surface are preserved. The large missing segment of the periarticular and metaphyseal region was reconstructed using a combination of techniques. The surfaces opposing areas of breakage were removed digitally, and initial attempts to reconstruct the area were performed using automated tools in Geomagic that extend curvature of the existing surface. However, because of the size and complexity of the missing area, automated reconstruction did not produce realistic morphology. Therefore, the automated reconstruction was digitally resculpted by the

author, following curvature of existing surface morphology (olecranon fossa rim, medial shaft border above and below the break) as a guide. Error introduced by this resculpting process should be considered in assessment of results for this individual.

TM 1517

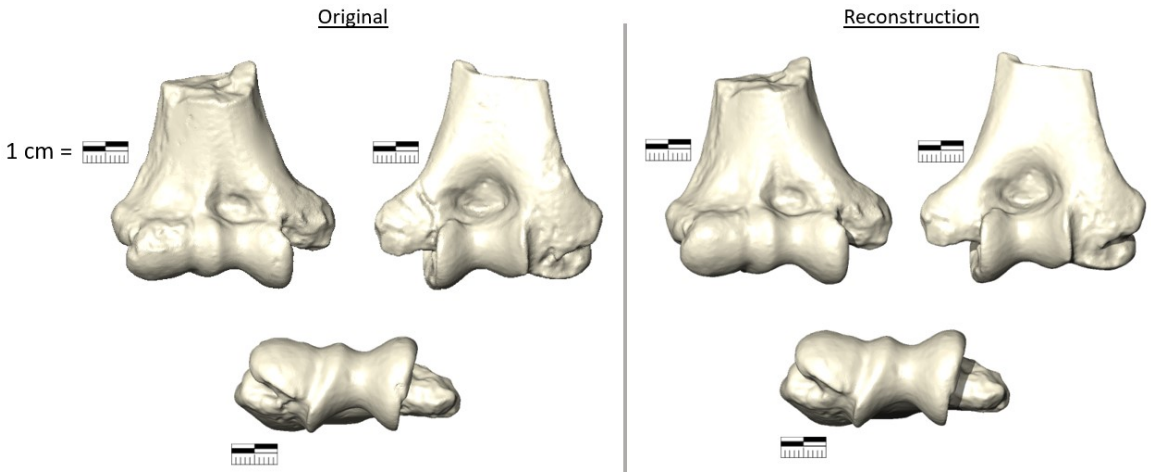

Figure 2-10 TM 1517 original (left) and reconstruction (right)

TM 1517 is a partial right humerus belonging to the type specimen of *Paranthropus robustus*, found at Kromdraai in close association with a skull, proximal ulna, two phalanges and a talus (Broom, 1938; Schepers and Broom, 1946). The entire distal articular surface and periarticular region are well-preserved. Cracking on the posterior surface of the medial epicondyle and pitting on the capitulum have been repaired.

2.2 Asymmetry

2.2.1 Measurements and Rationale

Chapter 3 addresses the issue of morphological asymmetry of the distal humerus interpreted as reflecting asymmetric loading patterns. As discussed in Chapter 1, there is strong evidence that long bone diaphyses in general and the humeral midshaft region specifically exhibit an adaptive bone response to mechanical loading (e.g., Ruff et al., 2006; Shaw, 2011). However, the extent to which adaptive remodeling is present in metaphyseal end periarticular epiphyseal regions of the upper limb is unclear (Haapasalo et al., 2000; Nadell and Shaw, 2016). The degree to which these regions exhibit response to loading is important to assess because they have recently been used for taxonomic assignments of isolated early hominin postcrania (Susman et al., 2001; Lague, 2014). The extent to which different traits respond to loading is also important for assessing their utility in reconstructing past behavior (e.g., Ward, 2002; Kivell, 2016: Ruff et al., 2016, 2018).

First, asymmetry was quantified in each of the regions of interest. Then, asymmetry in each region was compared to a proxy for habitual asymmetry in loading. Because bone increases in strength and rigidity under conditions of increased mechanical loading (see summary in Ruff et al., 2006), handedness in modern humans, and the resultant asymmetric loading of the upper limb, results in bilateral asymmetry of the humeral midshaft (Jones et al., 1977; Trinkaus et al., 1994; Haapasalo et al., 2000; Bass et al., 2002; Auerbach and Ruff, 2006; Shaw and Stock, 2009; Shaw, 2011; Warden

et al., 2014; Nadell and Shaw, 2016; Sládek et al., 2016). This creates differences in cross-sectional diaphyseal properties between the right and left humerus that are likely to reflect loading differences rather than differences in genetics, size, nutrition, etc., because these latter factors are held constant within an individual (Roy et al., 1994; Steele and Mays, 1995; Auerbach and Ruff, 2006; Blackburn, 2011; Warden et al., 2014). Therefore, bilateral asymmetry of cross-sectional properties of the humeral diaphysis was selected as a proxy for asymmetry in mechanical loading.

In this study, percent asymmetry in polar section modulus (Zp) at 40% of biomechanical bone length from the distal end was used as a proxy for handedness and associated asymmetric loading of the upper limb. The 40% section is used because this section replicates the differences in mechanical properties present at midshaft (Ruff, 2002; Nadell and Shaw, 2016), but it avoids the potential impact of the deltoid tuberosity. To obtain cross-sectional properties at this and other locations in the humerus, peripheral quantitative computed tomography (pQCT) was employed, using a Stratec XCT Research SA scanner. pQCT is ideally suited to this type of analysis because of its voxel size (down to 90 microns), facilitating resolution of thin cortices in the distal humerus (Ferretti et al., 1996; Ruff et al., 2012). The pQCT system is also equipped with software that uses the images obtained in scanning to compute standard section properties including: areas, second moments of area and section moduli, average cortical thickness, as well as bone density. Zp is proportional to torsional rigidity and to twice bending strength. It has been used in many previous studies of limb bone

structural properties (Ruff, 2003a, 2008, 2009, Ruff et al., 2013, 2016) and is an appropriate parameter to assess average bending.

To determine whether metaphyseal end periarticular epiphyseal regions of the distal humerus exhibit a coordinated response to asymmetric loading (approximated by diaphyseal asymmetry), three cross sections through the distal portion of the bone were defined relative to standardized measurements of the humerus (Figure 2-11). Bones were oriented in standardized anatomical position prior to measurement, with the humeral shaft supported such that it lay parallel to the measurement surface (see Ruff, 2002). The distal articular surface was oriented such that its long axis also lay parallel to the measurement surface. Distance between the most proximal point of the humeral head and the most distal point of the lateral trochlear crest was recorded as biomechanical length using an osteometric board. The 40% cross section, used as a proxy for load-dependent remodeling, was based on this distance. The first of the three distal humeral cross sections is also a percentage of this length, taken at 18%. The 18% site was chosen for analysis because it is equivalent to that presented by Lague(2015). Additionally, it is similar to Susman's (Susman et al., 2001) 19% section based on maximum length, which was used for taxonomic assignments, as well as being close to the 20% location included in previous studies of some nonhuman taxa and fossil hominins (Ruff et al., 2016). Both the 40% and the 18% cross sections lie perpendicular to the long axis of the humeral shaft. Figure 2-11 shows the location of all cross sections measured in this study.

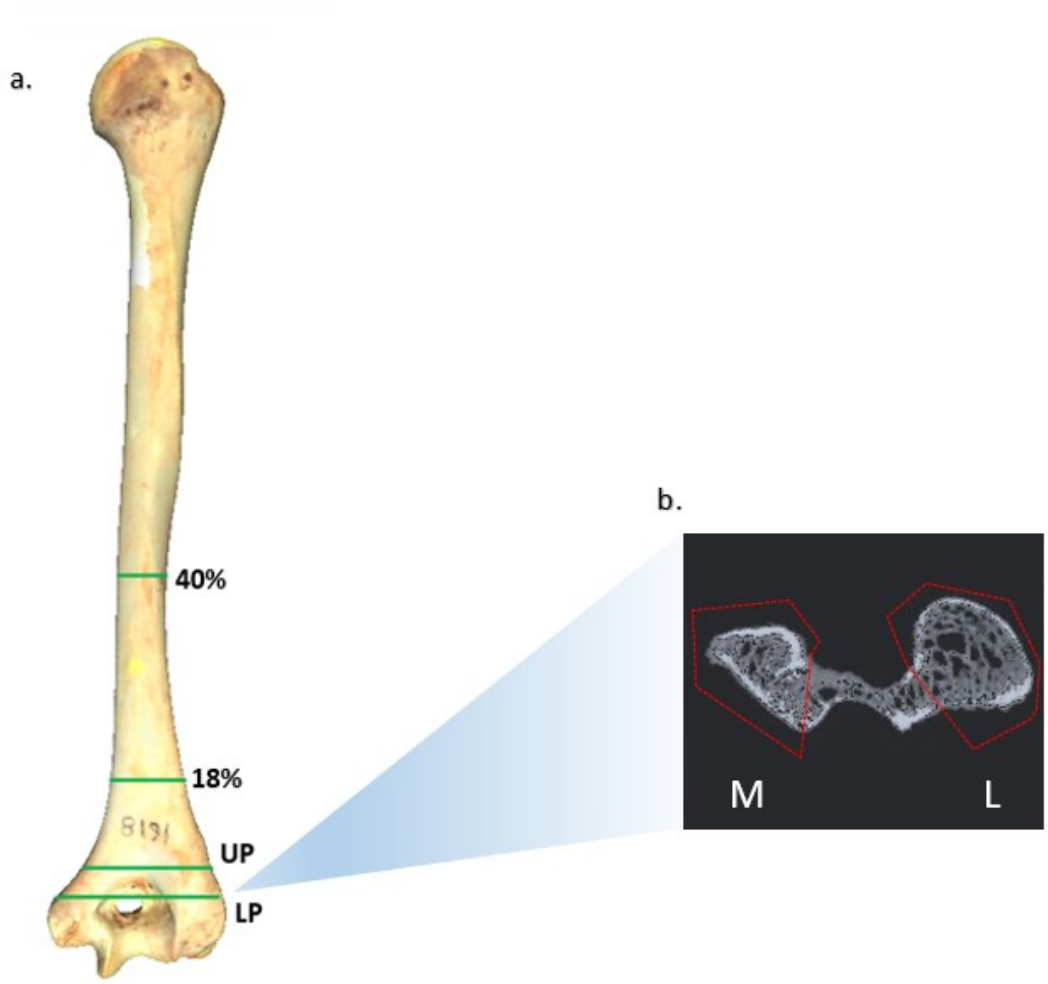

Figure 2-11 Location of the 40% comparison section and the three distal humeral cross sections analyzed. All cross sections were taken perpendicular to the humeral shaft. UP=Upper Pillar, LP=Lower Pillar, percentages are measured from the distal end and based on biomechanical length. Medial and Lateral pillar ROIs depicted.

In addition to the control located at 40% bone length and the 18% section, two additional cross sections were taken perpendicular to the humeral shaft. The first, at the proximal rim of the olecranon fossa, is called the upper pillar (UP), because it intersects the proximal portion of the medial and lateral olecranon pillars. This section is usually slightly proximal to midway between the distal end of the humerus and the 18% section

(see Figure 2-11). The final cross section, the "lower pillar" section (LP), was calculated as midway between the upper pillar section and a transverse plane through the medial epicondyle. These pillar sections resemble Senut's outlines (Senut, 1981a). The LP section was subsequently divided into medial and lateral regions of interest (ROIs) in order to examine the medial and lateral olecranon pillars independently. Senut (1981a, 1981b) asserts that olecranon pillar shape varies in part because of different patterns of loading between taxa. The two pillar ROIs were examined to determine contralateral asymmetry and whether the size of the pillars might be responsive to loading. Pillar ROIs were defined by the inflection point of the connection between each pillar and the floor of the olecranon fossa, indicated in Fig. 11b.

Orientation for pQCT scanning generally followed the procedure described in Ruff (2002) and above, with one difference: bones were oriented with the posterior portion of the shaft facing up. This was done because two of the cross sections are based on the olecranon fossa, and accuracy in marking this section and aligning during scanning was improved when this feature could be seen. Clay supports were placed under the proximal and distal shaft when necessary to elevate the shaft such that its entire length remained parallel to the support surface. The reversal of anteroposterior (AP) direction is not expected to significantly impact results. This position is held constant for all scans, and AP and ML distances remain the same as when the bone is measured in the more standard position. Neither the reversed nor the standard position reflects customary orientation during loading (Ruff, 2002).

Subsequent to scanning, data were extracted from the pQCT using built-in software (Stratec XCT SA1, Norland Stratec Medizintechnik GmbH, Birkenfeld, Germany)(Ferretti et al., 1996). Zp, discussed above, was extracted, as well as AP section modulus (Zx), which corresponds to AP bending strength, ML section modulus (Zy), which responds to ML bending strength, and total subperiosteal area of the cross section (TA). This allows for assessment of both average bending strength (Zp), as well as possible differences in strength dependent upon direction (Zx and Zy), as well as size (TA). Directional (right-dominant) asymmetry (%DA) was calculated for each of these properties according to recent conventions (Steele and Mays, 1995; Mays, 2002; Auerbach and Ruff, 2006; Sládek et al., 2016) :

$$Asymmetry = \frac{right - left}{(average\ of\ right\ and\ left)} \times 100$$

Absolute asymmetries were also calculated, but did not provide additional insights and are therefore not presented. Correlation between %DA in these properties and %DA of Zp at the 40% section was interpreted to reflect the degree to which these properties may be affected by the same asymmetry in loads that create cross-sectional asymmetry near midshaft.

Centroid size (Cz) %DA of six geometric morphometric (GM) landmark sets (distal 18% of bone, distal 10% of bone, periarticular region, articular region, capitulum, and trochlea, landmarks and subsetting (discussed in section 2.3) was also compared to shaft %DA to determine to what degree centroid size is influenced by the same

mechanical factors. This was done as a way of quantifying variation in the articular and periarticular regions where a beam model, the basis for calculation of cross-sectional properties, is inappropriate. This was of interest because while articulations are generally found to be more symmetric than diaphyses (Trinkaus et al., 1994; Lieberman et al., 2001; Ruff et al., 1991; Auerbach and Ruff, 2006), some studies have found evidence that articular (Frost, 1979; Hamrick, 1996, 1999; Plochocki, 2004) and periarticular (Blackburn and Knüsel, 2006) dimensions also adapt to mechanical loading. Centroid sizes are used as a scaling variable in GM analyses (Bacon, 2000; Lague, 2014), and mechanical adaptation of these measures would also complicate their use in this way. Two linear measurements were also used to assess asymmetry of the articular and periarticular regions: biepicondylar breadth, another potential scaling variable (Carretero et al., 2009; De Castro et al., 2012), and articular breadth. Articular breadth was measured directly from specimens in anatomical position (orientation described above), while biepicondylar breadth was measured digitally, as the distance between landmarks placed on the most projecting points of the medial and lateral epicondyles.

In subsequent analyses, %DA of both cross-sectional properties and centroid sizes were tested for differences on the basis of population and estimated sex, in order to evaluate the hypothesis that activity patterns, subsistence strategies, and gender roles may influence observed patterns in bilateral asymmetry of a diverse sample. Such relationships have been found in previous studies (Auerbach and Ruff, 2006; Sladék et al., 2007; Sládek et al., 2016).The six populations chosen (the American Terry (Black) and

Terry (White), the Native American Indian Knoll, Illinois, and Puye, and the ancient Egyptian Lisht populations) represent a variety of lifestyles including variation in both degree and type of activity. Recent work suggests that shifts in manipulative behavior associated with changes in agricultural and weapons technology significantly affected asymmetry of the upper limb in terminal Pleistocene and Holocene Europe (Sládek et al., 2016). This study tests whether these differences are also observed in non-European populations.

2.2.2 Statistical methods

First, means and standard deviations were calculated for asymmetry of all cross-sectional properties and centroid sizes in the full sample. None of the %DA distributions included in this study were normal according to a Kolmogorov-Smirnov test. This is common for percentage data, for which arcsine transformation is generally recommended (Sokal and Rohlf, 1995). However, arcsine transformations did not reliably produce normal distributions for these variables, and therefore non-parametric tests were performed on non-transformed data. Asymmetry of each property was tested against the null hypothesis of no significant asymmetry using a Wilcoxon signed rank test with Bonferroni correction.

Significant correlation (Pearson) of %DA of each of the 14 cross-sectional properties, six centroid sizes, and two breadths, and correlations of %DA with Zp %DA at 40% bone length were calculated in MATLAB R 2017a (The MathWorks, Inc., Natick, MA). For graphical presentation, reduced major axis (RMA) regression of each of these

metrics on shaft asymmetry was performed using gmregress code from the MATLAB Central File Exchange (Trujillo-Ortiz, 2014). RMA regression was chosen to account for error in both x and y (Rayner, 1985).

The Kruskal-Wallis test (equivalent to ANOVA), was used to test whether directional asymmetry of each property varied between populations. Following a positive result, post-hoc comparisons were made using Mann-Whitney U-tests with Bonferroni correction. For sex comparisons, Mann-Whitney U-tests were run on each property. Finally, sex differences within populations were also tested using Mann-Whitney U-tests using an alpha level of 0.05. Corrections were not made for the possible inflation of Type I error due to multiple comparisons, because our interest is not in the significance of any one comparison. Rather, the pattern of group differences – whether one group shows a consistent increase or decrease in asymmetry across measures – was of interest, and the risk of obscuring such a pattern due to inflated Type II error was of greater concern, given the small sample sizes available for some of our archeological populations.

2.3 Geometric Morphometrics

A geometric morphometric (GM) study was conducted in order to assess whether there are functional or taxonomic trends in distal humeral morphology that could be used to make inferences about fossil hominins. Given long-lasting doubts as to the discriminative power of distal humeral features (Straus, 1948; Ward, 2002; Lovejoy et al., 2016), it was important to first quantify variation within and among extant taxa.

Previous studies have been technologically limited in their ability to fully quantify humeral morphological variation, because they have required the definition of fixed, preferably homologous, landmarks for either linear measurements or GM techniques, both two-dimensional (Knussman, 1967; Patterson and Howells, 1967; McHenry, 1976; Bacon, 2000; Lague, 2014) and three-dimensional (Tallman, 2010; Holliday and Friedl, 2013). Such techniques may not be able to fully capture features that are key to understanding both phylogenetic and functional differences in the distal humerus, which has long been understood to suffer from a deficit of clear landmarks (Lague and Jungers, 1996) due to the "irregular and frequently ill-defined form and contour" of certain features (Straus, 1948). The current study overcomes this limitation by using three-dimensional sliding semilandmark techniques. These do not rely on discrete, user-positioned landmarks, but instead use a large number of semilandmarks that are able to quantify a continuous surface through algorithmic movement of the landmark set to a position that minimizes differences between individuals, but remains an accurate representation of the original surface.

2.3.1 GM Method Background

Before discussing specific analyses undertaken in this study, a brief overview of geometric morphometric techniques incorporating landmarks is warranted.

2.3.1.1.1 Fixed landmarks

GM studies of fixed landmarks rely on points known as Type I, II, and III landmarks, according to the type of data they represent (Bookstein, 1997). Type I landmarks refer to an intersection of tissues, type II to points that are locally defined (local minima and maxima, tips of projecting features), while Type III landmarks are defined with reference to distant points or the bone as a whole. Geometric morphometric work traditionally gives preference to Type I landmarks, because their homology is certain and their placement is reliable. Type II and Type III landmarks more closely replicate traditional morphometric linear measurements, but are less precise, and have therefore been dispreferred.

This presents a problem in analysis of postcrania, especially the distal humerus. The morphology of the bone contains few, if any, Type I landmarks. Most regions of interest are best quantified by a combination of Type II and Type III landmarks – often these landmarks reference both local morphology and global coordinates (e.g., “most anterior point along the maximum of curvature of the lateral trochlear crest”). Though these landmarks contain information of interest, relative to Type I landmarks they are deficient – they cannot be placed without reference to other portions of the bone. On the humerus, one component of their placement does not carry new information about the structure – while landmarks are placed along distinct biological structures, their exact placement is determined with respect to reference planes or as distances

between other landmarks to improve reliability, rather than as a measure of important biological shape.

2.3.1.1.2 Sliding Landmarks

Semilandmark represents biologically homologous structures that are deficient in Type I landmarks as a series of geometric curves and surfaces in order to make use of all relevant information (Gunz et al., 2005). Spacing of semilandmarks is produced as a byproduct of the statistical analysis of shape, rather than relying on user placement. This allows for the placement of a much larger number of landmarks, which do not need to be placed at Type I, II, or III landmarks – they may be placed anywhere across a surface. Indeed, semilandmarks should be placed across the entire surface, sampling all areas that may vary.

The reason this does not introduce undue error into the data is that final position of the semilandmark is not determined by its initial placement. Semilandmarks are compared to the positions of the same set of landmarks on a template surface. They are then allowed to slide tangent to their own surface in the direction that minimizes the bending energy of the thin plate spline interpolation function between the target and reference specimen. (i.e., relaxation of the splines). This movement is constrained depending on the type of feature each landmark is meant to represent. In this analyses, most landmarks are allowed to slide along a plane tangent to the surface. However, landmarks placed along the edges of the articular surface are considered curve landmarks, and are treated differently. These landmarks are restricted to sliding along a

tangent vector. The semilandmarks are then projected back to the original surface. The process is iterative. In this study, landmarks are slid and projected four times before creation of a Procrustes average (discussed below). This average becomes the new template to which landmarks slide, and the procedure is repeated. This continues until the landmark Procrustes average stabilizes.

2.3.1.1.3 Procrustes Superimposition

Comparison of shapes in this study relies upon the techniques of Procrustes superimposition, as does the sliding landmark technique described above. In generalized Procrustes analysis, shape configurations are scaled, translated and rotated such that Procrustes distance between them is minimized (Gower, 1975). This allows for comparison of shapes of different sizes, locations, and orientations. The analyses presented here analyses also allow reflection, in order to compare right and left humeri. After superimposition, the Procrustes average is the average position of each landmark. The analyses performed in the following studies follow a partial Procrustes procedure, which differs from generalized Procrustes in that scale of each landmark set is scaled to unit size one, rather than allowing scale to fluctuate in order to improve fit. A centroid size (square root of sum of squared distances of landmarks to average position) is extracted from each configuration that quantifies the relative size of the original shape.

2.3.2 Data Collection

The first step in this process is production of surface models. Three-dimensional models of the full sample described in sections 2.1.1 and 2.1.2 were produced by the author or provided by other researchers, as noted in Table 2-1 Total sample) and Table 2-2 Fossils included in this study). This sample includes 643 humeri in total, including seven populations of modern humans and three great ape genera (see Table 2-1). Surface models produced by the author were created using two NextEngine desktop 3D laser scanners running ScanStudio (Version 2.0.2) using a series of orientations and scanning revolutions designed to capture the entire humerus. Full bone scans were taken in standard definition (0.1 mm accuracy). Additional scans of the distal end were taken in high definition macro mode (67,000-268,000 points per square inch, .05 mm accuracy) (NextEngine Inc., Santa Monica, CA). Because this scanning process results in several surface models, each of which captures the original surface incompletely, scans were then imported into Geomagic wrap software version 2015.1.0.1919 (3D Systems, Cary, NC), cleaned, and merged to create a surface model of the whole bone.

Scan data for surface models provided by Dr. J. M. Plavcan and Dr.C. Ward were collected using a Konica-Minolta Vivid 9i (Konica-Minolta, Tokyo, Japan). Alignment of point cloud data was performed using Konica-Minolta Polygon Editing Tool software and the PolyWorks V 11.0 (InnovoMetric, Québec, Canada) IMAlign module, followed by overlap reduction and merging of point clouds with medium smoothing using the IMMerge module. The low levels of difference between Konica-Minolta and Next Engine

scanners have previously been shown to be comparable to differences between repeated trials with a single scanner (Sholts et al., 2010), and other work shows that differing scan protocols and data point density do not significantly bias volume and surface area (Guidi et al., 2007; Aguilar et al., 2009; Sholts et al., 2010). Such data have been combined successfully in previous studies (Hammond et al., 2013, 2016), and differences in scanners and protocols is not expected to bias results.

For all surface models, where a patent supratrochlear foramen was present, this feature was filled with a thin plane in order to prevent landmarks from sliding between the anterior and posterior surfaces of the bone. To increase computational speed, the original surface models were decimated to 150,000 faces, resulting in approximately 75,000 vertices with 0.6mm spacing (dependent upon surface size), smoothed and remeshed.

Humeri were oriented to anatomical position using the following procedure: Bones were oriented such that the first PC of the surface model (and therefore the long axis of the shaft; as defined by automated tools in Avizo Standard Edition 7.1.10 (Visualization Sciences Group (VSG), Hillsboro, OR)) defined the Z axis. Each specimen was then manually rotated such that the central axis of the distal articular surface (the axis of rotation, assessed visually) defined the X axis. Thirty total fixed landmarks were placed on the distal humerus for use as control points for the placement of the semilandmarks. Depictions in Table 2-3 show the position of these initial points. Points were positioned based on visual assessment in Avizo using built-in curvature mapping as

a guide for identifying local maxima and minima on features of interest. Twenty-one of these landmarks are on the distal articular surface itself.Landmarks 28 and 29 were placed with the aid of a clipping plane perpendicular to the shaft and intersecting landmark 27.

Table 2-3 List of Fixed Landmarks

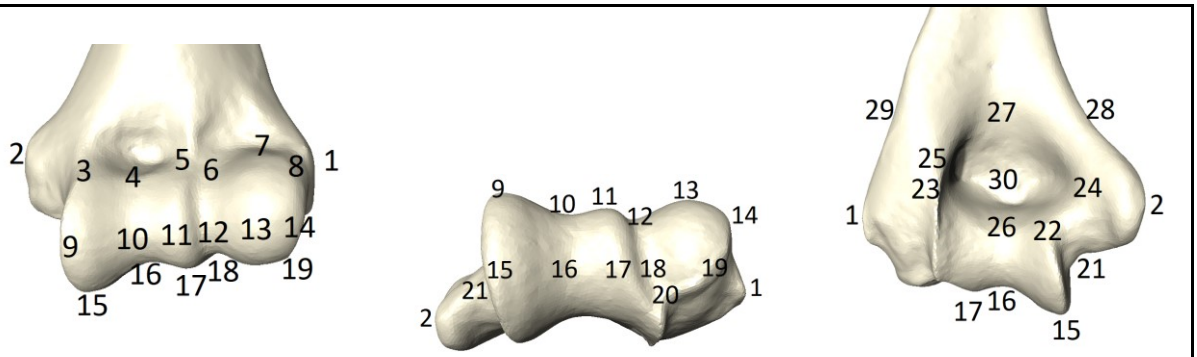

Anterior view | Inferior View | Posterior View

	1	Lateral Epicondyle
	2	Medial Epicondyle
Most proximal (anterior)	3	Medial trochlear border
	4	Trochlear groove
	5*	Lateral trochlear crest
	6	Zona conoidea
	7	Capitular margin
	8	Lateral edge of capitulum
Most Anterior	9	Medial trochlear border
	10	Trochlear groove
	11*	Lateral trochlear crest
	12	Zona conoidea
	13	Capitular maximum of curvature
	14	Lateral edge of capitulum
Most Inferior	15	Medial trochlear border
	16	Trochlear groove
	17*	Lateral trochlear crest
	18	Zona conoidea
	19	Lateral edge of capitulum
Posterior	20	Capitulum – posterior border ends at the zona conoidea
	21	Medial epicondyle – base meets trochlea

	22	Medial trochlear crest – posterior end
	23*	Lateral trochlear crest – posterior end
	24	Olecranon fossa – most medial point
	25	Olecranon fossa – most lateral point
	26	Trochlear groove – posterior end
	27	Olecranon fossa – most proximal point
	28	Medial supracondylar crest –medial extent of a plane intersecting landmark 27 and perpendicular to the long axis of the bone
	29	Lateral supracondylar crest- lateral extent of the plane described in 28
	30§	Olecranon fossa – deepest point

The landmarks listed above were designed to replicate and update into three dimensions points used in previous studies of the distal humerus (McHenry, 1976; Bacon, 2000; Lague, 2014; Rosas et al., 2015). However, they proved insufficient for satisfactory placement of the 988 sliding semilandmarks. They were therefore used in the creation of a larger set of 129 control points, as demonstrated in Figure 2-12.

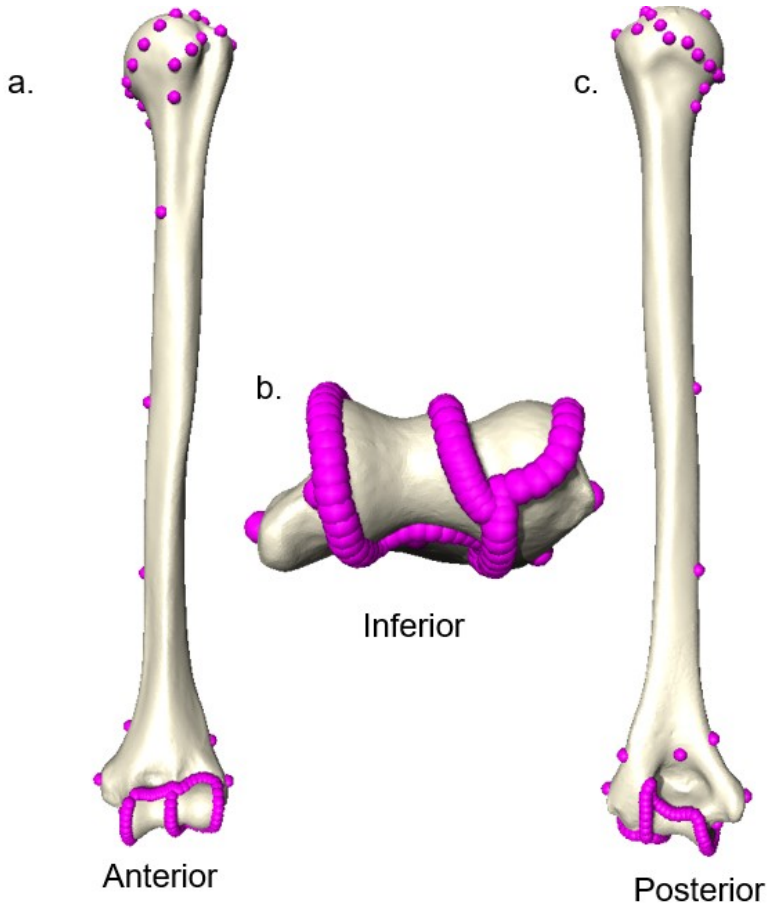

Figure 2-12 Additional control points.

These control points can be divided into three sets:

1) Proximal landmarks: 25 registration points were placed along the humeral head, neck, and tubercles. Detailed description of these landmarks is omitted here, because they were used for registration only. Morphology of the proximal humerus is excluded from the following analysis.

2) Shaft landmarks: Four landmarks were spaced evenly from the base of the lesser trochanter to the inflection point that forms the beginning of the medial epicondyle.

3) Distal landmarks: The 21 landmarks on the articular surface and an additional 40 control points evenly spaced along the articular border but without strict definition were used to create a series of b-splines along the articular border and lateral trochlear crest. Each spline was then resampled to create a series of evenly spaced landmarks along homologous regions (Table 2-4), for a total of 95 final landmarks defining the articular border. After creation of these edge landmarks, points on the face of the trochlea and capitulum were discarded, in favor of applying evenly spaced semilandmarks across each articulation. Fixed landmarks 1, 2, 21, 27, and 29 (

were retained in the control set. Table 2-4 below summarizes these landmarks, which can be seen in Figure 2-12.

Table 2-4 List of control point regions

Region	**Number of landmarks**
Humeral head and tubercles	25
Medial Humeral Shaft	4
Retained Fixed Landmarks	5
Capitulum (border)	20
Lateral trochlear crest, anterior portion: Proximal-most point to intersection with termination of the capitulum	15
Lateral trochlear crest, posterior portion: Intersection with capitulum to termination at olecranon fossa	10
Posterior trochlea	15
Medial trochlear crest	20
Anterior border of trochlea	15
Total	129

An initial template was created by hand placing 988 semilandmarks on a single human humerus. This template was then projected to a member of each genus using a thin plate spline (TPS) interpolation function that directly mapped the 129 control points described above onto the same 129 landmark positions on one member of each genus.

This TPS function was then applied to the total 988 semilandmark set, moving these landmarks to their approximate position on each bone. The interpolated 988-landmark set was then projected to the nearest point on the surface of the selected bone. Placement of these landmarks was adjusted, retaining homologous regions while correcting any poor spacing that occurred during the warping and projection process due to any large differences in morphology. These new templates were used to create the initial landmark placement for congeneric humeri. Using the same procedure by which the genus-specific templates were created, for each individual in the total sample, initial placement of semilandmarks was done by warping and then projecting template points. Figure 2-13 shows an example of initial landmark placement using this procedure.

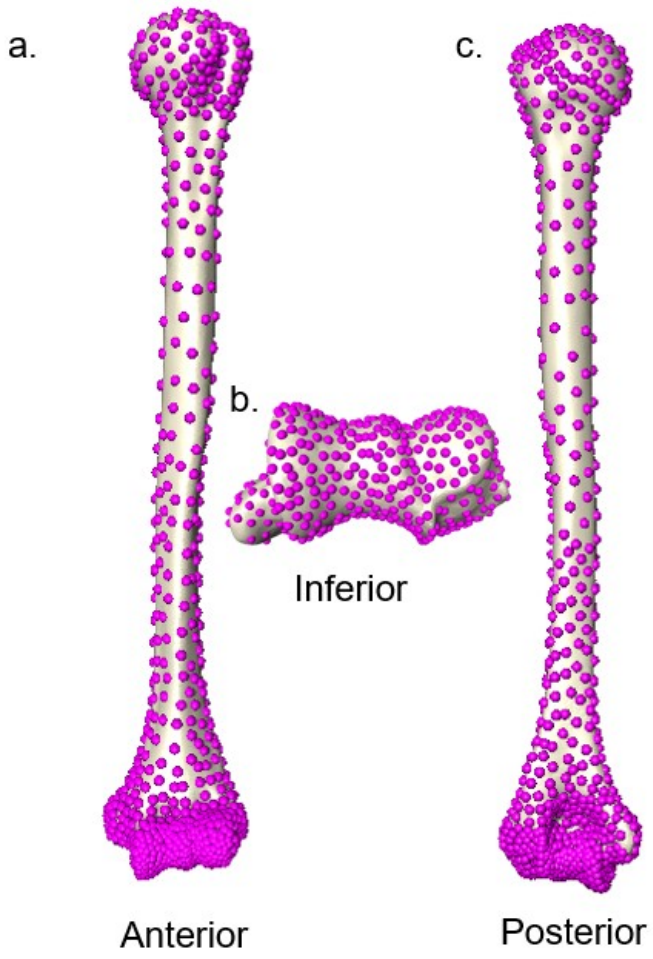

Figure 2-13 Semilandmark initial positions applied to bone.

Fossils

For fossils, all of the 129 control points that could be accurately assessed on the specimen were placed on its surface model. To create the initial semilandmark positions, the set of control points on the original template bone was subset to match the number of points available on the fossil. As above, these were used to warp the human template using the control points on the fossil. Prior to projection, this created a 'phantom bone'; the warped semilandmark points that did not correspond to preserved

morphology found their approximate positions based on extrapolation of the data available.

All points were projected to the fossil surface model and visually examined; in all cases, these phantom points projected to the most proximal remaining point of the model, which was the point of fossil breakage. All points projecting to this break were discarded. Nearby points that projected to areas within a few millimeters of a break were also discarded, in order to eliminate points that might move onto the broken area during sliding. The landmark ID numbers of the remaining points were recorded for later use.

Sliding procedure

In this analysis, two types of sliding landmarks were used: curve and surface. Curve landmarks were defined as those along the border of either the proximal articular surface (26 landmarks) or the distal articular surface (51 landmarks). Landmarks on all other regions of the bone were defined as surface landmarks.

Landmarks were slid to minimize bending energy of the thin-plate spline interpolation function relative to an updated Procrustes average (Sylvester, 2013) using Matlab programs developed by Adam D. Sylvester (JHU), Christine M. Harper (JHU), and the author. Surface landmarks were allowed to slide in along a plane tangent to the surface of the bone (two degrees of freedom), while curve landmarks were constrained to one degree of freedom, allowing them to slide along a vector tangent to the border

of the articular surface. The border of the articular surface was defined by the articular landmarks described in rows 4-9 of Table 2-4 , excluding the anterior lateral trochlear crest landmarks. They are depicted on the distal end of the humerus in Figure 2-12. A spline was fit through these landmarks and resampled to increase the density, resulting in several hundred possible vertices along the curve of the spline (variable dependent on total length of articular border). When landmarks slide along tangent vectors and planes, they often slide off of the original (curved) surface. Consequently, subsequent to sliding, new surface coordinates were projected to the nearest vertex in the original surface model, while new curve landmarks were projected to the spline as defined above.

Landmarks were initially slid to the human template bone. An iterative process of sliding and Procrustes alignment was carried out until the sliding landmarks and the Procrustes average reached stable configurations (in practice this took approximately three rounds). In the initial analysis, the landmark set for the full bone was slid at once. However, in this scenario, the position of proximal landmarks placed a measure of constraint on the distal landmarks that were the focus of this analysis, creating an inappropriate comparison for the fragmentary fossil material. To release this constraint, for each landmark subset (discussed below), an additional round of sliding was performed in which only the landmarks under analysis were applied to the bone and allowed to slide with the rest of the landmark set removed. The resulting configurations

were examined visually, and it was determined that there were no problematic artifacts of this procedure present in our results.

2.3.3 Statistical methods

In principal components analysis (PCA), large numbers of variables can be reduced by linear transformation into a set of variables where most variation (and therefore likely most important information) is contained in only a few. This smaller set of variables is created by orthogonal transformation of the original data to a new set of axes, or principal components (PCs). The transformation is defined such that the first principal component describes the highest amount of variance. Each subsequent principal component defines the direction of next-most variance, constrained to a plane orthogonal to the preceding components. The resulting principal components scores are then by definition uncorrelated with each other. In the case of geometric morphometric data, when principal component analysis is performed on landmark sets that have been superimposed during Procrustes analysis, this results in principal components that describe the ways in which shapes are most different from each other.

The full 988-landmark dataset was subset into six regions of interest, illustrated in Table 2-5 below. They include the distal 40%, distal 18%, distal 10%, and the isolated periarticular, articular, and distal diaphyseal (40%-18%) regions. Fossils were included where all landmarks present in the subset under investigation could be placed on the fossil. Table 2-5 makes note of this.

The six regions were defined based on evidence that different regions - diaphyseal, periarticular, and articular - may vary in terms of developmental asymmetry (see above and Chapter 2); the different functional implications of variation in morphology in these regions (e.g., muscular attachment sites versus articular surfaces); and differential regional preservation of fossils (Table 2-5). Individual PCAs were performed on these regional landmark sets to assess relationships between humans, great apes, and fossil hominins.

Table 2-5 Landmark Subsets

SEMILANDMARK ANALYSES

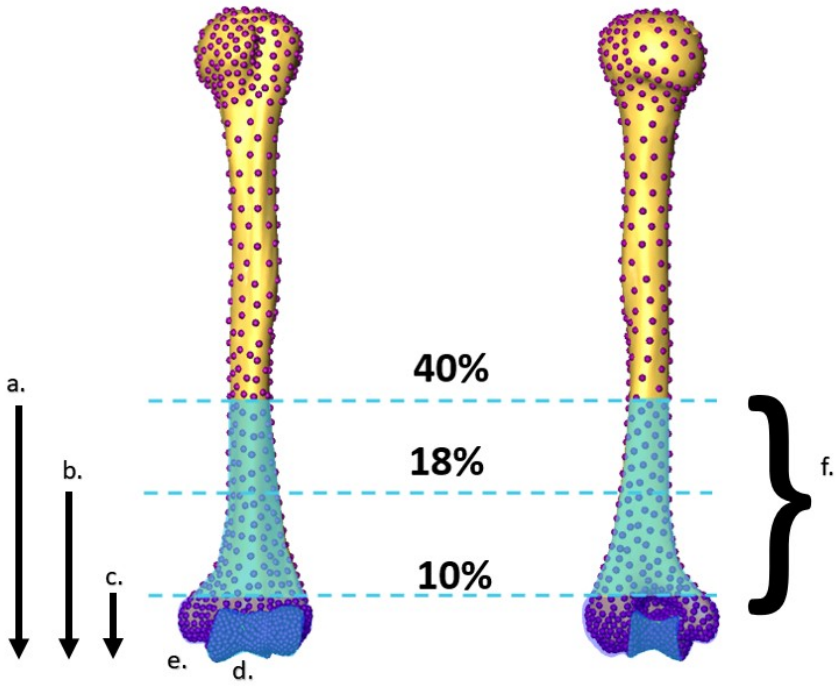

Region	*Number of Landmarks*	*Fossils Included*
Distal 40% (a)	736	A.L. 288-1 (R), StW 431, KNM-ER 739
Distal 18% (b)	625	A.L. 288-1 (R), StW 431, KNM-ER 739, KNM-ER 1504, Gombore IB-7594
Distal 10% (c)	558	A.L. 288-1 (R+L), StW 431, TM 1517, KNM-ER 739, SKZ 10924, SK 24600, KP 271, KNM-ER 1504, Gombore IB-7594
Articular Surface (d)	307	A.L. 288-1 (R+L), StW 431, TM 1517, KNM-ER 739, SKZ 10924, SK 24600, KP 271, KNM-ER 1504, KNM-ER 6020, Gombore IB-7594
Periarticular Surface (up to 10%, excludes articular surface) (e)	251	A.L. 288-1 (R+L), StW 431, TM 1517, KNM-ER 739, SKZ 10924, SK 24600, KP 271, KNM-ER 1504, Gombore IB-7594
Shaft (10% to 40%) (f)	178	A.L. 288-1 (R), StW 431, KNM-ER 739

For each PCA analysis, a MANOVA was performed in R to determine the effects of species, sex, and side (right or left) on the data. Each PC representing more than 1% of variation was treated as a dependent variable. Tukey HSD post-hoc tests were run using a 0.05 alpha level to identify significant differences.

2.4 Size

2.4.1 Overview

For the study of allometry in distal humeral properties, body masses derived from femoral head dimensions (as described below) were compared to a series of centroid sizes and two linear breadths (biepicondylar and articular). While some error may be introduced through the process of mass estimation, these mass estimates are independent of humeral properties. The correlation of size measures to each other was compared to determine the ability of distal humeral properties to act as a proxy variable for body mass.

Three of the size measures (centroid size of the distal 10%, biepicondylar breadth, body mass) were then used to investigate scaling of the distal humeral morphological characteristics demonstrated . This was achieved by regressing components that distinguish extant hominids from each other in the GM analysis in Chapter 4 on each of the three size measures (PC1 for all regions, as well as PC2 for the periarticular region). Fossils were then added, and the allometric relationships in the extant sample were used to interpret these results. Residuals from the human line were

calculated for the modern sample and for fossil hominins and used to examine temporal and taxonomic trends.

2.4.2 Sample

For this study, the extant sample was divided by genus. Two hundred forty-six humans, 47 *Pan*, 44 *Gorilla*, and 22 *Pan* were included. See section 2.1.1 for narrative description of the sample and Table 2-1 for sex breakdown. Where both left and right humeri were available for an individual, prior to analysis one side was selected for inclusion using a pseudorandom number generator. The sample is consistent across analyses.

Nine fossil hominins were included. These are listed in Table 2-2 with scan source and description of any reconstruction performed. Narrative description of the fossil sample can be found both in section 2.1.2 and in Chapter 1. Of the fossils listed, only KNM-ER 6020 was omitted. This was necessary because none of the three size measures (body mass, centroid size of the distal 10%, biepicondylar breadth) were available. Both left and right humeri were included for A.L. 288-1.

2.4.3 Body Mass

Body masses for the extant sample were estimated using equations based on femoral head SI breadths (Burgess et al., 2018; Ruff et al., 2018b). Some femoral head breadths were measured by the author with digital calipers; others were drawn from the literature or shared by other researchers. These contributions are listed in Table 2-6.

Table 2-6 Source of femoral head breadths.

Sample	Museum	Source of Femoral Head Breadths
Non-Pygmy Modern Humans	NMNH	K. G. Zelazny
Babongo/Babinga	MdH	K. G. Zelazny
	IRSNB	Auerbach & Ruff, 2006
Great Apes	NMNH	K. G. Zelazny
	MCZ	K. G. Zelazny
	RMCA	(Ruff, 2002)
	CNMH	C. M. Harper

Modern human body masses were calculated from femoral head prediction equations in Ruff et al. (2018). For great apes, known body masses were used where available (3 *Pan troglodytes*, 5 *Pan paniscus*, 23 *Pongo*. See Burgess et al., 2018). Additional *Pan* and *Pongo* body masses were calculated using genus-specific femoral head equations, while *Gorilla* body masses were calculated using femoral head body mass equations for African apes (Burgess et al., 2018).

Fossil body masses were drawn from Ruff et al. (2018). Special note should be made of the body mass for KNM-ER 1504. The body mass used is that calculated for 1503/5. This is done on the basis of the Leakey's judgment that all three specimens are likely from the same individual (Leakey, 1973; Leakey and Leakey, 1978). All three were found in the same locality and at the same level as the humerus, within several meters of each other. However, this association and therefore this body mass is slightly more uncertain than that for A.L. 288-1 and StW 431. No body masses were available for the other fossils included in this study.

2.4.4 Other Measures of Size

One measure of size included in the initial assessment of distal humeral scaling, ML articular breadth, was obtained from caliper measurements. This was taken with the humerus in anatomical position (described in section 2.2.1), as described in Ruff (2002). Biepicondylar breadth was calculated as the distance between landmarks placed on the medial and lateral epicondyles rather than by measurement with calipers. This allowed for inclusion of both extant and fossil specimens not physically available to the author.

Eight of the size measurements included were distal humeral centroid sizes. A number of different centroid sizes were assessed here, because while centroid size has been used in the past to scale humeral morphological features, centroid size necessarily varies upon the features and landmarks included. Landmark sets vary substantially between previous studies, partially due to the constraints of two-dimensional analyses. Therefore, the 988 landmarks in the current study were subset and analyzed as described above in section 2.3, resulting in a total of eight centroid sizes.

In brief, sliding landmarks placed on the humerus as a whole were subset into distinct regions, based either on length percentage (100%, 40%, 18%, 10%), feature (articular surface, trochlea, capitulum), or a combination of the two (periarticular region defined as the distal 10% excluding the articular surface). While trochlear and capitular morphological results are omitted in Chapter 4 in favor of interpretation of the articular surface as a whole, these were extracted and divided into 210 trochlear landmarks and 97 capitular landmarks for these analyses. A partial Procrustes analysis was performed

on these data in order to extract centroid size. This procedure was identical to that performed for the other regions.

2.4.5 Data Processing and Statistical Analyses

Each of the possible size measures, including body mass, was log-transformed prior to analysis. First, correlations between the ten distal humeral properties and body mass were calculated (calculations performed in MATLAB R 2017a, The MathWorks, Inc., Natick, MA). This included the eight centroid sizes, biepicondylar breadth, and articular breadth. In order to quantify scaling relationships, reduced major axis (RMA) regression of each of the ten size measures individually on body mass was performed using gmregress code from the MATLAB Central File Exchange (Trujillo-Ortiz, 2014). Model II techniques such as RMA are recommended when both variables are measured with error (Rayner, 1985; Hofman, 1988; Aiello, 1992) and are in general well suited to examination of scaling relationships, though results from Model I and Model II bivariate regression techniques are similar when correlations between variables are high, as is the case for most of the relationships between body mass and humeral size in this study. Standard error (SE) of the RMA regression slopes was also calculated in MATLAB. In order to understand scaling differences between taxa, differences in RMA slope were assessed in R using the smatr package (Warton et al., 2012), which also confirmed initial regression statistics. Parametric tests require statistically equivalent slopes for tests of elevation; because this assumption was not met here and elevation differences were not a key point of interest in this study, differences in elevation were not tested.

Correlation values alone can produce a misleading impression of the strength of relationships, because they are partially dependent on range, slope and sample size (Smith, 1984). Therefore, percent standard error of the estimate (%SEE) is also provided. This was calculated using the method described by per Organ and Ward (2006) for RMA, with calculation of %SEE per Smith (1984) and Ruff (2003) based on log-transformed data:

$$\%SEE = \exp(SEE + 4.6052) - 100$$

While multiple methods exist for size correction of morphological studies and characterization of allometry (Klingenberg, 2016), the primary focus of this study was to understand the influence of differences between possible scaling factors rather than to perform a study of allometry per se. The secondary focus was to examine the possible effects of size on key findings of the unscaled analysis presented in Chapter 4. Rather than a multivariate regression of global shape on size, therefore, RMA bivariate regressions of selected PCs of interest on log-transformed size variables were performed. This allows for direct comparison between the scaled and unscaled analyses and tests for the influence of allometry on the morphological results presented more fully in Chapter 4. Though less common than other techniques, this method has nevertheless been used in a number of studies of allometry (O'Higgens and Jones, 1998; Singleton, 2002; Zollikofer and Leo, 2002).

Fossil residuals from the modern human regression line were also calculated and compared to the estimated age of each fossil in order to ascertain morphological change

over time. For comparison, +/- 2 SEE for the human sample is provided; 95% of modern humans are expected to fall within these bounds.

3 Results: Asymmetry

To determine the likelihood that variation in distal humeral properties is influenced by, and therefore potentially indicative of, behavior during life, this study examines patterns of bilateral asymmetry in distal humeral structural properties in humans. Cross-sectional properties are chosen for analysis here because many studies show that one aspect of developmental plasticity is the increase in strength and rigidity of long bone diaphyses under increased mechanical loading (e.g. Hsieh et al., 2001; Bass et al., 2002; Robling et al., 2002; see additional references in Ruff, 2006) and they are therefore a good choice for examining the influence of *in vivo* use. This has been repeatedly demonstrated for the humerus, which experiences lateralized development in response to asymmetric loading of the upper limb in humans (Jones et al., 1977; Trinkaus et al., 1994; Haapasalo et al., 2000; Bass et al., 2002; Shaw and Stock, 2009; Shaw, 2011; Warden et al., 2014; Nadell and Shaw, 2016; Sládek et al., 2016). The resulting bilateral asymmetry is typically assessed in the middle region of the diaphysis (Shaw, 2011). Here we use a section at 40% of bone length from the distal end, to avoid complications associated with variations in size of the deltoid tuberosity.

In this chapter, asymmetry at the 40% section is used as a proxy for handedness and related asymmetry in loads in order to evaluate effects on more distal humeral regions, which are less well understood, though these regions may also be responsive to these and other loads in different ways not assessed here. Understanding the degree to

which loading patterns affect distal humeral cross sections is particularly important because distal diaphyseal cross-sectional morphology between 15-20% bone length has been used to make inferences about fossil hominin taxonomy (Lague and Jungers, 1996; Susman et al., 2001). The degree to which distal humeral centroid size (Cz) may be affected by loading is also considered in order to examine potential impact on its use as a scaling factor in studies of humeral allometry (Bacon, 2000; Lague, 2014; discussed further in Chapter 5). Centroid sizes of the periarticular and articular regions, as well as centroid sizes of the trochlea and capitulum, also provide a better way of quantifying "size" differences between these regions, for which cross-sectional properties based on a beam model are inappropriate. This chapter first addresses patterns of asymmetry in distal humeral cross sections and centroid sizes generally, and then considers the effect of sex and population (which vary in their life histories) on these relationships.

All analyses presented in this chapter are based on percent asymmetries between right and left humeri (%DA), calculated per Auerbach and Ruff (2006) as described in Chapter 2. Analyses of absolute asymmetry were also conducted, but did not produce substantially different conclusions and were overall less informative than directional analysis, so are not included in the following results.

3.1 Distal Humeral Asymmetry

Table 3-1 shows the percent bilateral asymmetry of each distal humeral property measured in the entire pooled human sample, examines whether these asymmetries

are significantly different from the null hypothesis of zero asymmetry, and determines whether asymmetry differs between regions and properties.

Table 3-1 Mean %DA by property
***=p<0.001, **=p<0.01, *=p<0.05. UP=upper pillar, LP=lower pillar. Medial pillar and lateral pillar are ROIs within the lower pillar cross section. Definitions of each region can be found in Chapter 2. Significant differences in asymmetry between cross sections on the basis of Mann-Whitney U tests with Bonferroni correction are listed by reference to property numbers in the first column.

Asymmetry in Cross-Sectional Properties and Centroid Size

	Property	Mean %DA	Standard Deviation	Significant Property Differences
1	**Zp 40%*** **	7.32	11.4	5,8-10,12,13,14,16-21
2	**Zp 18%*** **	7.36	11.2	5,8-10,12,13,14,16-21
3	**Zx 18%*** **	5.49	11.3	14,16-21
4	**Zy 18%*** **	6.46	12.4	14,16-21
5	**TA 18%*** **	4.30	8.1	1,2,14,16-21
6	**Zp UP*** **	3.64	12.5	16-21
7	**Zx UP*** **	3.97	11.2	14,16-21
8	**Zy UP** **	2.62	13.8	1,2,21
9	**TA UP*** **	2.83	8.2	1,2,17,18,21
10	**Zp LP ***	2.53	17.1	1,2,21
11	**Zx LP*** **	6.48	15.4	14,16-21
12	**Zy LP***	2.04	17.9	1,2
13	**TA LP*** **	2.86	9.1	1,2,16-18,21
14	**Medial Pillar TA**	-0.36	15.9	1-5,7,11,15
15	**Lateral Pillar TA*** **	4.34	14.0	14,16-21
16	**Distal 18% Centroid Size*** **	0.96	1.4	1-7,11,13,15,21
17	**Distal 10% Centroid Size*** **	0.85	1.4	1-7,9,11,13,15
18	**Periarticular Centroid Size*** **	0.48	1.6	1-7,9,11,13,15,19,20
19	**Articular Centroid Size*** **	1.24	1.8	1-7,11,15,18,21
20	**Trochlear Centroid Size*** **	1.29	2.1	1-7,11,15,18,21
21	**Capitular Centroid Size*** **	-1.40	10.3	1-11,13,15,16,19,20

The results shown in the table demonstrate that the degree of asymmetry varies depending on the region and property studied. Asymmetry is highest in section moduli (Zp, Zx, and Zy) of the diaphysis, both at the 40% section that represents the midshaft

region, and at 18%, near the section studied by Lague (2015) and Susman et al. (2001). Asymmetry of section moduli at the 18% location is not significantly different from that at the 40% location. Mean asymmetry in the upper pillar section (UP) is lower than asymmetry of the 18% section, but this difference is only significant for the ML section modulus (Zy) and total area (TA) of the cross section. Mean asymmetry of three of four measures of the lower pillar section (Zp, Zy, and TA) are significantly lower than Zp at 40% and 18%, and means of Zp and Zy are lower than corresponding UP measures, though not significantly. Asymmetry in Zx of the lower pillar appears much higher than other measures of the upper and lower pillar sections, but does not differ from them significantly. While area of the medial lower pillar is not significantly asymmetric, area of the lateral pillar is highly asymmetric. Overall, there is evidence for a slight proximo-distal decline in asymmetry. This is consistent with findings in Auerbach and Ruff (2006) that asymmetries of articular and periarticular measures tend to be less pronounced than asymmetry of the diaphysis.

Centroid size asymmetries are significantly lower than most, but not all those of cross-sectional properties. Mirroring the possible trend in cross-sectional asymmetries, centroid size asymmetries also show a trend of declining asymmetry across the distal diaphysis and periarticular metaphysis. However, articular centroid size asymmetry is significantly higher than periarticular centroid size asymmetry.

3.2 Correlations of Asymmetry

Table 3-2 shows the correlations of %DA in cross-sectional properties and centroid sizes with polar section modulus %DA at 40%. Asymmetry at 40% is referred to as shaft asymmetry later in the text. Based on correlations with asymmetry at 40%, there is a clear trend in the degree to which distal humeral properties within the total pooled human sample respond to the forces affecting the midshaft region. The correlations decrease in magnitude moving distally down the humerus, but remain statistically significant throughout. Correlation is highest for the most proximal cross section, 18% (equivalent to the ~19% section studied by Lague (2015) and Susman et al. (2001)), and declines distally, where sections are less beam-like. This somewhat recapitulates the overall trend in asymmetry described above. The periarticular region appears to be more responsive to the loads attributable to handedness than the articular region despite higher asymmetry in the articular region, which may reflect the greater effect of non-mechanical factors (e.g., genetic) on articular surface variability (Trinkaus et al., 1994; Lieberman et al., 2001; Ruff et al., 1991; Auerbach and Ruff, 2006). Results also indicate that this response is higher in the trochlea than in the capitulum. In fact, the capitulum is the only region for which asymmetry is not linked at all to %DA of the shaft. This may be the result of more mechanical load being transmitted through the trochlea than the capitulum, at least in humans. The capitulum is also the only feature for which centroid size shows a significant left bias (Table 3-1),

possibly indicating growth of this feature is inhibited by trochlear growth, perhaps as a constraint on articular size.

There is a pattern of declining correlation moving distally from midshaft that echoes the proximo-distal decline in asymmetry described in the previous section. It is not unexpected than sections closer together are more tightly correlated, but the resulting pattern suggests that this may be due to dissipation of forces across the bone, though other factors also influence the degree of total asymmetry, especially in the articular region. The results show that both cross-sectional properties and centroid sizes covary with asymmetry at 40%, and it is likely that both types of measurement are affected by the loading regime that produces asymmetry at midshaft. Where centroid sizes include measured cross-sectional levels, correlation magnitudes are similar between the two types of measurement. (i.e., periarticular centroid and LP). Figures for cross-sectional results by region follows Table 3-2. Centroid sizes are addressed in section 3.2.3.

Table 3-2 Correlations with shaft asymmetry (Zp 40%). ***=p<0.001. UP=upper pillar, LP=lower pillar. Medial pillar and lateral pillar are ROIs within the lower pillar cross section. Definitions of each region can be found in Chapter 2.

%DA in Cross-Sectional Properties and Centroid Size Correlation with Zp 40% Percent Asymmetry	
Property (Percent Asymmetry)	r
Zp 18%	0.84***
Zx 18%	0.83***
Zy 18%	0.77***
TA 18%	0.77***
Zp UP	0.62***
Zx UP	0.73***
Zy UP	0.55***
TA UP	0.58***
Zp LP	0.49***
Zx LP	0.48***
Zy LP	0.46***
TA LP	0.46***
Medial Pillar TA	0.38***
Lateral Pillar TA	0.27***
Distal 18% Centroid Size	0.52***
Distal 10% Centroid Size	0.51***
Periarticular Centroid Size	0.46***
Articular Centroid Size	0.37***
Capitular Centroid Size	0.05
Trochlear Centroid Size	0.29***

3.2.1 Distal Diaphysis

All cross-sectional asymmetries of the 18% section are highly correlated with asymmetry at 40% (r = 0.77-0.84). This indicates significant response of the structural properties of this region to the same factors that produce asymmetry at 40% (i.e., handedness). The magnitude of asymmetry of this region is similar to that seen at 40% (compare x and y axes).

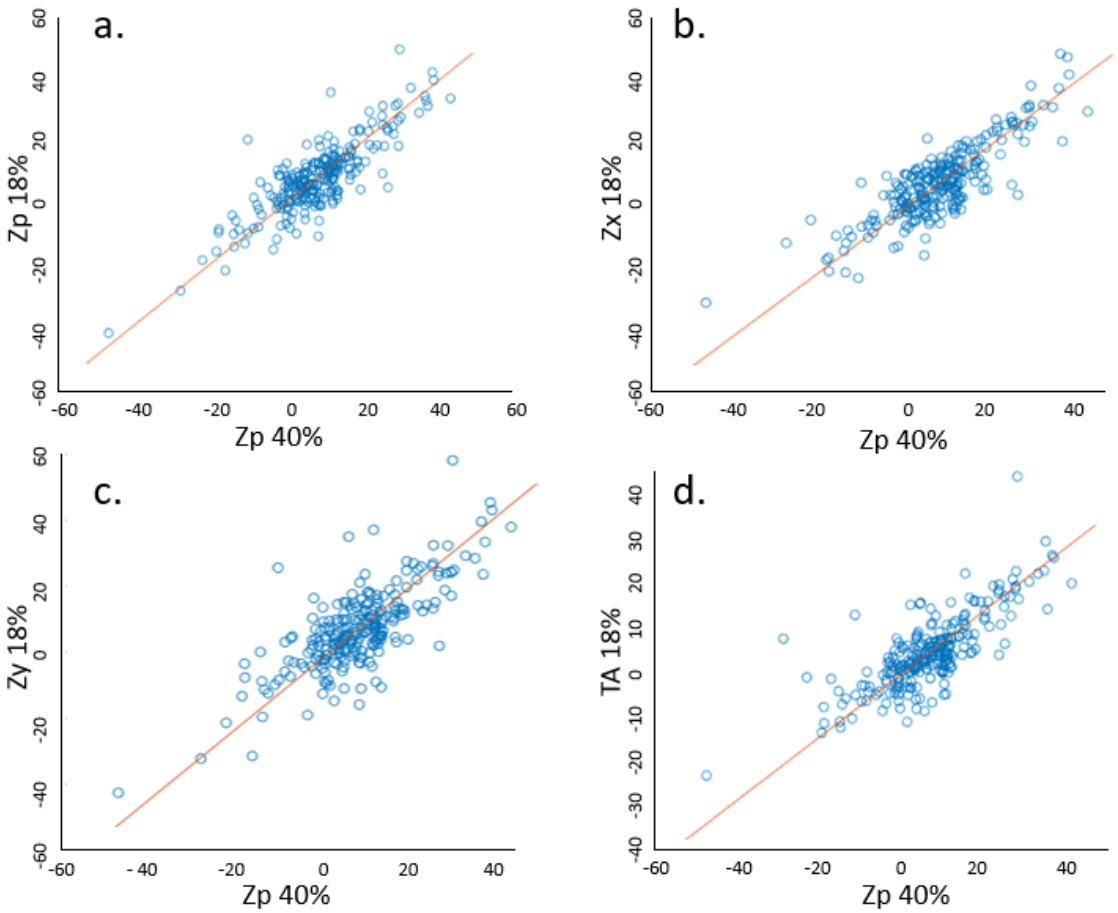

Figure 3-1 Correlation between percent asymmetry at 18% and 40%
RMA regression of %DA in each of four properties against %DA Zp at 40% is shown. See Table 2 for statistics.

3.2.2 Olecranon Region

Upper Pillar

At the proximal rim of the olecranon fossa, asymmetry in each of the cross-sectional properties for the upper pillar section (Zp, Zx, Zy and TA) is significantly correlated with ZP 40% asymmetry (r=0.55-0.73). The correlation is strongest for Zx (Figure 3-2 b).

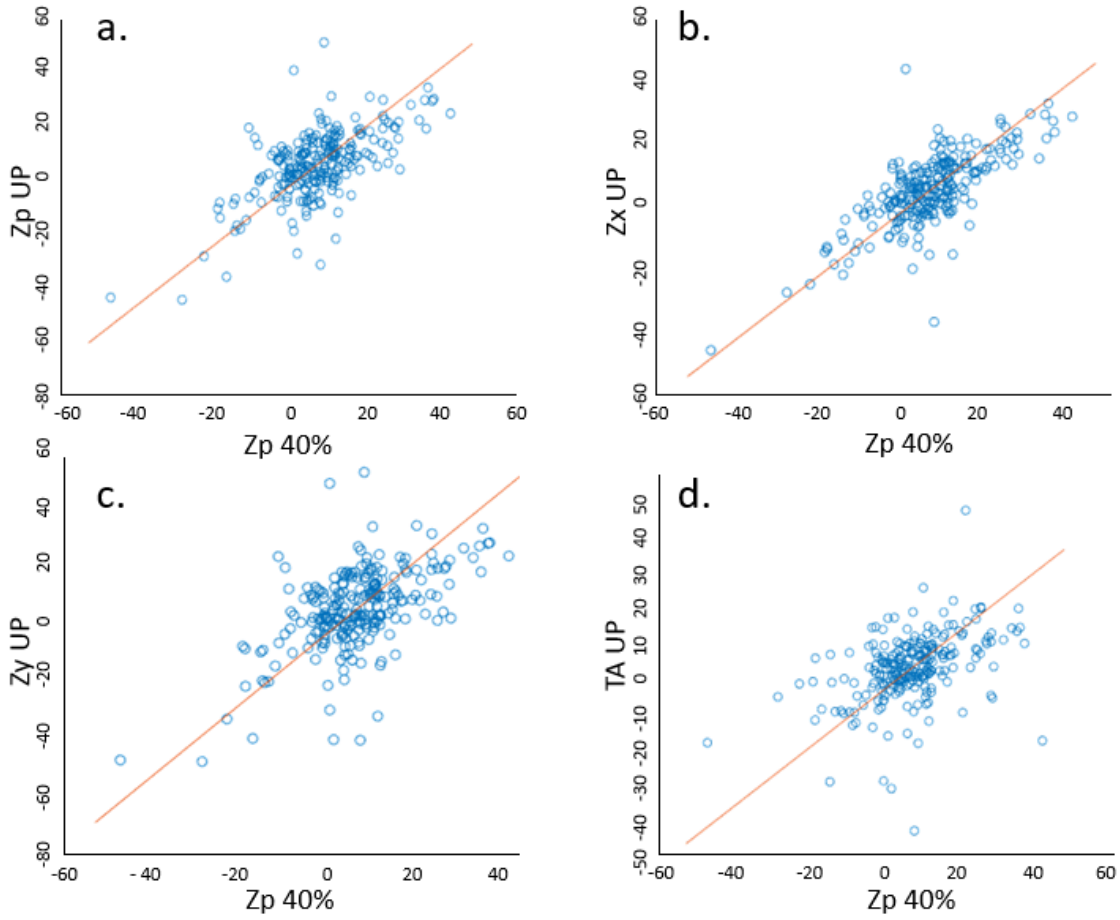

Figure 3-2 Correlation between percent asymmetry in the upper pillar section (UP) and 40% RMA regression of %DA for each of four properties against %DA in Zp at 40% is shown. See Table 2 for statistics.

Lower Pillar

Moderate correlations (r = 0.46-0.49) between shaft asymmetry and %DA in lower pillar cross-sectional properties are highly significant, though application of a beam model to this section is of arguable utility due to invagination of the olecranon fossa, (i.e., a very irregular cross section). Separate ROIs were defined for the medial and lateral pillars within this section. %DA of total cross-section area of each of the

pillars is significantly correlated with shaft asymmetry (Figure 3-4). A slightly stronger correlation is seen for the medial pillar than the lateral.

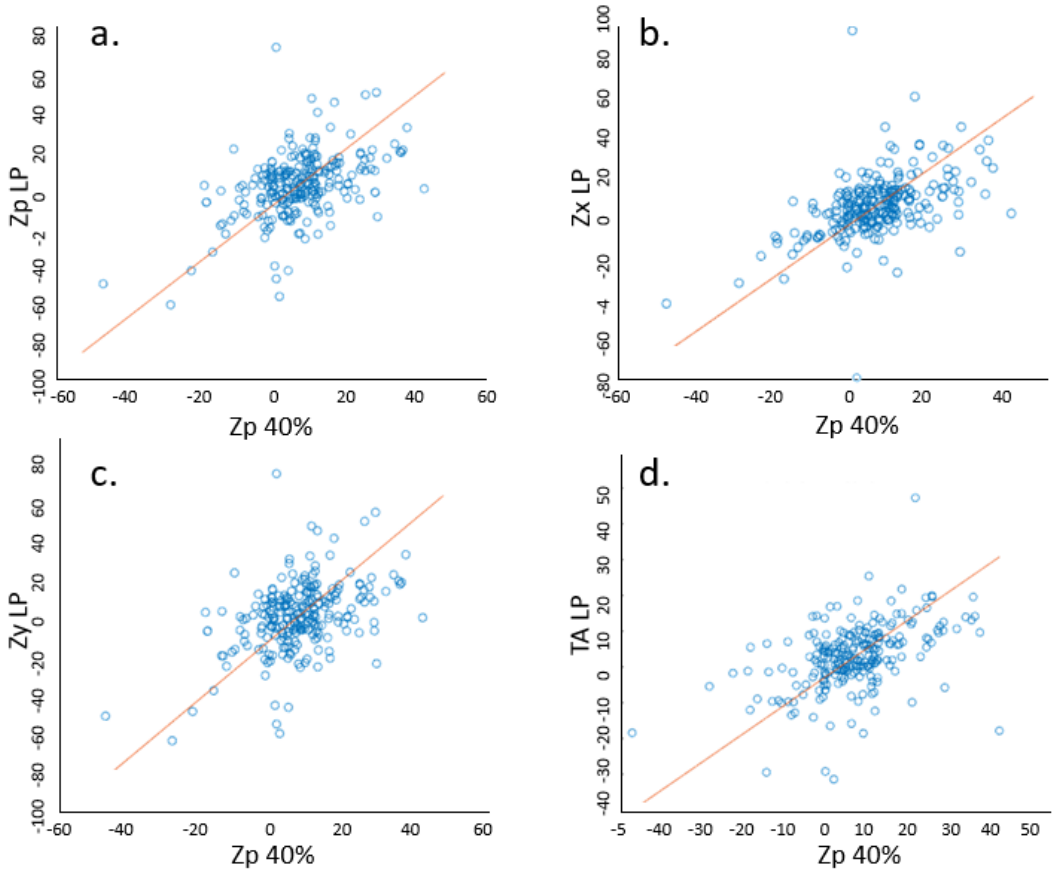

Figure 3-3 Correlation between asymmetry of the lower pillar section (LP) and 40% RMA regression of %DA in each of four properties against asymmetry in Zp at 40% is shown. See Table 2 for statistics.

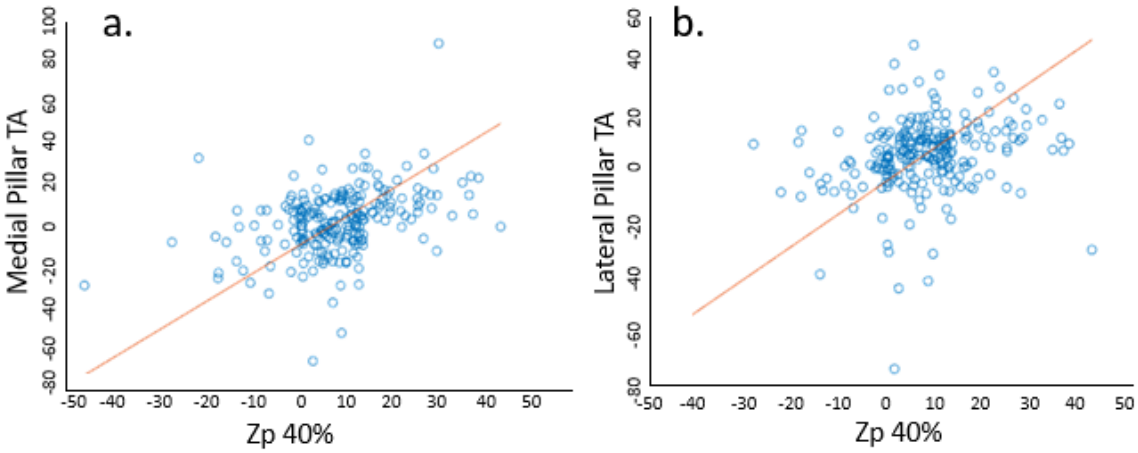

Figure 3-4 Correlation between total area asymmetry of the olecranon pillars and 40%. RMA regression of %DA in total area of each pillar cross section against asymmetry in Zp at 40% is shown. See Table 2 for statistics.

3.2.3 Centroid size

In the course of geometric morphometric (GM) analyses (Chapter 4), size of the studied surfaces was extracted as centroid size. This provides another method of measuring distal humeri that can be evaluated for association with handedness by correlation with shaft asymmetry. This is particularly important, because centroid size (Cz) is used as a scaling factor in humeral analyses where body size is not available (Bacon, 2000; Lague, 2014). In the GM analysis presented in Chapter 5, 988 landmarks are distributed across the entire humerus and subdivided into discrete regions (see GM methods, Chapter 2). Centroid size is extracted for the whole humerus and for each region separately. These data allow us to investigate the degree to which overall size of humeral regions varies in conjunction with estimates of handedness. Figure 3-5 shows the relationship between asymmetry in centroid size and asymmetry of the shaft.

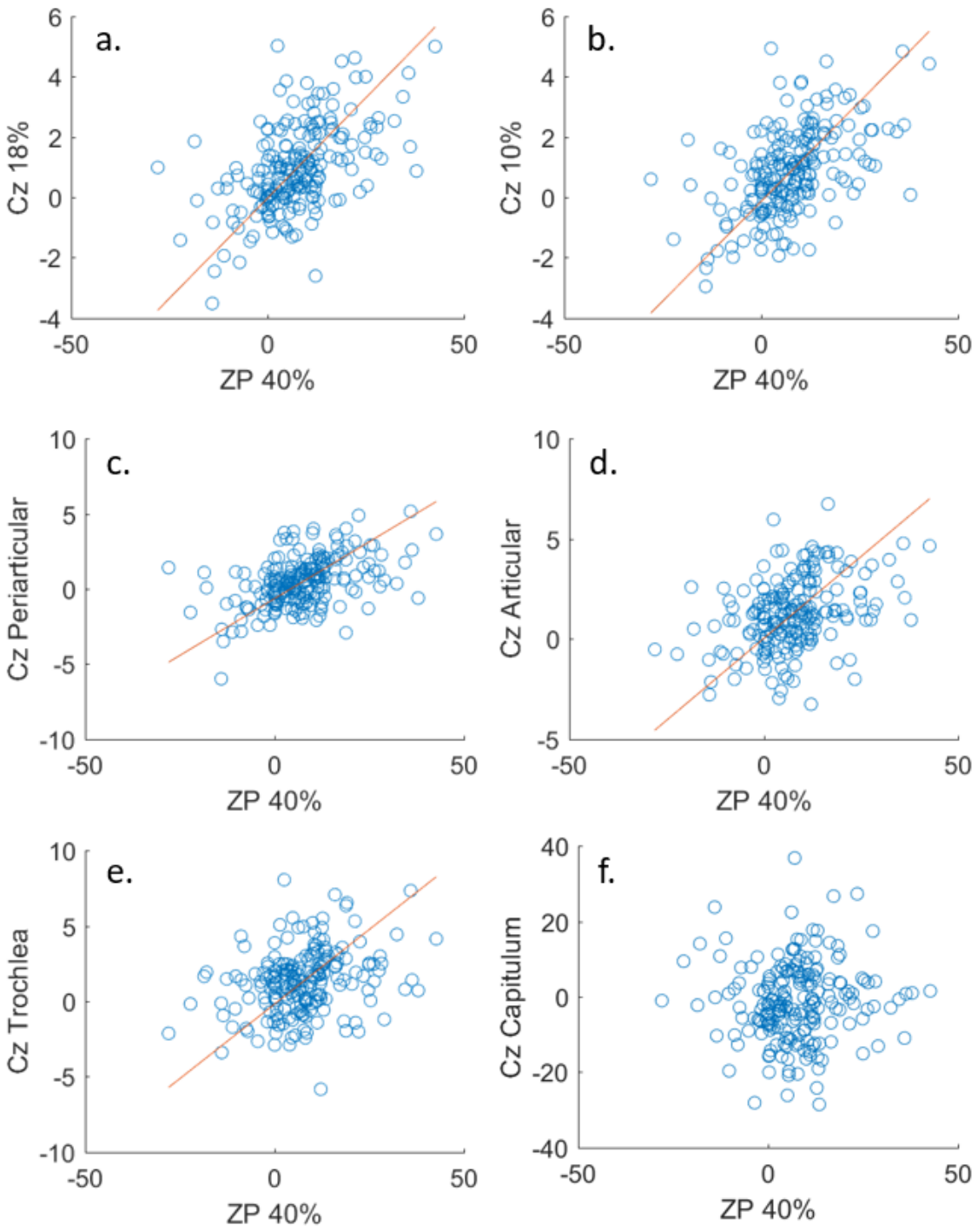

Figure 3-5 Correlations between Centroid Size Asymmetry (Cz) and Zp 40%.
RMA regression of %DA in total area of each pillar cross section against asymmetry in Zp at 40% is shown. See Table 2 for statistics.

Centroid size asymmetry follows the same trend of declining correlation with shaft asymmetry that is seen in cross-sectional properties. Between right and left humeri, there is up to an 8% difference (trochlea, Figure 3-5 e.) in centroid size for regions that show significant correlations with shaft asymmetry (all regions excluding the capitulum). Centroid sizes based on regions that include more proximal bone regions (18% Figure 3-5 a; 10%, Figure 3-5 b) have higher correlations with Zp 40% asymmetry, while more distal regions are less correlated with shaft asymmetry. While periarticular centroid size is more strongly correlated with shaft asymmetry than articular centroid size, both correlations are significant, indicating centroid size plasticity is not restricted to diaphyseal and metaphyseal regions.

Centroid sizes of the distal 18%, 10%, and periarticular region encompass cross sections included in this analysis. The periarticular region and the distal 10% region both include the upper and lower pillar sections, including both medial and lateral olecranon pillars. The distal 18% also generally includes the 18% section in addition to these measures, though it is important to note that percentages referred to by the centroid sizes are calculated to encompass the distal 18% of the average bone of the combined great ape and human sample (see details in Chapter 2), while percentages for cross-sectional analyses are measured on individual bones, and therefore not directly comparable. Centroid sizes can be thought of as summarizing the multiple cross sections they include, which explains in part why correlation for centroid size of distal 18% is lower than that for the 18% cross section and correlation of the 10% centroid is lower

than that for the upper pillar section. However, the periarticular region has a similar degree of correlation with shaft asymmetry as the lower pillar section. This is interesting because unlike the 18% and 10% centroids, this section omits the articular region, and is instead chiefly composed of the olecranon pillars and the epicondyles. As noted previously, articular response to asymmetric loading of the more proximal shaft appears to occur primarily at the trochlea, for which there is a significant correlation with shaft asymmetry, rather than the capitulum, for which there is not.

3.3 Effects of Sex and Population

Bilateral asymmetry of the upper limb can be indicative of patterns of manipulative behaviors, including transitions in subsistence strategies and division of labor by sex (Sládek et al., 2016). Both population and especially sex also have the potential to affect bilateral asymmetry through genetic and hormonal effects (Trinkaus et al., 1994; Auerbach and Ruff, 2006; Sladék et al., 2007; Sládek et al., 2016). This section examines the influence of demographics on asymmetry of the distal humeral regions included in this study.

3.3.1 Population

There are significant population differences for all cross-sectional asymmetries and three of the five centroid sizes significantly correlated with shaft asymmetry. Table 3-3 presents the mean %DA for each population and notes significant differences between groups for each property, based on significant Kruskal-Wallis results with

Mann-Whitney U post-hoc comparisons. Graphical representation of selected properties can be found in Figure 3-6.

Table 3-3 Population Differences in Asymmetry
Mean asymmetry of each property is given by population. Centroid size is omitted because it was not significantly correlated with shaft properties in section 3.2.3. Significant effect of population subject to Kruskal-Wallis marked for properties,***=p<0.001, **=p<0.01, *=p<0.05. Significant between group comparisons are marked for each population. B=Terry (Black), W=Terry (White), K= Indian Knoll, I=Illinois, P=Puye, L=Lisht. Multiple comparison results based on Mann-Whitney U post-hoc test with Bonferroni correction, equivalent to alpha=0.05.

		POPULATION DIFFERENCES					
	$X^2(5)$	*Terry (Black)*	*Terry (White)*	*Indian Knoll*	*Illinois*	*Puye*	*Lisht*
Zp 40%* **	41.212	4.08^{K}	6.51^{K}	$18.9^{B,W,I,L}$	4.82^{K}	10.8^{L}	$1.47^{K,P}$
Zp 18% * **	23.966	5.31^{K}	6.21^{K}	$17.3^{B,W,L}$	7.27	8.7	1.09^{K}
Zx 18% * **	30.205	3.09^{K}	4.04^{K}	$16.3^{B,W,I,L}$	3.67^{K}	7.69	1.1^{K}
Zy 18% * **	27.108	4.65^{K}	4.9^{K}	$18.3^{B,W,I,P,L}$	5.34^{K}	6.49^{K}	1.59^{K}
TA 18% * **	29.466	2.89^{K}	3.23^{K}	$11.2^{B,W,I,L}$	3.53^{K}	6.1	0.478^{K}
Zp UP * **	28.965	1.81^{K}	1.86^{K}	$15^{B,W,I,P,L}$	3.46^{K}	4.81^{K}	-2.01^{K}
Zx UP * **	22.349	2.7^{K}	1.94^{K}	$13.4^{B,W,I,L}$	3.13^{K}	4.87	1.41^{K}
Zy UP * **	26.348	1.14^{K}	0.795^{K}	$14.3^{B,W,I,P,L}$	1.93^{K}	3.34^{K}	-2.85^{K}
TA UP * **	21.180	2.37^{K}	2.71^{K}	$7.75^{B,W,I,L}$	2.1^{K}	3.7	-2.1^{K}
Zp LP*	14.812	1.48^{K}	2.44^{K}	$10.9^{B,W,L}$	-0.276	4.45	-4.22^{K}
Zx LP**	15.286	5.17^{K}	3.88^{K}	$13.5^{B,W}$	4.99	12.7	1.47
Zy LP*	13.371	1.34	2.06	10.5^{L}	-1.0	3.26	-4.78^{K}
TA LP**	15.120	3.23	2.32	4.9	2.23	5.58	-2.28
Medial Pillar TA*	15.038	1.17	-0.75	1.28	-4.48	5.21^{L}	-9.45^{P}
Lateral Pillar TA*	11.702	5.45^{L}	5.89	4.17	6.0^{L}	1.57	$-2.49^{B,I}$
Distal 18% Cz * **	23.204	0.759^{K}	0.652^{K}	$2.08^{B,W,I}$	0.817^{K}	1.52	0.847
Distal 10% Cz**	16.827	0.624^{K}	0.64^{K}	$1.85^{B,W,I}$	0.652^{K}	1.27	0.804
Periarticular Cz	10.458	0.312	0.428	1.3	0.375	0.714	-0.093
Articular Cz**	17.934	0.928^{K}	0.815^{K}	$2.31^{B,W}$	1.14	1.62	2.11
Trochlear Cz	6.370	1.16	0.906	2.11	1.13	1.64	1.88

Differences are most striking in the Indian Knoll population, which consistently has much higher values of right-dominant asymmetry. The Indian Knoll population is pre-agricultural, probably subsisting through hunting and foraging (Webb, 2001), which has previously been thought to amplify asymmetry in other populations (Sládek et al., 2016). The Indian Knoll population differs from both Terry populations and the Lisht at

midshaft and all properties of the 18% and UP sections. It also differs from the Illinois population in eight of these nine measurements, and from the Puye in three (see Figure 3-6 a and b below). At the lower pillar section, which runs through the periarticular region, it differs from the Terry collection in Zp and Zx and from the Lisht in Zp and Zy (Figure 3-6 c). The Indian Knoll population appears most similar to the Puye, from which it differs only in asymmetry of three cross-sectional measurements. The two groups do not differ in centroid size asymmetry (discussed further below). Distinction of the Indian Knoll population is less clear more distally: the medial pillar differs only from the Lisht, and the lateral pillar does not differ significantly from any population.

Selected cross-sectional properties divided by population are presented in Figure 3-6 below. Figure 3-6 a-c highlight the strong asymmetry in the Indian Knoll population, while Figure 3-6 d and e show subtle but significant left-handed asymmetry in the Lisht at the olecranon pillars.

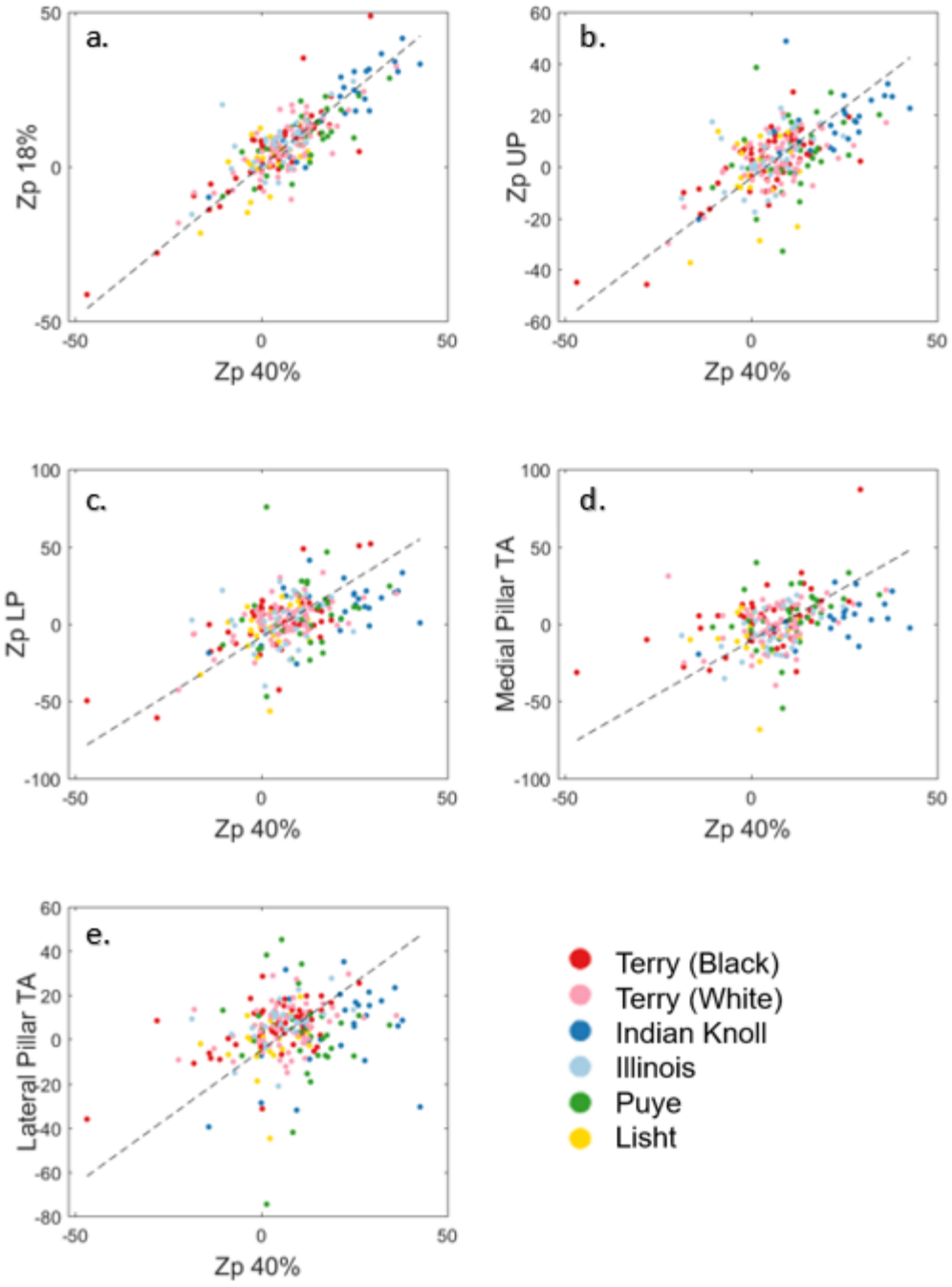

Figure 3-6 Population differences in cross-sectional properties. See Table 3-3 for statistics.

While there is a significant effect of population on asymmetry of all cross-sectional sizes, only three of the five centroid sizes significantly correlated with Zp 40% show the

same effect (Table 3-3). Centroid size asymmetry of the distal 18%, 10%, and articular region is significantly impacted by population, but asymmetry of the periarticular and trochlear centroids is not. For the centroid sizes affected, the amplified asymmetry seen in the Indian Knoll population is the primary difference. Asymmetry in the Indian Knoll population differs significantly from both Terry populations in three of the five centroid sizes, and from the Illinois population in two (Table 3-3). These relationships are demonstrated in Figure 3-7.

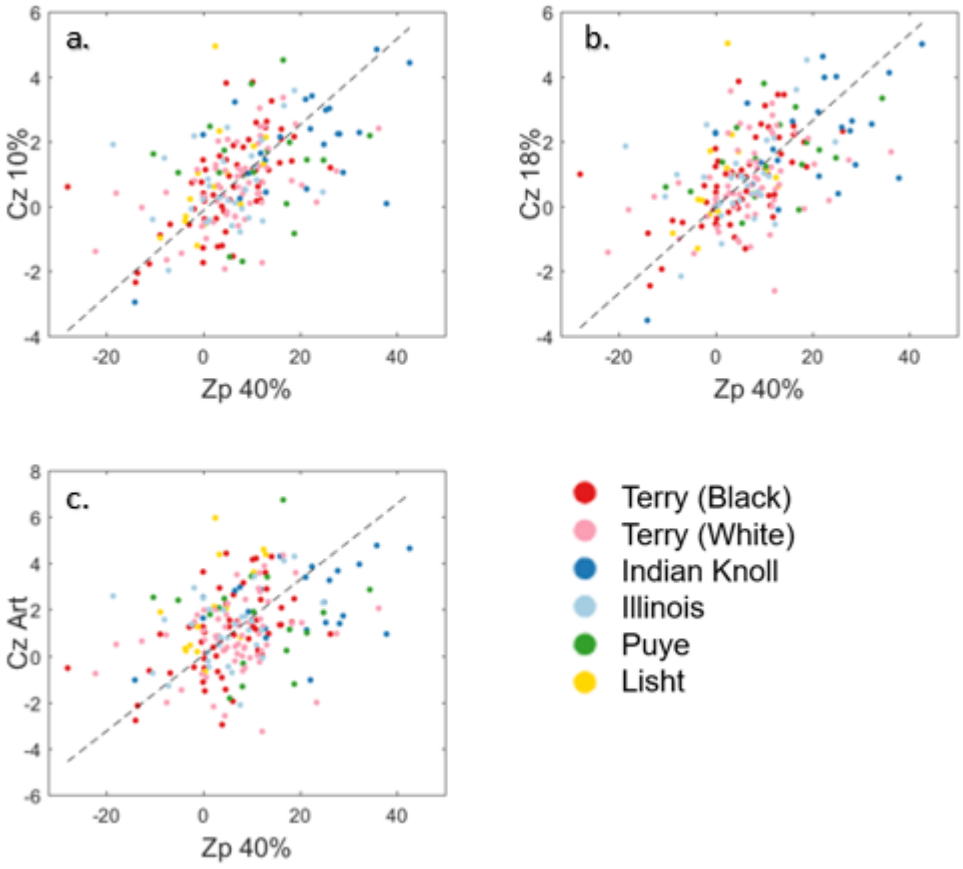

Figure 3-7 Population differences in centroid size asymmetry. See Table 3-3 for statistics.

3.3.2 Sex

Males and females differ significantly in the degree of asymmetry present in several of their cross-sectional properties, shown in Table 3-4 and Figure 3-8. Sex differences are concentrated in the more proximal sections (though see following section for within population effects). They are significant for all properties assessed at the 18% section and two properties of the upper pillar section (Zx and TA), but are also significant for total area of the lower pillar section and of the medial olecranon pillar.

Table 3-4 Mean asymmetry by sex.
Asterisks indicate significance levels of Mann-Whitney U test. ***=p<0.001, *=p<0.05.

	SEX DIFFERENCES		
	p	*Male*	*Female*
Zp 40%* **	<0.0001	10.21	3.97
Zp 18%* **	<0.0001	10.18	4.09
Zx 18%* **	<0.0001	8.54	1.94
Zy 18%* **	<0.0001	9.15	3.33
TA 18%* **	<0.0001	6.40	1.88
Zp UP	0.417	3.87	3.36
Zx UP * **	<0.0001	6.01	1.63
Zy UP	0.481	2.56	2.69
TA UP* **	<0.0001	4.21	1.23
Zp LP	0.701	1.91	3.23
Zx LP	0.386	7.15	5.72
Zy LP	0.540	1.20	2.97
TA LP*	0.020	4.01	1.57
Medial Pillar TA* **	<0.0001	2.48	-3.59
Lateral Pillar TA	0.550	4.60	4.05
Distal 18% Cz	0.530	1.04	0.89
Distal 10% Cz	0.848	0.84	0.86
Periarticular Cz	0.562	0.41	0.55
Articular Cz	0.897	1.21	1.27
Trochlear Cz	0.637	1.35	1.22

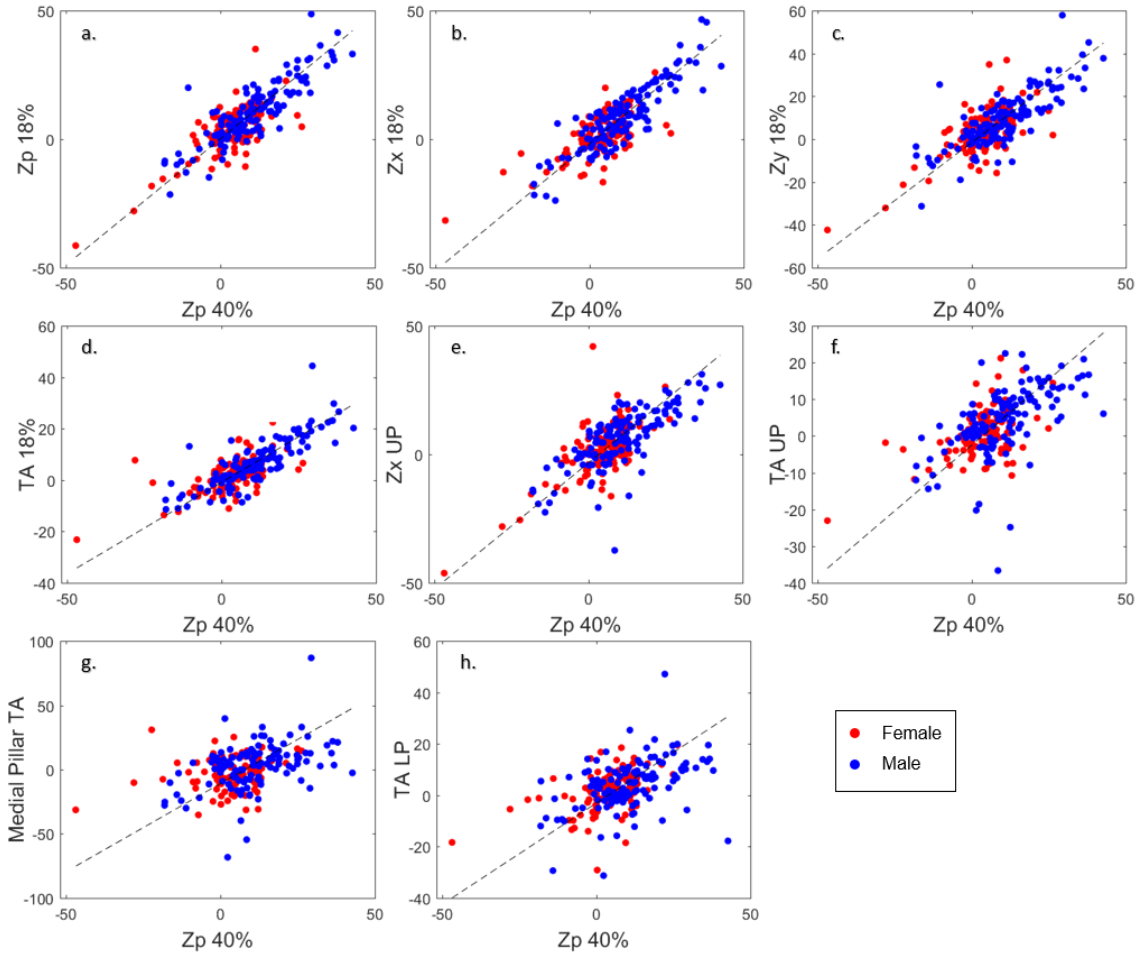

Figure 3-8 Sex differences in centroid size asymmetry. See Table 3-4 for statistics.

3.3.2.1 Sex within Population

The results discussed above appear to be primarily due to significant differences between the sexes in the three Native American populations, especially the Indian Knoll population. Table 3-5 below shows sex differences within populations, highlighting those that are significant. These are presented graphically in Figure 3-9. As discussed in section 3.3.1 above, the Indian Knoll population has significantly higher asymmetry than other groups. However, within this population the sexes diverge significantly. Especially high

asymmetry is found in males in this population. This is statistically significant for all cross-sectional properties at 18%, as well as Zx at both the upper and lower pillar. This effect is also seen in the proximal sections of the Puye (Zp 40%, Zp and Zx 18%), as well as a selection of properties in the Illinois, although in the Illinois it appears to involve TA more than section moduli (significant differences in Zx of 18%, as well as TA of 18%, UP, LP, and the medial pillar).

Table 3-5 Sex differences within populations. Letters represent significance levels of Mann-Whitney U test. a=p<0.001, b=p<0.01, c=p<0.05.

	Black F / M	**White** F / M	**Indian Knoll** F / M	**Illinois** F / M	**Puye** F / M	**Lisht** F / M
Zp 40%	2.45/2.12	5.16/7.82	**10.04/22.7[b]**	2.12/7.2	**5.65/15.08[b]**	0.23/2.95
Zp 18%	3.45/4.62	4.56/7.81	**7.13/21.66[b]**	4.62/9.6	**4.06/12.56[b]**	1.51/0.59
Zx 18%	1.27/-0.82	2.76/5.27	**7.6/20.05[c]**	**-0.82/7.63[c]**	**3.31/11.33[b]**	-1.09/3.72
Zy 18%	1.81/1.82	2.66/7.07	**11.26/21.3[c]**	1.82/8.45	3.74/8.78	4.36/-1.73
TA 18%	1.16/-0.23	2.09/4.33	**5.16/13.81[b]**	**-0.23/6.86[a]**	3.69/8.1	1.05/-0.2
Zp UP	2.25/3.27	1.72/1.99	13.78/15.51	3.27/3.62	5.87/3.93	0.56/-5.09
Zx UP	0.41/1.28	1.44/2.43	**5.79/16.39[c]**	1.28/4.76	5.34/4.48	-1.8/5.25
Zy UP	1.75/1.58	0.64/0.95	14.28/14.3	1.58/2.25	5.43/1.6	0.71/-7.13
TA UP	1.96/-1.79	1.56/3.82	2.96/9.67	**-1.79/5.54[b]**	3.47/3.89	-1.6/-2.71
Zp LP	3.33/2.5	3.35/1.58	10.08/11.32	2.5/-2.87	3.98/4.86	-2.45/-6.33
Zx LP	5.06/5.62	4.65/3.17	**4.78/17.38[b]**	5.62/4.41	9.68/15.28	6.01/-3.98
Zy LP	3.44/1.96	2.82/1.34	11.61/10.01	1.96/-3.78	2.92/3.56	-2.95/-6.99
TA LP	2.76/-0.99	2.44/2.21	-0.28/7.23	**-0.99/5.24[b]**	4.49/6.54	-2.69/-1.77
Medial Pillar	-2.06/-12.25	-1.44/-0.11	-5.14/3.98	**-12.25/4.49[b]**	2.43/7.38	-9.38/-9.52
Lateral Pillar	4.44/4.63	5.5/6.23	-1.11/6.27	4.63/9.53	7.32/-2.89	-2.79/-2.18
18% Cz	0.81/0.5	0.64/0.67	1.83/2.19	0.5/1.06	1.6/1.43	1.04/0.56
10% Cz	0.64/0.72	0.74/0.53	1.62/1.94	0.72/0.6	1.69/0.76	0.61/1.1
Periarticular Cz	0.36/0.52	0.47/0.39	1.34/1.29	0.52/0.26	1.45/-0.2	-0.13/-0.04
Articular Cz	1.04/1.01	0.96/0.66	2.21/2.35	1.01/1.24	2.17/0.94	1.66/2.77
Trochlear Cz	1.16/1.14	0.98/0.82	1.32/2.43	1.14/1.12	1.94/1.28	1.45/2.52

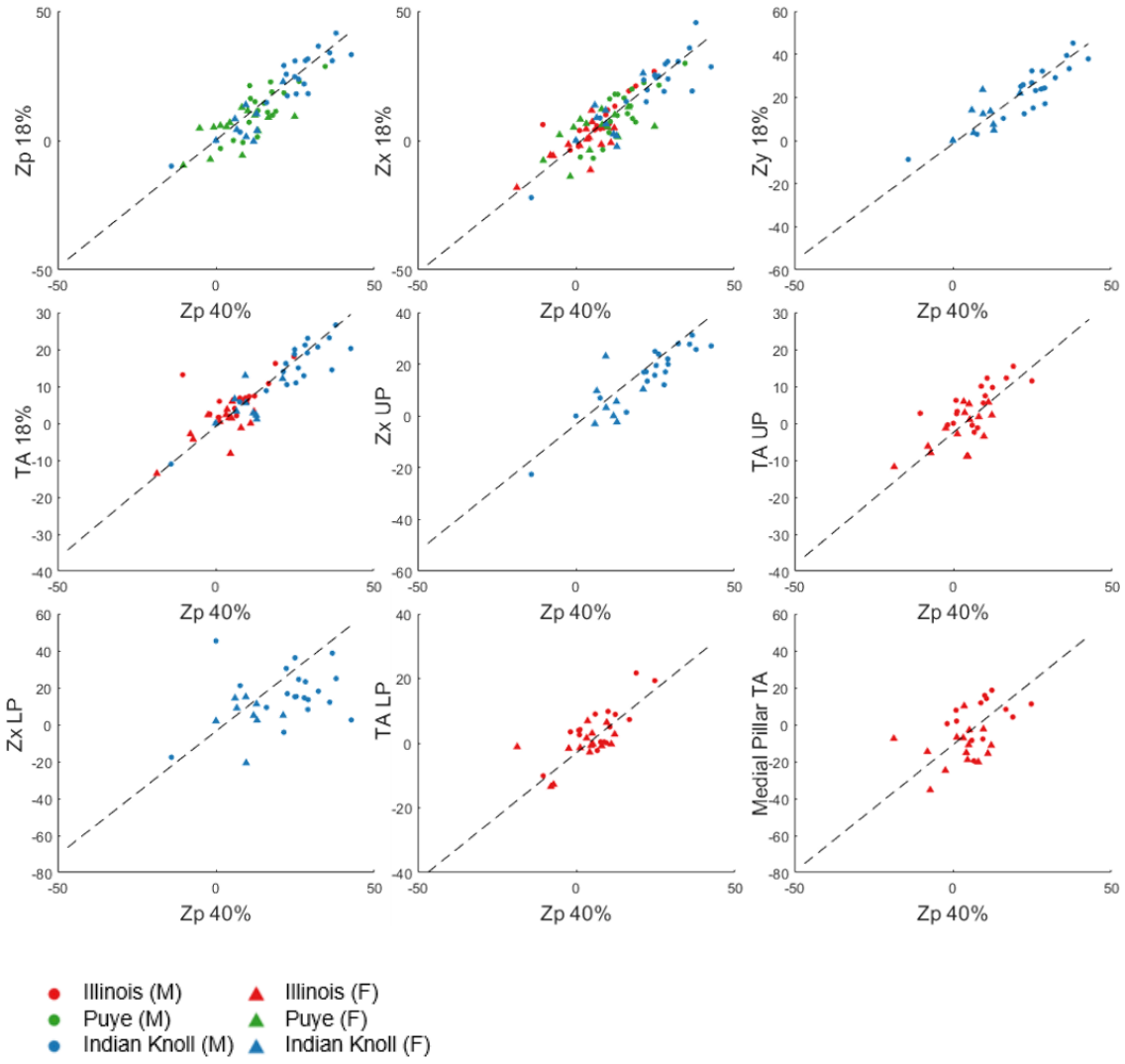

Figure 3-9 Significant sex differences within populations. See Table 3-5 for statistics.

3.4 Summary

In summary, there is significant bilateral asymmetry across the distal humerus, with a slight trend of declining asymmetry and a strong trend of declining correlation with shaft %DA moving distally. Both cross-sectional properties and centroid sizes conform to this pattern. Both cross-sectional %DA and centroid size %DA are nevertheless significantly correlated with 40% shaft asymmetry almost without

exception. There are both population and sex differences in degree of asymmetry that are potentially linked to behavioral differences. Sex differences in asymmetry (males greater) are found exclusively in the shaft and pillar regions. Strong asymmetry is particularly characteristic of the pre-agricultural Indian Knoll population, especially in males, though sex-related variation also exists within other populations.

4 Results: Geometric Morphometrics

In the literature, despite many reports of morphological differences between taxa (Knussman, 1967; McHenry and Corruccini, 1975; McHenry, 1976; Senut, 1980, 1981a; b; Senut and Tardieu, 1985; Aiello and Dean, 1990; Rose, 1993; Lague and Jungers, 1996; Bacon, 2000; Yokley and Churchill, 2006; McHenry and Brown, 2008; Lague, 2014, 2015; Rosas et al., 2015; Di Vincenzo et al., 2015), there have long been doubts that distal humeral morphology can provide locomotor or phylogenetic insights when evaluating fossil hominins (Straus, 1948; Lovejoy et al., 2016). This is largely due to the wide range of morphological variability within hominid taxa, which is substantial (Straus, 1948). However, previous studies may not have been able to fully capture important variation in distal humeral morphology due to technological constraints. These studies have in general been restricted to two dimensions (but see Tallman, 2010; Holliday and Friedl, 2013) and have relied on the ability to place individual fixed landmarks at reliably homologous points on the bone. This study re-examines distal humeral morphology in three dimensions using sliding semilandmark techniques that create a fuller picture of the distal humerus. Because different regions of the distal humerus may be impacted by different mechanical and genetic factors (Trinkaus et al., 1994; Haapasalo et al., 2000; Lieberman et al., 2001; Auerbach and Ruff, 2006; Blackburn and Knüsel, 2006; Shaw, 2011; Nadell and Shaw, 2016), this study also

considers whether these different regions vary in their power to uncover taxonomic and functional variation.

4.1 Distal 10%

4.1.1 Average Morphology

The first region considered is the distal 10% of the humerus. This region, determined by the landmarks present on the distal 10% of the average post-Procrustes position of landmarks in the full extant sample, captures both the articular and periarticular features discussed in previous studies of the distal humerus. To illustrate these differences, the average landmark positions of the human and the combined great ape sample are shown in Figure 4-1.

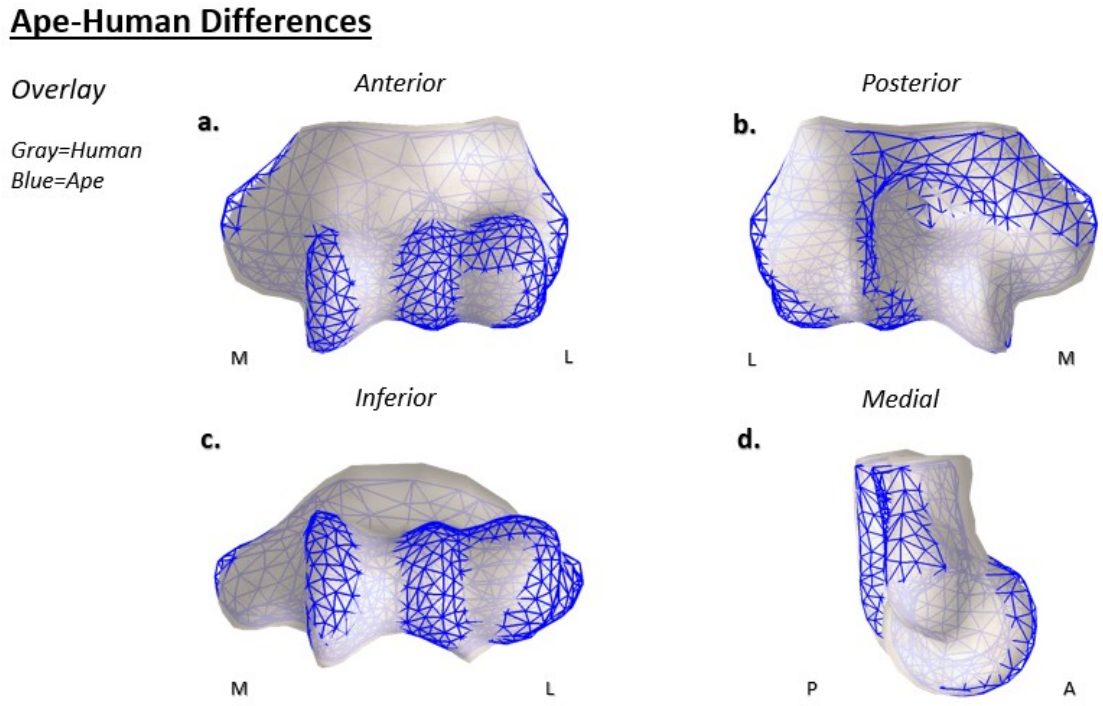

Figure 4-1 Differences between the distal 10% of the Procrustes average morphology of humans and the average shape of pooled non-human hominids.

The distal humeri of humans and great apes primarily differ in the epicondyles, the degree of articular relief, and the orientation of the periarticular region relative to the articular surface. The medial epicondyle of great apes is proximal to that of humans (Figure 4-1 a), while in humans the medial epicondyle is expanded inferiorly. Humans show less articular relief than great apes, particularly observable in the low profile of the lateral trochlear crest. The medial trochlear crest of humans appears smaller anteriorly but larger posteriorly, which can be understood as a shift in the position of this feature rather than its size. The periarticular region also appears shifted relative to the articular surface. In humans, the periarticular region appears shifted and expanded anteriorly. This is particularly notable along the medial portion of the bone (Figure 4-1 d), and results in an apparent alignment of the articular axis and medial pillar, while in great apes the medial pillar appears offset posteriorly. It should, however, be noted that rotation is allowed during Procrustes superimposition, so this could equally signify a shift in the opposite direction among humans.

Figure 4-2 shows the average shape of the distal humerus for each of the extant taxa in this analysis. Because species variation within *Pan* is not significant in the subsequent analyses, their morphology is presented at the genus level. *Pongo* species are pooled due to sample size considerations, though some locomotor differences may exist between species. Gorilla species are presented individually because they differ in subsequent analyses. Differences in their average morphologies are further examined in Figure 4-3.

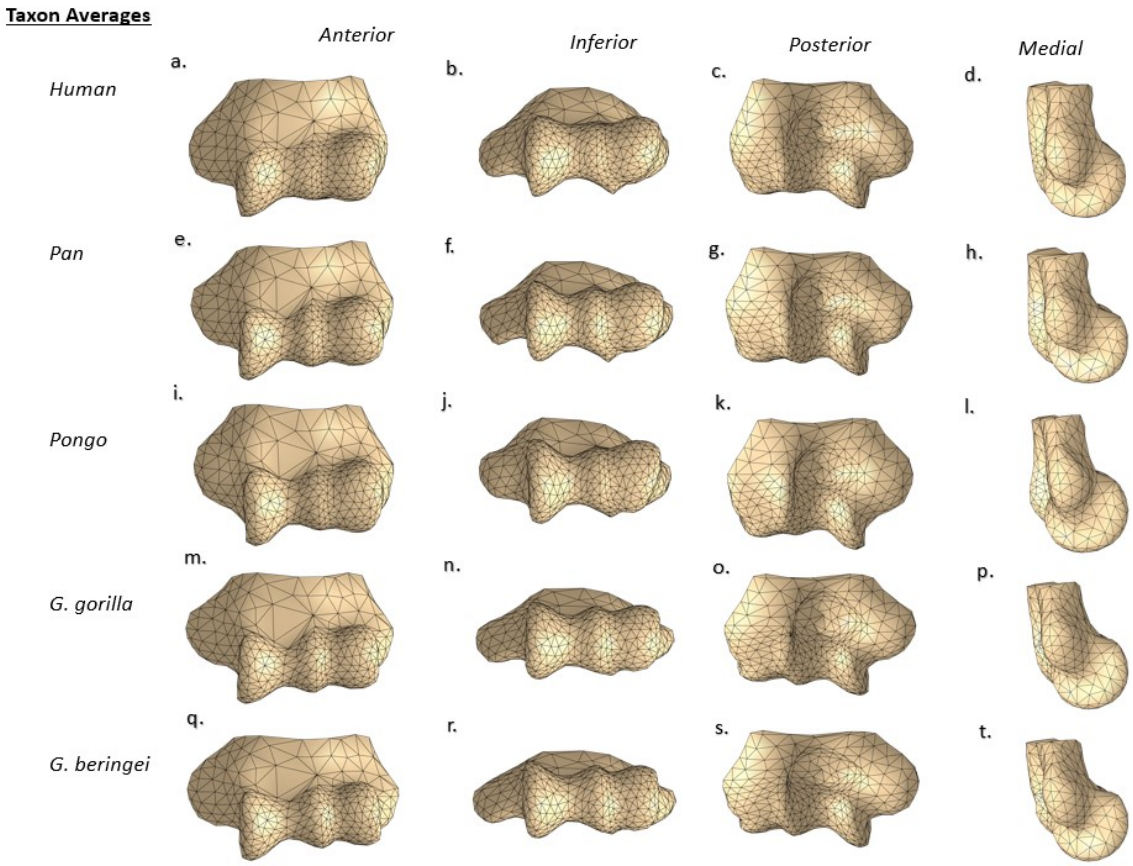

Figure 4-2 Procrustes average shape of the distal 10% of the humerus by taxon.

As noted by previous authors, differences between species are subtle. In addition to the overall human-great ape differences described above, particular traits can be noted in specific great ape taxa. Overall, apes are mediolaterally expanded relative to humans, with particularly developed lateral trochlear crests. Differences between great apes are clearest in the overall shape of the medial epicondyle (Figure 4-2 column 1). In *Pan* and *G. gorilla*, the medial epicondyle is particularly projecting and proximally located. In *Pongo*, the epicondyle is less projecting, which is associated with decreased proximodistal tapering. In *G. beringei*, the medial epicondyle is projecting,

but does not appear to be as proximally located as in the other African apes. Subtle differences are also observable in the shape, orientation and size of the capitulum, particularly its sphericity in *Pan*, and in the overall dimensions and orientation of the articular surface, which appears proximodistally compressed in both gorilla species.

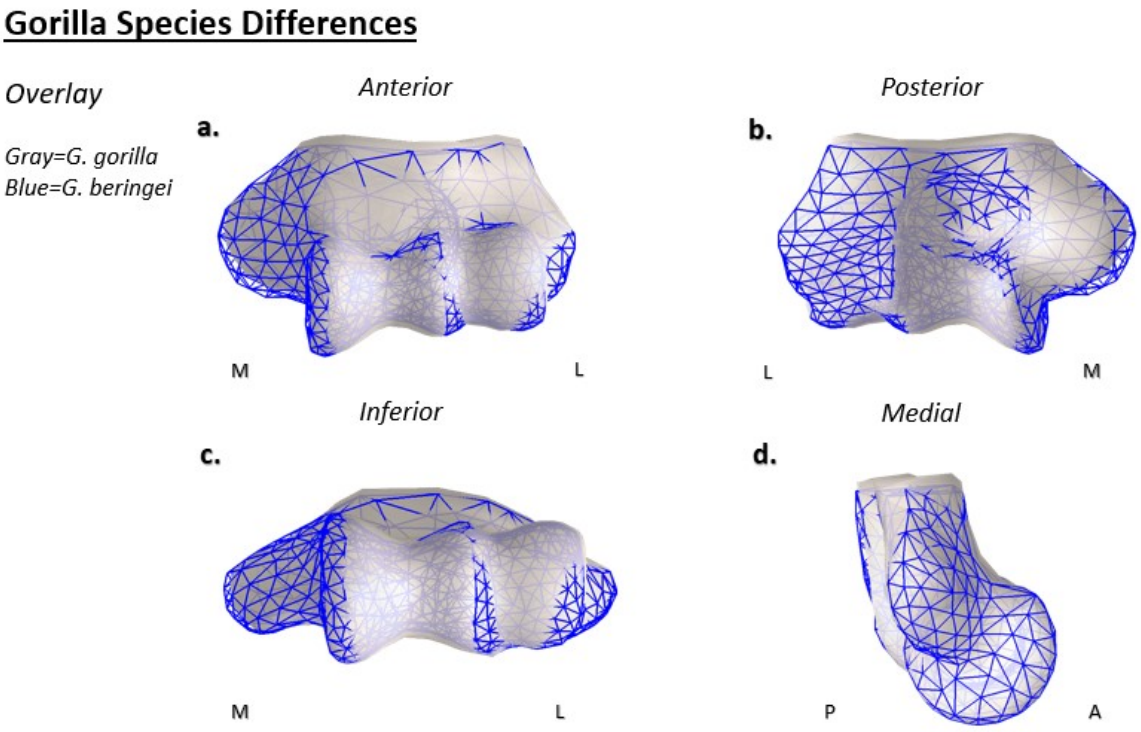

Figure 4-3 Differences between the distal 10% of the Procrustes average morphology of *G. gorilla* and *G. beringei.*

Gorilla species differ from each other primarily in the inferior expansion and greater projection of both epicondyles in *G. beringei* and the apparently shallower trochlear groove in *G. gorilla* (Figure 4-3 a). However, when overlaid, there are also sweeping subtle differences across the morphology. Because Procrustes tends to spread differences across sets of points (Zelditch et al., 2012), the apparent inferior expansion

of the epicondyles in *G. beringei* may indicate a proximal shift of the articular surface.

4.1.2 PCA

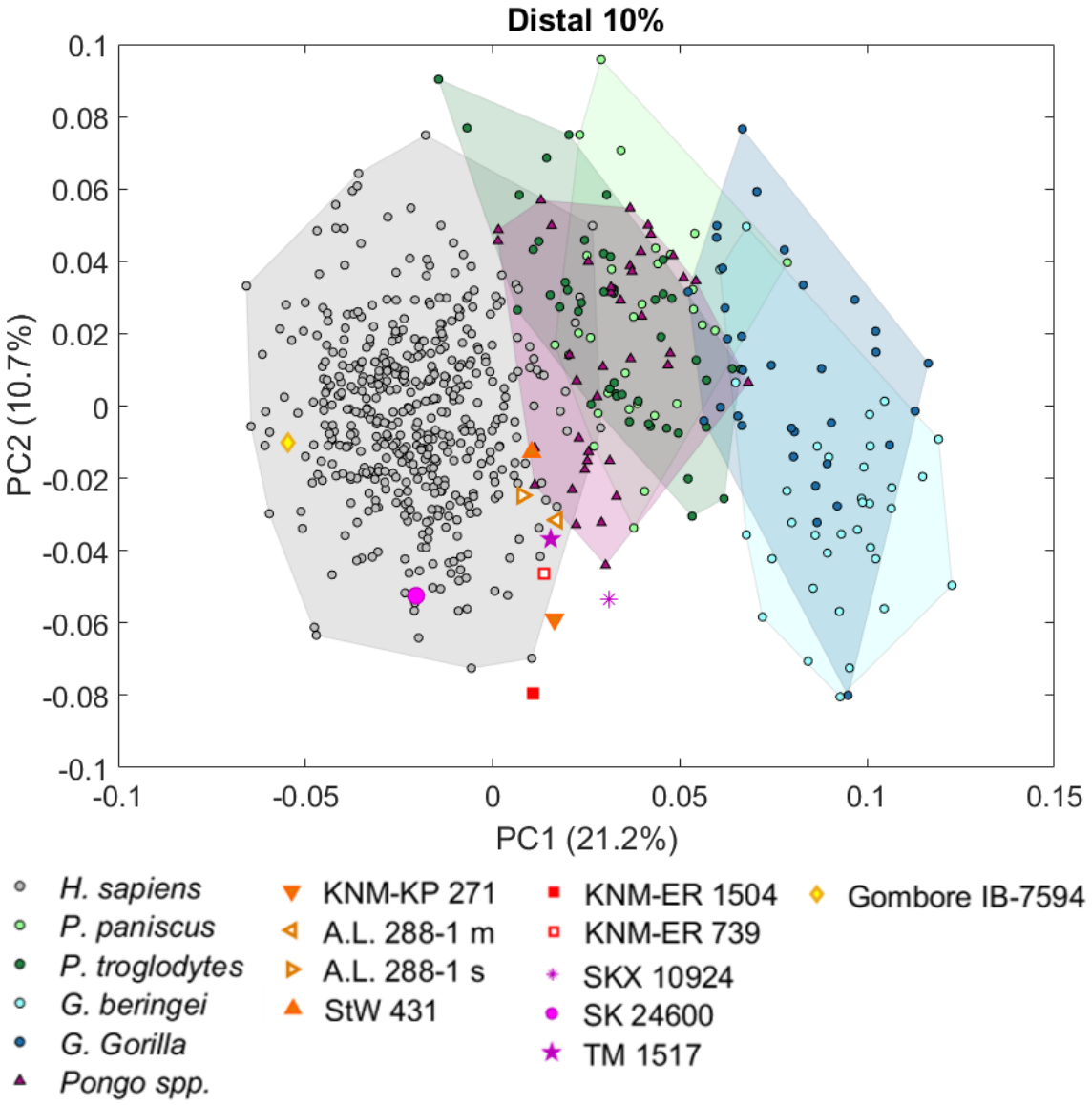
Distal 10%
PC2 (10.7%)
PC1 (21.2%)
0.1
0.08
0.06
0.04
0.02
0
-0.02
-0.04
-0.06
-0.08
-0.1
-0.1
-0.05
0
0.05
0.1
0.15
H. sapiens
P. paniscus
P. troglodytes
G. beringei
G. Gorilla
Pongo spp.
KNM-KP 271
A.L. 288-1 m
A.L. 288-1 s
StW 431
KNM-ER 1504
KNM-ER 739
SKX 10924
SK 24600
TM 1517
Gombore IB-7594

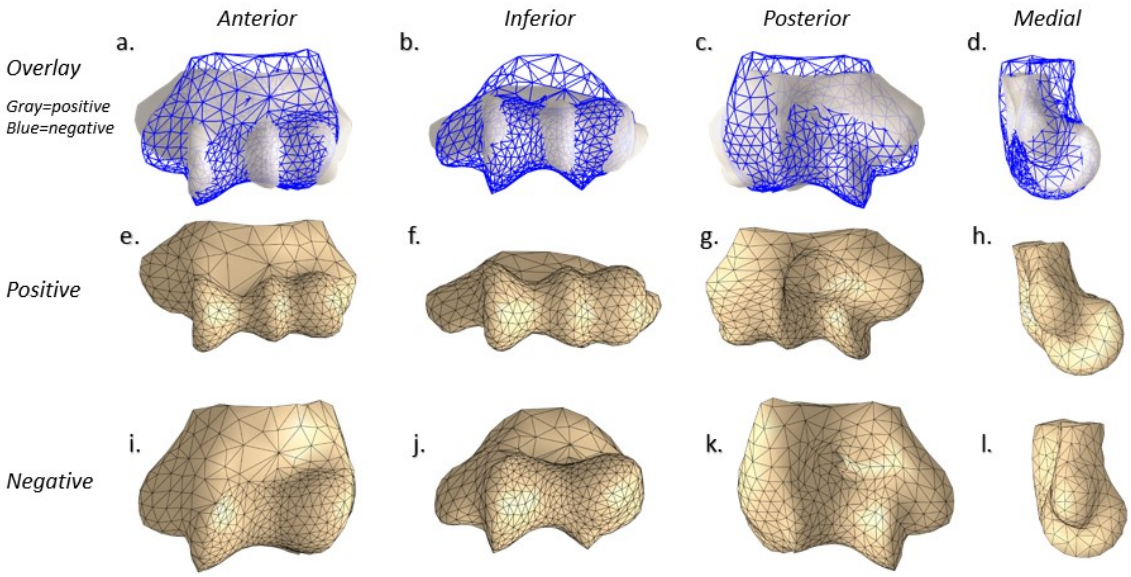

Figure 4-4 Results of the principal component analysis performed on 558 sliding landmarks on the distal 10% of the humerus, including nine fossil humeri that preserve this region. Visualizations show projected morphology at three standard deviations along PC1.

PC1 captures and accentuates the human-ape differences described above. There is a clear difference between humans (negative, Figure 4-4 row 3) and great apes (positive, Figure 4-4 row 2). There is minimal overlap between the great ape and human ranges on PC1 (Figure 4-4). Gorillas differ from the other great apes, showing an extreme form of the ape morphology. MANOVA on the collection of all PCs holding greater than 1% of the variation (17 PCs) shows a significant effect of species, and Tukey HSD post-hoc tests show highly significant differences between humans and all nonhuman hominids on PC1 ($p<0.001$). *Pongo* and both species of *Pan* are also significantly different than both species of *Gorilla* ($p<0.001$), but not from each other.

The divide between humans and nonhuman hominids is driven by prominent characteristics of both the articular and periarticular regions. As in other studies and the average morphologies described above, great apes have overall mediolateral expansion of the periarticular region, prominent epicondyles, and greater articular relief (Figure 4-4 row 1). The traits that appear to drive PC1, described in more detail below, in large part reflect the differences in the average morphologies of humans and great apes described above.

In the periarticular region, the medial epicondyle of great apes is AP narrow and positioned proximally to that of humans; it often bears an upturned cap. In humans with an analogous projection, this feature points medially or inferiorly rather than superiorly, while the medial epicondyle as a whole is AP wider and distal to that of great apes. This combination of features in humans creates the appearance of an inferior projection, while in great apes the medial epicondyle is projected parallel to the mediolateral plane. The superior portion of the medial olecranon pillar is angled anteriorly (Figure 4-4 d). In profile, the long axis of the human medial pillar appears to intersect the trochlear axis of rotation (Figure 4-4 d). In great apes the pillar is ML narrower relative to humans, and its superior portion is angled posteriorly. This reflects an overall anterior shift of the ape trochlea, while the human trochlea lies in line with the periarticular surface. Not apparent in the average morphologies, but frequently commented on in the literature, the human olecranon fossa is wide, with sloping walls that blend into the articular surface (Figure 4-4 k), while the olecranon fossa of great apes is deep, narrow, and

clearly defined (Figure 4-4 g). Like the olecranon fossa, the posterior trochlea of humans is broad, while that of apes is narrow, with a prominent and extended lateral crest.

Differences between human and great ape articular morphology appear to be driven largely by relative development of the trochlear crests. Great apes have a prominent lateral trochlear crest, which creates the appearance of a deep zona conoidea and trochlear groove. In humans, this crest is significantly reduced (Figure 4-4 i, j), and in individuals that fall at the negative observed extremes of PC1, results in a morphology where the trochlea is nearly continuous with the capitulum. This morphology is true to observed morphology in humans. An example is shown in Figure 4-5 below.

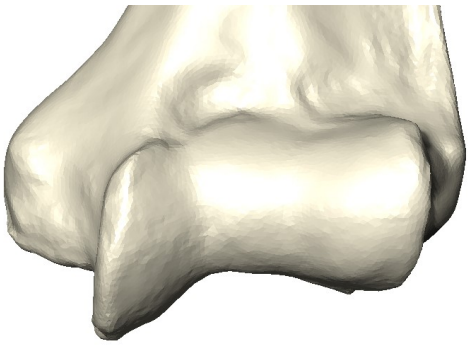

Figure 4-5 Example of low articular relief in humans, a male from the Terry (Black) population.

The trochlear groove also appears deeper in great apes because the medial trochlear surface has a sharper incline and is taller than that of humans on the anterior surface. On the inferior and posterior surface, the medial trochlea of great apes does not project as far inferiorly and posteriorly as in humans, in part due to the general anterior shift in the position of the trochlea. In great apes, both trochlear crests are

orthogonal to the axis of the articular surface, while in humans the medial trochlear crest is sharply angled, pointing inferomedially, away from the capitulum. This can also be seen in the taxon-specific average morphologies (Figure 4-2 a), though it was not noted as one of the most obvious differences. In great apes, the capitular surface itself extends farther posteriorly and remains broad on the inferior surface than in humans (Figure 4-4 f), where the capitular border angles towards the trochlea and terminates on the inferior portion of the bone.

Fossil hominins, with the exception of IB-7594 and SK 24600, fall near the positive (more ape-like) edge of the human range near its overlap with *Pan* and *Pongo*, indicating a somewhat intermediate morphology in these traits. However Gombore IB-7954 (*H. erectus*), falls on the extreme negative end of the human range. This appears to be driven by the orientation of the trochlea relative to the medial epicondyle and medial olecranon pillar; in IB-7594, as in humans, these features are in one plane, while in great apes the anterior surface is set anteriorly and the medial pillar posteriorly. IB-7594 also has a markedly angled medial trochlear crest, large olecranon fossa, wide posterior trochlea, and abbreviated capitulum, though damage to this last feature may have some influence on our results. SK 24600 also falls within the human range along PC1. Like IB-7594, it shares the human-type relative position of the medial pillar and trochlea; it also has an inferiorly elongated medial epicondyle, relatively low lateral trochlear crest and wide posterior trochlea.

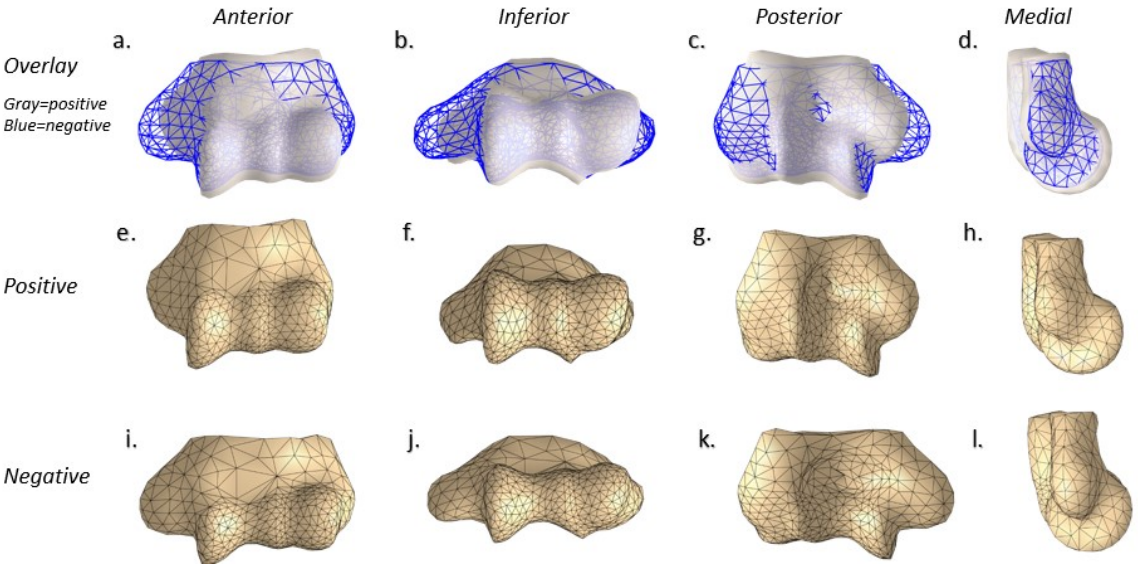

Figure 4-6 Visualizations of projected morphology at three standard deviations along PC2.

Humans and great apes overlap broadly along PC2 (Figure 4-4), though humans are significantly lower than both species of *Pan* ($p<0.001$), and have a smaller but significant difference with *Pongo* and *G. gorilla* ($p<0.05$). The latter two taxa have a higher mean position on PC2. *G. beringei* is the only group lower than humans on PC2. In fact, *G. beringei* is significantly lower on PC2 than all other groups, including *G. gorilla* ($p<0.001$). *Gorilla gorilla* is not significantly different from the other great apes, nor are they different from each other.

Humans and *G. beringei* are the only two species whose means plot negatively on PC2. This positioning is particularly noticeable in *G. beringei*, which differs significantly from all other great apes. PC2 generally captures relative mediolateral to anteroposterior proportions of the articular and periarticular surfaces (Figure 4-6). Negative scores on PC2 indicate an ML wide periarticular surface with AP and

proximodistal narrowing of the articular surface. This essentially indicates a smaller articulation relative to the periarticular surface for negative PC2 scores. The positive values of PC2 seen in *Pan* and *G. gorilla* correspond to relative AP thickening, particularly of the articular surface. Compared to *G. gorilla* and other groups, *G. beringei* has a slightly larger medial epicondyle, expanding the mediolateral proportions of the periarticular region. AP and proximodistal attenuation of the articular surface in *G. beringei* and deepening of the trochlear groove (see Figure 4-2, Figure 4-3) drive its negative position on PC2. While the human mean on PC2 is slightly below zero, the human range encompasses nearly the entire ape range. This suggests that in humans, these traits are variable either due to variation in the mechanical demands of manipulative tasks, or due to the absence of locomotor constraints. This contrasts with the results for *G. beringei*, whose range of variation is more constrained, though a small number of outliers lead to the appearance of significant overlap with *G. gorilla*.

The range of the fossils along PC2 is remarkably similar to that of *G. beringei*. All fossil hominins score negative along PC2, though all except KNM-ER 1504 also fall within the human range. IB-7594 has the highest position, near the mean for modern humans. The exceptionally low position of KNM-ER 1504 on PC2 appears to be driven by an articular surface that is particularly AP and proximodistally attenuated (see images in Chapter 1 and Chapter 2), especially in relation to prominently projecting epicondyles. However, while attenuation of the articular surface appears to be driven by depth of the

trochlea in *G. beringei*, in KNM-ER 1504 this attenuation is at least partially driven by the low profile of the trochlear crests.

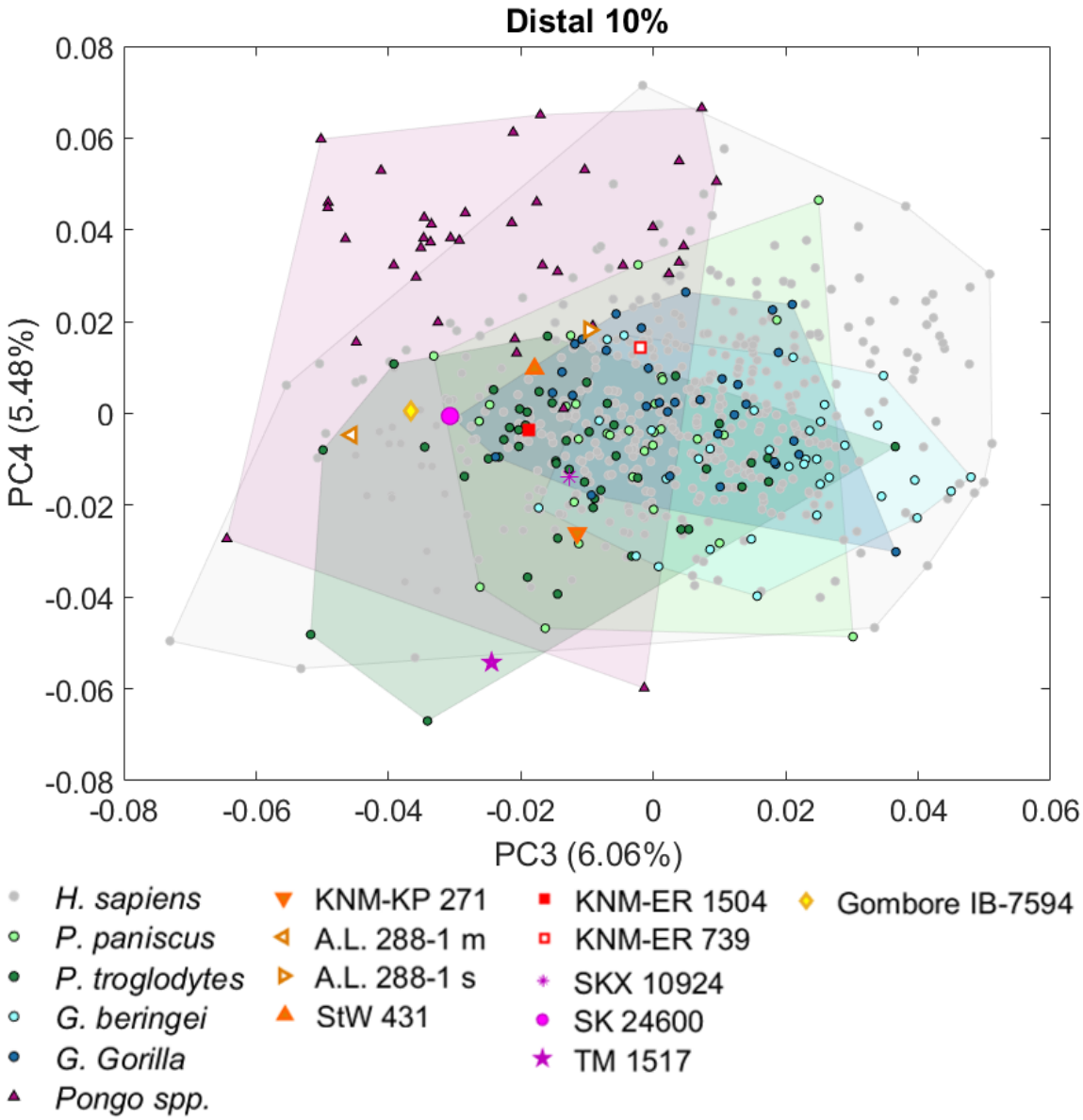

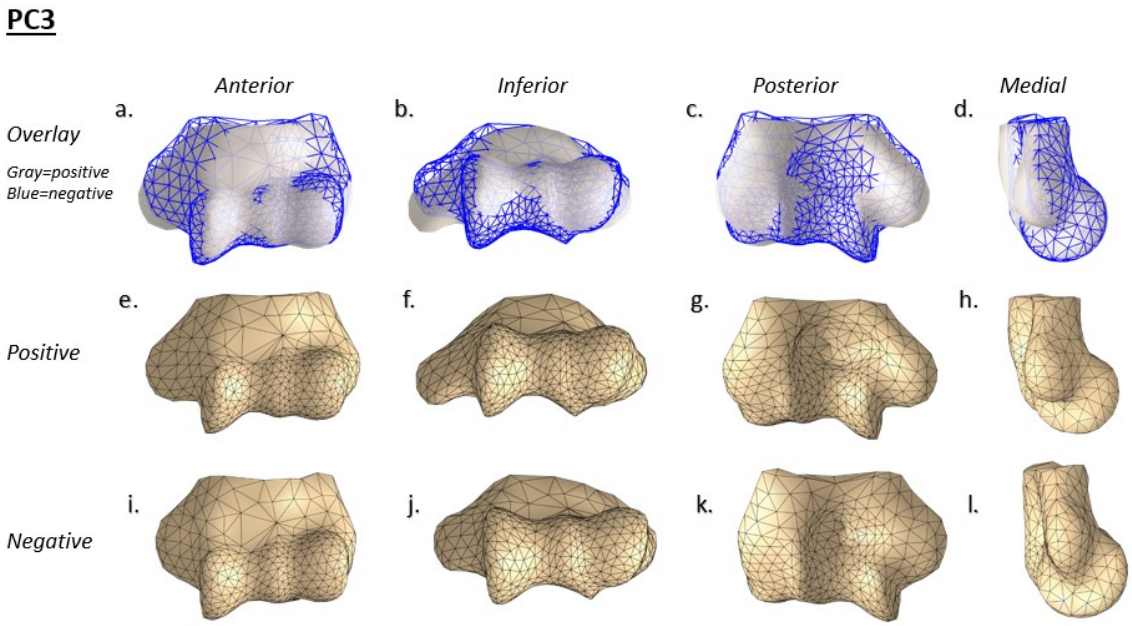

Figure 4-7 PCs 3 and 4 for the 558 landmarks on the distal 10% of the humerus. Visualizations show the projected shape at three standard deviations along PC3.

As on PC2, *G. beringei* are significantly different from all other groups along PC3 (*H. sapiens, P. paniscus, P. troglodytes* $p<0.001$, *G. gorilla* $p<0.01$) (Figure 4-7). PC3 also divides *Pongo* from all other species (*H. sapiens, P. paniscus, G. gorilla, G. beringei* $p<0.001$, *P. troglodytes* $p<0.01$), though this distinction is less apparent. As on PC2, humans have a broad range along this axis, overlapping with each of the great ape species, but significantly different from *P. troglodytes* ($p<0.01$) in addition to *Pongo*.

Gorillas are positive on PC3, as is the mean for modern humans, while *Pan* and especially *Pongo* are negative. At the positive extreme of PC3, the medial and lateral portions of the periarticular surface are extended posteriorly, creating a curved profile with the olecranon fossa as its inflection point Figure 4-7 column 2). This is driven by posterior extension of the medial epicondyle and inflation of the lateral olecranon pillar.

The olecranon fossa is large and deep. It is particularly expanded medially. For these positive values of PC3, the articular surface appears mediolaterally compressed; this is due to a narrower medial trochlea and capitulum. The narrowed capitulum is also particularly convex.

The high position of gorillas, and especially *G. beringei*, is driven by mediolateral compression of the capitulum. *G. beringei* also has a posteriorly angled medial epicondyle and a slight bulge of the lateral pillar, as well as a deep olecranon fossa and sharply angled medial trochlea.

Pongo's low position on PC3 is driven by the position of its epicondyle; while the medial epicondyle of humans and African apes is angled posteriorly, the medial epicondyle of orangutans is roughly parallel with the articular surface. This is also observable in the average morphologies (Figure 4-2 j). In addition, the lateral pillar of *Pongo* is concave, compared to the posterior bulging of the human lateral pillar; this trait also contributes to a negative score on PC3.

While humans have only a slight posterior angle to the medial epicondyle (Figure 4-2 b), they have a strong posterior swelling of the lateral pillar, explaining their slightly positive average on PC3. While many humans have characteristics captured by PC3, these traits do not appear tightly linked within modern humans. This partially explains the wide range of variation of the human range on PC3.

All fossils score negative on PC3, near the orangutans and unlike the majority of the human sample. KNM-ER 739 is closest to the average human, while IB-7594 and A.L.

288-1m are near the negative extreme of the human range. This is likely due to the position of the medial epicondyle; in the fossils, this feature is less posteriorly angled than for the average modern human (see images in Chapters 1 and 2). Neither do the fossils have dramatic swelling of the lateral olecranon pillar, though this trait varies between specimens.

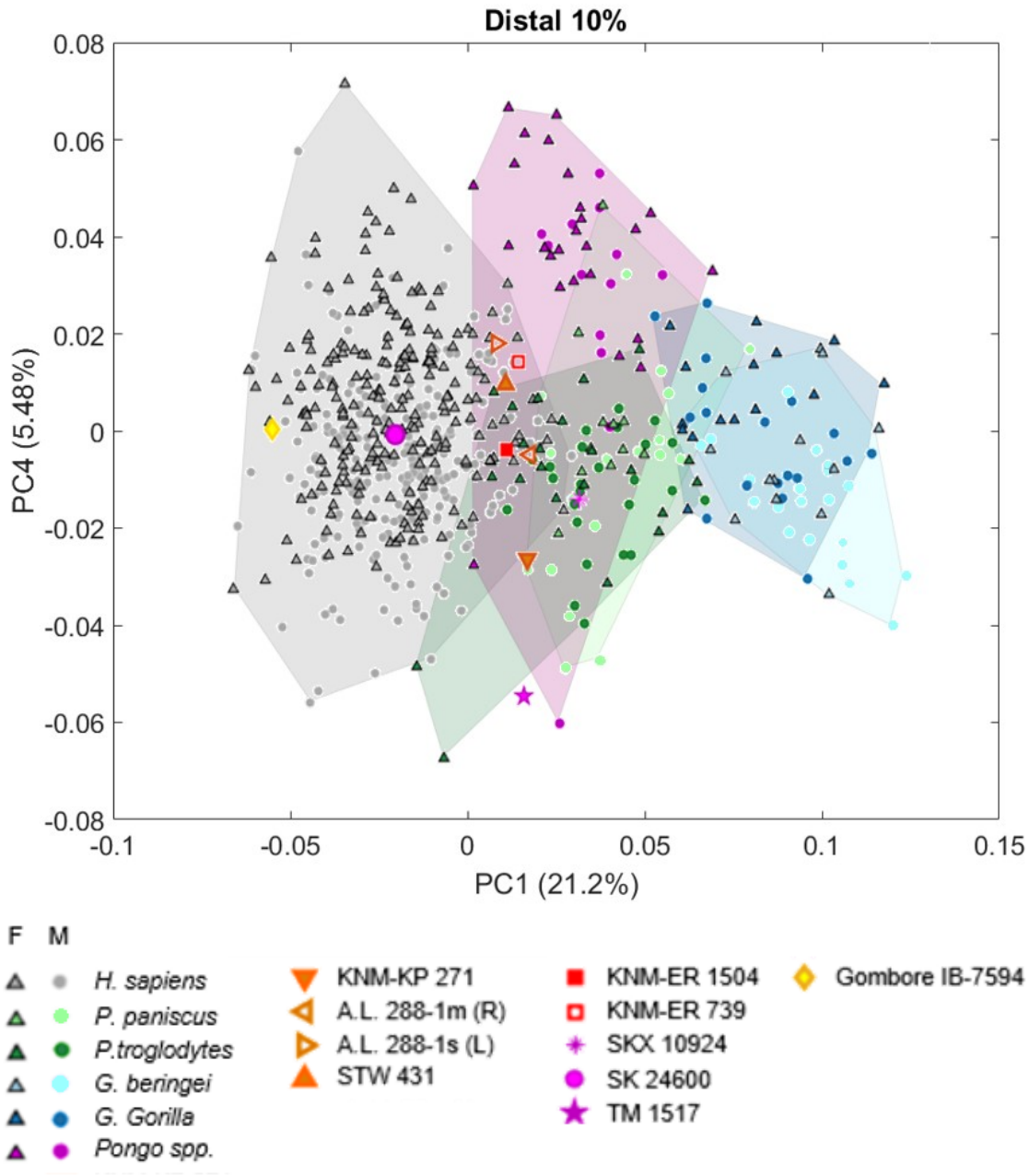
Distal 10%
PC4 (5.48%)
PC1 (21.2%)
0.08
0.06
0.04
0.02
0
-0.02
-0.04
-0.06
-0.08
-0.1
-0.05
0
0.05
0.1
0.15
F M
H. sapiens
P. paniscus
P.troglodytes
G. beringei
G. Gorilla
Pongo spp.
KNM-KP 271
A.L. 288-1m (R)
A.L. 288-1s (L)
STW 431
KNM-ER 1504
KNM-ER 739
SKX 10924
SK 24600
TM 1517
Gombore IB-7594

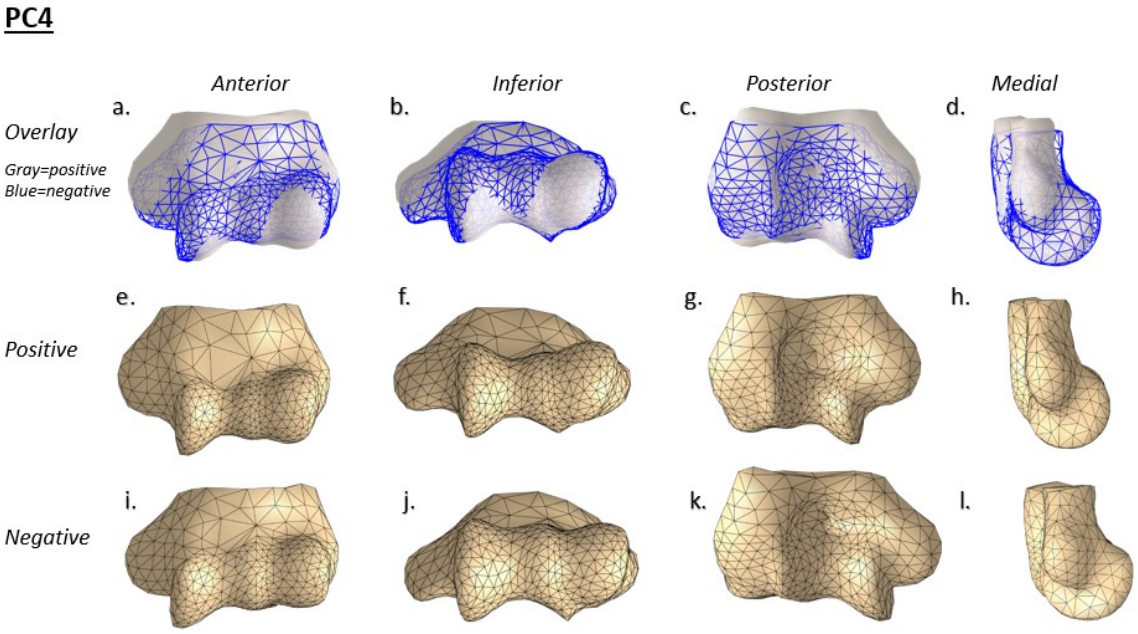

Figure 4-8 PC1 vs PC4, highlighting sex differences on PC4. Visualizations of projected morphology at three standard deviations along PC4.

Pongo has significantly higher values on PC4 than all other species ($p<0.0001$); this is the clearest difference between groups captured on this axis (Figure 4-8). The means of *P. troglodytes* and *G. beringei* are also significantly lower than *H. sapiens* and *G. gorilla* ($p<0.01$). There is also a significant difference on the basis of sex, with females scoring significantly higher than males overall.

Positive values of PC4 indicate a reduced trochlea and a relatively expanded medial supracondylar crest. Reduction of the trochlea occurs primarily anteriorly in the anteroposterior direction and is associated with a relative proximodistal elongation of the capitulum. The relative expansion of the medial supracondylar crest has the effect of creating a less acute angle between the medial pillar and the biepicondylar line, and is associated with proximodistal expansion of the olecranon fossa.

Pongo exhibits most of these traits. While *Pan*, *Gorilla* and humans have a relatively narrow, angled medial pillar terminating in a medially projecting medial epicondyle, the medial and lateral pillars in *Pongo* are of equivalent breadth and exhibit roughly equivalent angles of excursion; the medial epicondyle in *Pongo* is also shorter. While the trochlea of *Pongo* does not appear significantly reduced, the capitulum is superoinferiorly expanded and more ovoid compared to the more spherical condition seen in humans and African apes.

The high position of females relative to males on PC4 (Figure 4-8) appears to be driven by slight proximodistal expansion of the olecranon fossa and the capitulum. This expansion is also visible across all parts of the periarticular surface except the medial epicondyle; it may therefore be related to reduction of the medial epicondyle and trochlea rather than expansion of the surrounding area.

Fossil hominins fall below *Pongo* on PC4, unlike PC3. They are generally intermediate in these traits, with the exception of TM 1517, which appears at the negative extreme on this axis. This is likely due to its extremely short capitulum, which may be affected by damage to this feature.

4.2 Articular region

The distal 10% of the humerus was then split into two regions: the articular surface, and the periarticular surface. Analysis of the articular region alone captures much the same suite of morphological differences seen in analysis of the distal 10% of the bone. However, analysis of this region in isolation enables us to clarify potentially

divergent trends in different bone regions (i.e., articular and periarticular). Analysis of this region in isolation slightly alters our understanding of fossil hominin morphology, and allows for analysis of an additional fossil specimen (KNM-ER 6020).

4.2.1 Average Morphology

As in the previous analyses, taxa differ in their morphology. Figure 4-9 shows differences between the average human and the average nonhuman hominid.

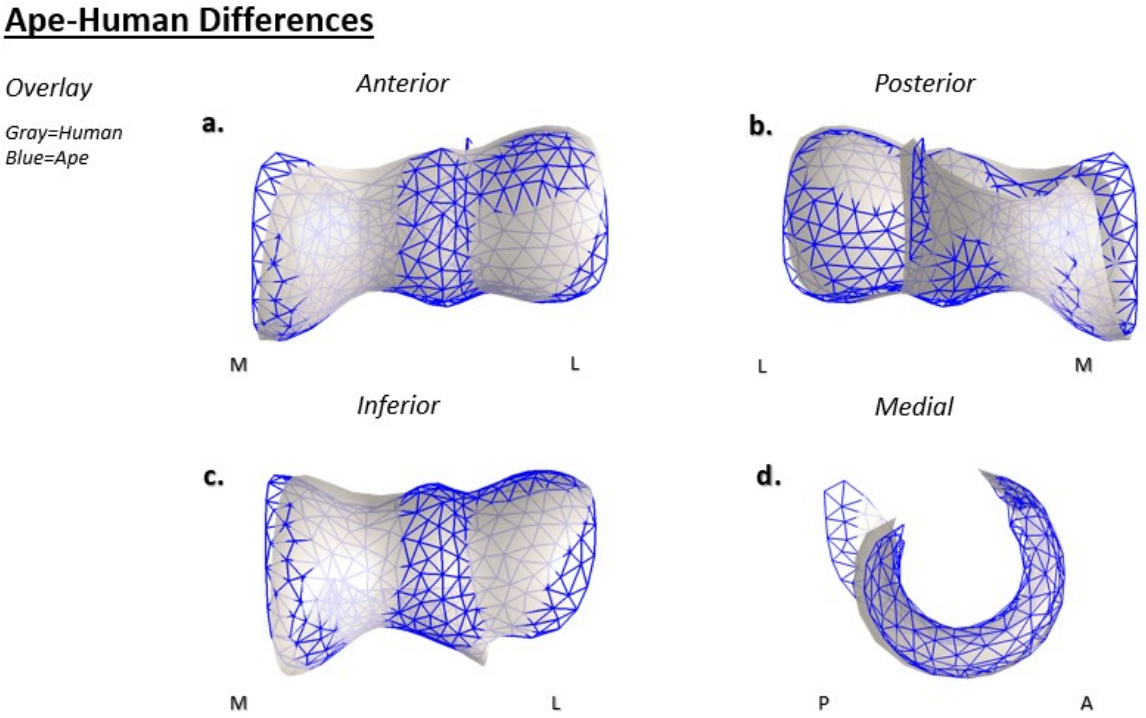

Figure 4-9 Differences between the Procrustes average articular morphology of humans and and the average shape of pooled nonhuman hominids.

The characteristics of the articular surface noted in discussion of the average shapes of the full distal 10% are again observable. The human average has lower articular relief and a lower lateral trochlear crest than great apes (Figure 4-9 a). The

trochlear groove of humans is shallow on the anterior surface but deeper in great apes (Figure 4-9 c). The edge of the articular surface also differs between human and apes. In great apes, the start of the medial and lateral trochlear crests is in roughly the same transverse plane, slightly more distal than the beginning of the capitulum (Figure 4-9 a). In humans, the beginning of the trochlear crest is further distal than in great apes, and is also more medial, creating the appearance of angulation across the proximal border of the full articulation. The posterior trochlea is slightly wider in humans than in great apes (Figure 4-9 b).In great apes the projection of the posterolateral trochlea onto the lateral wall of the olecranon fossa can be seen in the curvature of the proximolateral peak at the corner of the posterior trochlea (Figure 4-9 b).

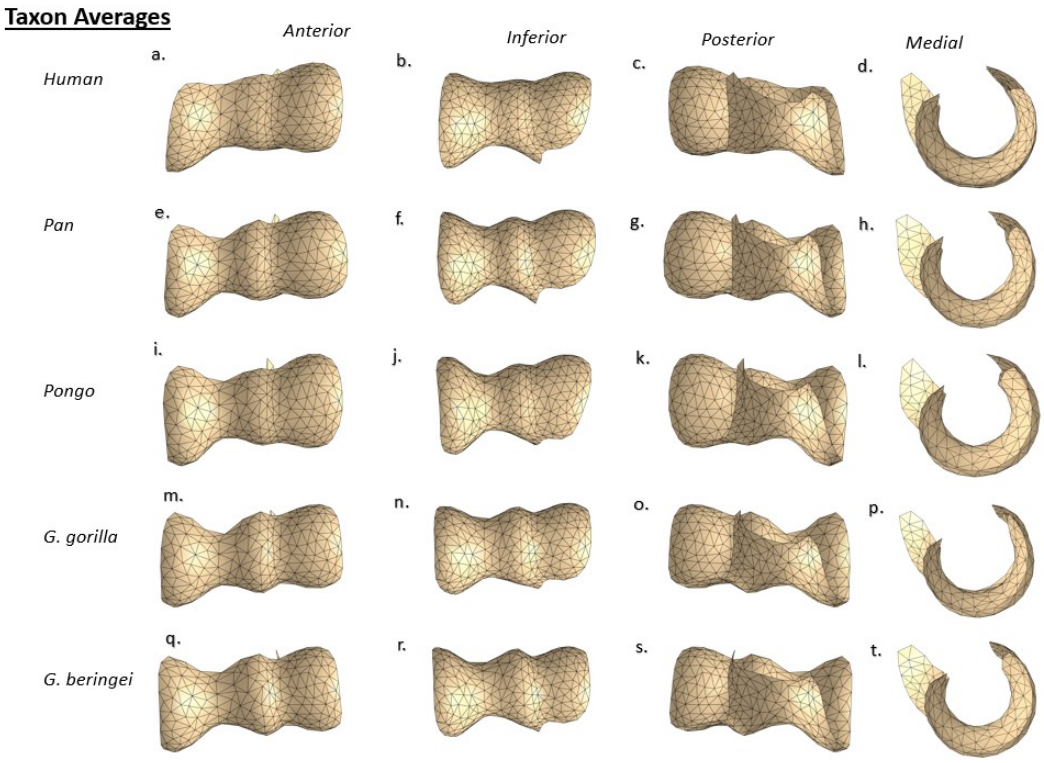

Figure 4-10 Procrustes average shape of the humeral articular surface by taxon.

Nonhuman hominids do however differ between taxa. As in the distal 10% averages, the capitulum of *Pan* is particularly spherical. In *Pongo*, it is proximodistally elongated. Also in *Pongo*, the medial half of the trochlea is large relative to its lateral part (when compared with other great apes), and the posterior trochlea is narrow (Figure 4-10 I and k). The two gorilla species have a smaller capitulum relative to the trochlea, and share a distinct narrow peak of the proximolateral corner of the posterior trochlea (evidence of extension along the lateral olecranon fossa). Unlike in analysis of the distal 10%, there are relatively few differences between *G. gorilla* and *G. beringei* (Figure 4-11 below), though the trochlear groove is slightly shallower inferiorly in *G. gorilla* and its anterior trochlear surface appears slightly more mediolaterally compressed.

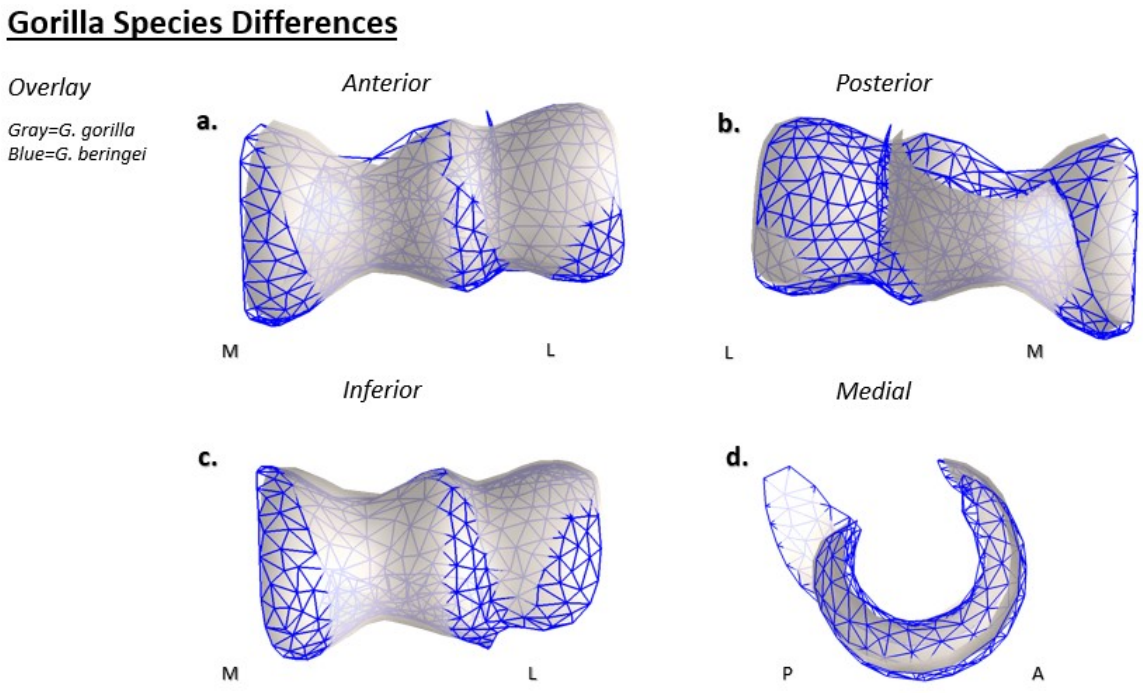

Figure 4-11 Procrustes average shape of *G. gorilla* compared to *G. beringei*.

4.2.2 PCA

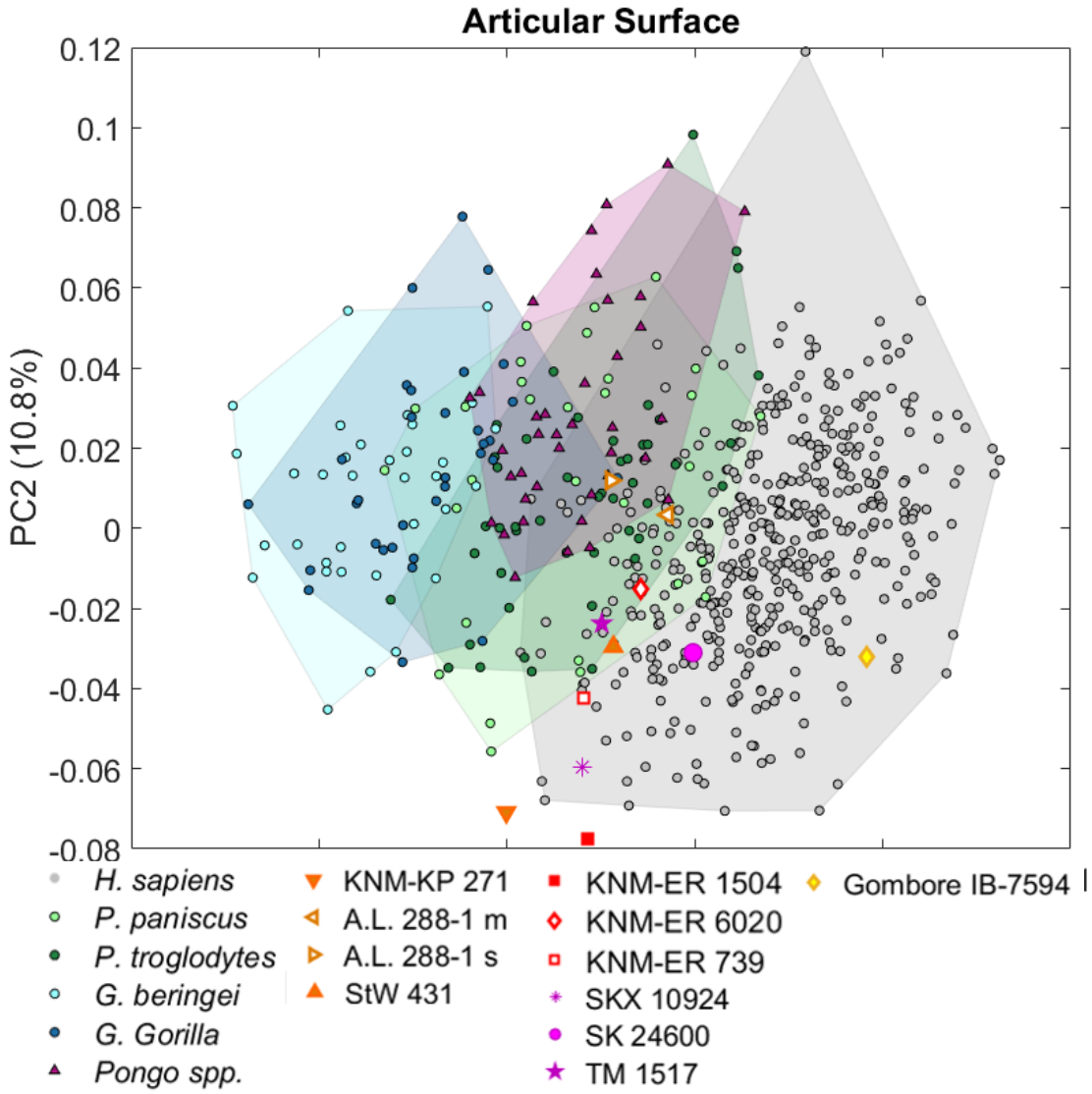
Articular Surface
PC2 (10.8%)
0.12
0.1
0.08
0.06
0.04
0.02
0
-0.02
-0.04
-0.06
-0.08
H. sapiens
P. paniscus
P. troglodytes
G. beringei
G. Gorilla
Pongo spp.
KNM-KP 271
A.L. 288-1 m
A.L. 288-1 s
StW 431
KNM-ER 1504
KNM-ER 6020
KNM-ER 739
SKX 10924
SK 24600
TM 1517
Gombore IB-7594

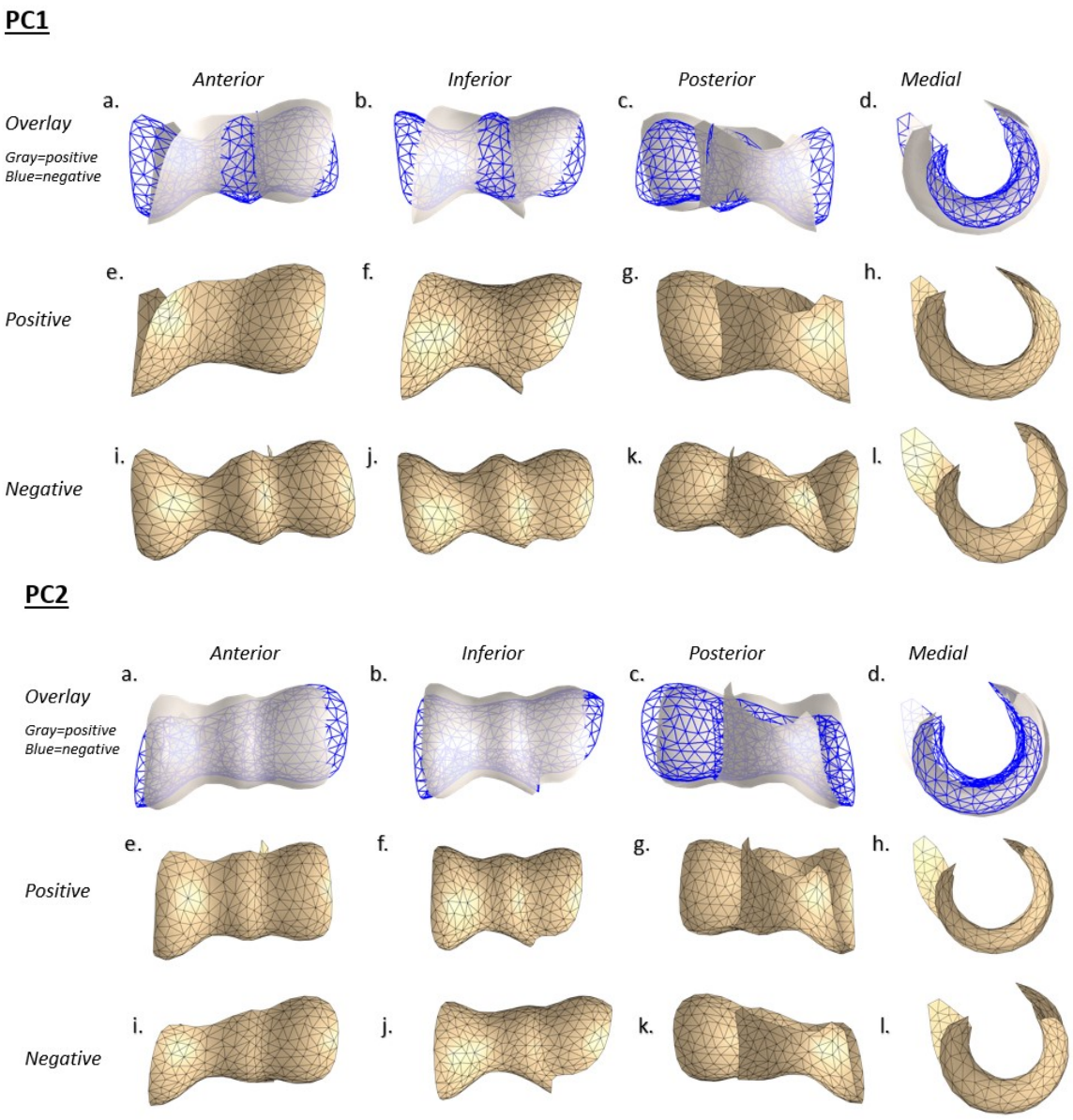

Figure 4-12 PCA of the 307 sliding landmarks on the articular surface. Visualizations show projected morphology at three standard deviations along PCs 1 and 2.

In the PCA of the articular surface, a combination of PC1 and PC2 separates humans from great apes (Fig. 2-1). The human range (positive on PC1, slightly negative on PC2) is characterized by a trochlea with low articular relief, blending gradually into a capitulum that is large anteriorly but which terminates on the inferior surface of the

bone. The human trochlea is also notable for the inferomedial angulation of the medial trochlear crest and the wide trochlea at its termination in the olecranon fossa. Great apes are characterized by relatively high articular relief and a capitulum that extends across the entire inferior aspect of the bone, as well as a trochlea that is markedly narrow at its termination and curves onto the lateral wall of the olecranon fossa.

There is some evidence of a taxonomic trend in hominin articular morphology. All australopiths lie in the region where the human and nonhuman ranges overlap. A.L. 288-1 in particular lies in a region shared by humans, both species of *Pan,* and *Pongo*; her left humerus lies nearer the central *Pan* cluster than the human one due to its articular relief. As groups, *P. boisei* (KNM-ER 1504, KNM-ER 739) and *P. robustus* (SKX 10924, SK 24600, TM 1517) are farther from the great ape range and closer to modern humans. Individuals in these taxa that fall outside the human range do so in ways that are not ape-like, such as KNM-ER 1504, which has an exaggerated degree of mediolateral expansion of the articular surface (see images in Chapters 1 and 2). While the oldest *P. robustus* individual within the group (TM 1517) lies in a region of ape overlap, the other two *P. robustus* individuals do not. There is a positional difference in SKX 10924, which in the distal 10% analysis was slightly outside the human range and close to that of *Pongo*; without the inclusion of periarticular features this association disappears, highlighting the low relief and wide posterior trochlea of the human-like articular surface. As in the earlier analysis, IB-7594 is at the extreme edge of human variation and appears nearly "super-human", significantly differing from the other

fossils; this is likely due to proportions of the trochlea, but may be exaggerated by damage to the capitulum.

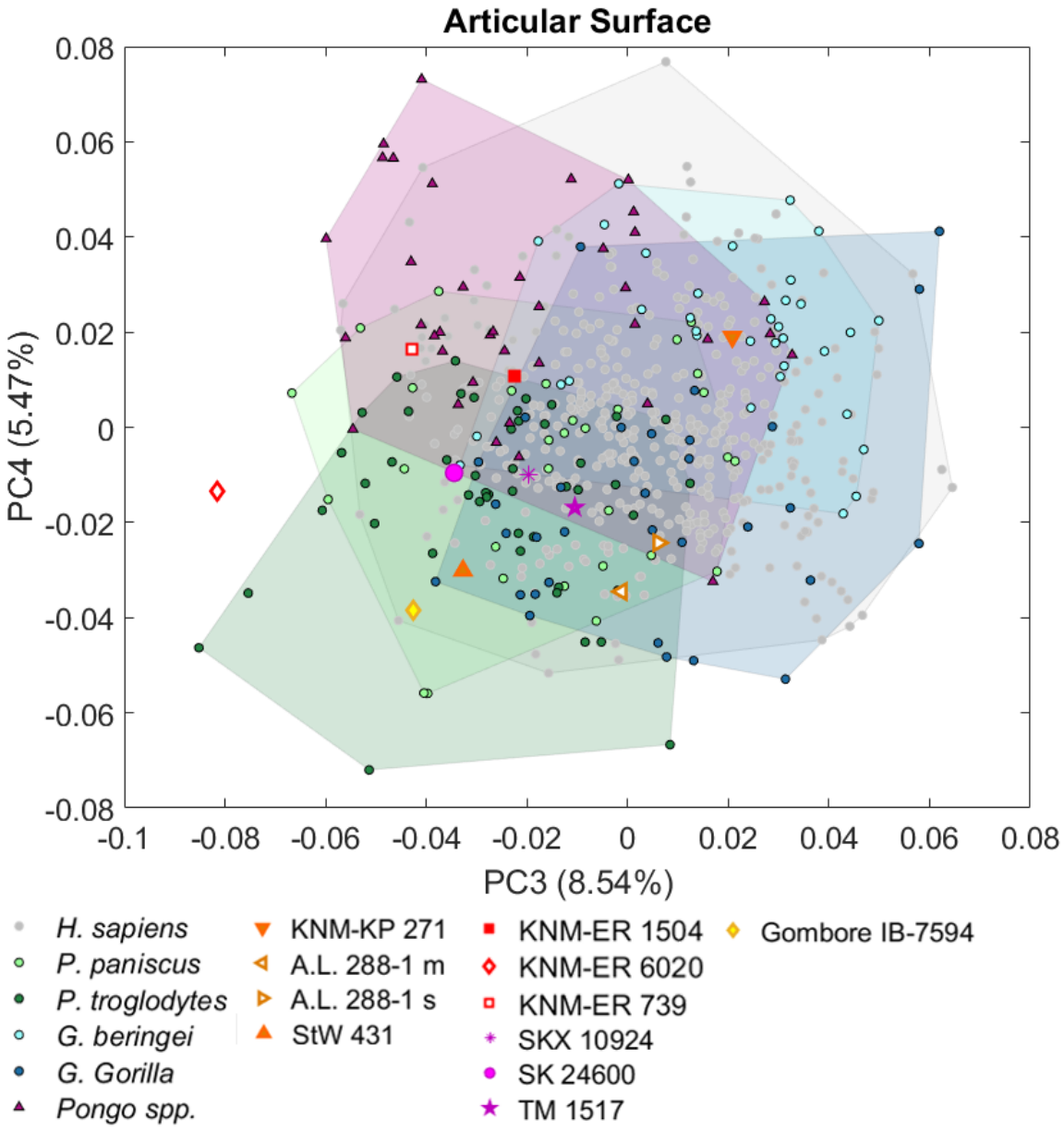

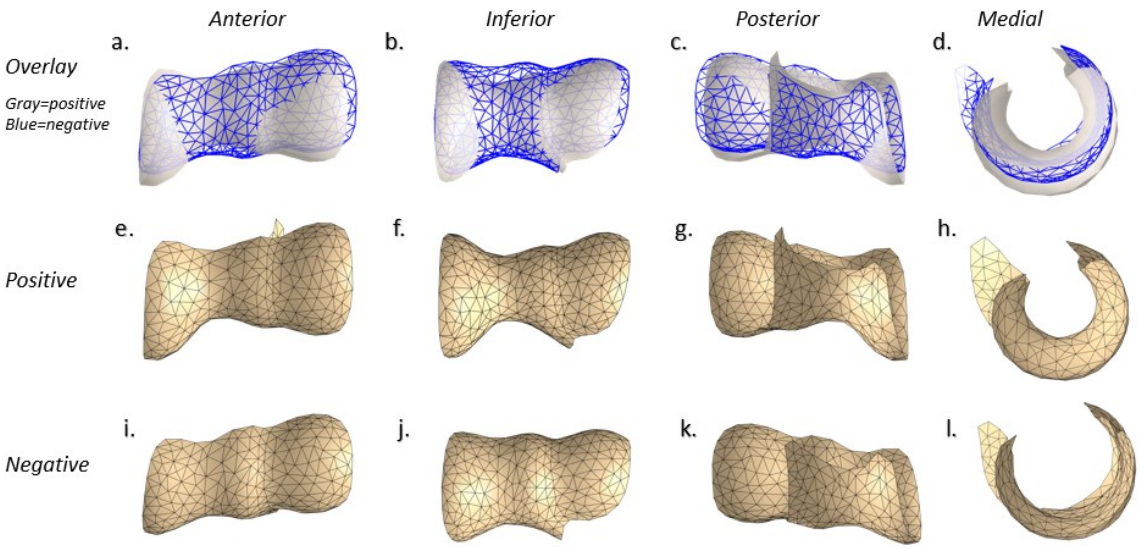

Figure 4-13 PCA of the 307 sliding landmarks on the articular surface. Visualizations show projected morphology at three standard deviations along PC 4.

The other PC of particular interest is PC4 (Figure 4-13), which quantifies depth of the trochlear groove as well as exaggeration of the medial relative to the lateral trochlear crest. This PC distinguishes *Pongo* and *G. beringei* from all other groups ($p<0.0001$). This supports suggestions above that the apparent attenuation of the *G. beringei* articular surface along PC2 of the 10% analysis is due to a pronounced trochlear groove. The trochlear groove is likewise more pronounced in *Pongo*, but the AP breadth of the articular surface and height of the medial trochlear crest in *Pongo* overshadow this trait. These traits are variable in the fossils and in humans, but are particularly pronounced in KNM-ER 1504, KNM-ER 739, and KP-271. There is no apparent temporal or taxonomic trend in these features: KNM-KP 271 (*A. anamensis*) and A.L. 288-1 (*A. afarensis*) fall on opposite ends of the distribution, and early *Homo* (IB-7594) lies nearest *A. africanus* (StW 431).

4.3 Periarticular Region

4.3.1 Average Morphology

Periarticular averages also echo differences seen in the distal 10% region. Average shapes for this region can be seen in Figure 4-14 below. Humans and nonhuman hominids differ primarily in the projection of the lateral epicondyle and position of the medial epicondyle. The anterior median surface of the periarticular region is also more projecting in humans than in great apes. In contrast with the previous analyses, when the periarticular region is considered in isolation, *Gorilla* species differ little from each other. *Pongo*, however, differs from the African apes in the orientation of the medial epicondyle (Figure 4-15 c), which is orthogonal to the periarticular surface in orangutans but posteriorly inflected in African apes.

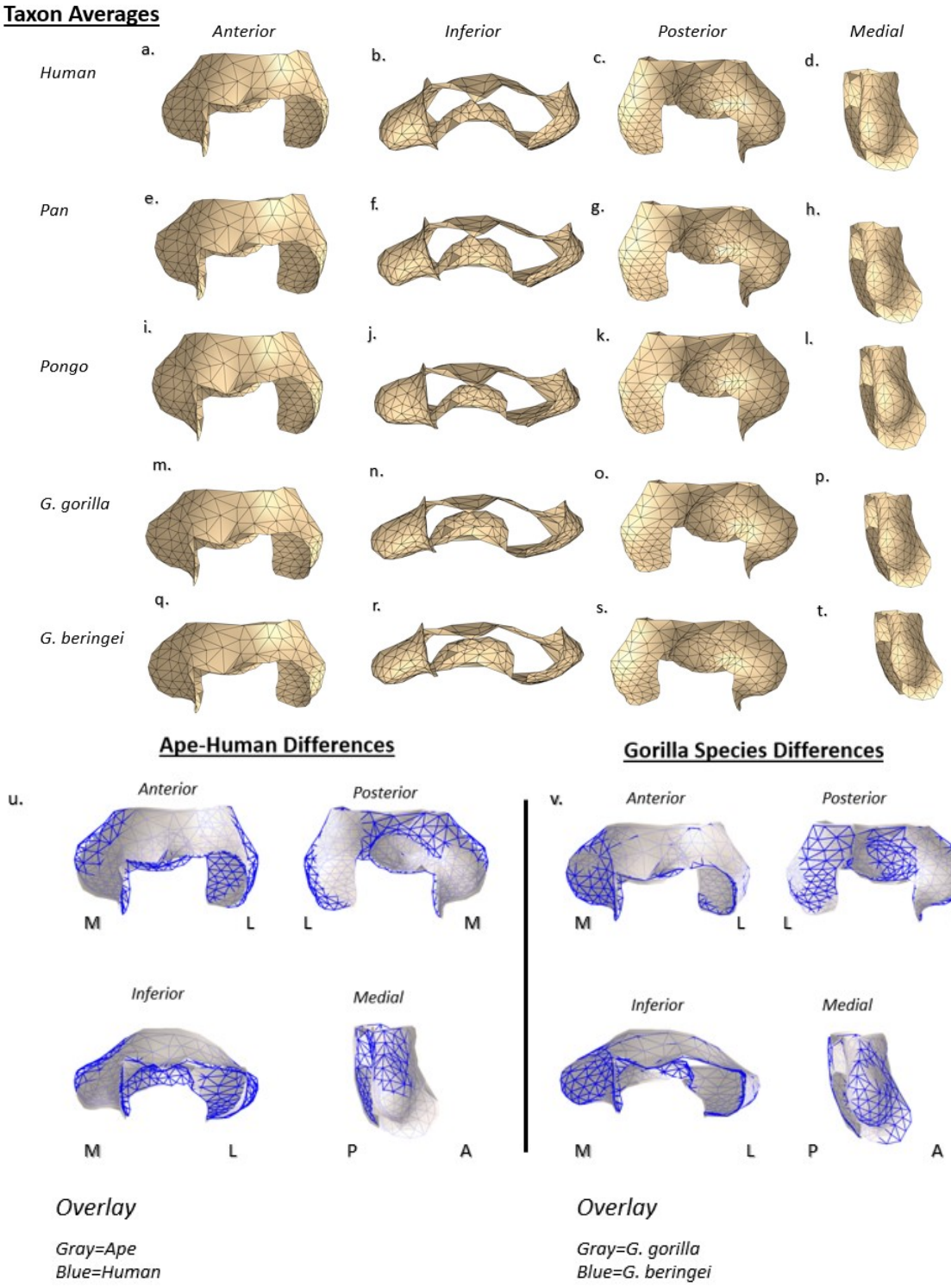

Figure 4-14 Procrustes average shape of the humeral periarticular surface by taxon. This figure also shows comparisons between a generalized great ape morphology (average shape of pooled non-human hominids) and that of humans and between the two gorilla species.

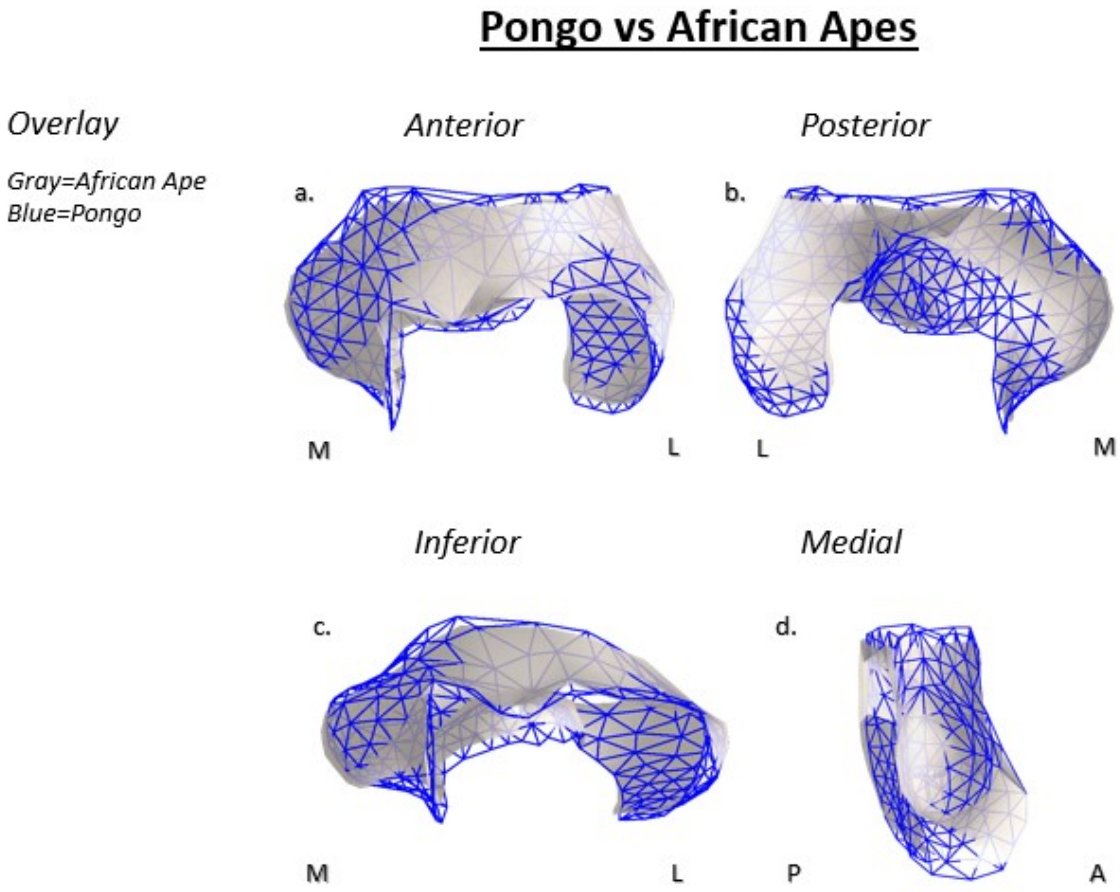

Figure 4-15 Differences between average periarticular morphology of humans and other nonhuman hominids.

4.3.2 PCA

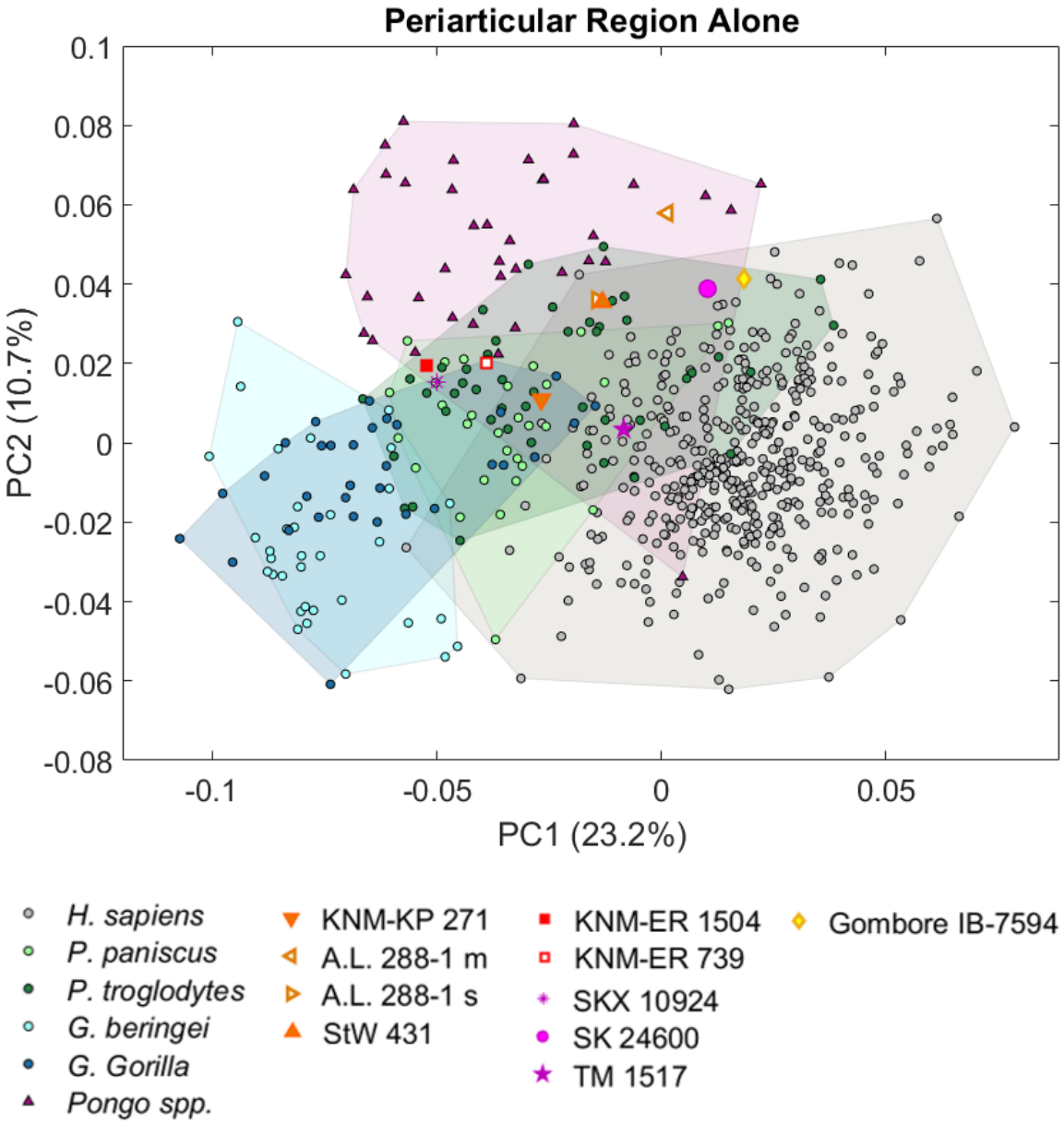
Periarticular Region Alone
0.1
0.08
0.06
0.04
0.02
0
-0.02
-0.04
-0.06
-0.08
PC2 (10.7%)
-0.1
-0.05
0
0.05
PC1 (23.2%)
H. sapiens
P. paniscus
P. troglodytes
G. beringei
G. Gorilla
Pongo spp.
KNM-KP 271
A.L. 288-1 m
A.L. 288-1 s
StW 431
KNM-ER 1504
KNM-ER 739
SKX 10924
SK 24600
TM 1517
Gombore IB-7594

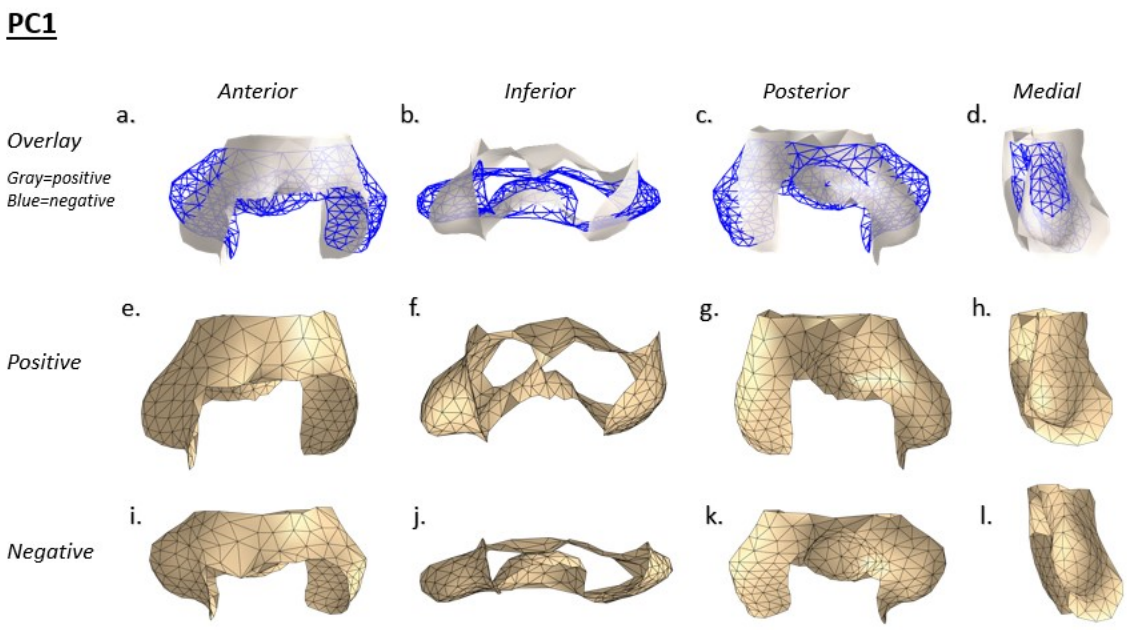

Figure 4-16 PC1 and PC2 based on analysis of the 251 periarticular landmarks and visualization of their extremes.

Principal component analysis of the periarticular region alone yields quite different results from the articular analyses (Figure 4-16). The combination of PCs 1 and 2 clearly distinguishes all genera from each other. Humans are divided from apes by their high position on PC1, but have a wide range on PC2. Gorillas are distinguished by their low position on both PCs, with *G. beringei* significantly lower on PC2 than lowland gorillas ($p<0.0001$). *Pan* and *Pongo* are both intermediate on PC1, but while *Pan* is likewise intermediate on PC2, Pongo is significantly higher on this axis than all other groups ($p<0.0001$); this order of nonhuman ape species along PC2 resembles a locomotor grade (i.e., from most arboreal to most terrestrial). The range of *Pan* overlaps minimally with each of the other three groups; there is no overlap between any other pair of genera. The only species that are not distinguishable from each other on the

combination of PCs 1 and 2 are *P. paniscus* and *P. troglodytes*; this is consistent with the other analyses.

Positive values of PC1, as in humans, show relative AP thickening of the periarticular region. The medial olecranon pillar is particularly affected. The ape range on PC1, by contrast, has a relatively flattened profile that emphasizes mediolateral proportions. As seen in the 10% analysis, in humans the medial epicondyle extends farther distally and inferiorly than in apes and is thicker, while the ape medial epicondyle projects further medially, often has a distinct knob-like projection on its superior border, and is relatively under-developed along its inferior border. Fossil hominins are mainly low on PC1; this puts them mostly outside the human range. This is likely due to the notable AP flatness of the periarticular surface of most specimens. TM 1517, SK 24600 and IB-7594 are exceptions; these fall at the periphery of the human range. Fossil hominins as a group also show relatively strong development of the medial epicondyle along its superior rather than inferior border; this is particularly apparent in KNM-ER 1504, KNM-ER 739 and SKX 10924. TM 1517 is an exception, with a strongly projecting but inferiorly directed medial epicondyle. While there is no linear progression from ape-like to human-like morphology in these groups, there are differences among taxa. While australopiths fall near the human range (though within apes), *P. boisei* is distinctly ape-like and not human-like. *P. robustus* spans the range from very ape-like (SKX 10924) to human-like (SK 24600, and to a lesser degree, TM 1517). IB-7594 (*Homo erectus*) is the most like modern humans, though very similar to SK 24600.

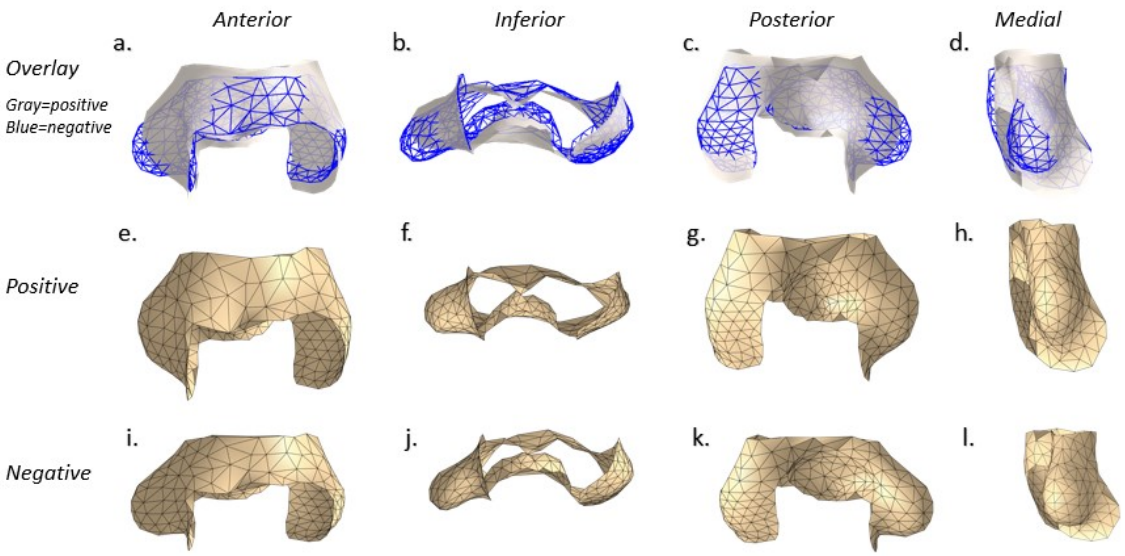

Figure 4-17 Visualization of periarticular PC2.

PC2 relates to overall mediolateral expansion and transverse curvature. Low values on PC2, as in gorillas, indicate an emphasized projection of a posteriorly angled medial epicondyle which has a marked concave slope at its intersection with the distal shaft. This feature is paired with enlargement of the olecranon fossa and inflation of the lateral pillar. The overall effect is a region that appears to wrap posteriorly as it expands mediolaterally. By contrast, the medial epicondyle of orangutans, high on PC2, lies roughly parallel with the mediolateral axis of the bone and blends gradually into the shaft due to expansion of the medial supracondylar crest. The olecranon fossa is narrow and deep, and the posterior border of the lateral pillar is flat. The effect is a periarticular region which lies in a coronal plane. Humans and *Pan* are intermediate on PC2, but show more posterior curvature than *Pongo*, emphasized by posterior projection of the medial epicondyle. Fossil hominins are high on PC2, though generally lower than *Pongo*.

This reflects that the periarticular region, in addition to being anteroposteriorly flattened, is not posteriorly curved.

The combination of low PC1 and high PC2 values places most fossil hominins outside the human range. IB-7594, TM 1517 and SK 24600 fall at the border of the combined human range, within its overlap with *Pan*, while the remaining specimens (KNM-KP 271, A.L. 288-1, StW 431, KNM-ER 1504, KNM-ER 739, SKX 20934) are more closely associated with *Pan* than *Homo* and lie near its range of overlap with *Pongo*.

4.4 Diaphysis

4.4.1 Average Morphology

Moving proximally, average shape of the distal shaft also differs between humans and apes, though this difference is more subtle than those observed in previous sections (Figure 4-18, below).

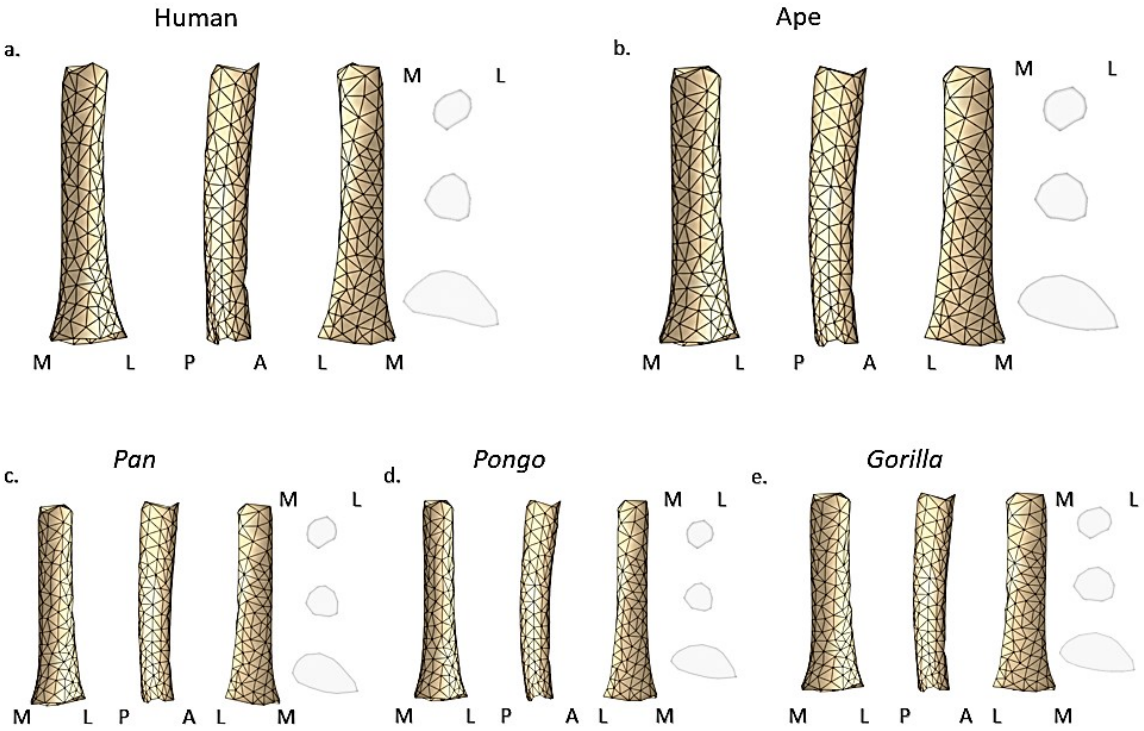

Figure 4-18 Procrustes average shape of the distal shaft (40-18%) of the humerus by taxon.

Great apes and humans differ primarily in the relative emphasis of the anteroposterior dimension. Distally, human cross sections are triangular. Progressing proximally, the anteroposterior dimension of the medial portion of the humerus remains prominent in humans, resulting in an ovoid shape with an AP oriented long axis. In great apes, distal shaft cross sections are more rounded. Moving proximally, this trend continues, and cross sections of apes appear round rather than ovoid. Differences between ape taxa are more apparent in the distal portion of the shaft, primarily in the location of greatest AP diameter (Figure 4-18); this may be influenced by relative development of the lateral trochlear crest.

4.4.2 PCA

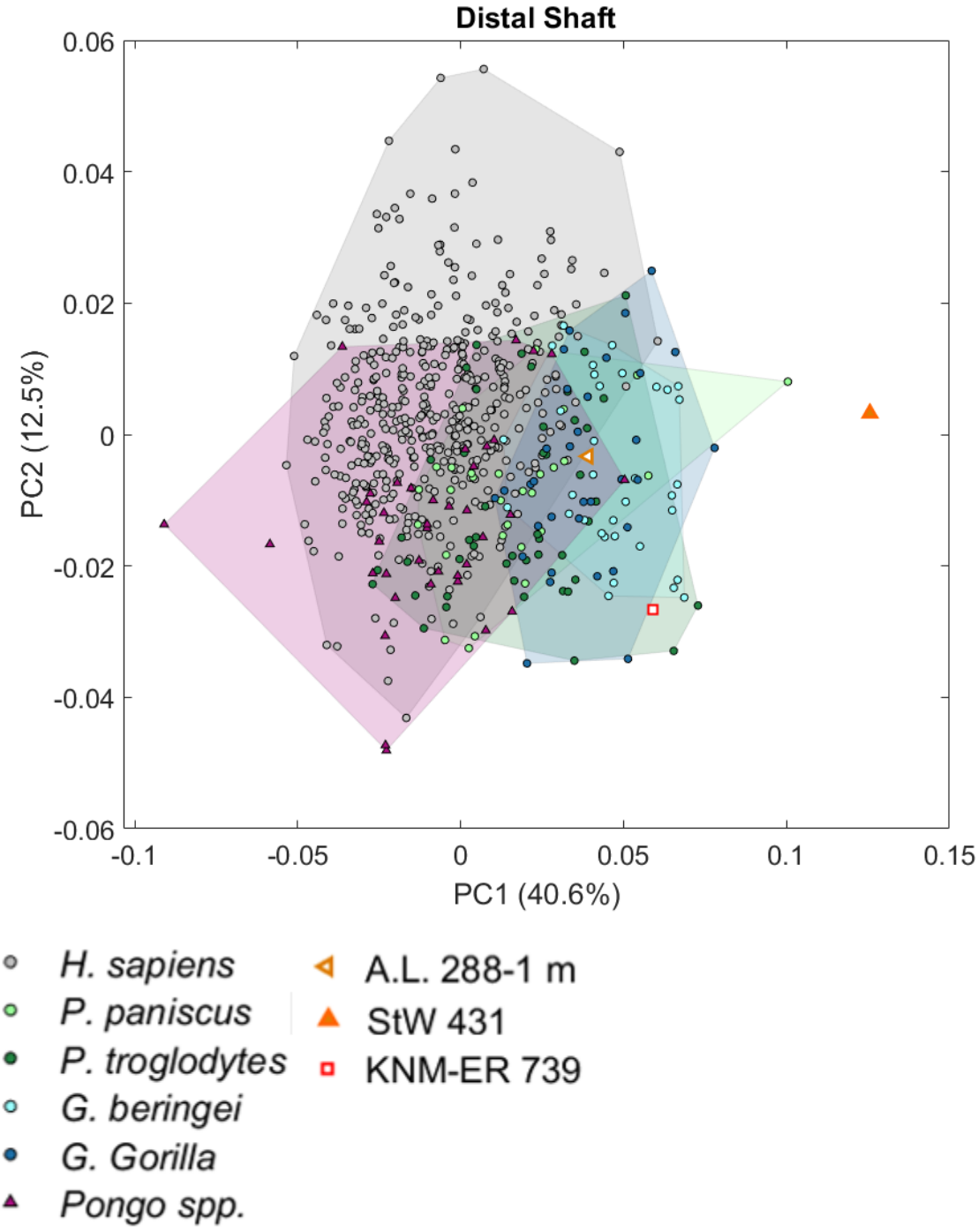
Distal Shaft
0.06
0.04
0.02
0
-0.02
-0.04
-0.06
PC2 (12.5%)
-0.1
-0.05
0
0.05
0.1
0.15
PC1 (40.6%)
H. sapiens
P. paniscus
P. troglodytes
G. beringei
G. Gorilla
Pongo spp.
A.L. 288-1 m
StW 431
KNM-ER 739

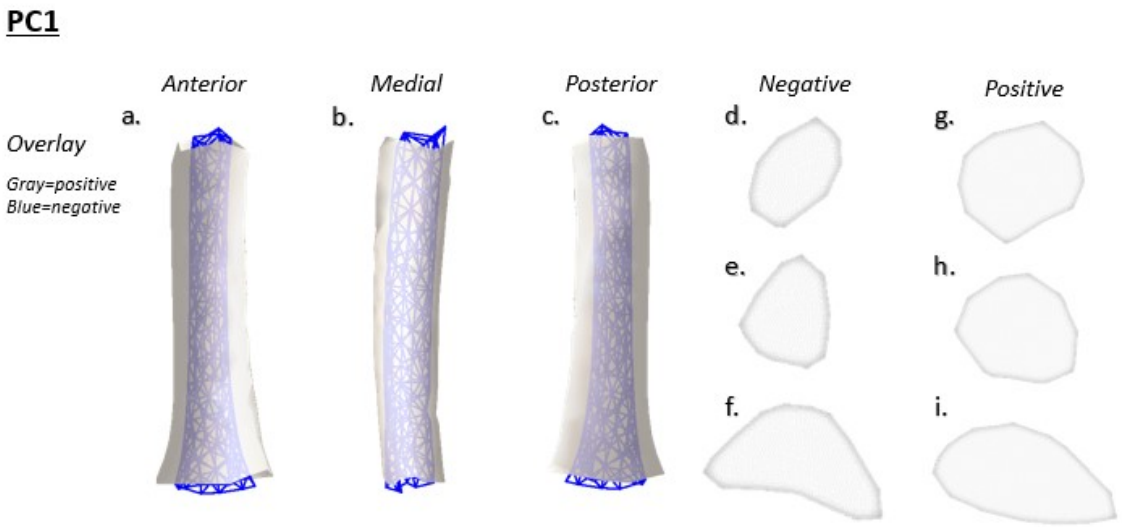

Figure 4-19 PCA and visualization of the 178 shaft landmarks falling between 10% and 40% of bone length. Inferior views are enlarged to clarify cross-sectional shape.

Analysis of the distal shaft reaffirms the human-fossil divide seen in the periarticular region (Figure 4-19). On PC1, human shaft morphology is significantly different from all nonhuman hominids except *Pongo* ($p<0.0001$), while on PC2 humans differ from all other groups ($p<0.05$). Among the apes, *Pongo* is lower on PC1 than the four other species ($p<0.001$), while the two species of gorilla are higher than all other species ($p<0.05$). Great apes do not differ significantly among themselves on PC2. While there is significant overlap between the ranges of the six groups, A.L. 288-1 and KNM-ER 1504 lie within the *Pan-Gorilla* range, while StW 431 exceeds the range of all extant taxa. This specimen falls at the positive extreme of PC1, nearest *Gorilla*. This association is driven by divergence on PC1, which quantifies 40.6% of the variation and describes the relationship between the points of greatest ML and AP breadth. High values of PC1 in the African apes are a result of mediolateral and anteroposterior expansion and the

cross-sectional shape of the distal shaft; overall, the distal shaft is more robust. In these groups, at the base of the shaft (10%) the region of greatest mediolateral breadth is offset from the posterior border of the cross-section by approximately one third of the total AP bone thickness. There is a convex curve away from the point of greatest AP thickness on both the posterior and anterior border, creating a rounded appearance, though the lateral border of the contour is narrowed and elongated. This general pattern, characterized by both anterior and posterior convex curvature, is seen throughout the shaft. At 40%, this results in a circular cross section; between the 10 and 40% sections, the shaft is ovoid with a mediolateral major axis. By contrast in humans, the point of greatest ML breadth is along the posterior border of the cross section and is narrower than in *Pan* and *Gorilla*. At the base of the shaft, the posterior border is concave, reflecting a slight depression above the olecranon fossa which is not present at high values of PC1 (apes). AP breadth at the midline in humans is accentuated at this section and throughout the shaft by a sharp incline to the medial and lateral borders. On the more distal portion of the shaft, this results in a roughly triangular cross section; near midshaft, this presents as a narrow ellipse with anteroposterior major axis that is angled laterally. Humans are also more positive on PC2. This indicates an increase in the thickness of the medial and lateral portions of the bone; this is likely because the expanded supracondylar crests in great apes are thin by comparison to the relatively undeveloped human supracondylar crests. Fossils are intermediate to low on PC2, but high to extremely high on PC1; this reflects the fact that these three specimens lack the

exaggerated AP breadth characteristic of humans, and have a robust distal shaft characterized by mediolateral expansion with a rounded posterior contour.

4.5 Distal 40% and 18%

Addition of shaft morphology to morphology described in earlier analyses appears additive, combining the results observed in the articular, periarticular, and shaft subsets (Figure 4-20). PC1 in both analyses of the distal 40% (Figure 4-20) and 18% (Figure 4-21) separates human and great ape morphologies. In fossil hominins, inclusion of the shaft with the articular and periarticular regions creates a clear distinction between StW 431 and other fossil hominins (Fig. 5-1). While A.L. 288-1 and KNM-ER 739 are intermediate between apes and humans in analysis of the distal 40% of the bone, falling near the border between humans, *Pan* and *Pongo*, StW 431 falls squarely within the gorilla range (Figure 4-20). This is evidently the result of a relatively robust shaft, and is not apparent in any analyses that do not include shaft morphology. This relationship is, however, seen in analyses that include smaller portions of the shaft. In analysis of the distal 18% of the bone (Figure 4-21), StW 431 falls in the center of the great ape range, while A.L. 288-1 and KNM-ER 739 fall within the human cloud. Though A.L. 288-1 and KNM-ER fall on the side of the human distribution closer to apes, they appear less ape-like than in the distal 10% analysis, indicating the part of the distal shaft between 10 and 18% is particularly more human-like than the shaft as a whole. KNM-ER 1504 falls close to KNM-ER 739; as in the periarticular analysis, these two *P. robustus*

specimens form a cloud that is more ape-like than A.L. 288-1, which is older. IB-7594 is again nearly ‘super-human’, as it in all analyses except that of the periarticular surface.

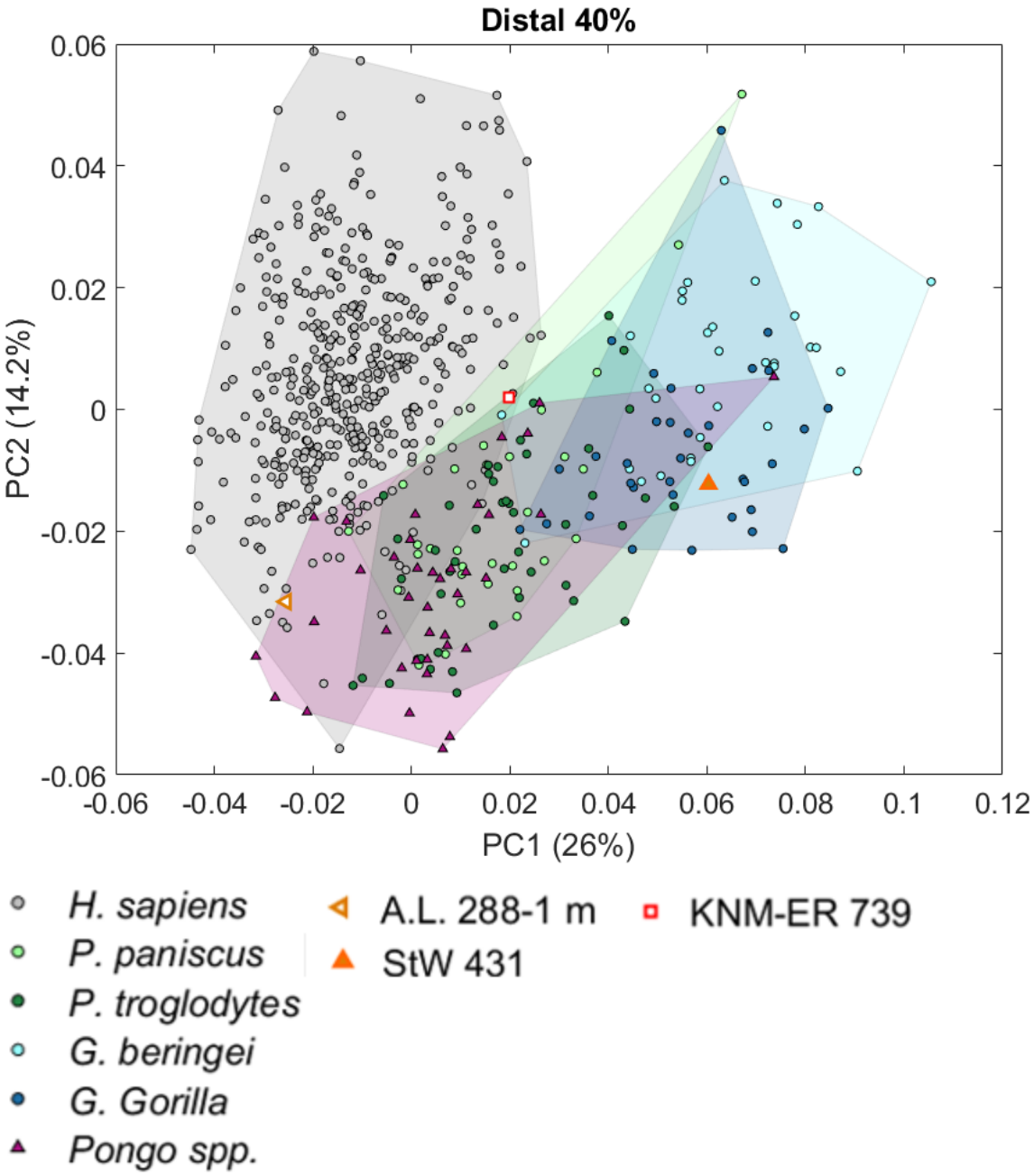
Distal 40%
0.06
0.04
0.02
0
-0.02
-0.04
-0.06
PC2 (14.2%)
-0.06
-0.04
-0.02
0
0.02
0.04
0.06
0.08
0.1
0.12
PC1 (26%)
H. sapiens
P. paniscus
P. troglodytes
G. beringei
G. Gorilla
Pongo spp.
A.L. 288-1 m
StW 431
KNM-ER 739

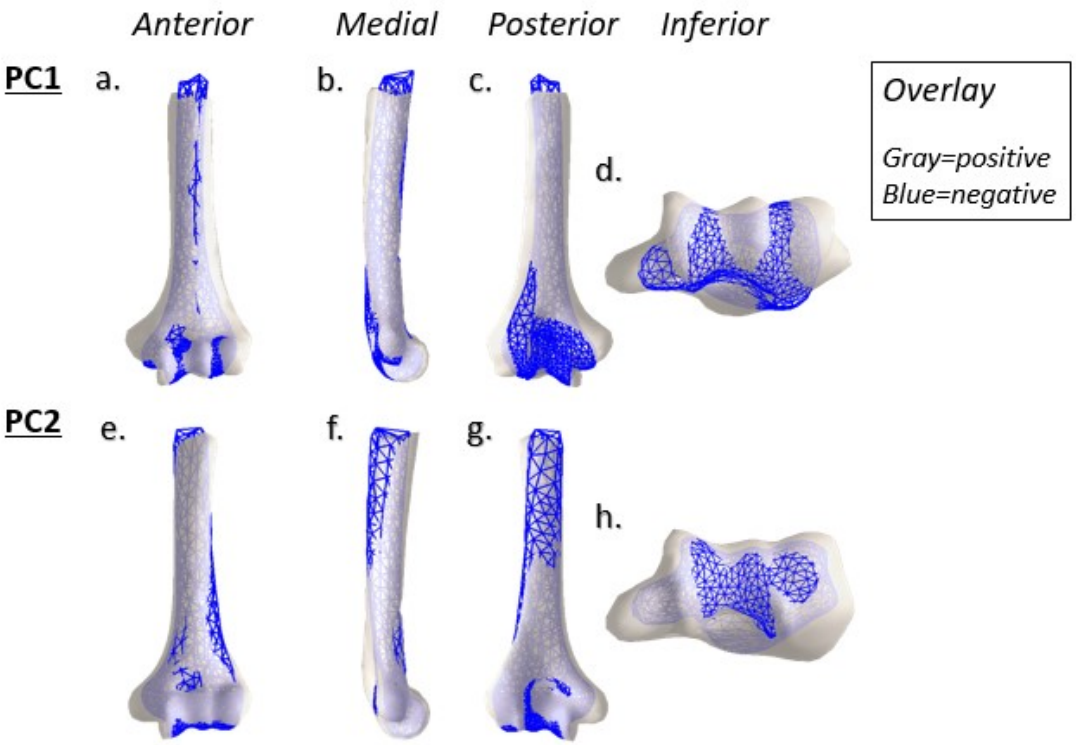

Figure 4-20 PCs 1 and 2 of the PCA performed on 736 landmarks on the distal 40% of the humerus.

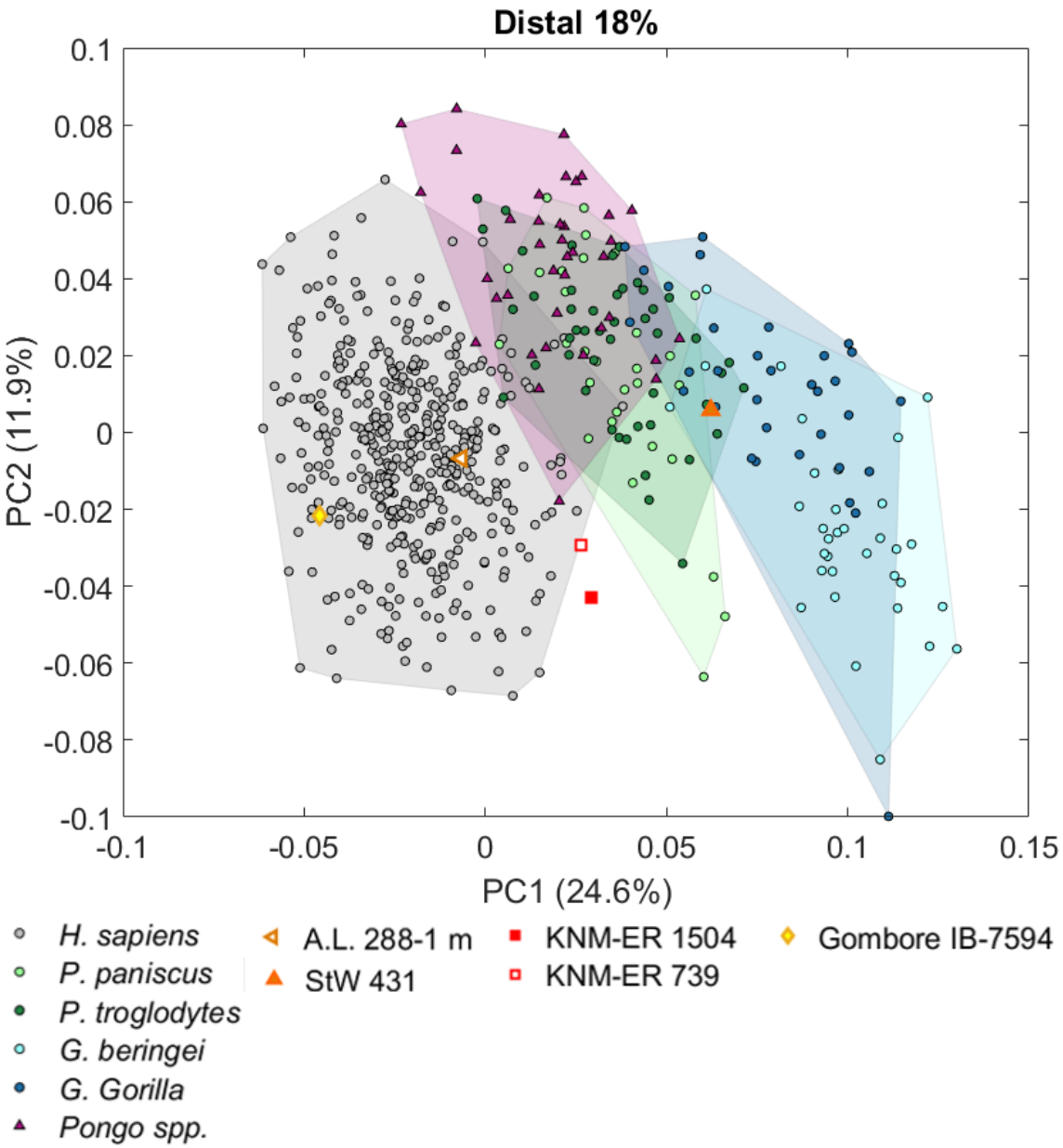
Distal 18%
PC2 (11.9%)
PC1 (24.6%)
0.1
0.08
0.06
0.04
0.02
0
-0.02
-0.04
-0.06
-0.08
-0.1
-0.1
-0.05
0
0.05
0.1
0.15
H. sapiens
P. paniscus
P. troglodytes
G. beringei
G. Gorilla
Pongo spp.
A.L. 288-1 m
StW 431
KNM-ER 1504
KNM-ER 739
Gombore IB-7594

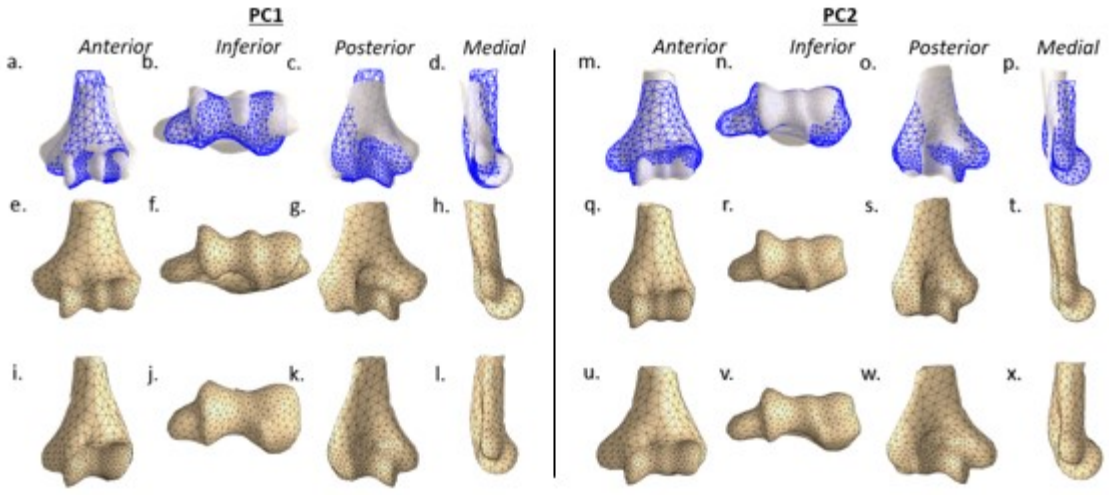

Figure 4-21 Results of the principal components analysis performed on 625 landmarks on the distal 18% of the humerus.

4.6 Summary

Distal humeral morphology differs statistically significantly between humans and great apes in all subregions of the distal humerus, though ranges of variation overlap. Key features differentiating great apes from humans generally include a more robust shaft, a more proximally located medial and more projecting lateral epicondyle, and a more developed lateral trochlear crest, though variation exists within and among taxa. Humans, by contrast, have a relatively gracile shaft and overall narrow ML proportions, increased anteroposterior breadth of the periarticular region, and a wide posterior trochlea that does not extend onto the sloping walls of their wide olecranon fossa. Regions also differ in their relative size. For example, humans and *G. beringei* appear to have smaller articular surfaces relative to the periarticular region. Fossil hominins show different affinities depending upon which portion of bone is analyzed. The shaft and periarticular regions of fossil hominins are more ape-like than the articular surface.

There is limited evidence of temporal or phylogenetic trends in fossil hominin distal morphology. The most salient among these is the difference between Gombore IB-7594 (*H. erectus*), which consistently lies at the extreme end of the human range (and distant from apes), and other fossils which are generally intermediate between humans and great apes or fully ape-like. Despite the limited ability of these features to discriminate between fossil taxa, SK 24600 is notably more human-like than SKX 10924 in every analysis that discriminates between humans and great apes (Figure 4-4, Figure

4-12, Figure 4-16), possibly supporting assignment of SK 24600 to *Homo* per Lague (2014) and contra Susman et al. (2001).

5 Results: Allometry

Morphological variation in the distal humerus cannot be assumed to be purely a function of behavioral use or phylogeny. Many other factors play a role in humeral morphology. Body size is one of these factors. Not all aspects of humeral morphology scale isometrically, and therefore some differences between distal humeri of very small and very large individuals is attributable to size (Bacon, 2000; Lague, 2014). This is important for interpretations of fossil morphology, which have been used to support both functional and phylogenetic claims. However, assessment of scaling effects first relies on an effective measure of size. Because body mass is often unavailable for fossil hominins, two humeral characteristics, centroid size and biepicondylar breadth, have been used in some previous studies to investigate allometry of the distal humerus (Bacon, 2000; Carretero et al., 2009; De Castro et al., 2012; Arias-Martorell et al., 2015; Di Vincenzo et al., 2015; Lague, 2015). This chapter first examines the relationship of these measures to body mass and demonstrates how use of different size measures can affect morphological analyses. Fossil hominins are then interpreted within this context.

5.1 Correlations between humeral properties and body mass

Distal humeral dimensions are strongly correlated with estimated body mass derived from femoral head SI breadth. Table 5-1 provides the correlation between body mass and ten potential body size surrogates, including eight centroid sizes and two linear breadths, in the present study samples, as well as RMA slope, standard error of

the slope, and number of individuals included in each analysis. However, because large ranges, large slopes, and small sample sizes can amplify correlation values and give a misleading impression of the strength of relationships (as noted by Smith, 1984), %SEE is also provided in Table 5-1. While the following analysis is not designed for prediction per se, %SEE provides a method of evaluating how well the measures reflect body mass and serves as a comparison for correlation values, which can be inflated in highly sexually dimorphic species (i.e., gorillas and orangutans). Notably, while all measures in gorillas are well correlated with body mass ($r > 0.90$), when %SEE is examined it is evident that the high correlations in gorillas can largely be understood as the effect of a large range in body mass, as %SEEs are not substantially lower in gorillas and *Pongo* than in other taxa.

Table 5-1 Relationship between humeral properties and body mass (logged).

Sample	*Measurement (ln)*	*n*	*r*	*Slope*	*SE slope*	*%SEE*
Humans	**Biepicondylar Breadth (Landmarks)**	246	0.83	0.58	0.022	7.19
	Articular Breadth (Calipers)	237	0.87	0.64	0.021	6.52
	Centroid Size Full Bone	246	0.68	0.44	0.022	8.58
	Centroid Size 40%	246	0.79	0.54	0.022	7.64
	Centroid Size 18%	246	0.85	0.56	0.019	6.48
	Centroid Size 10%	246	0.88	0.57	0.018	5.89
	Periarticular Centroid Size	246	0.86	0.56	0.019	6.23
	Articular Centroid Size	246	0.87	0.63	0.021	6.56
	Trochlear Centroid Size	246	0.84	0.65	0.023	7.27
	Capitular Centroid Size	246	0.82	0.60	0.023	7.45
Combined Great apes	**Biepicondylar Breadth (Landmarks)**	113	0.97	0.40 [d]	0.009	9.09
	Articular Breadth (Calipers)	67	0.96	0.34	0.012	9.47
	Centroid Size Full Bone	113	0.91	0.30 [d]	0.012	13.5
	Centroid Size 40%	113	0.94	0.31 [c]	0.010	11.1
	Centroid Size 18%	113	0.97	0.35 [d]	0.008	8.69
	Centroid Size 10%	113	0.98	0.37 [d]	0.008	7.61
	Periarticular Centroid Size	113	0.97	0.37 [d]	0.008	8.03
	Articular Centroid Size	113	0.97	0.36	0.008	8.36
	Trochlear Centroid Size	113	0.96	0.38 [c]	0.010	9.66
	Capitular Centroid Size	113	0.94	0.32 [c]	0.010	11.3
Pan	**Biepicondylar Breadth (Landmarks)**	47	0.79	0.42 [d]	0.041	8.64
	Articular Breadth (Calipers)	23	0.77	0.34	0.050	7.92
	Centroid Size Full Bone	47	0.56	0.31 [d]	0.043	10.7
	Centroid Size 40%	47	0.76	0.33	0.034	8.08
	Centroid Size 18%	47	0.83	0.31	0.027	6.59
	Centroid Size 10%	47	0.85	0.33	0.027	6.36
	Periarticular Centroid Size	47	0.83	0.36 [d]	0.031	7.11
	Articular Centroid Size	47	0.83	0.36	0.031	7.07
	Trochlear Centroid Size	47	0.74	0.35	0.037	8.72
	Capitular Centroid Size	47	0.73	0.39	0.043	9.39
Gorilla	**Biepicondylar Breadth (Landmarks)**	44	0.95	0.39 [d]	0.019	7.55
	Articular Breadth (Calipers)	24	0.95	0.37	0.025	7.87
	Centroid Size Full Bone	44	0.91	0.28 [d]	0.018	8.32
	Centroid Size 40%	44	0.95	0.37 [a,d]	0.019	7.41
	Centroid Size 18%	44	0.96	0.37 [d]	0.017	6.73
	Centroid Size 10%	44	0.97	0.38 [d]	0.014	5.52
	Periarticular Centroid Size	44	0.97	0.38 [d]	0.014	5.41

	Articular Centroid Size	44	0.96	0.39 [d]	0.017	6.50
	Trochlear Centroid Size	44	0.95	0.42 [a,d]	0.020	7.40
	Capitular Centroid Size	44	0.91	0.38 [a,b,d]	0.025	9.84
Pongo	**Biepicondylar Breadth (Landmarks)**	22	0.92	0.32 [a,b,c]	0.028	10.1
	Articular Breadth (Calipers)	20	0.88	0.29	0.033	12.1
	Centroid Size Full Bone	22	0.80	0.20 [a,b,c]	0.028	12.9
	Centroid Size 40%	22	0.84	0.24 [c]	0.030	12.6
	Centroid Size 18%	22	0.93	0.28 [a,c]	0.024	9.06
	Centroid Size 10%	22	0.94	0.29 [a,c]	0.023	8.58
	Periarticular Centroid Size	22	0.93	0.27 [a,b,c]	0.023	8.77
	Articular Centroid Size	22	0.90	0.31 [c]	0.031	11.2
	Trochlear Centroid Size	22	0.88	0.33 [c]	0.035	12.4
	Capitular Centroid Size	22	0.91	0.32 [c]	0.031	10.9

Great ape genera that differ from each other in slope ($p<.05$) are noted: a=differs from combined sample, b=differs from *Pan*, c=differs from *Gorilla*, d=differs from *Pongo*. Slope differs significantly ($p<.01$) between humans and all other samples for all measures, and therefore these differences are not noted. Elevation differences are not provided, because slope differs by taxon in all cases.

Logged centroid size of most landmark configurations is especially strongly correlated with logged body mass, despite the fact that eight different landmark sets sampling eight different regions of bone were tested. Within genera, logged centroid size of the distal 10% is most strongly correlated with logged body size in humans, *Pan*, *Pongo*, and the combined nonhuman sample ($r = 0.85$-0.98, %SEE = 5.89-8.58), while centroid sizes of 10% and periarticular regions are equally well correlated with body mass in gorillas ($r = 0.97$, %SEE = 5.53, 5.41 respectively). While periarticular rather than articular centroid size is more strongly correlated with body mass in Nonhuman genera, articular centroid size is also strongly correlated with body mass and the difference between the two does not rise to the level of significance using Fisher's z-transformation ($p>.05$ in each genus and the combined great ape sample). Centroid

sizes of landmark sets incorporating larger portions of the bone (full bone, 40%) are significantly poorer correlates than size of the distal end alone; this is likely because of the influence of bone length (which varies relative to body mass) on the centroid size of these landmark sets.

While biepicondylar breadth is a less highly correlated measure of body size than centroid size, it is nevertheless correlated with body mass. The lowest correlation for biepicondylar breadth is 0.79, in *Pan*. It is more highly correlated with body mass in gorillas (r=0.95), but %SEE for biepicondylar breadth is lowest in humans (%SEE = 7.19). However, within humans, articular breadth is a slightly but significantly better measure of size than biepicondylar breadth ($p<.05$). This trend is reversed in great apes, where biepicondylar breadth is more strongly correlated with body mass than articular breadth, though this does not rise to the level of significance in any taxon ($p>0.05$).

In Figure 5-1, RMA regressions of six of the ten size measures listed in Table 5-1 are shown. Centroid sizes including regions above the distal 10% are omitted because of the poorer correlations of these regions with body mass. The omitted regions are also less frequently preserved in the fossils.

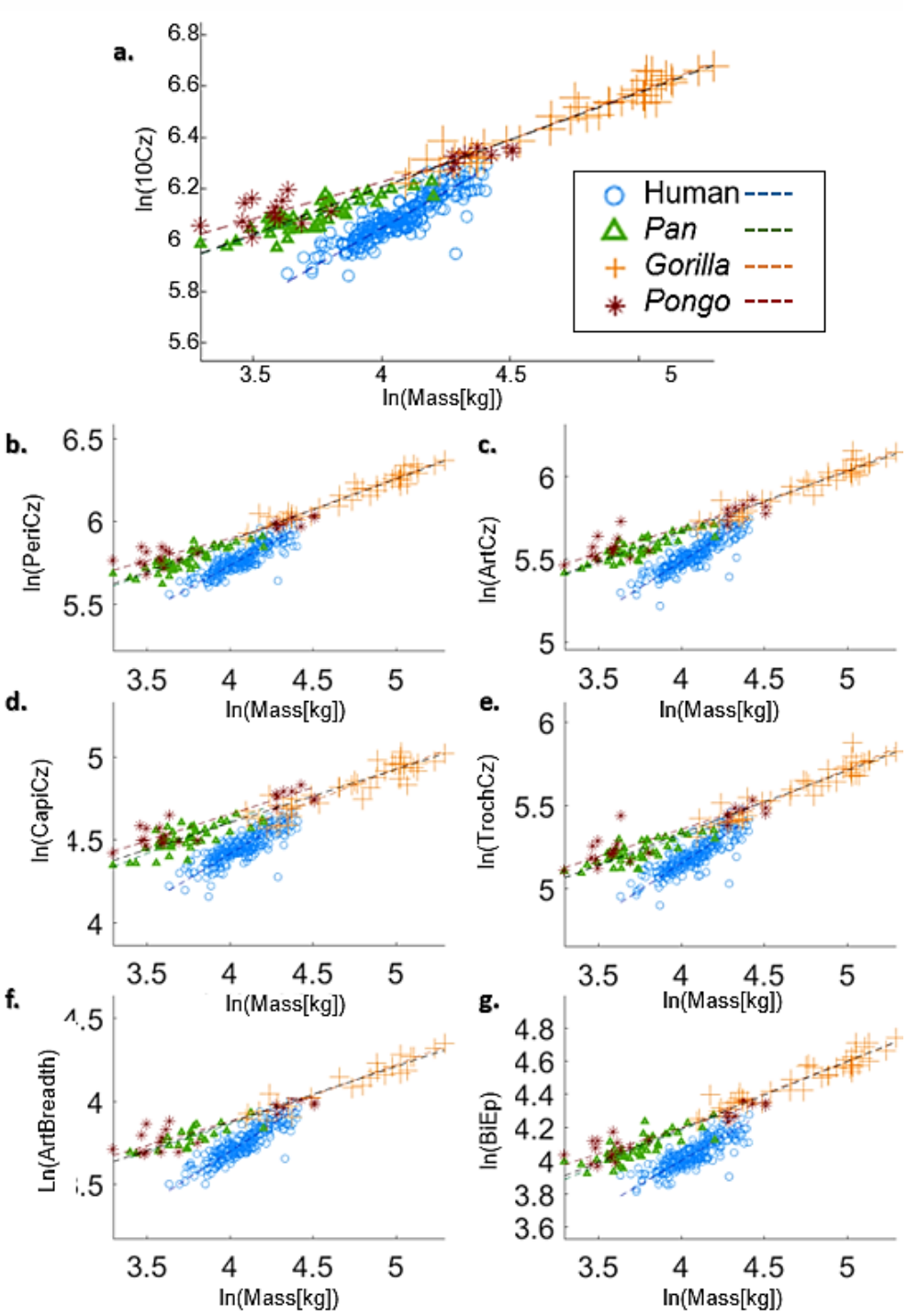

Figure 5-1 Plots of selected measures of size against estimated body mass. 10Cz=centroid size distal 10%, PeriCz=periarticular centroid, ArtCz=articular centroid, CapCz=capitular centroid, TrochCz=trochlear centroid, ArtBreadth=articular ML breadth, BiEp=biepicondylar ML breadth.

Relative to body mass, humeral articular, epicondylar, and centroid sizes of the six examined regions are smaller in humans than in great apes (see Figure 5-1 above). This is however less true of large humans. Due to high positive allometry within humans (Table 1, Figure 5-1), large humans are relatively more ape-like in their humeral proportions, while small humans are quite unlike nonhuman hominids. This is relevant for fossil comparisons, given the low estimated body masses of many early hominins (Ruff et al., 2016). When the degree of allometry (i.e., slope), within humans is compared between distal humeral dimensions, there is a statistically significant difference ($p<.001$) in the scaling of different regions. Within humans, there is particularly strong positive allometry of the articular surface: articular breadth, articular centroid size, and trochlear centroid size are significantly more positively allometric than all non-articular measures of size ($p<.01$). Thus, larger humans have relatively larger articulations compared to periarticular dimensions (or the distal humerus as a whole). However, the RMA slope of the capitular regression does not follow this pattern, suggesting that it is primarily the trochlea that is driving this result.

All great apes have large distal humeral properties for their body masses compared to humans (Figure 5-1, a-g). However, scaling relationships (slopes) vary between taxa. Slope of the regression is low for orangutan humeral properties, higher in chimpanzees, and, among great apes, highest in gorillas (see Table 5-1). These scaling relationships are shown to differ significantly between taxa for several of the properties presented. Humans display very high positive allometry, as discussed above. Thus, there

appears to be an arboreal-terrestrial gradient, with the more arboreal taxa exhibiting more isometric relationships between distal humeral size and body mass. There is evidence that these differences are statistically significant. RMA slopes for orangutans differ from the gorilla regression for every property except articular breadth, from *Pan* in three measures (most notably, biepicondylar breadth and periarticular centroid size), and from the combined great ape regression in five measures. In addition to their consistent difference from orangutans, gorillas differ in slope from the combined great ape sample in both trochlear and capitular centroid size, as well as centroid of the distal 40%, and from *Pan* in capitular size.

5.2 Effect on PC Scores

While distal humeral features are strongly correlated with estimated body mass, use of these measures to scale analyses of humeral shape is potentially circular, given that these features are themselves the subject of analysis. Taxonomic differences in the relationship between centroid size and body mass in particular presents challenges in analyses including multiple species. It is therefore necessary to assess the potential bias these measures introduce into size-scaled analyses. In this section, the potential effects of allometry on the principal components (PCs) of interest in Chapter 4 are considered, and how scaling using three different size measures influences morphological interpretation is examined. The size measures incorporated in these analyses reflect scaling variables used in the literature: body mass, biepicondylar breadth, and centroid size. Centroid size of the distal 10% was chosen for use in these analyses because it was

the most highly correlated with body mass, which is a standard scaling variable with numerous advantages (Jungers, 1984). Because the 10% centroid size most closely reflects body mass, it represents the best case scenario for incorporating allometric effects using centroid size, which is necessary for fossil specimens without body mass estimations.

In the GM analysis in Chapter 4, great apes and humans consistently separated along PC1, regardless of bone region analyzed. Figure 5-2**Error! Reference source not found.** shows the allometric relationships present in PC1 scores of four regions (distal 10%, articular surface, periarticular surface, shaft) and by regressing PC scores on the three measures of size. Humans show a significant correlation ($p<.001$) between PC1 scores for three of four regions (distal 10%, articular surface, shaft) and logged body mass (Figure 5-2**Error! Reference source not found.** a,d,g,j), though the relationships are weak (10%: $r=0.26$, Articular: $r=-0.33$, Shaft: $r=0.28$). No great ape taxa show a significant relationship between PC1 scores and size, but, when apes are pooled, this relationship is significant and similar in direction to the relationship seen within humans. However, while human periarticular PC1 scores are not correlated with body mass, this variable is correlated with size among great apes (discussed below).

The same size-shape relationship that is seen with respect to body mass arises when PC scores are regressed against logged centroid size (Figure 5-2**Error! Reference source not found.** b,e,h,k). When regressed against logged biepicondylar breadth, periarticular PC1 scores are significantly ($p<.05$) correlated with size as are scores along

the first PC of the three other regions, though periarticular PC1 score is not significantly correlated with either body mass or centroid size among humans. Among humans, wherever a significant correlation between PC1 scores and size exists, large humans have humeri that are more ape-like, while small human humeri are less ape-like (discussed below). This is most apparent in the articular and periarticular (scaled by biepicondylar breadth, Figure 5-2**Error! Reference source not found.** i) analyses. While there is also a strong allometric trend in the shaft, a much wider range of human body sizes overlap with the great apes.

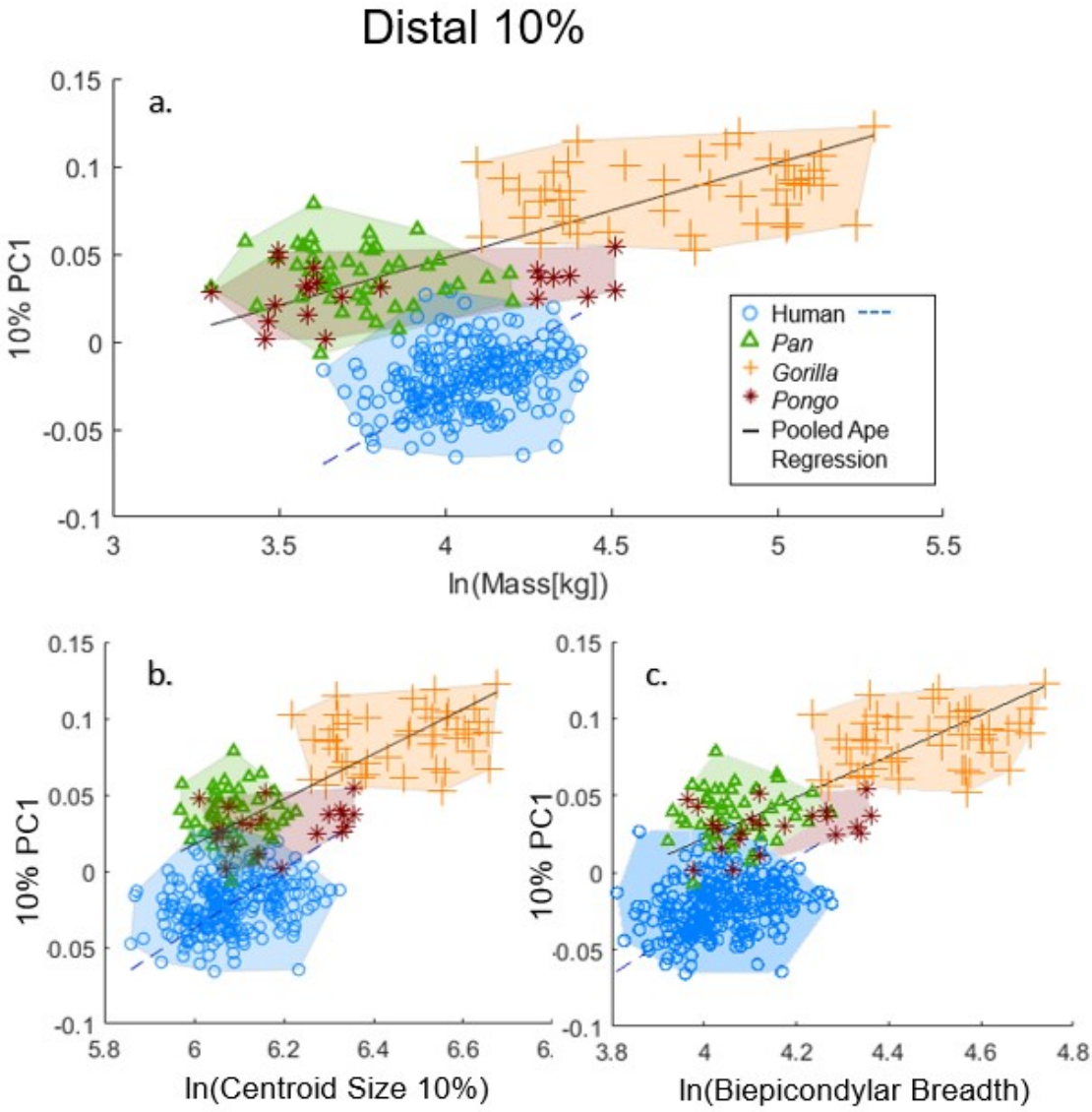
Distal 10%
a.
10% PC1
ln(Mass[kg])
Human
Pan
Gorilla
Pongo
Pooled Ape Regression
b.
10% PC1
ln(Centroid Size 10%)
c.
10% PC1
ln(Biepicondylar Breadth)

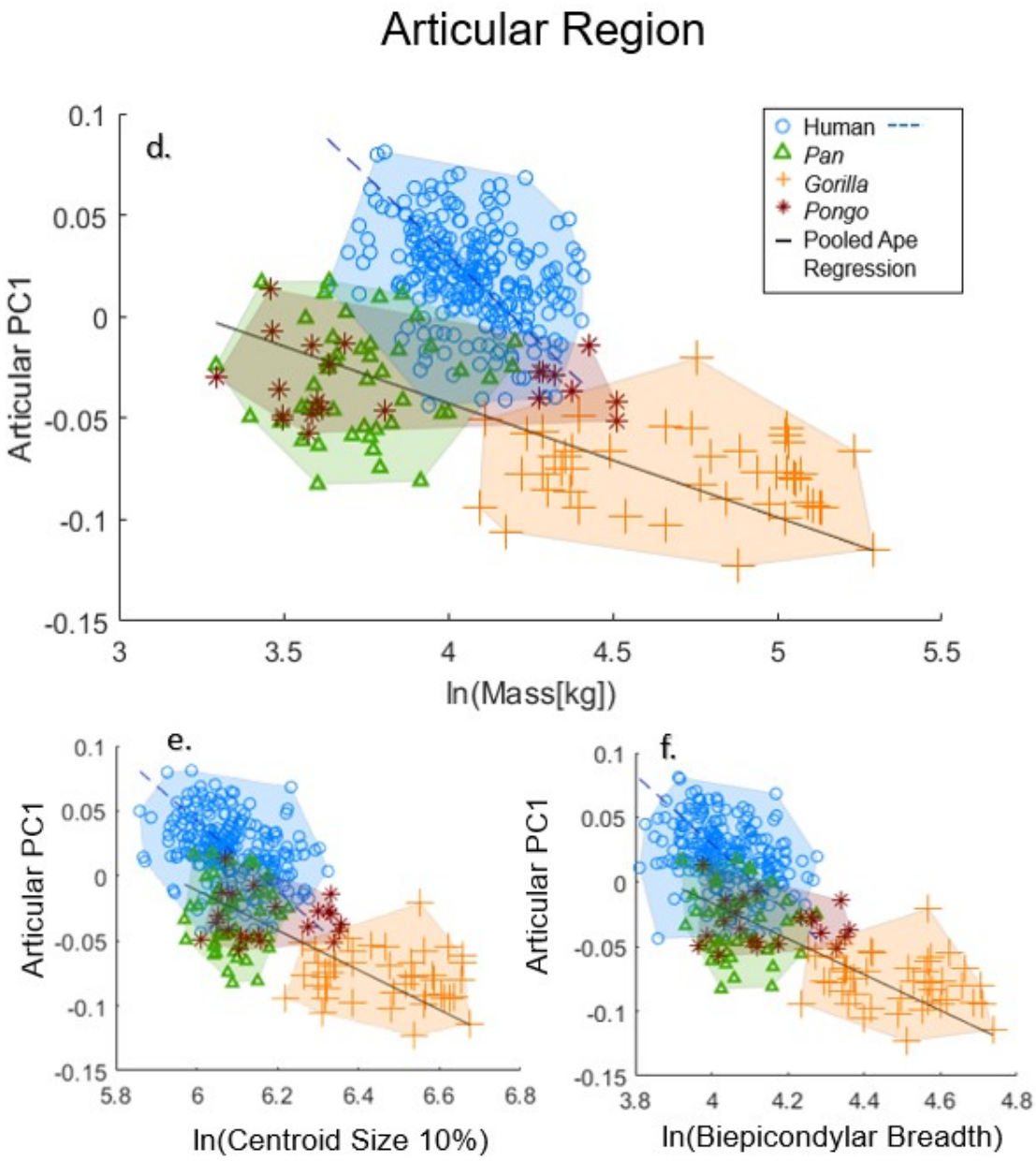
Articular Region
d.
Human
Pan
Gorilla
Pongo
Pooled Ape Regression
Articular PC1
ln(Mass[kg])
e.
ln(Centroid Size 10%)
f.
ln(Biepicondylar Breadth)

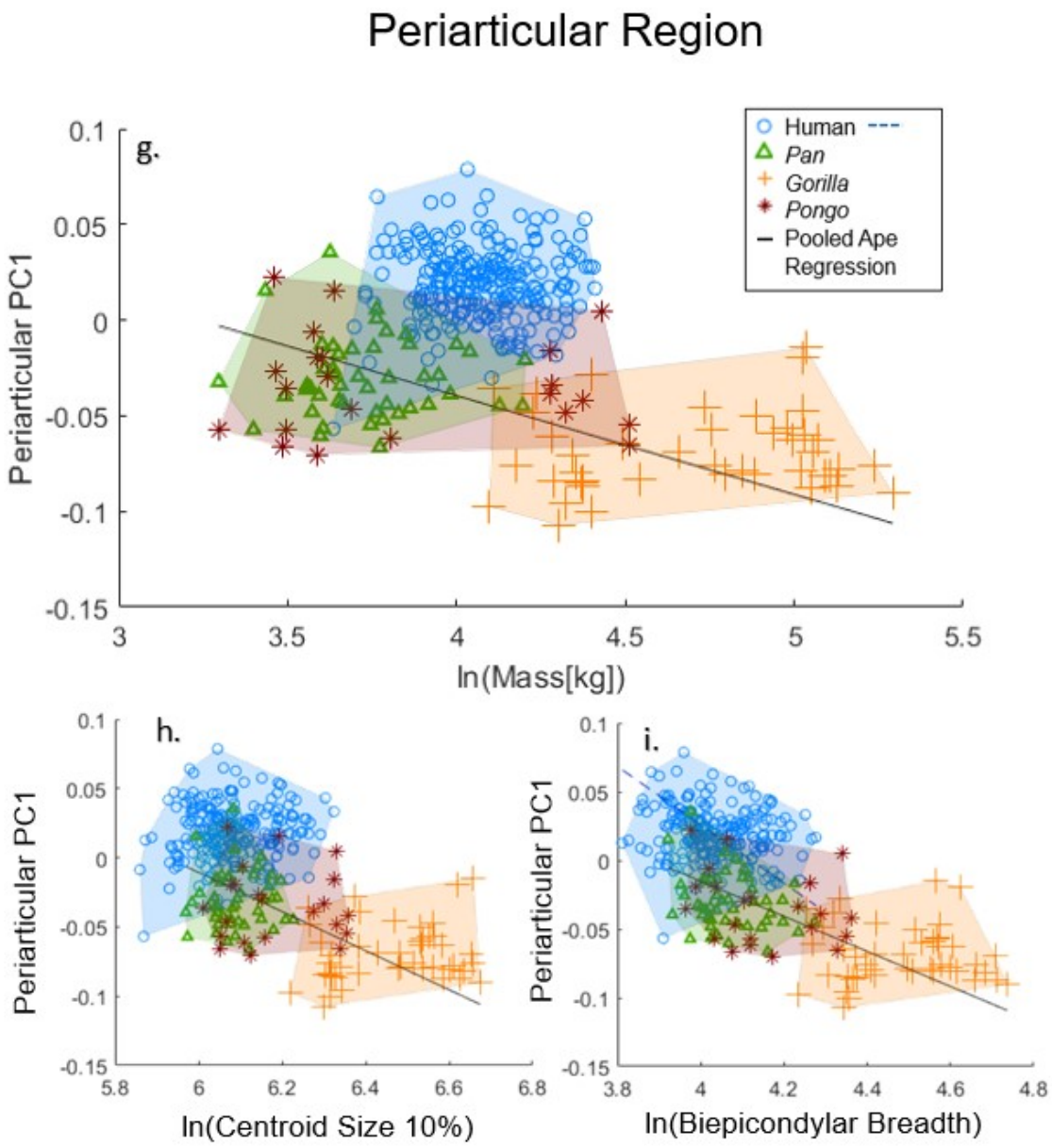
Periarticular Region
g.
Human
Pan
Gorilla
Pongo
Pooled Ape Regression
Periarticular PC1
ln(Mass[kg])
h.
ln(Centroid Size 10%)
i.
ln(Biepicondylar Breadth)

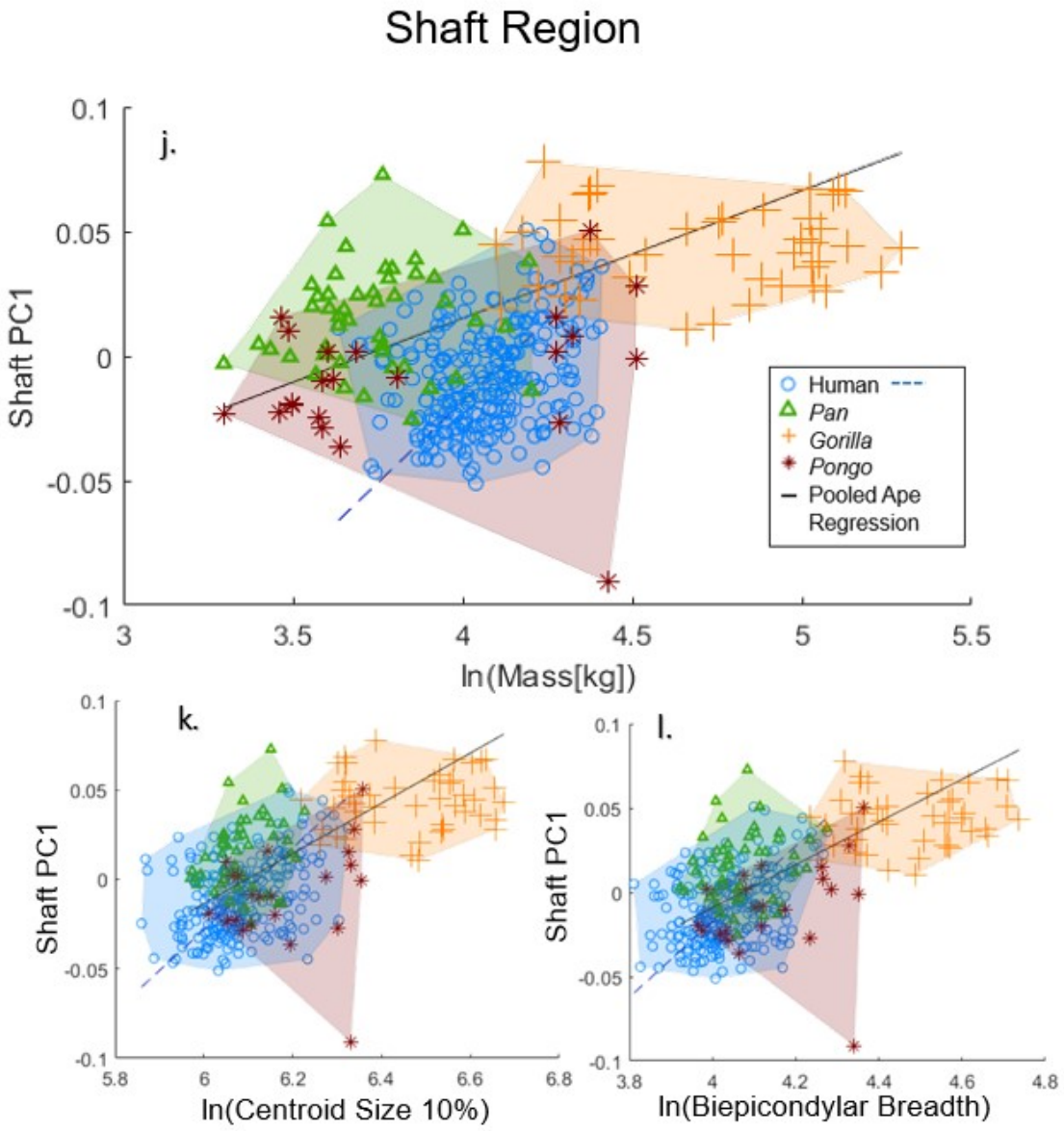

Figure 5-2. Regression of PC1 scores (y axis) on body mass, centroid size of the distal 10%, and biepicondylar breadth. Within-group RMA regression lines are shown where significant.

In Figure 5-3, the results of this allometric trend are demonstrated through depiction of size-related changes of the distal 10%, which includes both articular and periarticular features. The difference between large and small individuals is depicted by the predicted shape of the distal 10% region at extremes of the regression of PC1 scores

on body mass (used to create warps of expected shape at minimum and maximum observed body mass). Ape-like features of large humans include a marked lateral trochlear crest with an associated deep zona conoidea and trochlear groove as well as a more proximally oriented medial and larger lateral epicondyle, while smaller humans have diminished lateral trochlear crests and lesser articular relief, medial trochlear crests that extend further distally, inferiorly oriented medial epicondyles, and a posteriorly expanded articular surface (see Chapter 4 for full comparative morphometric discussion).

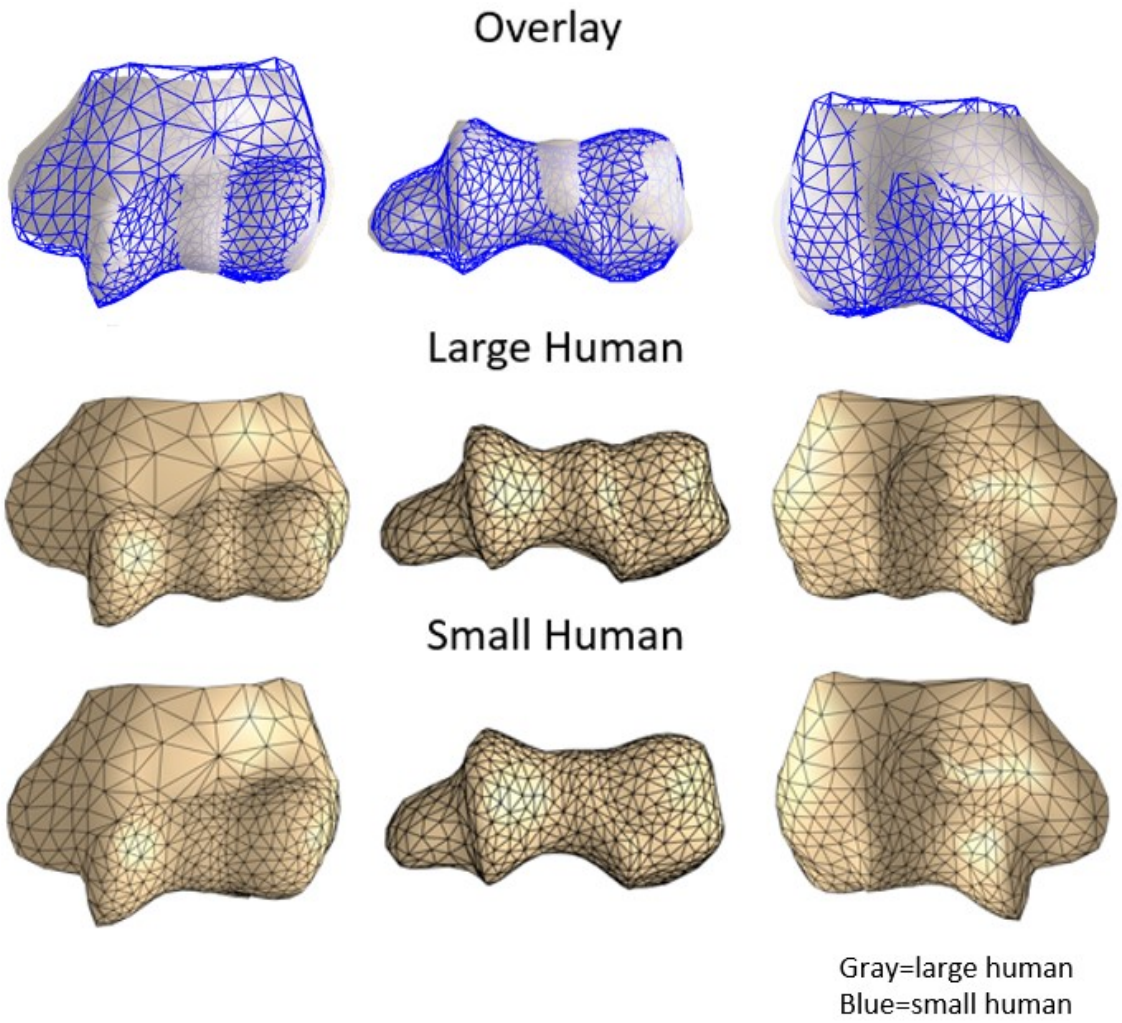

Figure 5-3. Expected shapes of the distal 10% at minimum and maximum human body mass based on RMA regression of PC1 scores on body mass.

However, interpretation of this effect differs slightly depending on the size measure used (see Figure 5-2**Error! Reference source not found.**). Because human distal humeri are small relative to body mass, both centroid size and biepicondylar breadth create a false equivalence between human humeri and those of significantly lighter great apes. For individuals of approximately average mass, many humeri scaled by either by centroid size or biepicondylar breadth appear more similar to apes than is

actually the case (when scaled against body mass). In both the distal 10% and in the articular surface, PC1 scores differ more between humans and great apes of comparable body mass than it does between humans and great apes with comparable biepicondylar breadths or centroid sizes. Likewise, because of the difference in scaling of distal humeral size with body mass, use of centroid size or biepicondylar breadth as a size measure underestimates the size of small humans. Use of different size measures does not appear to strongly affect intertaxon differences among nonhuman hominids, though while no individual great ape taxon has a significant correlation between PC1 scores and size, there is a trend across great ape taxa as a whole.

The periarticular region warrants special attention because of the ways in which it differs from the other three regions analyzed in the overall trends seen in PC1. As noted above (Figure 5-2**Error! Reference source not found.** g-i), in the periarticular region heavier humans are no more like great apes than small humans (g). This is also true for 10% centroid size (h), but there is some convergence between larger humans and nonhuman taxa when scaled against biepicondylar breadth (i). This is perhaps not surprising, because PC1 of this landmark set reflects overall mediolateral expansion. Because of a significant scaling trend among great ape taxa, the smaller great ape genera (*Pan*, *Pongo*) are more human-like on PC1, but this is not true within any individual ape taxon.

A different pattern emerges for PC2, which in the morphological analysis in Chapter 4 appeared to reflect an arboreal-terrestrial gradient among the great apes.

Figure 5-4 shows PC2 scores regressed against the three measures of size, revealing an interesting combination of trends in humans, great apes, and orangutans.

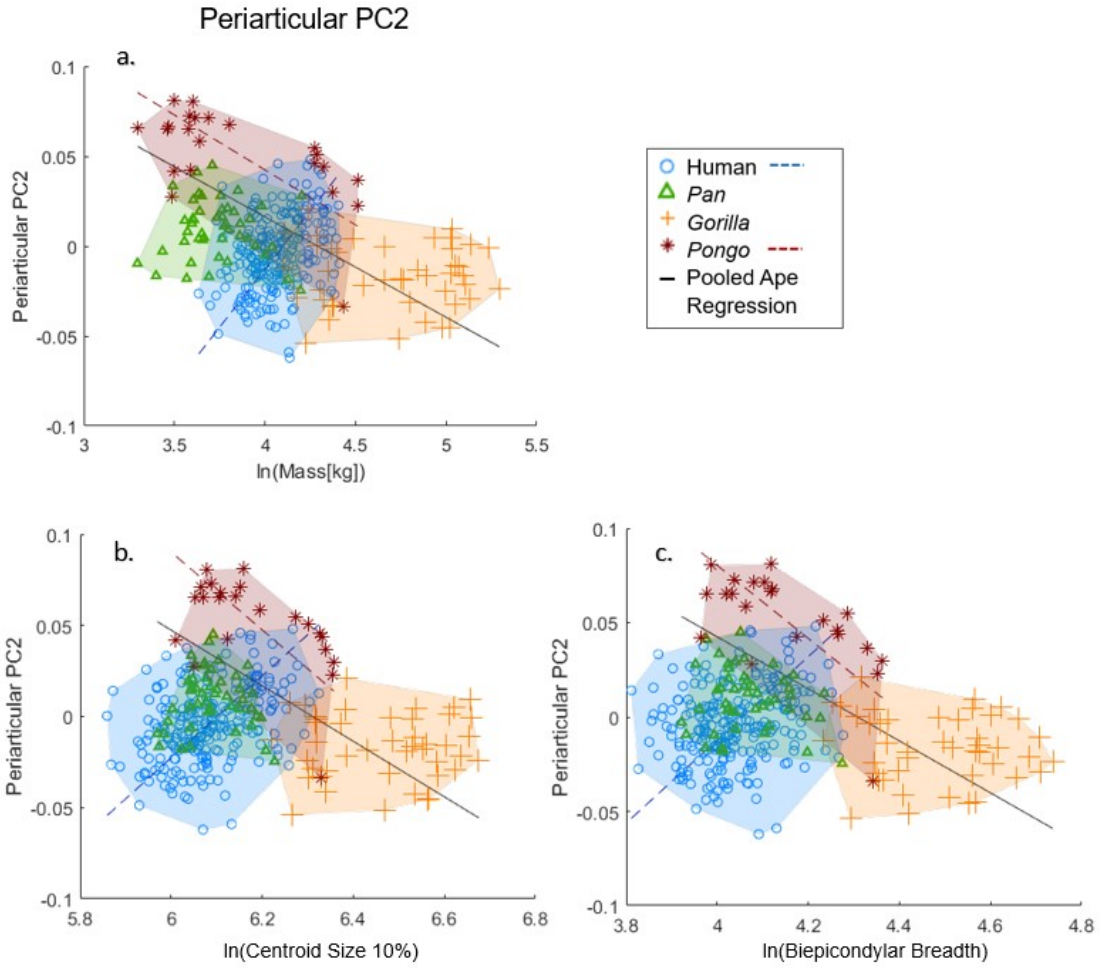

Figure 5-4 Periarticular PC2 regressed on three measures of size. Within-group RMA regression lines are displayed for populations with significant correlations.

Both humans and great apes are significantly correlated with all three measures of size; however, the directions of these correlations are in opposition to each other. While there is a size trend among humans, it cannot be said that large humans are more ape-like on PC2; humans overlap with nearly the entire ape PC2 range. At best, larger

humans are more chimpanzee-like or more orangutan-like, while small humans are more gorilla-like. However, the relationship between and among the great apes is more interesting, in part because on periarticular PC2, there is a significant relationship between size and shape both across genera and within *Pongo*. The size-shape relationship on PC2 suggests that the arboreal-terrestrial gradient among great apes presented in Chapter 4 may be due in part to differences in size. However, because size and locomotor differences parallel each other to some extent (Cant, 1987; Remis, 1995), these factors are difficult to disentangle. That chimpanzees are lower on PC2 than orangutans despite similar mass may possibly argue for locomotor effects, but this possibility should be explored in greater detail.

5.3 Fossil interpretation

The size relationships within and among extant taxa provide the necessary context for understanding how size may influence fossil hominin morphology. In the following section, nine fossil hominins (KNM-KP 271, A.L. 288-1, StW 431, KNM-ER 1504, KNM-ER 739, TM 1517, SK 24600, SKX 10924, and Gombore IB 7594; KNM-ER 6020 is omitted because the selected size measures are not available) are interpreted within this context in order to further understand whether and how use of different size measures is likely to affect interpretation of fossils.

5.3.1 Size estimation

Three of the ten fossil hominins in this study have body masses estimated from femoral dimensions (see Ruff et al., 2018; estimated body mass for KNM-ER 1504 is that

calculated for KNM-ER 1503/5 - see Chapter 2 for justification for association of KNM-ER 1503/5 with 1504). Figure 5-5 shows the relationship between body mass, centroid size, and biepicondylar breadth for these three individuals. These results impact our understanding of these specimens, and also serve to demonstrate relationships that may be present but not currently assessable in other fossil hominins.

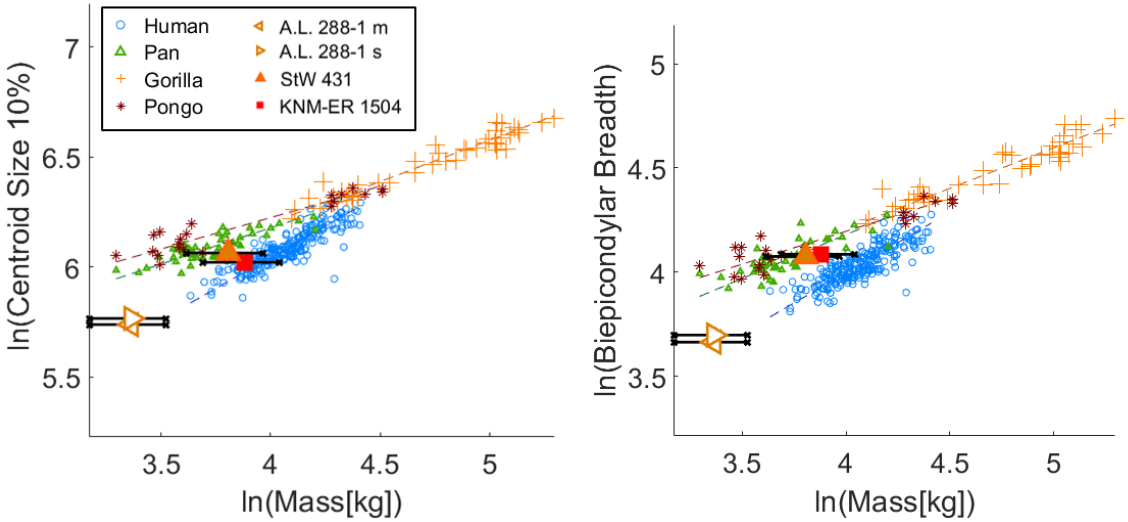

Figure 5-5. Log-log regression of centroid size of the distal 10% (10Cz) and biepicondylar breadth (BiEp) against body mass, with the addition of A.L. 288-1, KNM-ER 1504 and StW 431. RMA regression lines in colors corresponding to genus markers.

The diminutive A.L. 288-1 (*A. afarensis*) has a strikingly human-like relationship between body mass and both other measures of size, falling almost directly on the trajectory of the human regression line. This is not the case for the other two fossils. The biggest difference is seen in biepicondylar breadth. The epicondyles of StW 431 (*A. africanus*) and KNM-ER 1504 (*P. boisei*) are extremely large relative to estimated body mass; these individuals from more recent taxa diverge considerably from the human regression line, falling within the chimpanzee range. If body mass estimates are correct,

use of biepicondylar breadth as a scaling factor for these individuals would overestimate size (at least, using a human model). The relationship of centroid size to body mass of StW 431 and KNM-ER 1504 is somewhat different than that seen for the epicondyles. While centroid size of StW 431 remains within the chimpanzee range, it falls near the range of human-ape overlap. Centroid size is human-like relative to estimated body mass in KNM-ER 1504 (as well as A.L. 288-1); this measure is therefore less likely than biepicondylar breadth to bias allometric analyses.

5.3.2 Fossil Shape

To investigate the possible impact of allometry on interpretation of fossil morphology, the position of fossils on PC1 of the distal 10%, articular, periarticular and shaft analyses, as well as PC2 of the periarticular analysis were placed in the context of the regressions presented in section 5.2 above. Their position relative to the human regression line was analyzed in the context of both fossil age and taxonomy. This was done in order to understand how comparison to humans of similar size rather than to all humans in the modern size range changes interpretation of which fossils are most or least like *Homo sapiens*.

For each of the fossils, the RMA residual to the within-human regression line was calculated for each of the five target PCs (see above). Results were omitted where the within-human correlation was not significant (i.e., periarticular PC1 scores against body mass and centroid size). Figure 5-6 (Distal 10% PC1), Figure 5-7 (articular PC1), Figure 5-8 (periarticular PC1; residual plots omitted for c. and d. due to lack of significant allometry

in humans), Figure 5-9 (shaft PC1), and Figure 5-10 (periarticular PC2) show fossil PC scores placed in the context of regression on different size measures. Below each bivariate plot, fossil residuals from the human regression line are plotted against time. A description of general trends is given below, which are similar across analyses unless otherwise noted.

a.

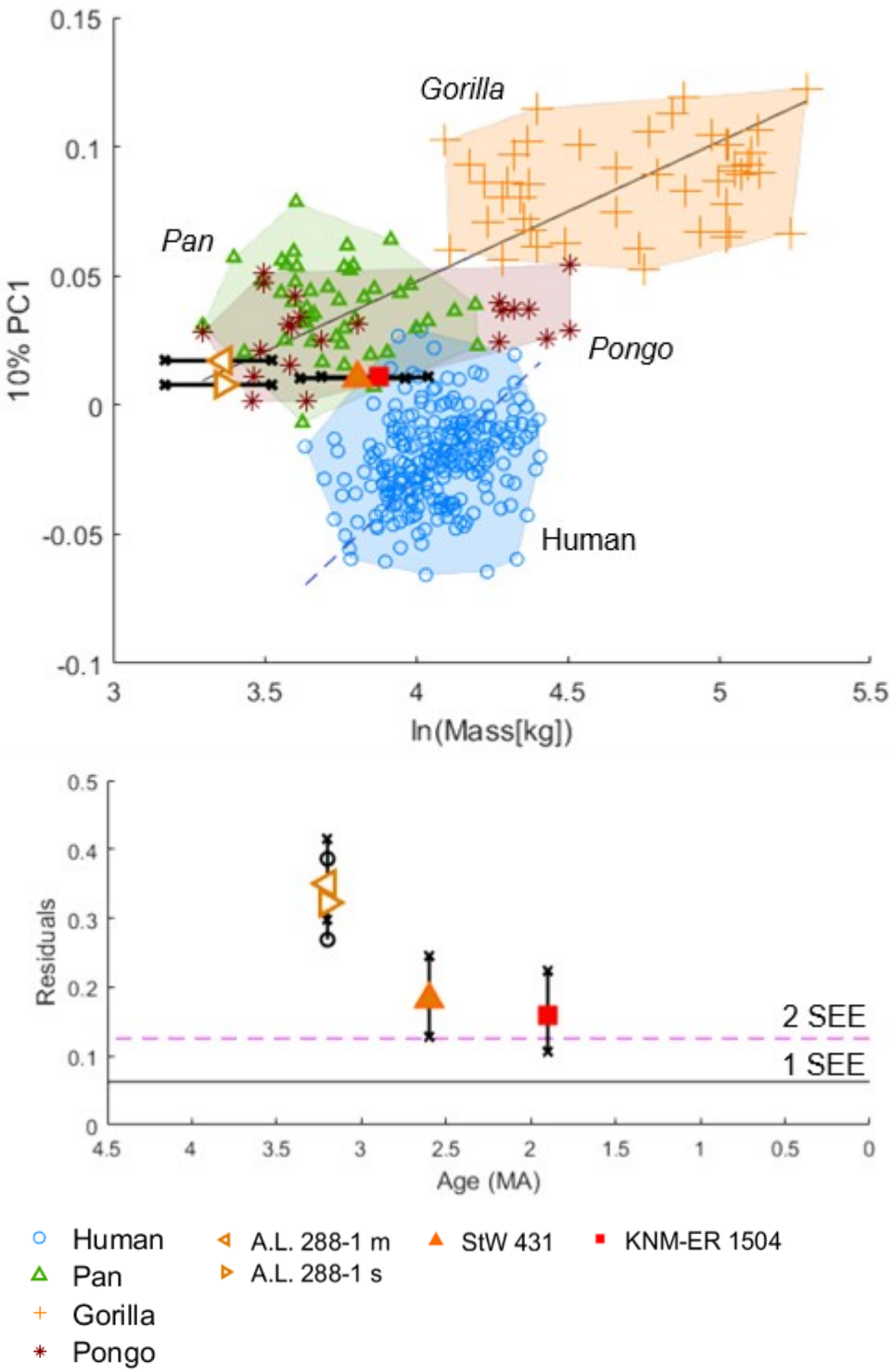
Gorilla
Pan
Pongo
Human
10% PC1
ln(Mass[kg])
Residuals
2 SEE
1 SEE
Age (MA)
Human
Pan
Gorilla
Pongo
A.L. 288-1 m
A.L. 288-1 s
StW 431
KNM-ER 1504

b.

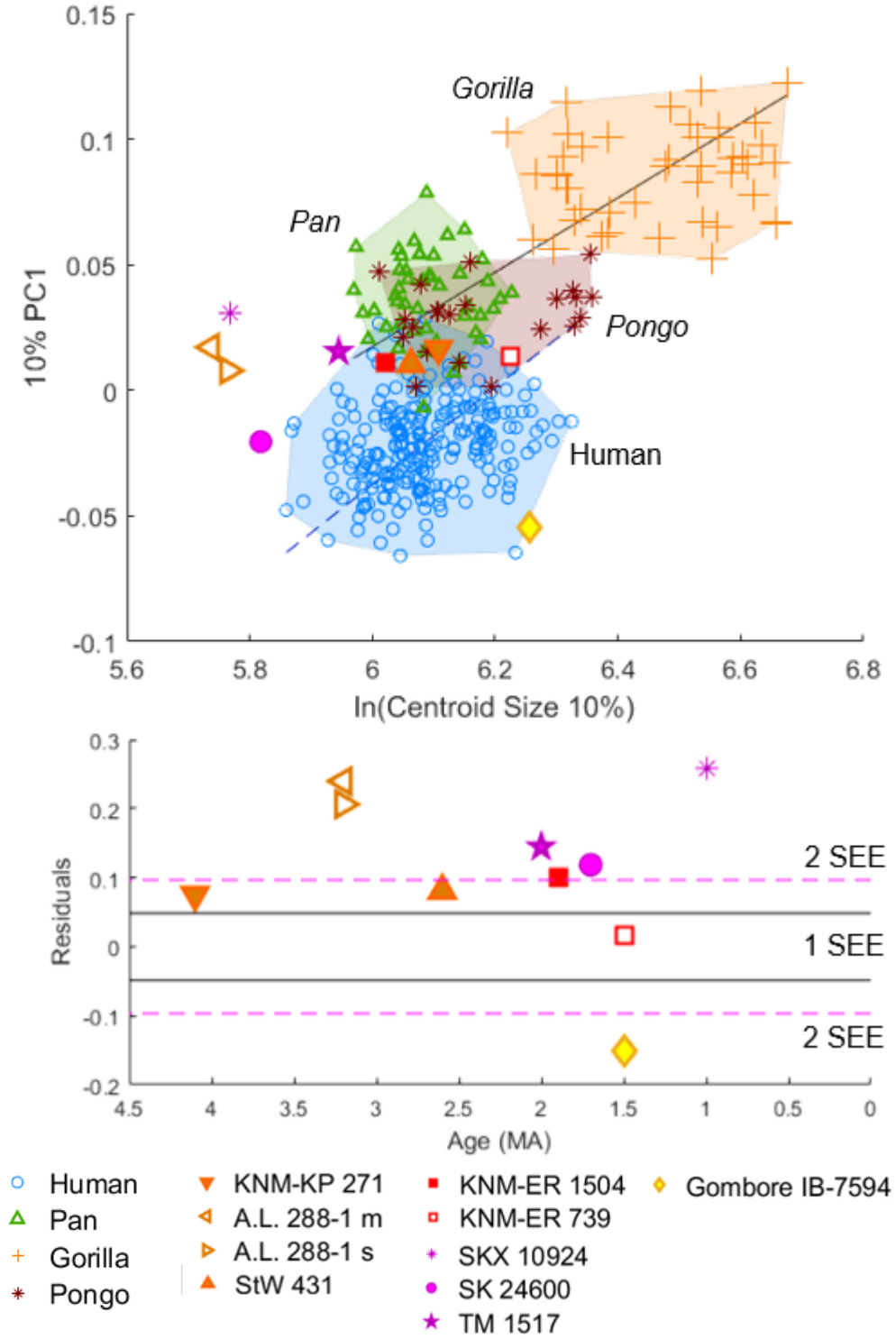
Gorilla
Pan
Pongo
Human
10% PC1
ln(Centroid Size 10%)
Residuals
2 SEE
1 SEE
2 SEE
Age (MA)
Human
Pan
Gorilla
Pongo
KNM-KP 271
A.L. 288-1 m
A.L. 288-1 s
StW 431
KNM-ER 1504
KNM-ER 739
SKX 10924
SK 24600
TM 1517
Gombore IB-7594

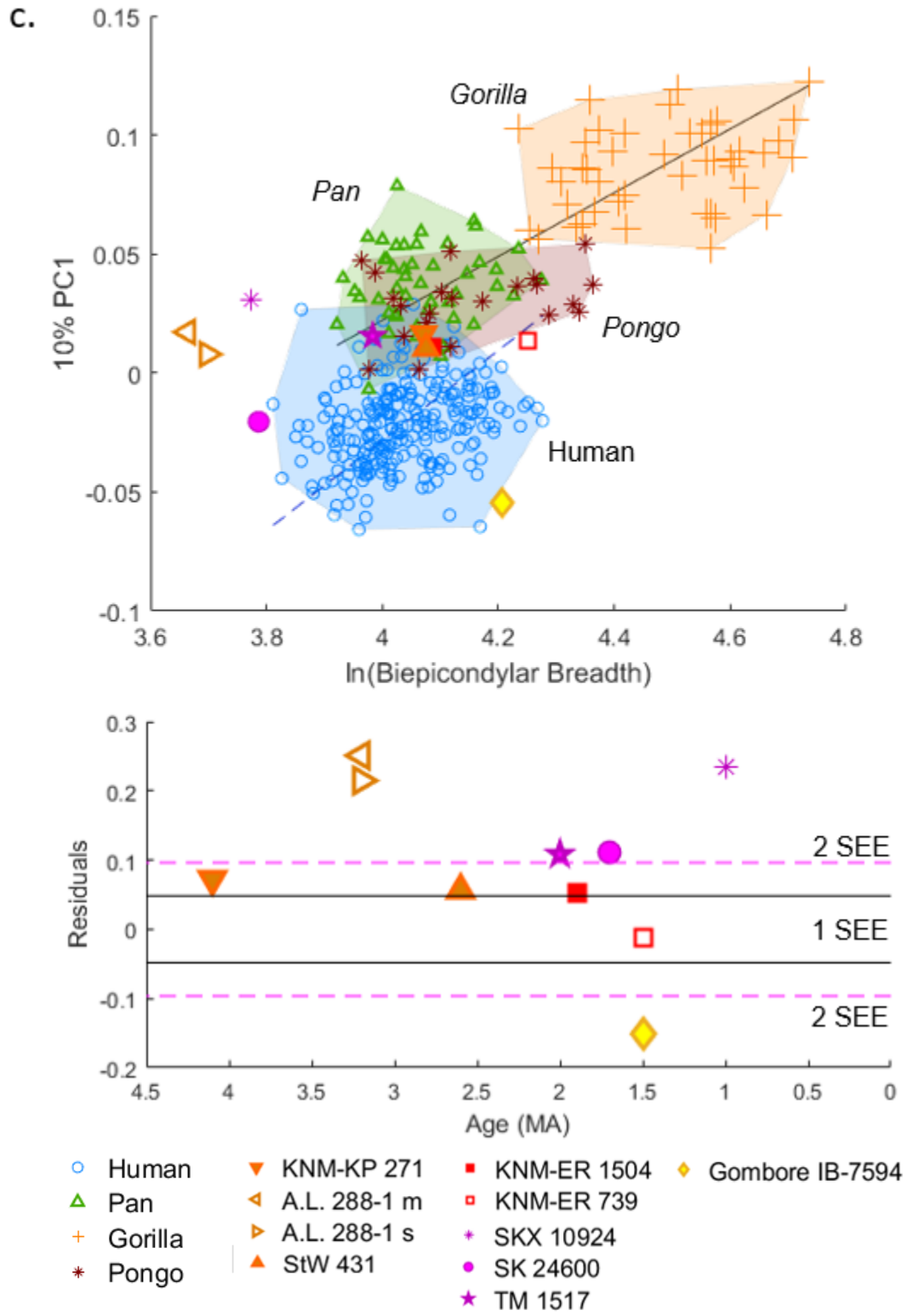

Figure 5-6. PC1 of the distal 10%, scaled by body mass, centroid size and biepicondylar breadth. Residuals are plotted against fossil age, with SEE of the human regression as reference.

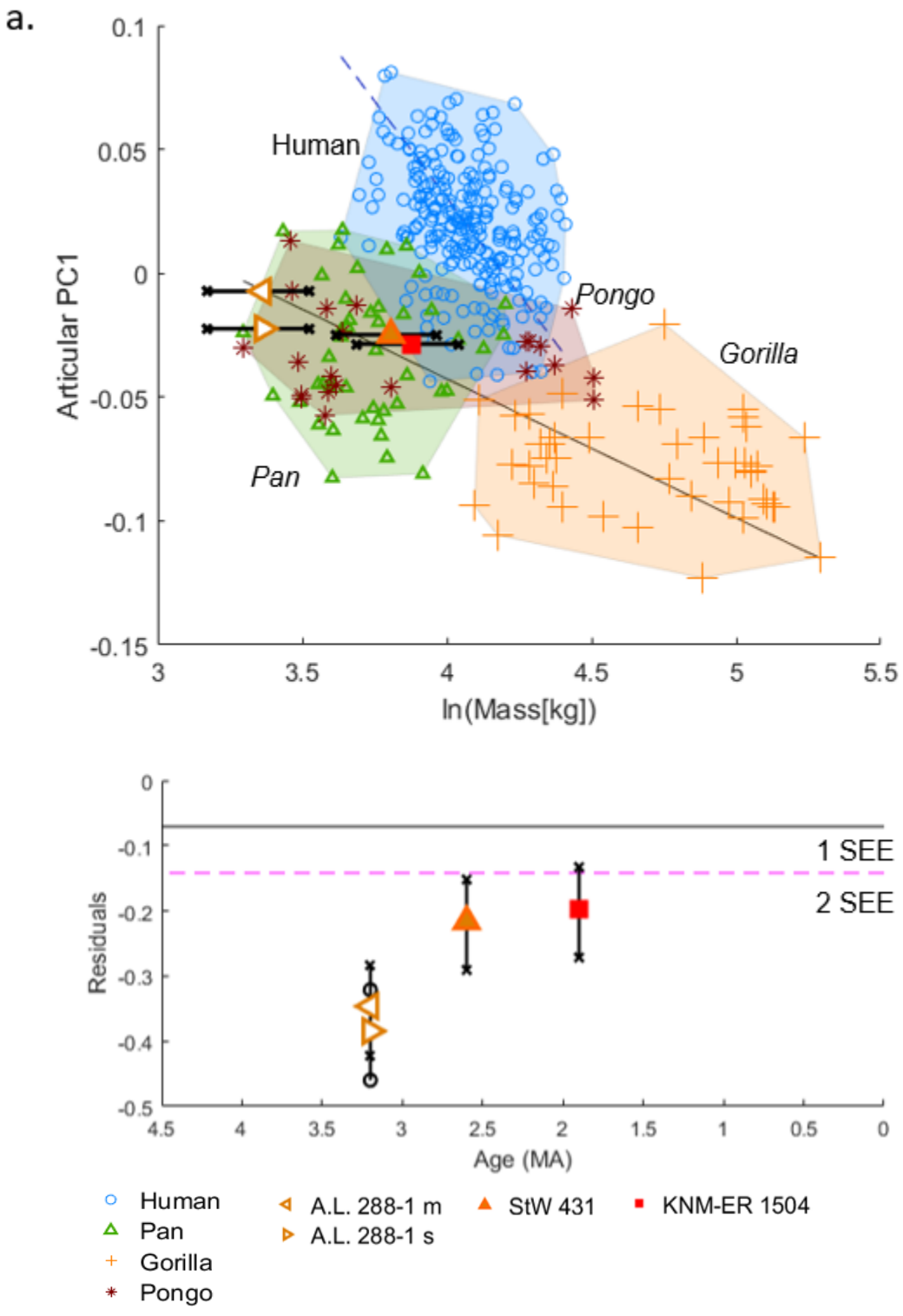
a.
Articular PC1
ln(Mass[kg])
Human
Pongo
Gorilla
Pan
Residuals
Age (MA)
1 SEE
2 SEE
Human
Pan
Gorilla
Pongo
A.L. 288-1 m
A.L. 288-1 s
StW 431
KNM-ER 1504

b.

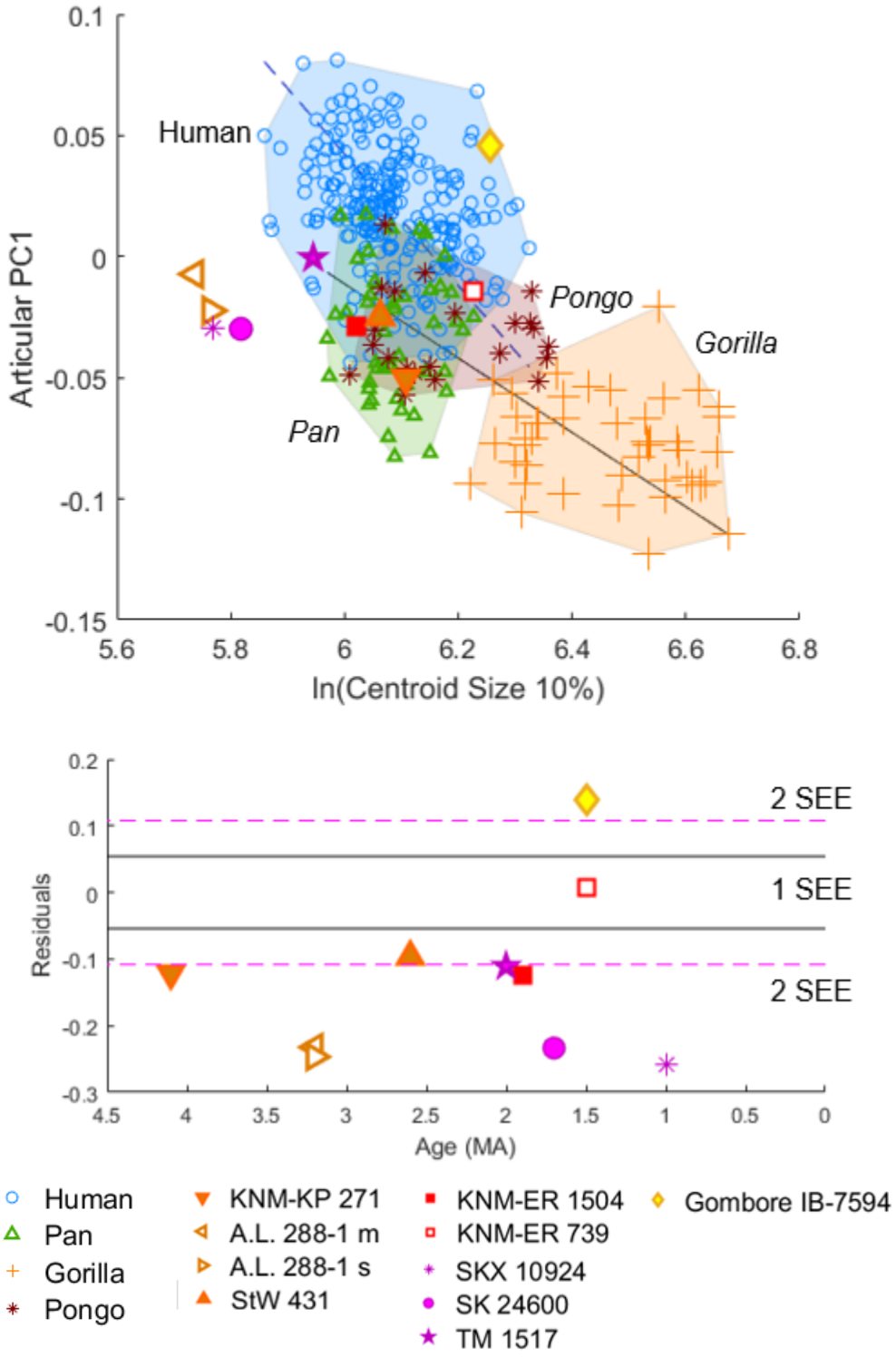
Human
Pongo
Gorilla
Pan
Articular PC1
ln(Centroid Size 10%)
0.1
0.05
0
-0.05
-0.1
-0.15
5.6
5.8
6
6.2
6.4
6.6
6.8
2 SEE
1 SEE
2 SEE
Residuals
0.2
0.1
0
-0.1
-0.2
-0.3
4.5
4
3.5
3
2.5
2
1.5
1
0.5
0
Age (MA)
Human
Pan
Gorilla
Pongo
KNM-KP 271
A.L. 288-1 m
A.L. 288-1 s
StW 431
KNM-ER 1504
KNM-ER 739
SKX 10924
SK 24600
TM 1517
Gombore IB-7594

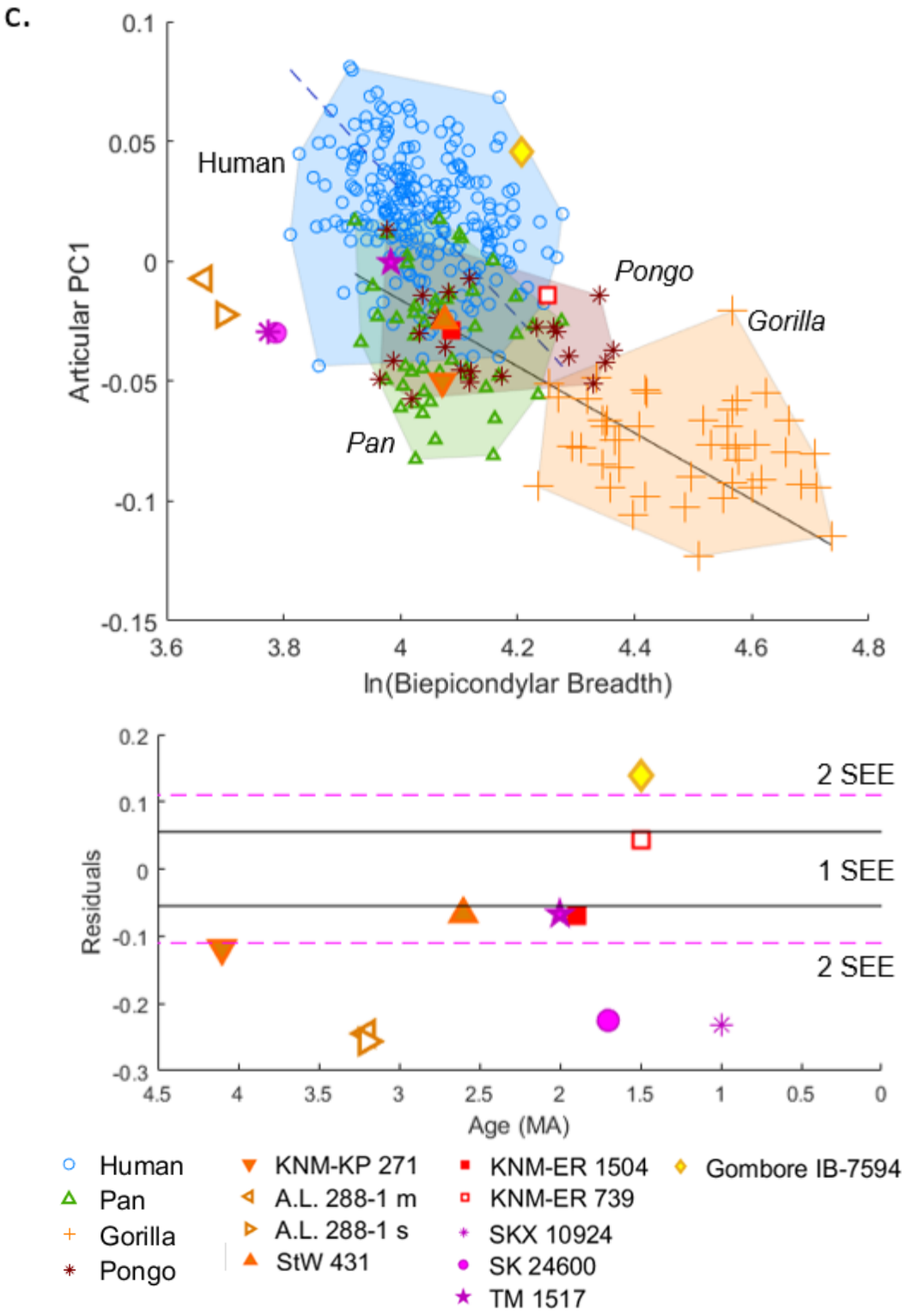

Figure 5-7. PC1 of articular shape scaled by body mass, centroid size and biepicondylar breadth. Residuals are plotted against fossil age, with SEE of the human regression as reference.

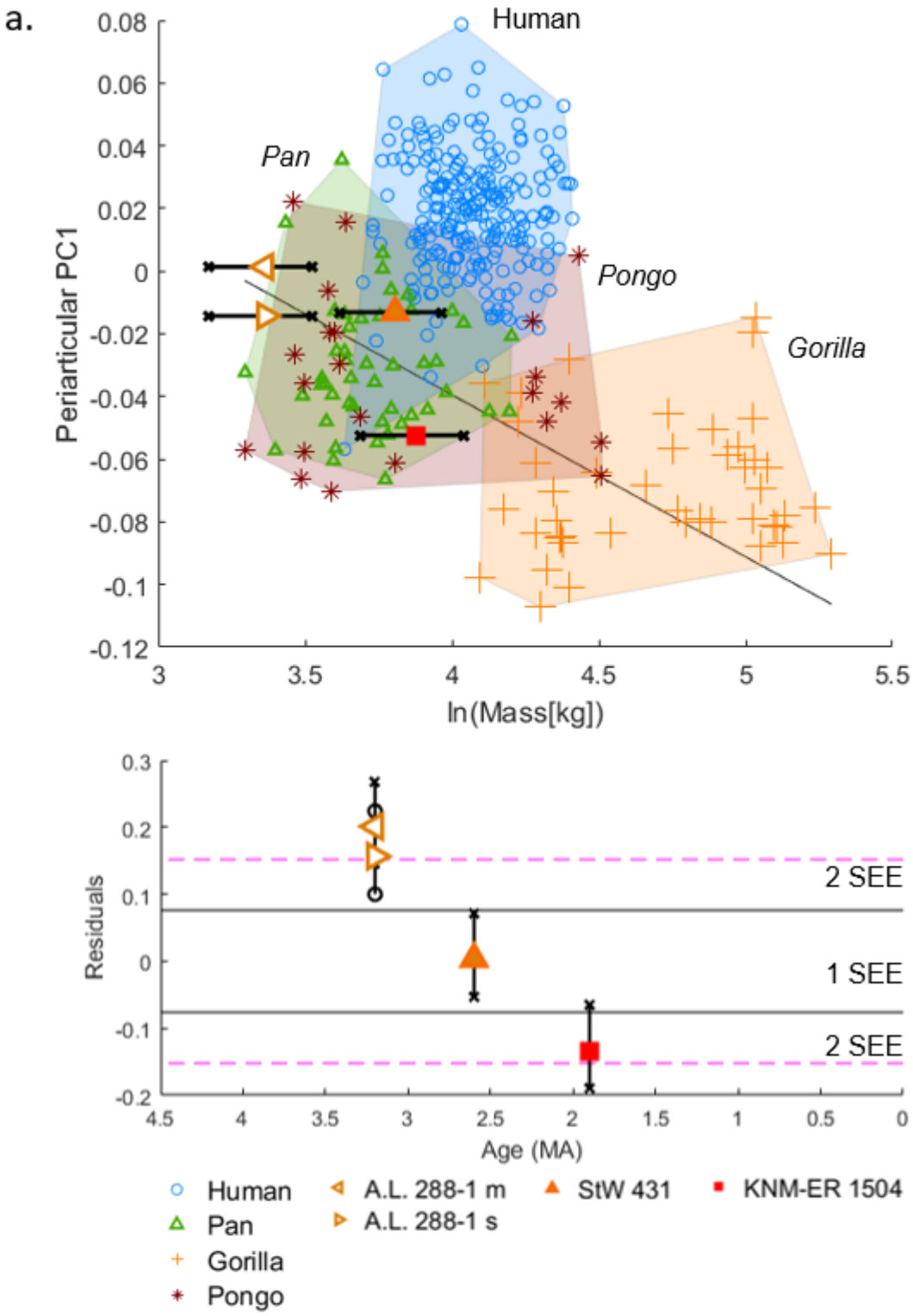
a.
Human
Pan
Pongo
Gorilla
Periarticular PC1
ln(Mass[kg])
Residuals
2 SEE
1 SEE
2 SEE
Age (MA)
Human
Pan
Gorilla
Pongo
A.L. 288-1 m
A.L. 288-1 s
StW 431
KNM-ER 1504

b.

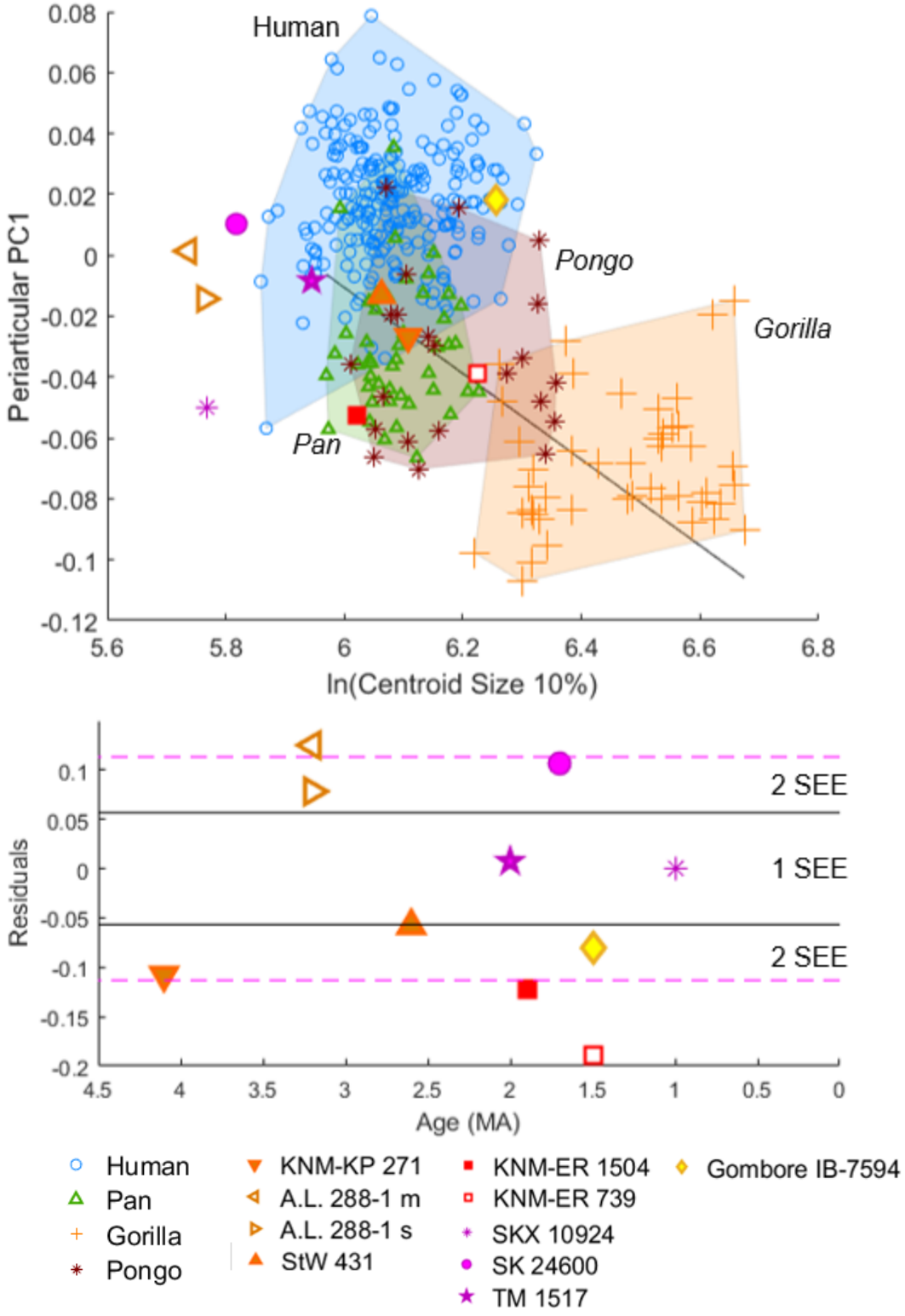
Human
Pongo
Gorilla
Pan
Periarticular PC1
ln(Centroid Size 10%)
0.08
0.06
0.04
0.02
0
-0.02
-0.04
-0.06
-0.08
-0.1
-0.12
5.6
5.8
6
6.2
6.4
6.6
6.8
Residuals
Age (MA)
2 SEE
1 SEE
2 SEE
0.1
0.05
0
-0.05
-0.1
-0.15
-0.2
4.5
4
3.5
3
2.5
2
1.5
1
0.5
0
Human
Pan
Gorilla
Pongo
KNM-KP 271
A.L. 288-1 m
A.L. 288-1 s
StW 431
KNM-ER 1504
KNM-ER 739
SKX 10924
SK 24600
TM 1517
Gombore IB-7594

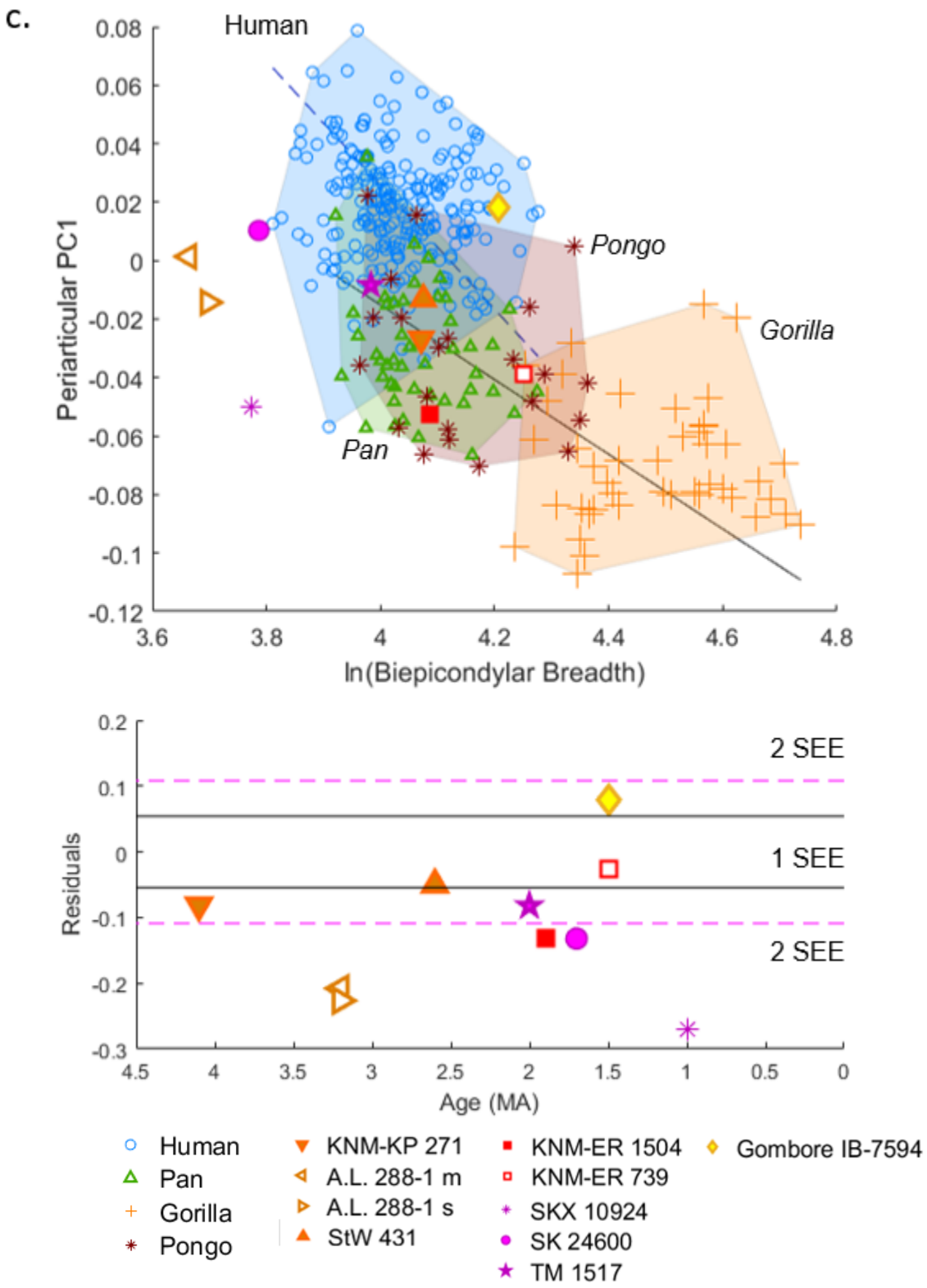

Figure 5-8 PC1 of the periarticular region scaled by body mass, centroid size and biepicondylar breadth. Residuals are plotted against fossil age, with SEE of the human regression as reference.

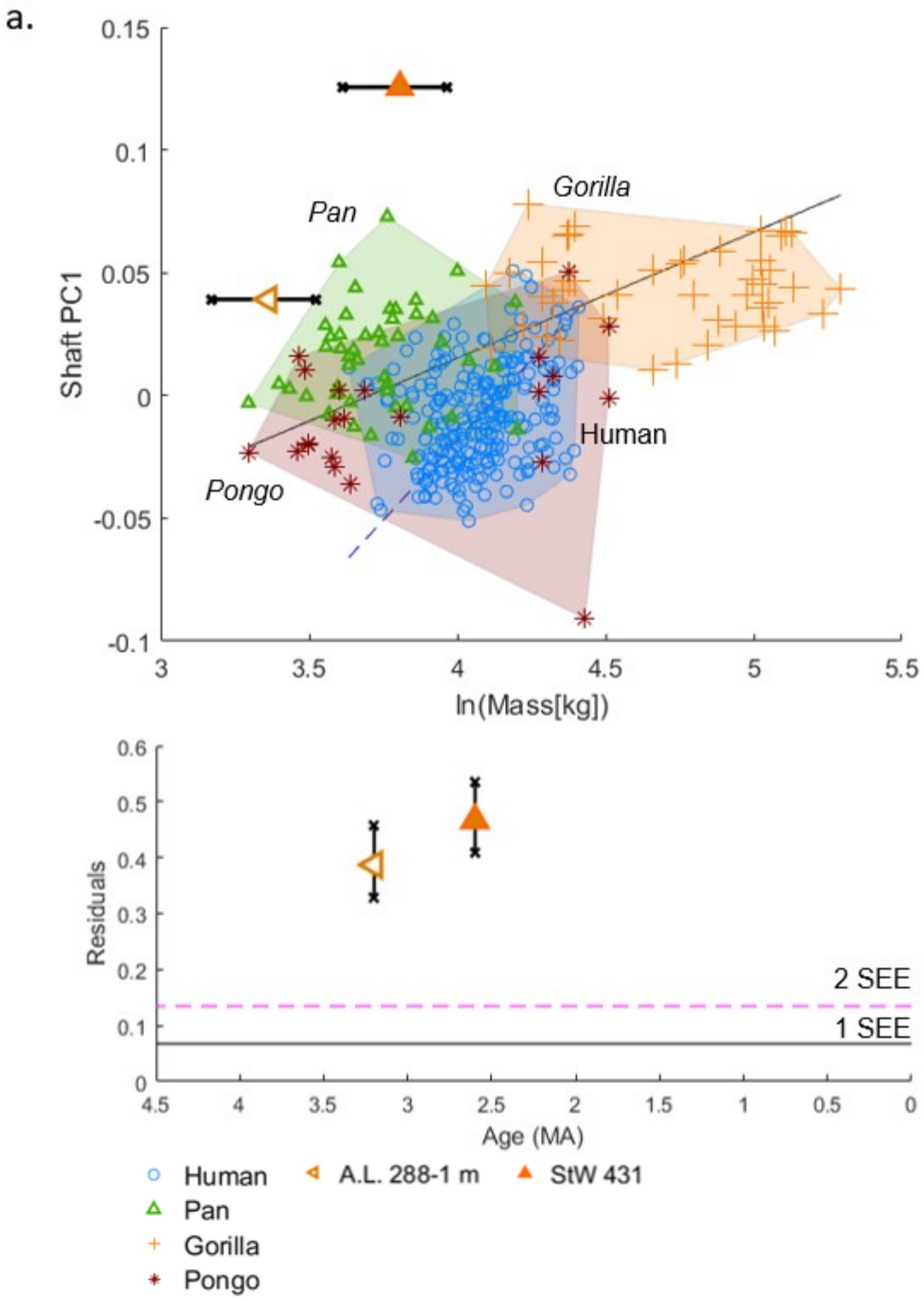
a.
Shaft PC1
ln(Mass[kg])
Pan
Gorilla
Human
Pongo
Residuals
Age (MA)
2 SEE
1 SEE
Human
Pan
Gorilla
Pongo
A.L. 288-1 m
StW 431

b.

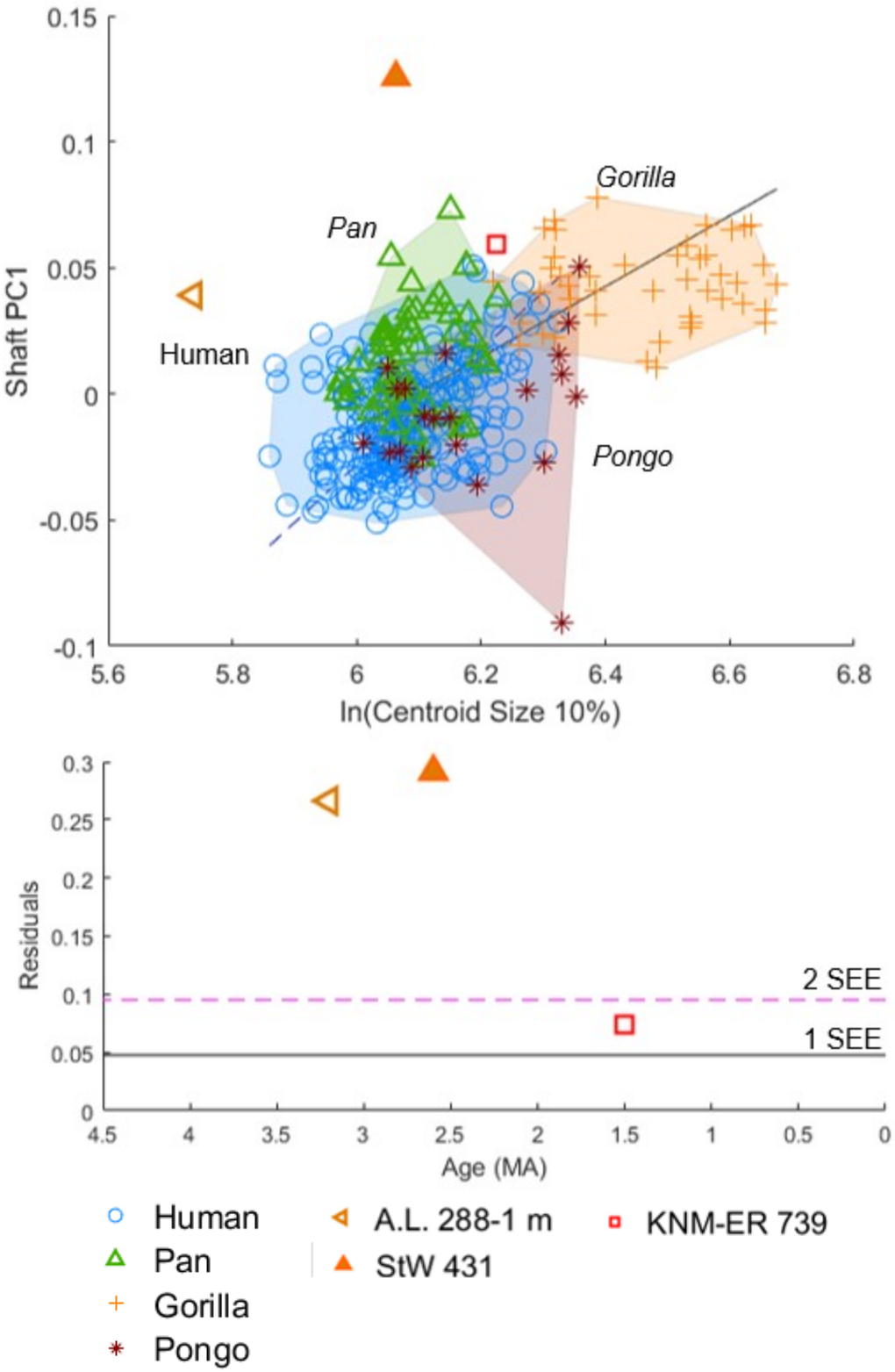
Shaft PC1
0.15
0.1
0.05
0
-0.05
-0.1
5.6
5.8
6
6.2
6.4
6.6
6.8
ln(Centroid Size 10%)
Gorilla
Pan
Human
Pongo
Residuals
0.3
0.25
0.2
0.15
0.1
0.05
0
4.5
4
3.5
3
2.5
2
1.5
1
0.5
0
Age (MA)
2 SEE
1 SEE
Human
Pan
Gorilla
Pongo
A.L. 288-1 m
StW 431
KNM-ER 739

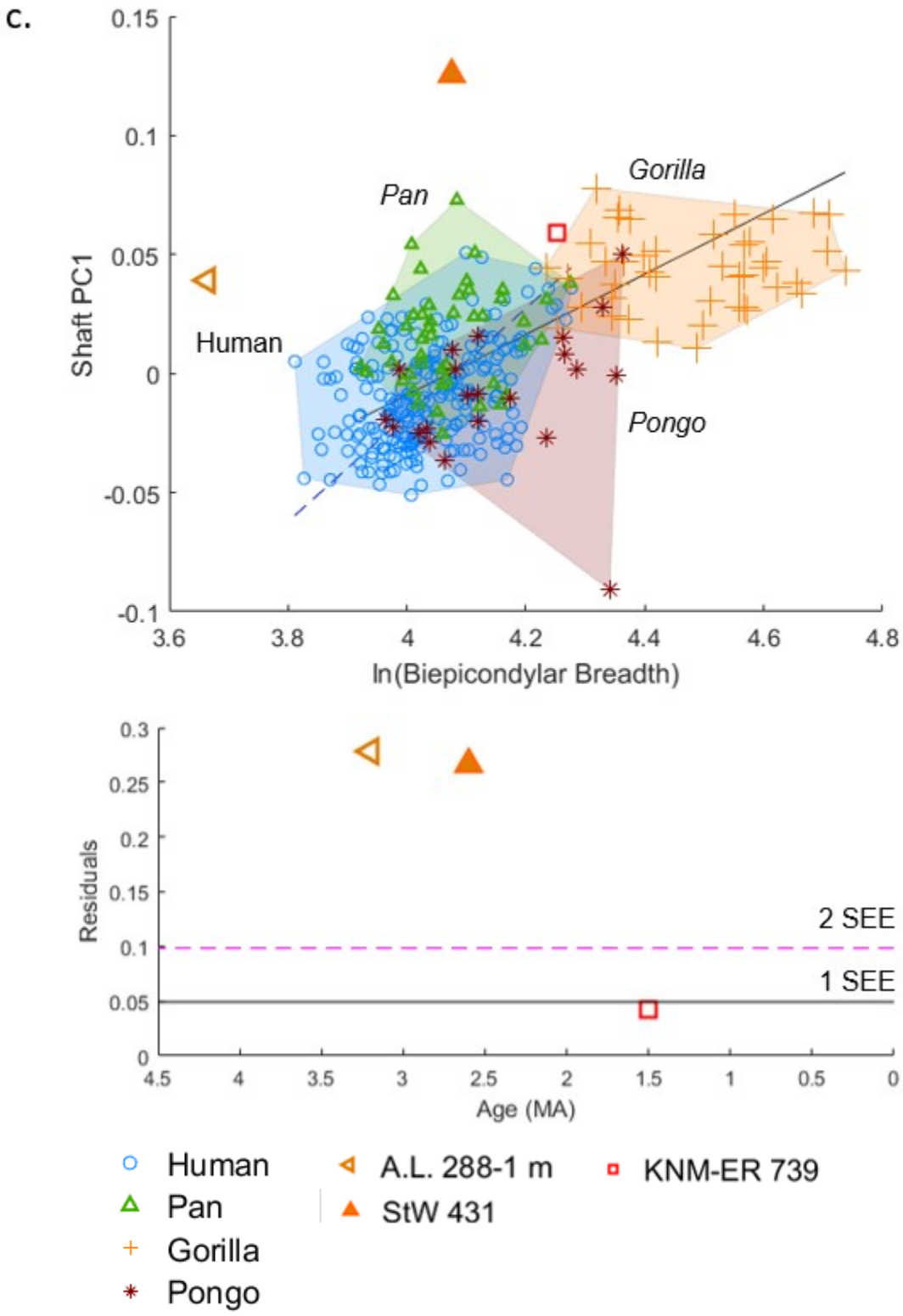

Figure 5-9. PC1 of shaft shape scaled by body mass, centroid size and biepicondylar breadth. Residuals are plotted against fossil age, with SEE of the human regression as reference.

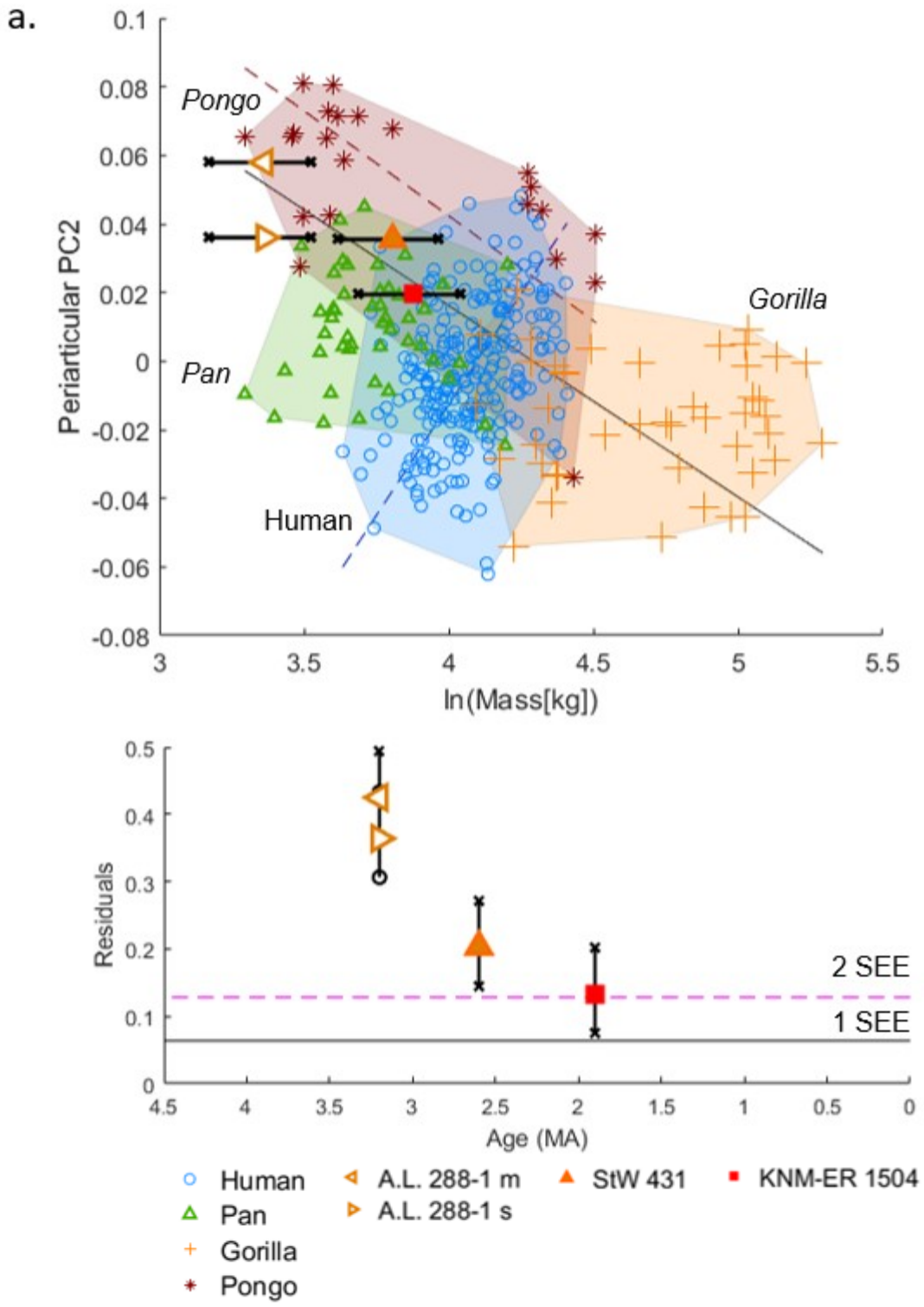
a.
Pongo
Gorilla
Pan
Human
Periarticular PC2
ln(Mass[kg])
Residuals
2 SEE
1 SEE
Age (MA)
Human
Pan
Gorilla
Pongo
A.L. 288-1 m
A.L. 288-1 s
StW 431
KNM-ER 1504

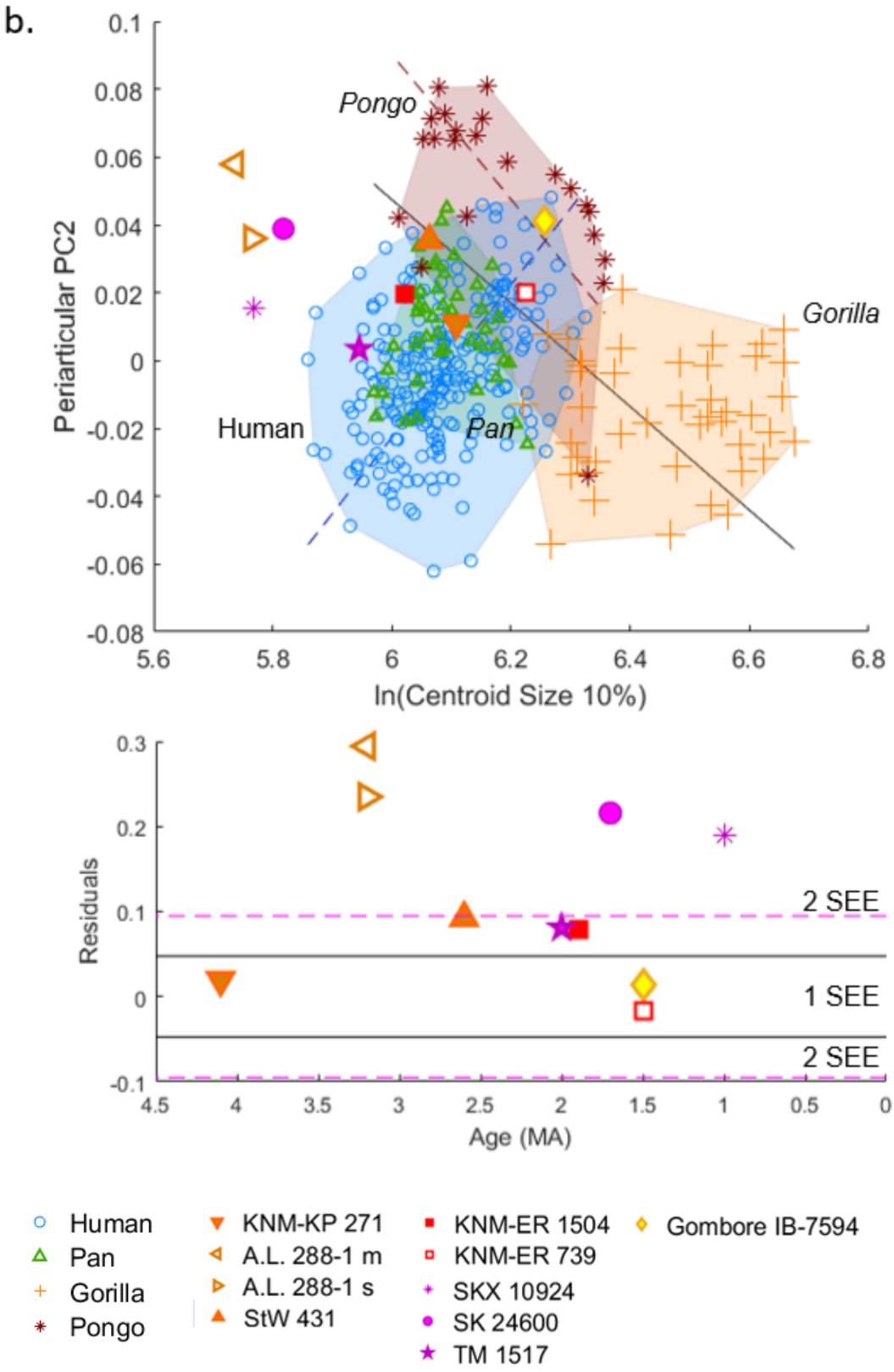
b.
Periarticular PC2
ln(Centroid Size 10%)
Pongo
Gorilla
Human
Pan
Residuals
Age (MA)
2 SEE
1 SEE
2 SEE
Human
Pan
Gorilla
Pongo
KNM-KP 271
A.L. 288-1 m
A.L. 288-1 s
StW 431
KNM-ER 1504
KNM-ER 739
SKX 10924
SK 24600
TM 1517
Gombore IB-7594

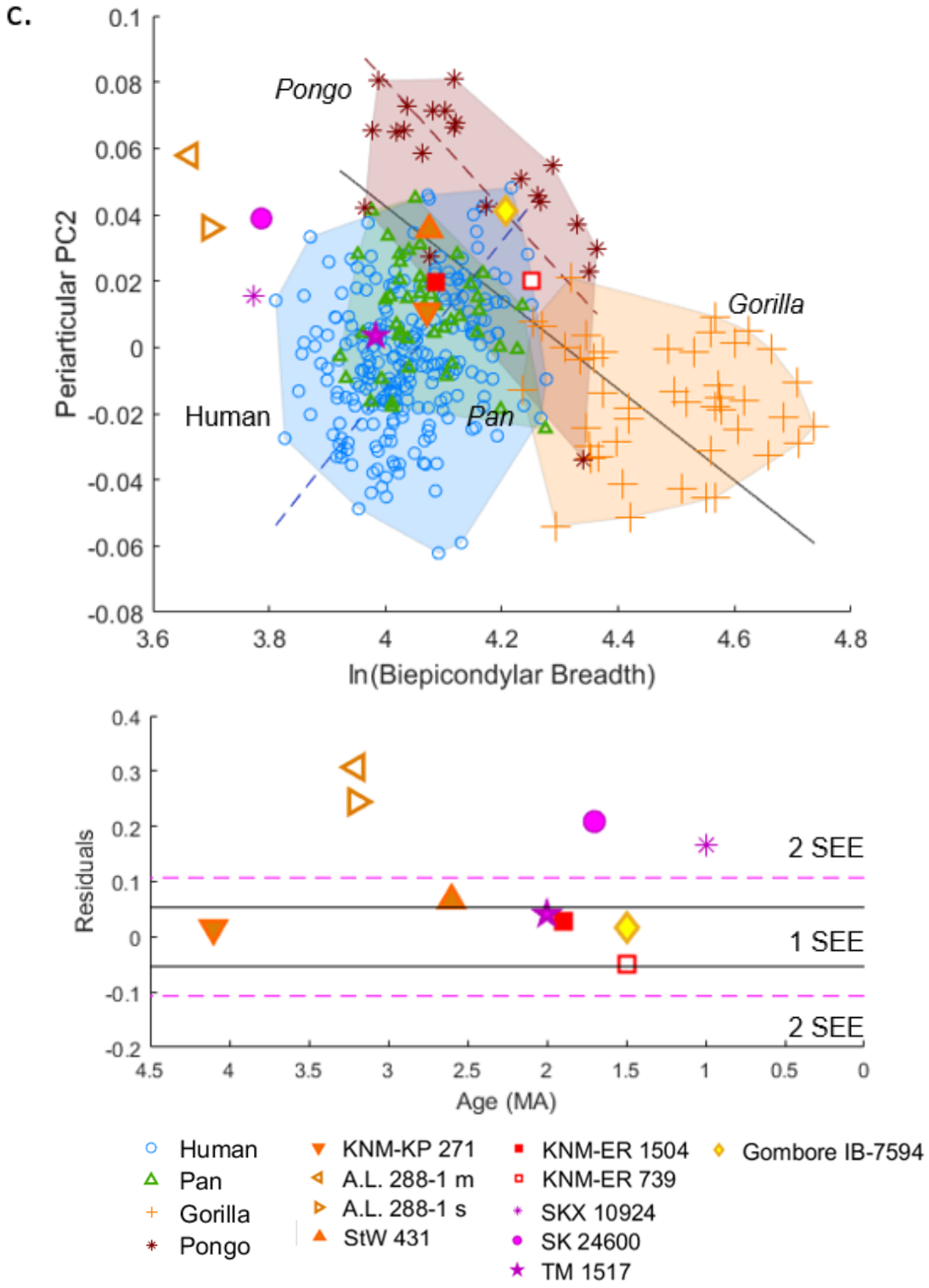

Figure 5-10. PC2 of periarticular shape scaled by body mass, centroid size and biepicondylar breadth. Residuals are plotted against fossil age, with SEE of the human regression as reference.

While in Chapter 4 fossil hominins appeared either human-like or intermediate between humans and great apes on PC1 (in articular morphology and the distal 10%), when these results are plotted against size variables , fossil hominin morphology, with the exception of Gombore IB 7594, generally appears ape-like, though several individuals remain within the human range due to overlap between humans and other hominids. This is true for PC1 scores of the distal 10% (Figure 5-6) and articular surface (Figure 5-7), and both PC1 and 2 scores of the periarticular surface (Figure 5-8 and Figure 5-10). Interestingly, fossil hominin shaft morphology (Figure 5-9), which in Chapter 4 appeared ape-like, appears to diverge strongly from both humans and great apes when scaled against size. While fossil hominin shafts are nevertheless more ape-like absolutely, strong positive allometry of the human shaft erodes the difference between the very robust KNM-ER 739 and humans and amplifies the human difference from A.L. 288-m.

Differences between unscaled and scaled analyses had the strongest effect on interpretation of small individuals. A.L. 288-1 (Lucy) is the smallest fossil specimen in the sample. It is important to note that this specimen falls below the observed human body size range, and so requires extrapolation of the regression line. In analyses that do not account for allometry, A. L. 288-1 is at the edge of the range of modern human morphology (see Chapter 4 for full discussion of geometric morphometric results). Scaled by body size, however, A.L. 288-1 clearly exceeds the human range if current

body mass estimations are accurate. This is true for all bone regions analyzed (Figure 5-6 through Figure 5-10). In these analyses, A.L. 288-1m is consistently the farthest from the expected human morphology of all fossils analyzed, though in most analyses it is matched by SKX 10924 (but see Figure 5-10, periarticular PC2). Contra Lague (2014), who found KNM-KP 271 to be the least human-like fossil specimen, KNM-KP 271 is consistently near or within the expected range (+/- 2 SEE) of modern humans in these size-scaled analyses.

Fossils generally show the same relationship to the human range regardless of landmark set or PC analyzed. The following associations are found with relationship to centroid size. StW 431 is relatively human-like in all but the shaft (Figure 5-9). KNM-ER 1504 and KNM-ER 739 (*P. boisei*) are respectively near or within the human range, with TM 1517 (*P. robustus*) approximately following the trend for KNM-ER 1504 for all analyses. Gombore IB 7594 shows a different pattern from the other fossils. While it is sometimes outside the modern human range (see distal 10% , Figure 5-6 and articular, Figure 5-7) it is always on the opposite side of the regression line from the majority of great apes. This usually differentiates it from the other fossils, which tend to be more ape-like (see Figure 5-6, Figure 5-7, Figure 5-8 a.). The only PC scores for which this is not true are scores on PC2 of the periarticular surface. SKX 10924 (*P. robustus*) is consistently far outside the human range. While SK 24600 sometimes joins SKX 10924, as in analysis of the articular surface (Figure 5-7) and to some extent periarticular PC2 scores (Figure 5-10), in general the two diverge. Of the two, SK 24600 is more human-

like, especially on periarticular PC1, though both are more ape-like than predicted for humans of comparable size (Figure 5-8; see also distal 10% PC1, Figure 5-6).

These observations vary slightly depending on the scaling variable used, with fossils moving in relation to each other and to the human distribution, but these differences are, in general, slight. It is however notable that use of body mass as a scaling variable appears to amplify differences between humans and fossils, while fossil-human differences are diminished by use of centroid size and biepicondylar breadth, as noted earlier for comparisons between modern humans and great apes. When scaled by body mass, all three individuals for which it is available have articular, shaft, and distal 10% morphology outside the human +2 SEE range (see subfigure a. in Figures 5-6, 5-7, and 5-9; because periarticular PC1 scores show no correlation with body mass, it was not assessed here, but see periarticular PC2, Figure 5-10). When scaled by centroid size or biepicondylar breadth, however, both StW 431 and KNM-ER 1504 fall within the range of modern humans for all PCs other than PC1 of the shaft (Figure 5-9); the shaft of StW 431 remains an outlier in shaft morphology regardless of size measure, and the shaft of KNM-ER 1504 is not preserved and therefore cannot be assessed.

The size measure used also affects the relationship between fossil hominins and great apes. When scaled by body mass, the shaft, periarticular and articular morphology of A.L. 288-1 is clearly similar to that of chimpanzees and orangutans of similar size. However, the relationship between great apes and humans changes when scaled by centroid size or biepicondylar breadth. This creates a morphological space that is

unoccupied by the extant hominids (compare subfigures a. and b. in Figures 5-6, 5-7, and 5-8, and to some extent, Figure 5-10.). In analyses that include fossils, this space is occupied by A.L. 288-1, SKX 10924, and SK 24600. These fossil hominins therefore appear morphologically distinct from both nonhuman hominids and humans, but this is arguably an artifact of inaccurate scaling of individuals with a human-like relationship between humeral size and body mass but more ape-like morphology.

It is difficult to argue for a temporal trend in hominin humeral morphology based on these results. When humeral morphology is assessed relative to allometric trends, Lucy (*A. afarensis*), the second oldest fossil in the sample, consistently has one of the highest residuals to the human regression for each PC studied, and therefore can be said to possess one of the least human-like morphologies when size-scaled. However, SKX 10924, the youngest fossil in the analysis, differs nearly as much or more from modern humans in three of the four regions where its affinities can be assessed (10% PC1 Figure 5-6; Articular PC1 Figure 5-7; Periarticular PC1 Figure 5-8), and remains significantly divergent from humans on the fourth (Periarticular PC2, Figure 5-10). KNM-KP 271 and StW 431, representatives of the two other *Australopithecus* species and bracketing A.L. 288-1 in age, are both more human-like than A.L. 288-1 for all regions. It is possible that some taxonomic trends are present in other taxa. The two putative *P. boisei* (KNM-ER 1504 and KNM-ER 739) are consistently human-like for all regions, while the combined tentative *P. robustus* sample (TM 1517, SKX 10924, SK 24600) is less so. Gombore IB 7594, our *Homo erectus* specimen, either falls within the range of its expected

morphology, or diverges from it in a way that appears ‘super-human’. While this creates a more diverse range of morphologies present in the more recent fossils (between 1 and 2 Mya) compared to the older ones as noted elsewhere (McHenry and Brown, 2008; Lague, 2014), the small sample size prior to this this time period is such that broader statements about morphological progression or diversification are difficult to assess.

5.4 Summary

Body mass is strongly correlated with distal humeral properties, including both centroid size and biepicondylar breadth. A variety of landmark configurations were tested to determine whether the relationship between centroid size and body mass is dependent upon the region sampled. Centroid size of the distal 10%, inclusive of both the articular and periarticular surfaces, appears to be the best proxy for body mass, but centroid size of all regions showed high correlations. Most centroid sizes are more tightly correlated with body mass than is biepicondylar breadth, but landmark sets that include diaphyseal regions weaken this correlation and are not recommended as a scaling variable.

Despite strong correlations between body mass and distal humeral size within taxa, there is significant variation among taxa in scaling relationships of humeral properties to estimated body mass. In addition to having larger distal humeri relative to body mass, the centroid size and biepicondylar breadth of great apes scale differently with body mass than that of humans, being closer to isometric in great apes and very positively allometric in humans. Thus, larger humans are more ape-like in proportions.

A.L. 288-1 shows the same relationship between distal humeral size and body mass as modern humans, StW 431 has a relatively larger distal humerus, while KNM-ER 1504 appears like modern humans in relative centroid size but not biepicondylar breadth (larger). When scaled relative to all three size measures, distal humeral morphology, as assessed by scores on PCs 1 and 2 (Chapter 4), is generally closer to great apes in larger humans. Fossil hominins (except IB 7594) are not generally more human-like than ape-like in morphology when size scaled. However, use of different size parameters has some effect on comparisons: when scaled against body mass, there is a greater difference in morphology between modern humans and great apes, and fossil hominins are more ape-like, compared to results using distal humeral centroid size or biepicondylar breadth. No definitive temporal trends in size-scaled morphology are evident among fossil hominins, although there is some suggestion of taxonomic differences.

6 Discussion

Despite previous assertions that the distal humerus “is of extremely limited value in taxonomic and phylogenetic studies” (Straus, 1948) and “its morphology is generally not … likely to be informative about locomotion (or phylogeny) … within hominoid postcrania” (Lovejoy et al., 2016), results presented in the previous chapters demonstrate that although distal humeral variation is subtle and the factors affecting it complex, with careful analysis it can provide valuable insights into morphological adaptation. This chapter considers the impact of these findings on understanding of diaphyseal, periarticular, and articular developmental plasticity, the effect of different methods of size estimation and allometry on interpretation of humeral morphology, and the ability of the distal humerus to address questions of function and phylogeny across hominin evolution.

6.1 Developmental Plasticity

Understanding the response of the distal humerus to mechanical loads is important for correctly interpreting morphological variation, both within and between taxa. Variation may be misinterpreted if the impact of mechanical loading on distal humeral traits is overlooked, leading to inaccurate conclusions about the degree of developmental "noise" present in humeral morphology. As noted previously, developmentally plastic traits are useful for inferring living behavior (Ward, 2002; Ruff et al., 2018a), while those that are more genetically canalized are preferable for

understanding phylogenetic relationships. Clarifying the degree to which mechanical forces influence humeral traits improves efforts to use humeral characteristics in reconstructing both function and phylogeny.

Because bilateral asymmetry in limb bone dimensions is not observed very early in development (Blackburn, 2011), we interpret asymmetry among adults to be a product of developmental plasticity during growth. Mechanical adaptation of the humeral midshaft in response to the asymmetric loading pattern caused by modern human handedness is well-documented (Jones et al., 1977; Trinkaus et al., 1994; Haapasalo et al., 2000; Bass et al., 2002; Shaw and Stock, 2009; Shaw, 2011; Warden et al., 2014; Nadell and Shaw, 2016; Sládek et al., 2016), but evidence for metaphyseal and epiphyseal effects has been equivocal (Hamrick, 1996; Haapasalo et al., 2000; Plochocki, 2004; Nadell and Shaw, 2016). The study of bilateral asymmetry presented in Chapter 3 suggests that all regions of the humerus - diaphysis, metaphysis, and both articular and periarticular epiphyseal regions - are responsive to loading but that the effect is smaller in more distal regions. All measures in this study except total area of the medial olecranon pillar are shown to be significantly asymmetric, and all except capitular centroid size show right-handed asymmetry, demonstrating the response of distal humeral properties to right-dominant loading of the upper limb.

In addition, asymmetry of distal humeral properties is correlated with asymmetry near midshaft for all dimensions except capitular centroid size, supporting the association of distal asymmetry with mechanical loading. This is consistent with

previous evidence for upper limb articular (Plochocki, 2004; Auerbach and Ruff, 2006) and periarticular (Auerbach and Ruff, 2006) bilateral asymmetry. In the current study, there is a slight proximo-distal decline in both the degree of asymmetry present and correlation with midshaft asymmetry. This pattern is reflected in both mechanical properties and centroid sizes. The decline is consistent with the suggestion in Auerbach and Ruff (2006) that in general, asymmetry of articular and periarticular measures tends to be less pronounced than asymmetry of diaphyses, but puts these findings in the context of a broader gradient along the entire distal humerus.

There are a few possible reasons for the distal decline in asymmetry and correlation with midshaft lateralization. Spatial factors almost certainly play a role in the similarity of nearby cross-sections. Physical proximity likely creates similar mechanical environments. Bending moments, which are likely to be greater near midshaft, may decline distally. Because bending is expected to stimulate bone modeling during growth (although compressive forces on the articular surface are still high (Chadwick and Nicol, 2000), this would result in higher degrees of remodeling near midshaft. Another possible explanation is greater genetic constraint on developmental plasticity of the elbow articulation, with knock-on effects on periarticular regions. Articular surfaces are functionally integrated with opposing joint surfaces and evidence suggests that articular response to mechanical loading may occur through remodeling of underlying trabeculae and subchondral bone rather than the articular surface itself (Bouvier and Hylander, 1982; Radin et al., 1982; Ruff et al., 1991; Rafferty and Ruff, 1994; Lieberman et al.,

2001). However, results presented here show that despite a trend of declining asymmetry in centroid sizes of other regions, articular centroid size asymmetry is greater than that of any other region distal to 18% of bone length from the distal end. Because articular asymmetry does conform to the general proximo-distal trend of decreasing correlation with midshaft asymmetry, this finding may suggest greater developmental instability of articular size in response to factors other than those assessed in this study (i.e., overall mechanical loading of the humerus).

The capitulum is an exception to trends observed elsewhere in the humerus. Unlike any other region, the capitulum shows significant left rather than right bias. Capitular asymmetry is also not correlated with midshaft asymmetry, unlike other regions including the trochlea and total articulation. Correlation of trochlear but not capitular asymmetry with midshaft asymmetry may be explained in part by greater loading of the humeroulnar compared to humeroradial articulation when compressive forces are applied to the hand, at least in humans (Birkbeck et al., 1997; Pfaeffle et al., 2000). A possible explanation for left-dominant asymmetry of the capitulum is constraint on changes in total articular size. Under this hypothesis, trochlear expansion might necessitate reduction of the capitulum. Evidence for relatively high levels of right-dominant total articular asymmetry argues against this interpretation, and there is no evidence for a linear tradeoff between trochlear and capitular asymmetry (i.e., no negative correlation between their asymmetries). It is however possible that there is some less straightforward constraint on the relationship between total articular,

trochlear, and capitular size, or the mechanical loads transferred across the different components of the joint.

Results of population analyses in this study mirror those in Sládek et al. (2016), which found the highest asymmetry in hunter-gatherer populations (also see Ruff, 2018). This is thought to be due to greater engagement in uni-manual activities, based on evidence that spear thrusting (Schmitt et al., 2003) and unimanual throwing (Shaw and Stock, 2009) create interlimb load asymmetries. In the analysis presented here, the pre-agricultural Indian Knoll population shows significantly higher asymmetry in both cross-sectional properties and centroid sizes. This degree of asymmetry is not present in modern industrial populations, Native American groups that incorporate agriculture, or the agriculturalist 12th dynasty Egyptian Lisht population, suggesting that activity patterns rather than activity levels drive this asymmetry. Evidence of sex differences in this population reflect other findings by Sládek and others (Sládek et al., 2007; Sládek et al., 2016), and reflect likely differences in gender-specific activities. Sex differences are present only within the three Native American groups. The absence of an effect of sex in modern industrial populations or the Lisht suggests that these differences are not attributable to hormonal or genetic differences between males and females. However, differences in responsivity to mechanical stimuli have been observed in animal studies (see review in Wallace et al., 2017), and the possibility that population differences may be partially attributable to genetic factors cannot be discounted.

Regarding fossil hominins, the results presented here suggest that possible plasticity of distal diaphyseal shape should be more carefully considered when using the distal humerus for taxonomic identification (Susman et al., 2001; Lague, 2015), given evidence that mechanical properties and centroid sizes of the distal diaphysis appear responsive to loading. Evidence that laterality is present in upper limb mid-diaphyseal cross-sectional properties of chimpanzees (Sarringhaus et al., 2005) and the proximal diaphysis of A.L. 288-1 (Ruff et al., 2016) suggests that the patterned asymmetry presented here for humans could also be applicable to nonhuman taxa, including fossil hominins. Whether cross-sectional and centroid size responsiveness to loading is correlated with shape differences is unknown, though cross-species work suggests that cross-sectional diaphyseal shape becomes rounder with increasing time spent engaging in arboreal behavior (Carlson, 2005). These differences echo shape differences between the extant hominid taxa that have been used as a basis for understanding cross-sectional contours of fossil hominins (Lague, 2015). Within modern hominids, the triangular shape of human distal humeral diaphyses, compared to a more rounded, ovoid shape in great apes, is a key difference between extant taxa, and fossil hominins are noted to have anteroposteriorly flattened distal diaphyses, distinguishing them from modern humans (Senut, 1981a; Susman et al., 2001; Toussaint et al., 2003; Lague, 2015). The degree of flattening, posterior rounding, and anterior protrusion have been used to differentiate fossil taxa (Susman et al., 2001; Lague, 2015). However, the plasticity of these traits has not been assessed. Given evidence presented here that the

target region (15%-20% length) is significantly asymmetric and subject to remodeling in response to mechanical loads, the degree to which these characteristic traits are affected by the mechanical loading environment should be assessed in order to determine to what extent these traits could be modified by behavior.

Evidence for developmental plasticity across the distal humerus also has implications for allometric and morphometric studies. Significant bilateral asymmetry of centroid sizes and correlation with the effects of handedness complicate use of these properties as scaling variables, discussed further below. If the relative size of different distal humeral features is affected by use during life, then this has the potential to bias results when these features are used as "size" variables. (This also applies to evolutionary changes in distal humeral size relative to overall body size.)

In morphometric analyses, whether variation reflects function or phylogeny is often debated, though the two are not mutually exclusive. The findings in Chapter 3 support claims that there are functional insights to be gleaned from distal humeral morphology, and further suggest that some variation in this region may be useful for inferring living behavior. Diaphyseal regions appear to more strongly reflect actual use, at least among humans, and morphological variation in these regions may therefore be more likely to reflect differences in behavioral patterns and aid in reconstruction of the locomotor and manipulative repertoire of fossil hominins. Under this hypothesis, shaft differences are most likely to reflect variation in behavior, followed by the metaphysis and periarticular epiphysis. While some apparent developmental plasticity in the size of

the overall articulation and trochlea is observed, the morphology of these regions is more complex than that of periarticular and shaft regions and the correlation with shaft bilateral asymmetry is lower. Articular morphology is therefore less likely to be significantly impacted by *in-vivo* use, and more likely to reflect phylogeny and behavior at the species level.

6.2 Scaling

Chapter 5 addresses the relationship of distal humeral centroid sizes and biepicondylar breadth to body mass, because while significant allometric effects on distal humeral morphology have been proposed (Bacon, 2000; Lague, 2014), a number of previous studies have used properties of the distal humerus itself as scaling factors (Bacon, 2000; Carretero et al., 2009; De Castro et al., 2012; Lague, 2014; Di Vincenzo et al., 2015; Rosas et al., 2015). These analyses therefore quantify scaling with respect to distal humeral size, but not necessarily with respect to size of individuals. These are two separate questions. How morphology scales with centroid size or biepicondylar breadth may have some bearing on ontogenetic scaling, showing common features that arise when the distal humerus grows to an overall larger size, though ontogenetic data are necessary to truly understand growth allometries (Shea, 1984). Scaling by body mass addresses a different issue. Body mass creates biomechanical demands on the locomotor skeleton, and therefore has a strong influence on morphology of postcrania (Jungers and Susman, 1984; Jungers, 1990; Van der Meulen et al., 1996; Ruff, 2002; Perry et al., 2018). Scaling by body mass in great apes therefore provides information on

how the humerus responds to different locomotor requirements. In the upper limb of humans, which is freed from habitual locomotor demands, this relationship is less direct, although there is evidence that humeral shaft strength is related to body size in both static adult and ontogenetic scaling analyses of humans (Ruff, 2000a, 2003b). Humeral scaling relative to body size is of great interest in fossil hominins, whose locomotor repertoire is still under debate (see summaries in Stern, 2000; Ward, 2002). Body mass also has other advantages as a scaling variable. Use of body mass allows for comparison of scaling of different elements, even in the fragmentary fossil record (Jungers, 1990; Ruff, 2000b). Unlike many other scaling factors including centroid size, it is easily measurable in living animals, and therefore analyses scaled to body mass can be compared to extant physiological, behavioral, and ecological data (e.g. Schmidt-Nielsen, 1984; Calder, 1984). In modern humans, where centroid size is observed to be developmentally plastic (see above), body mass provides a measure of size that is independent from use of the upper limb in manipulation.

While body mass is strongly correlated with centroid size and linear breadths in all taxa studied, the strength of these relationships differs. Centroid size depends on the landmarks chosen to represent morphology, and it therefore differs between different studies (e.g. Bacon, 2000; Lague, 2014). This hinders direct comparison between allometric analyses. While landmark sets in the analyses described here are not independent, the degree to which they correlate with body mass varies depending on the region analyzed, despite the fact that overall humeral size of an individual is

invariant. Use of centroid size to scale regions that are likely to be developmentally plastic, especially the diaphysis, would introduce confounding effects, and centroid size of landmark sets including these regions are less highly correlated with body mass (possibly also because they are more dependent on bone length, which varies relative to body mass among taxa - e.g., see Jungers, 1985). Within taxa (and across great apes), centroid size of the periarticular region, which includes the epicondyles, olecranon fossa and olecranon pillars, is well correlated with body mass. Articular size and trochlear size are also strongly correlated with body mass, but centroid size of the entire distal 10% of the bone, including both periarticular and articular features, has the highest correlation. Biepicondylar and articular breadths are slightly more variable with respect to body mass than centroid size of landmarks found in the distal 10% of the bone, which is arguably the best comparison for previous studies using centroid size as a scaling factor because it encompasses all of the articular and periarticular features where traditional fixed landmarks have been placed (Bacon, 2000; Lague, 2014; but see Di Vincenzo et al., 2015). While the strong relationship of all centroid sizes and distal humeral breadths to body mass within taxa indicates that these measures provide similar information about size, the variation between them argues for use of a more consistent and easily replicable scaling factor.

Evidence indicates that articular size in primates may vary non-isometrically with body size (Swartz, 1989; Godfrey et al., 1991; Perry et al., 2018; see also Chapter 5 of this work) and that articular size relative to body mass varies with locomotor behavior

(Jungers, 1988; Ruff, 2002; Perry et al., 2018), resulting in relationships between humeral size and body mass that differ between taxa. In line with these findings, analyses in Chapter 5 show that centroid size and distal humeral breadths differ taxonomically in how they scale relative to body mass, especially between humans and great apes. Relative to humans, nonhuman hominids have larger distal humeri as measured by centroid size, as well as larger articular and biepicondylar breadths, in agreement with previous evidence (McHenry, 1992). The findings of previous comparative studies (Jungers, 1988; Swartz, 1989; Godfrey et al., 1991; Rafferty and Ruff, 1994; Jungers et al., 2002; Perry et al., 2018) suggest that this in part reflects the mechanical demands of different locomotor modes, because larger joints better dissipate larger joint reaction forces associated with use of the forelimb in locomotion (Godfrey et al., 1991; Ruff, 2002), and also allow for greater joint excursion (Ruff, 2002). Though experimental studies indicate that this is likely true at the species rather than individual level (Lieberman et al., 2001), the developmental plasticity of distal humeral centroid sizes discussed above suggests a possible effect of use, though this requires further testing. The same mechanical factors possibly affect biepicondylar breadth, which is a key component of the developmentally plastic periarticular region discussed above, and for which there is independent evidence of plasticity in orientation (Ibáñez-Gimeno et al., 2013b). Within apes, there are differences in how centroid size and biepicondylar breadth scale to body mass. Though the regression of each of these properties on body mass is close to expectations of isometry in all taxa, the regression

line for *Pongo* has a consistently lower slope than that of *Gorilla* and sometimes *Pan*. This may reflect functional or phylogenetic differences, or both.

Scaling by centroid size or biepicondylar breadth when comparing fossil hominins to modern humans assumes that fossils are most appropriately compared to humans of equivalent centroid size, and therefore makes the tacit assumption that fossil hominin centroids scale to body size like humans rather than other great apes. This is not necessarily the case. Multiple studies have noted that forelimb size is large relative to that of the hind limb in many early hominin taxa (Jungers, 1982; Hartwig-Scherer and Martin, 1991; McHenry and Berger, 1998a; b), with the exception of *H. erectus* (Latimer and Ward, 1993). However, the results of the present study corroborate the human-like scaling of humeral dimensions in A.L. 288-1 relative to body mass (Jungers, 1982 and implied in McHenry, 1992). These analyses also confirm the large size of the distal humerus of StW 431, for which both centroid size and biepicondylar breadth appear to scale as in great apes. McHenry (1992) found that the relationship between "elbow" size (product of capitular height and total articular width) and body mass appeared ape-like in KNM-ER 1504, but on this point the results of the present study are equivocal: distal humeral centroid size of KNM-ER 1504 appears to scale as in humans, while biepicondylar breadth scales as in great apes.

Apart from their effect on size-scaled morphometric analyses, the present results have implications for fossil hominin behavior and evolution. Human-like forelimb proportions of *A. afarensis* (A.L. 288-1) relative to body mass might suggest human-like

function, indicating loss of ape-like arboreal traits of the upper limb during active selection for bipedal postcranial traits proportions, as suggested in Ward (2002). However, relative strength of the humeral diaphysis relative to other postcranial elements in A.L. 288-1 suggests increased mechanical loading and likely use of the forelimb during locomotion compared to modern humans (Ruff et al., 2016). If the relative proportions of the distal humerus in A.L. 288-1 are indicative of more human-like elbow function, the retention of ape-like scaling in the distal humerus of *A. africanus* (StW 431) and possibly in *Paranthropus* (KNM-ER 1504), both of which are more recent than A.L. 288-1, must then be explained. Ape-like scaling in StW 431 may indicate retention of or reversal to arboreal behaviors, if simultaneous relaxation from the mechanical demands of arboreality and active selection for bipedal traits created the human-like scaling of A.L. 288-1. This would also explain the ape-like shaft morphology of StW 431 in the GM analyses of Chapter 4. Either the human-like or ape-like relationship between forelimb and body mass could be a result of phylogenetic inertia, depending on the relationship present in the last common ancestor (LCA). While evidence here suggests that generally ape-like scaling of forelimb dimensions to body mass could be ancestral, given the similarities between *Pongo* and the African apes, other evidence suggests that the forelimb of the LCA of humans and African apes was more generalized rather than (modern) ape-like in form (Lovejoy et al., 2009a,b; Lovejoy, 2010; Selby and Lovejoy, 2017) and therefore might have shared the condition seen in humans and in A.L. 288-1. McHenry and Berger (1998) suggest that a similar

pattern in fossil fore-to-hind limb proportions, which are human-like in A.L. 288-1 but ape-like in StW 431, imply homoplasy, possibly due to parallel evolution in *A. afarensis* and *Homo* (McHenry and Berger, 1998b), which is one possible explanation of the results of the current study. However, this could not be further tested here because body masses were not available for fossil *Homo* specimens included in the present study (Gombore IB-7593, possibly SKX 10924 or SK 24600). Equivocal evidence of scaling of size parameters in KNM-ER 1504 does not shed much light on this question, but because centroid size is a more global measure of size than biepicondylar breadth alone, it seems more accurate to say that distal humeral dimensions of the tentative *P. boisei* group from Koobi Fora (of which KNM-ER 1504 is a member) scale similarly to those of modern humans. However, whether this indicates retention of scaling relationships like those seen in *A. afarensis*, independent evolution, or another reversal is unclear.

The differences between centroid size, biepicondylar breadth, and body mass as measures of size result in differing conclusions about how fossils compare to extant groups in scaled morphometric analyses. Without going into detailed description of morphological variation within and among taxa (which are discussed at length in the following section, including consideration of allometric effects), some remarks on general patterns in size-scaled analyses are warranted. Three interesting results are observed irrespective of region:

1) While previous reports demonstrate allometric effects on shape of the distal humerus (Bacon, 2000; Lague, 2014), the results presented here suggest that

characteristic morphology of taxa uncovered through unscaled GM analyses may not always be affected. For example, there are no correlations within great ape taxa between size and PC1 scores (which differentiate great apes and humans), though morphology that is not associated with this division may be affected. If size of the distal humerus alone was a driving factor in the difference between human and great ape morphology, we might expect this relationship to be present within each taxon rather than in humans alone. The significant relationship between distal humeral size and PC1 scores when the upper limb is freed from locomotor constraints in humans suggests that allometric effects along this PC may be dependent to some degree on behavioral use of the upper/forelimb.

2) Distal humeral morphology of large humans is more great ape-like (marked lateral trochlear crest, deep zona conoidea and trochlear groove, more proximally oriented medial and larger lateral epicondyle) than in smaller humans. This is particularly true of articular morphology. This relationship is observed both with respect to body mass and centroid size in analysis of the distal 10% and of the shaft, but is especially pronounced in analysis of articular morphology. While many fossil hominins are small (Ruff et al., 2018b), fossil humeri span a wide range of sizes (Lague, 2014), including notably large individuals (KNM-ER 739, Gombore IB-7594). In unscaled analyses, because allometric effects along PC1 parallel the gradient between human and great ape morphology, the morphology of large fossil hominins should be interpreted cautiously (see below for description of features related to taxonomic distinctions and

subject to allometric effects). No relationship of periarticular PC1 morphology to body mass or centroid size is observed and therefore allometric effects are unlikely to be conflated with taxonomic distinctions along this axis.

3) There is an interesting pattern in the relationship of size-scaled fossil PC scores relative to size-scaled PC scores of extant taxa. When PC scores that capture interesting morphological variation in GM analyses (discussed below) are regressed on body mass, A.L. 288-1 appears ape-like, and its PC scores are consistent with apes of similar mass - small *Pan* and *Pongo* individuals. When the same variables are scaled to centroid size or biepicondylar breadth, there are no great apes of comparable size, so it is difficult to evaluate A.L. 288-1. In these latter analyses, it is an obvious outlier from both humans and great apes, though if the pooled ape regression line were extended beyond the observed centroid size range, A.L. 288-1 would still appear somewhat more great ape-like. A.L. 288-1 is joined by SKX 10924 and, to a lesser extent, SK 24600 in its near isolation from the extant hominids in analyses scaled by distal humeral size. It is plausible that, were body mass available for these latter two specimens, they would fall within the great ape cloud like A.L. 288-1. While these results could be reflective of a unique morphological pattern in fossil hominins (as suggested in Lague, 2014), a simpler explanation is that distal humeral morphology of at least some fossil hominins scales with body mass rather than centroid size, and that when scaled for body mass they would fall closer to great apes. These conclusions are tentative, given that they are based almost entirely on one individual (A.L. 288-1), but they would explain otherwise

puzzling patterns in the data. If true, it is interesting that the relationship of centroid size to body mass in A.L. 288-1 is human-like, which might reflect overall mechanical loading through the joint (see Chapter 3), but the relationship of distal humeral shape to body mass remains ape-like, suggesting either phylogenetic lag or other functional requirements on the loaded joint (e.g., muscle moment arms, need for greater stability in different postures) more similar to those in great apes.

6.3 Morphological variation

The GM analyses in Chapter 4 address the question of whether distal humeral morphology can be used to infer either phylogeny and/or locomotor behavior of fossil hominins. Existing work on this topic reports many morphological differences between taxa (Knussman, 1967; McHenry and Corruccini, 1975; McHenry, 1976; Senut, 1980, 1981a; b; Senut and Tardieu, 1985; Aiello and Dean, 1990; Rose, 1993; Lague and Jungers, 1996; Bacon, 2000; Yokley and Churchill, 2006; McHenry and Brown, 2008; Lague, 2014, 2015; Rosas et al., 2015; Di Vincenzo et al., 2015), but also raises doubt as to the utility of these differences in assessing the fossil record (Straus, 1948; Bacon, 2000; Ward, 2002; Lovejoy et al., 2016). These doubts are based on two factors. First, the distal humerus is simultaneously quite similar across hominids and highly variable within taxa (Straus, 1948), casting doubt on whether any individual feature or suite of features can confidently discriminate between species or between locomotor modes in individual specimens despite some differences between the average morphology of different species. The second is a question of evolutionary hypotheses. Whether ape-

like traits in fossil hominins should be interpreted as retention of selectively neutral primitive traits, stabilizing selection on traits with adaptive value, slow reduction of traits that confer a disadvantage, or developmental plasticity is unclear (Ward, 2002). The following section discusses the contribution of this thesis towards resolution of these questions, beginning with an assessment of morphological variation of extant hominids in three dimensions and an assessment of the factors that may drive this variation, based on our understanding of distal humeral plasticity and allometry. This framework is then applied to fossil hominins, with an emphasis on possible functional or phylogenetic implications.

6.3.1 Extant Hominids

All comparisons in the GM analysis in Chapter 4 (articular, periarticular, shaft, distal 10%, 18%, and 40%) distinguish humans and other great apes, with varying degrees of certainty; shaft-only comparisons are least able to discriminate between groups and show a near complete overlap between orangutans and the lower end of the human range, while fuller analyses (distal 10%, 18%, 40%) show almost no overlap between humans and nonhuman great apes. The distal 10% of the humerus incorporates most named features that are discussed in the literature with regard to distal humeral variation, including the olecranon fossa and olecranon pillars (Senut, 1981a; b) as well as articular surface morphology and the epicondyles (Knussman, 1967; Patterson and Howells, 1967; McHenry and Corruccini, 1975; McHenry, 1976; Senut, 1980; Rose, 1988, 1993; Bacon, 2000; Lague, 2014; Di Vincenzo et al., 2015), and is

therefore of particular interest (although it does not capture the distal diaphyseal cross-sectional morphology included in some studies (Susman et al., 2001; Lague, 2015) and quantified in other parts of the present analysis).

Humans differ from great apes primarily in the epicondyles, degree of articular relief, and relative orientation of the periarticular and articular regions. Humans are characterized by a more distal medial epicondyle, low articular relief in which the relative underdevelopment of the lateral trochlear crest is particularly notable, and an articular surface that is in line with the rest of the humerus rather than shifted anteriorly as in apes. This suite of differences is both visually observable in average human and average nonhuman hominid morphologies and is quantified by separation on PC1, which accounts for 21.2% of total morphological variation.

The first two traits, relative development and position of the epicondyles and overall articular relief, have been frequently commented on in the literature (Straus, 1948; Knussman, 1967; Patterson and Howells, 1967; McHenry, 1976; Senut and Tardieu, 1985; Aiello and Dean, 1990; Rose, 1993; Lague and Jungers, 1996; Bacon, 2000; Susman et al., 2001; Lague, 2014). Interestingly, reduced articular relief is also characteristic of Old World monkeys (Rose, 1988, 1993; Aiello and Dean, 1990), creating a parallel in this respect between the morphology of generalized quadrupeds and the distal humerus freed from locomotor demands. The apparent shift of the articular surface relative to the periarticular region in great apes has not been noted in the literature, but is likely related to the posterior bowing of the humeral shaft noted by

Holliday and Friedl (2013). It is hypothesized that long bone curvature increases but regulates bending moments such that they occur in a predictable direction (Bertram and Biewener, 1988) and may be especially useful in resisting loads incurred during terrestrial locomotion (Holliday and Friedl, 2013). Anterior position of the articular surface relative to the periarticular region in apes may maintain alignment of the proximal and distal humeral articular surfaces without requiring postural changes despite noted shaft curvature. The relative position of the articular surface is likely to alter moments of forces across the distal humerus, even in the absence of behavioral differences, by changing the distance to the axis of rotation of the joint.

However, there is both some overlap between the PC1 scores of humans and great apes and a significant allometric effect on the human morphology of this region. Large humans are significantly more like great apes in the features described above. There is no allometric effect on these traits within individual ape taxa, but in a pooled sample, these features are also more human-like in small great apes. In this way, differences between great ape taxa parallel size effects on these features in humans. This has implications for interpretation of fossil morphology, discussed in section 6.3.2 below.

The humeral distal periarticular and articular regions were also examined independently in order to determine whether differences between the function and possibly degree of genetic constraint characteristic of these regions (Rafferty and Ruff, 1994; Trinkaus et al., 1994; Ruff, 2002) are reflected in ways that can be used to aid in

discriminating function from phylogeny. Prior studies arguing that the distal shaft and periarticular region are particularly influenced by loadbearing and musculature (Jones et al., 1977; Ibáñez-Gimeno et al., 2013a), combined with evidence for increased developmental plasticity of the periarticular region compared to the articulation (presented in Chapter 3 and discussed above) suggest that morphology of the periarticular region is more likely to reflect behavior during life than the articular region. This has been difficult to quantify due to a paucity of repeatable landmarks, though functional effects on morphology of the olecranon pillars (Senut, 1980, 1981a; b) and epicondyles have been discussed (Senut and Tardieu, 1985; Lague, 2014). The epicondyles are often the only periarticular landmarks included in GM studies (Bacon, 2000; Lague, 2014, but see Di Vincenzo et al., 2015), although in studies of linear measurements, breadth of the olecranon pillars and olecranon fossa have also been measured (McHenry and Corruccini, 1975; McHenry, 1976; Lague and Jungers, 1996; McHenry and Brown, 2008). While these capture at least one dimension of each of the largest features of this region, they are unlikely to be able to quantify subtle variation.

As in the other analyses, humans and great apes separate along PC1 in analysis of the periarticular surface. This PC registers the expected differences in the epicondyles, with great apes falling along the end of the spectrum that indicates a medial epicondyle that is more projecting and more proximal than that of humans. PC1 also registers a difference in relative proportions of the periarticular region as a whole, in which the human periarticular surface is AP expanded, while the great ape surface is

ML expanded. This is likely a product of both development of the lateral supracondylar crest in apes (Knussman, 1967; Senut, 1980; Aiello and Dean, 1990) and the column-like structure that in humans extends down the anterior surface of the distal diaphysis before trifurcating above the coronoid fossa (Le Floch, 1982). Though the column itself is not present in the periarticular region as defined here, the ridges that descend from it are. Because there is no evidence of allometry in humans along this PC, interpreting this morphology does not run into the potentially confounding effects described above for the distal 10% as a whole. Lack of allometry in humans does not have any bearing on the hypothesis that this region might be responsive to function, because the human upper limb is used in manipulative tasks rather than locomotion, and therefore magnitude of forces need not scale with size.

On PC2, there is clear separation among the nonhuman hominids in periarticular morphology that appears to correspond to a locomotor grade, showing a progression from mountain gorillas to lowland gorillas, followed by chimps and bonobos and ending with orangutans. Modern human morphology, which is not subject to locomotor demands, is distributed widely across this grade, generally clustering in the mid-to-low range occupied by *Pan* and *Gorilla*. The difference between great ape taxa appears driven by increased development and retroversion of the medial epicondyle in African apes, especially *Gorilla*, although a broad suite of related changes create the impression that the entire periarticular surface is extending mediolaterally while wrapping posteriorly. Bolstering the argument for a locomotor effect of the suite of traits on PC2,

there is an allometric relationship within orangutans on this PC in which larger orangutans – which are more likely to engage in terrestrial fist-walking – are more like African apes in their morphology.

In addition to the indications of plasticity of periarticular size presented in Chapter 3, there is evidence in the literature that orientation of the medial epicondyle may be plastic in humans (Ibáñez-Gimeno et al., 2013b). Previous studies suggest that rotational efficiency is maximized in pronation when the medial epicondyle is posteriorly inflected (Ibáñez-Gimeno et al., 2014). In combination, this supports the idea that PC2 may capture functionally relevant traits related to rotational efficiency and hand position. In highly terrestrial apes (i.e*.,* gorillas), the forearm is fully pronated during knuckle-walking (Tuttle and Watts, 1985), while highly arboreal *Pongo*, and to a lesser extent, *Pan*, use a wider array of positional behaviors (Hunt, 1991; Thorpe and Crompton, 2006). As the site of attachment for the common flexor tendon, the medial epicondyle is intimately related to wrist flexion as well as pronation. The more medially projecting (*Pan* and *Gorilla*) or superoinferiorly broad (*Pongo*) medial epicondyle in great apes provides more surface area for muscle attachments, while differences in orientation may affect muscle moment arms, although full consideration of this possibility requires more direct mechanical modeling. These traits are likely to be adaptively significant in animals that use the forelimb for locomotion, and may therefore be selected upon, creating a locomotor signal in the morphological data. Given evidence of medial epicondyle plasticity (Ibáñez-Gimeno et al., 2013b), it is also

possible that this trait is developmentally labile (also see above), and could reflect direct evidence of contemporaneous behavior.

Articular (only) morphology does not show a terrestrial-arboreal trend. It does reaffirm a distinction between humans and nonhuman hominids, though there is significant allometry among humans in which large individuals are more ape-like. The overall gestalt is a mediolaterally expanded ape articular surface, compared to a human articular surface that appears narrower mediolaterally/larger anteroposteriorly. The mediolaterally expanded great ape articular surface suggests increased resistance to mediolaterally offset forces in the apes (Rose, 1993), useful during both arboreal and terrestrial locomotion. While both this analysis and that of the distal 10% region highlight the high degree of articular relief in great apes and weakening of this relief in humans, more of the specific features remarked upon in the literature are evident in the articular-only analysis. The human capitulum is broad anteriorly, relative to the trochlea. At its proximal origin, it is broader than that of great apes. However, inferiorly, the human capitulum narrows while the capitulum of African apes maintains its breadth. Compared to all nonhuman hominids, on the inferior surface of the bone, the human capitulum is abbreviated, as noted throughout the literature (Le Gros Clark, 1947a; b; Straus, 1948; Patterson and Howells, 1967; Senut and Tardieu, 1985; Aiello and Dean, 1990; Rose, 1993; Susman et al., 2001). Increased inferior breadth of the African apes is likely related to weight-bearing in a fully extended position (i.e., knuckle-walking).while complementary posterior extension of the capitulum in nonhuman great apes likely

extends range of extension. . This is likely useful in an arboreal context (Corruccini, 1975). The relatively broad anterior capitulum in humans perhaps reflects the decreased importance of extended relative to flexed postures in humans. On the trochlea, in addition to the low lateral crest seen in humans (described for the 10% region above), the medial trochlear crest is inferomedially angled, creating a narrow anterior trochlea despite a wide posterior trochlea in humans. The posterior trochlea of humans is abbreviated, not reaching into the olecranon fossa, but it is wide. The extension of the posterior trochlea in apes allows for hyperextension (Knussman, 1967; Aiello and Dean, 1990; Rose, 1993), and its mediolateral constriction, which is associated with a high posterior lateral trochlear crest and therefore greater curvature, likely lends stability in extended postures.

Distal shaft cross-sectional shape differs between humans and other great apes (Lague, 2015), largely due to posterior rounding in apes and anterior midline projection in humans, and has been used for taxonomic assignment in fossils (Susman et al., 2001; Lague, 2015). The results shown in Chapter 3 suggest that the entire distal humerus is asymmetric and therefore developmentally plastic, and that this asymmetry appears to be linked to the mechanical environment. The effects of mechanical environment appear to be strongest in the shaft, raising the possibility that distal diaphyseal shape differences may also be functionally mediated.

Chapter 4 includes an investigation of the morphology of a large segment of the distal shaft. The goal was to determine whether previous evidence of differing

diaphyseal cross-sectional shapes among hominid taxa were characteristic of the distal shaft as a whole (Susman et al. 2001; Lague, 2014). The possibility that functional differences observed in the periarticular region might extend into shaft morphology was considered, but analyses of the shaft region do not closely resemble analyses of the periarticular region. Unlike periarticular analyses, shaft analyses do not show a clear locomotor gradient among the apes. Neither is there a clear separation between humans and nonhuman hominids. Though PC1 explains 40.6% of the total variation in shaft morphology and the position of species along this axis generally replicates the associations found in Lague (2015), there is substantial overlap between humans and *Pongo*, and moderate overlap between humans and *Pan*. Nevertheless, shaft analyses presented hear appear to replicate the distal diaphyseal contour differences noted by Lague (2015) and Susman et al. (2001), and shows that similar differences appear throughout the distal shaft, not just at the 18% location.

Most differences between humans and African apes (but not *Pongo*) appear to reflect the influence of the column-like structure that begins directly distal to the crest descending from the greater tubercle at the level of the deltoid tuberosity. This column runs down the anterior surface of the human shaft near its mediolateral midpoint, which has the effect of expanding the AP dimensions of all human contours in approximately the median plane of the humerus. This shape has been referred to as 'triangular' by previous authors (Lague, 2015). The triangular morphology is most evident at the distal-most end of the shaft. The posterior surface is flat or slightly

concave, also noted by others (Senut, 1978; Susman et al., 2001; Lague, 2015). This differs from the African ape condition, which shows posterior convex rounding. The flat plane along the posterior human shaft appears to be an extension of the olecranon fossa and the roots of the olecranon pillars, when examined visually. The characteristically triangular human shape also appears to be affected by positioning of the supracondylar crests. The base of the triangle is formed by the medial-most and lateral-most portions of the bone. In humans, the medial and lateral margins of the bone lie flush with the posterior surface, but in apes, they are drawn anteriorly. More proximally, shape of the human shaft is compressed mediolaterally but remains triangular. Compared to contours of the distal-most shaft, at cross sections lying midway between 18 and 40%, in transverse section, the angle formed by the midline projection of the anterior surface is much more acute. Approaching midshaft, the human shaft remains mediolaterally compressed, but becomes ovoid rather than triangular.

Results of the analyses presented here support previous claims that the distal diaphysis of great apes is more rounded posteriorly (Lague, 2015). In the analyses presented in Chapter 5, typical great ape morphology is lachrymiform (teardrop-shaped) in distal cross section and nearly circular in cross sections near midshaft. Though in any given taxon the shape of cross sections varies between shaft levels, great ape cross-sectional morphology at any level appears more circular than in humans. However, there is considerable overlap between species as well as variation within them. There are especially high degrees of overlap between humans and *Pongo*, the two taxa that do

not engage in knuckle-walking (a similarity that has been noted elsewhere; see Holliday and Friedl, 2013 and Lague, 2015). This high variability in cross-sectional shape, along with apparent responsiveness of the diaphysis to loading, raises questions about use of diaphyseal shape as a discriminator between species. Responsiveness of the particular features included in previous studies (Susman et al., 2001; Lague, 2015) to loading is as yet unassessed, but it is possible that some aspects of this shape are developed through use, particularly size and possibly anteroposterior positioning of the lateral supracondylar crest, a prominent attachment for both flexor (brachioradialis) and extensor (extensor carpi radialis longus, edge of the triceps) musculature.

6.3.2 General Fossil Trends

Associations between fossil hominin humeri and specific extant species vary significantly depending upon the region under analysis. Fossil hominins are most similar to humans in articular morphology, but are more ape-like in both periarticular and shaft morphology (despite overlap between human and other great apes in the shaft). General commentary on morphological trends among fossils is presented below, followed by consideration of the cumulative evidence by taxon.

The great ape-like periarticular and shaft morphologies of most fossil hominins may have implications for the reconstruction of behavior. This could suggest in several taxa possible active maintenance of arboreal capabilities. Fossil hominin shaft morphology (preserved in A.L. 288-1, StW 431, and KNM-ER 739) and most periarticular morphology (barring Gombore IB-7594, SK 24600, and TM 1517) is clearly more “ape”-

like than human-like, and periarticular morphology aligns with the more arboreal *Pan* and *Pongo* rather than the more terrestrial *Gorilla* (Cant, 1987; Doran, 1993, 1996; Remis, 1995; Hunt et al., 1996). Allometric comparisons accentuate rather than diminish the ape-like qualities of fossils in both the shaft and periarticular region, with the possible exception of KNM-ER 739, whose ape-like shaft may be partially explained by its considerable size. This is interesting given findings here and elsewhere (McHenry, 1976) that the articular features of KNM-ER 739 are not more ape-like than those of other fossil hominins.

Analysis of the distal 10% of the humerus as a single unit appears to be primarily driven by differences in the articular surface but presents a clearer division between humans and great apes than analysis of the articular region in isolation, indicating that the relationship between articular and periarticular morphology may be taxonomically important. In both the articular-only and 10% analyses, fossil hominins are somewhat intermediate between humans and other great apes, but more closely associated with modern humans in the analyses presented here. However, when compared to individuals of comparable size, the shape of most fossils is notably ape-like with the exception of Gombore IB-7594, which falls at the extreme end of human variation in all analyses, and KNM-ER 739, whose ape-like qualities are partially explained by allometric trends. Without this allometric comparison, fossil morphology might indicate continued *in vivo* arboreal behavior affecting the periarticular region and shaft, despite decreasing adaptive importance of arboreality that resulted in changes to the articular surface

(Ward, 2002). However, allometric effects complicate this picture by suggesting that, relative to their size, many fossil hominins retain a substantially ape-like morphology even in the most distal (i.e., articular) features. With this consideration in mind, a completely human-like morphological pattern is much rarer in the fossil record than previously noted, alternately suggesting selective neutrality of distal humeral traits (Ward, 2002) or stabilizing selection on somewhat ape-like humeral features adapted for at least occasional arboreality. The emergence of *Homo* (Gombore IB-7594) appears to have either released constraints (likely related to arboreality) on humeral morphology, or created a new selective pressure possibly related to manipulation. The one relationship that is notably human-like in early hominins is that A.L. 288-1 has a small distal humeral centroid size relative to its estimated body mass. This size difference may be suggestive of lesser loading of the humerus than is the case in extant nonhuman hominids, but in this case, it is notable that there is no evidence for diminution in relative size of the distal humerus compared to body mass in StW 431.

There is some evidence of a temporal trend in articular morphology, though between-fossil taxonomic distinctions are unclear. Fossils assigned to *Australopithecus* lie at the extreme of the human range where overlap with *Pan* is significant, while *Paranthropus* falls further within the human range due to the influence of several individuals (SKX 10924, SK 24600, and KNM-ER 1504; although see below regarding the taxonomic assignment of SK 24600). The morphology of Gombore IB-7594 (*Homo erectus*) falls at the opposite extreme of the human ranges (i.e., non-ape-like).

Between taxa, consideration of allometric trends across regions may suggest that the morphology of *P. robustus* is slightly less like modern humans than that of *P. boisei*. Attribution of SK 24600 and SKX 10924 to *Homo* or *P. robustus* is uncertain in the literature (Susman et al., 2001; Lague, 2015), and this study is able to provide additional information that may help to clarify this issue. In both scaled and unscaled analyses, SK 24600 is more like modern humans than SKX 10924, across all regions. If these two specimens do represent two different taxa, as both Lague and Susman et al. argue, the present study concurs with Lague (2015) and contra Susman et al. (2001) that SKX 10924 represents *P. robustus* and SK 24600 is better assigned to *Homo*. However in most of the current analyses, SK 24600 closely resembles TM 1517, the type specimen of *P. robustus*, which argues against its classification as *Homo*, and perhaps suggests that all three individuals are conspecific.

6.3.3 Results by Taxon

6.3.3.1 A. anamensis

The morphology of KNM-KP 271 has often been considered to be strikingly similar to *Homo* despite its geological age (Patterson and Howells, 1967; McHenry and Corruccini, 1975; McHenry, 1976; Day, 1978; Senut, 1980; Senut and Tardieu, 1985; McHenry and Brown, 2008), with authors focusing on the small, weakly angled lateral trochlear crest, distally abbreviated capitulum, and weak lateral epicondyle, though conflicting evidence has also been presented (Feldesman, 1982; Hill and Ward, 1988;

Lague and Jungers, 1996; Lague, 2014). The current analyses do not find KNM-KP 271 to be particularly human-like as opposed to ape-like, but concur that KNM-KP 271 is more human-like than some other fossils, notably A.L. 288-1, and also the much more recent SKX 10924. In both scaled and unscaled GM analyses, KNM-KP 271 falls at the edges of the human range in analyses that include morphology of the articular surface (articular only, 10%), in contrast with previous size-scaled analyses that highlight extreme differences between KNM-KP 271 and modern humans (Lague, 2014). The periarticular morphology of KNM-KP 271, however, is moderately ape-like, falling within the *Pan* range and slightly outside the range of human variation. KNM-KP 271 also falls comfortably within the great ape range in all size scaled analyses, including those quantifying articular morphology. It is least like apes in unscaled analyses of the distal 10% region, where periarticular and articular traits are combined. In scaled analyses of this region, it falls within both the human and ape ranges of variation. The total evidence does not suggest that KNM-KP 271 was particularly adapted to life in the trees, but mild resemblance to apes in the periarticular region could suggest occasional climbing in this species, as has been suggested on the basis of primitive features in the hand and wrist of some specimens (Ward et al., 2001).

6.3.3.2 A. afarensis

This thesis finds strong evidence of ape-like characteristics in the distal humerus of A.L. 288-1 (*A. afarensis*), echoing studies on the ulna (Arias-Martorell et al., 2015), phalanges (Stern and Susman, 1983; Susman et al., 1984), and relative strength of the

humerus (Ruff et al., 2016). In unscaled analyses, the articular morphology of A.L. 288-1 falls within the ranges of *Pan, Pongo*, and *Homo*, but when body size and humeral size are considered, A.L. 288-1 is far outside the human – but not the nonhuman hominid – range. This is consistent with previous commentary on the marked lateral trochlear crest and deep zona conoidea of A.L. 288-1 (Johanson et al., 1982; Senut and Tardieu, 1985), but somewhat at odds with Lague (2014), who found A.L. 288-1 to be relatively more human-like than other members of the genus. This is not the case in the present analyses. In both the articular and distal 10% regions, A.L 288-1 is far less like modern humans than both *A. anamensis* (KNM-KP 271) and *A. africanus* (StW 431) when compared to individuals of equivalent size, though without consideration of allometry, the three species are morphologically similar. In the periarticular region and shaft, for which there is evidence of significant plasticity, A.L. 288-1, like KNM-KP 271 and StW 431, is ape-like, which may suggest active arboreal behavior in all three species. However, scaling of distal humeral size relative to body mass is definitively human-like in A.L. 288-1, and sharply differs from the scaling relationship seen in great apes. This echoes findings that the forelimb proportions of A.L. 288-1 were similar to those of modern humans (Jungers, 1982) and may reflect the increasing adaptive importance of bipedality over arboreality despite otherwise notably ape-like features in the upper limb (Ward, 2002). These results are consistent with findings that the elbow to knee breadth proportion in A.L. 288-1 is human-like, but its relative humeral to femoral diaphyseal strength proportion shows a markedly robust upper limb (Ruff et al., 2016) supporting

the inference that A.L. 288-1 walked bipedally on the ground but that arboreal behavior remained a significant component of the total locomotor repertoire of this individual.

6.3.3.3 A. africanus

Some previous evidence suggests that *A. africanus* (StW 431) was potentially more arboreal than other members of the genus (McHenry and Berger, 1998b; a). This study adds to the collection of evidence suggesting significant arboreality in *A. africanus* (Clarke and Tobias, 1995; McHenry and Berger, 1998b; a; Tallman, 2015; Ruff et al., 2016). Previous studies of the humerus note the similarity of StW 431 to gorillas (Lague and Jungers, 1996; McHenry and Brown, 2008), based on a strong lateral trochlear crest, large lateral epicondyle, and anteroposteriorly flattened periarticular region (Toussaint et al., 2003). This study does not find particular dissimilarities between StW 431 and other fossils on axes that divide humans from apes in the articular or periarticular regions, which include the previously discussed traits, but finds the shaft of StW 431 to be beyond the extremes of the modern great ape range. Like great apes, the shaft of StW 431 is extremely robust and bears a rounded posterior border. The extreme anterior expansion of the shaft of StW 431 does not create a triangular cross section as in humans, but also differentiates StW 431 from typical ape morphology. Strong differences between StW 431 and extant taxa cannot be explained by allometric effects, regardless of whether the morphology is scaled to body mass or to size of the distal humerus. Plasticity of the human shaft suggests that some of the observed morphology may be explained by remodeling in response to use; some portion of this variation may

also be due to reconstruction. This study also finds that size of the distal humerus of StW 431 is large relative to its body mass, as previous studies have implied (McHenry and Berger, 1998b), matching the nonhuman hominid but not the human scaling trend. However, this creates an interesting effect in size-scaled analyses: because the articular morphology of *A. africanus* is substantially the same as that of *A. afarensis* despite a significant difference in size (in the specimens included here), in analyses that consider allometry, StW 431 appears closer to the expected shape for humans of similar size than other members of the genus. This does not appear to reflect a change in morphology, but rather morphological stasis despite increasing body size. Whether this reflects stabilizing selection on these traits or their selective neutrality is a matter for debate.

6.3.3.4 P. boisei

Interestingly, though *P. boisei* has previously been noted to have a remarkably strong humeral diaphysis (Leakey, 1971; Domínguez-Rodrigo et al., 2013; Ruff et al., 2016), bearing a superficial similarity to female gorillas (McHenry, 1976), as well as marked posterior convexity (Lague, 2015), morphology of the shaft of KNM-ER 739 does not appear as extreme that of StW 431 in these analyses. The shaft is notably ape-like, and KNM-ER 739 falls among gorillas in unscaled analyses. However, regression of the relevant principal component scores against size indicates that much of the morphological difference between the shaft of KNM-ER 739 and modern humans could be explained by allometric trends in modern humans. Though KNM-ER 739 has one of the most extreme shaft PC1 scores in the unscaled analyses, positive allometry among

humans shows that this morphology falls within the bounds of expected morphology for humans of equivalent size, though no individuals in this particular sample reached such extreme morphology. Therefore, while shaft morphology of *A. afarensis* and *A. africanus* likely indicates nonhuman use of the upper limb, evidence is more tentative regarding the shaft of KNM-ER 739, which is more like great apes than humans, but cannot be definitively excluded from the latter. However, given evidence that the humerus of KNM-ER 739 is also quite strong, as in apes (Ruff et al., 2016), the balance of the evidence suggests arboreality, or other nonhuman upper limb use, at least in this individual.

Articular traits noted in the literature as distinguishing *P. boisei* from modern humans include a constricted trochlea and large capitulum (Leakey, 1971). Overall, articular morphology of *P. boisei* appears intermediate between humans and great apes, but taxonomic distinctions are difficult to determine due to a strong allometric trend in humans. The analyses presented find that allometry of the distal humerus could explain substantial portions of the differences between humans and KNM-ER 739, at least on the axis that separates human and nonhuman hominid morphology. Allometric scaling does not as clearly minimize differences between KNM-ER 1504 and modern humans because 1504 is substantially smaller than KNM-ER 739, but 1504 nevertheless lies within both the human and great ape ranges in scaled analyses.

However, morphology of the periarticular region of the putative *P. boisei* specimens strongly diverges from that of humans, and is quite ape-like. In fact, KNM-ER

739 and KNM-ER 1504 diverge more from modern human morphology in this region than any other fossil except SKX 10924. This reflects the marked flattening of the periarticular region, also noted by Lague of the distal diaphysis (Lague, 2015). This trait is also observed in *H. habilis* (Lague, 2015), and it has been argued the humeri here assigned to *P. boisei* (KNM-ER 739 and KNM-ER 1504) might be attributed to some form of early *Homo* other than *H. erectus* (Lague and Jungers, 1996; Lague, 2014). However, the periarticular morphology of *P. boisei* is farther removed from that of humans than any other fossil hominin species along the axis that separates humans and great apes. Given that periarticular morphology is plastic in response to loading, appears to differentiate locomotor modes within apes, and distinguishes great apes from humans, it seems likely that this is of functional as well as taxonomic significance. This could indicate greater arboreality of *P. boisei* at the species level.

6.3.3.5 P. robustus

In the face of uncertain taxonomy, this study began with the tentative assumption that both SK 24600 and SKX 10924 might belong to *P. robustus*, in addition to TM 1517, the type specimen. SK 24600 was assigned to *P. robustus* by Susman et al. (2001) and SKX 10924 was assigned to *P. robustus* by Lague (2014), but SK 24600 and SKX 10924 have each also been assigned to *Homo* (Susman et al., 2001; Lague, 2014). The results of this study generally support Lague (2015), contra Susman et al. (2001) that SKX 10924 represents *P. robustus* and SK 24600 is better assigned to *Homo* if assertions that the two specimens are not conspecific are correct (Susman et al., 2001;

Lague, 2014). SK 24600 is more like modern humans than any fossil hominin other than Gombore IB-7594, falling within the modern human morphological range and outside the great ape range in its articular morphology and in morphology of the distal 10%. TM 1517 and SK 10924 are intermediate between humans and apes for these regions. If attribution of SK 24600 to *P. robustus* were correct (per Susman, de Ruiter, & Brain, 2001), the morphological range of this species would extend farther into the human range than any other non-*Homo* species.

However, in the periarticular region, SK 10924 rather than SKX 24600 is an outlier from the possible *P. robustus* group, grouping instead with *P. boisei* (KNM-ER 739 and KNM-ER 1504) while both TM 1517 and SK 24600 are relatively human-like. However, Gombore IB-7594 (*Homo erectus*) lies nearer SK 24600 in periarticular analyses than does any other fossil including TM 1517, and therefore these findings support rather than refute possible association of SK 24600 with *Homo*, though they raise questions about the possible locomotor behavior of SKX 10924 (see discussions of periarticular traits above).

Application of modern human allometric trends to fossil morphology, however, casts some doubt on assertions that SKX 10924 and SK 24600 are not conspecific (Susman et al., 2001; Lague, 2014), and erodes some of the associations of SK 24600 with typically human morphology. In the articular region, both SKX 10924 and SK 24600 are substantially different from the morphology expected for their size, but TM 1517 is not. However, this may be partially accounted for by understanding that multiple PCs

contribute to the division between shape of the human and great ape articular surfaces, and fossils may not be subject to the same allometric trends that exist among modern humans.

Even if SK 24600 is better attributed to *Homo* rather than to *P. robustus*, considerable differences between SK 10924 and TM 1517 in their periarticular morphology suggest a wide range of variability in *P. robustus* in a region that has both locomotor and taxonomic significance for other taxa. SK 10924 appears clearly ape-like and therefore likely arboreal in its periarticular morphology, while TM 1517 falls within the modern human range. This range of diversity is larger than that seen between different species of *Australopithecus*, and much larger than variation between KNM-ER 1504 and 739 (*P. boisei*). However, both SK 10924 and TM 1517 do fall within the range of extant *Pan*, demonstrating that this degree of variability is not outside the realm of possibility for a living species. If attribution of SK 10924 to *P. robustus* is correct, this species may have engaged in arboreal behavior perhaps similar to that in *Pan*. However, it should be noted that the only definitive *P. robustus* specimen (TM 1517) is more like modern humans than any non-*Homo* fossil, falls within the range of human variation in both scaled and unscaled analyses of articular morphology, and falls only just outside the expected human range on PC1 of the distal 10%, which in absence of other specimens would align *P. robustus* more closely with modern humans.

6.3.3.6 Fossil Homo

The associations of Gombore IB-7594 in this study are clear throughout, supporting assignment to *Homo* (Chavaillon et al., 1977; Senut, 1980, 1981a; Senut and Tardieu, 1985; Bacon, 2000; Coppens, 2004; Di Vincenzo et al., 2015). In all analyses, Gombore-IB 7595 falls at the edge of the range of modern human variation farthest from great apes, except in the periarticular region, where it remains within the human range and is more human than any other fossil. Consideration of modern human allometry accentuates this difference to such a degree that Gombore IB-7594 appears outside the human range. Though it is inadvisable to draw a strong conclusion from a single data point, these results could suggest strong selection away from the great ape articular morphology and towards the human morphology in *Homo erectus*, possibly related to adaptation to tool use. Strong differences have been noted elsewhere in shape of the distal humeral diaphyses of *Homo cf. habilis* and *Homo erectus* (Lague, 2015) and in relative strength of the fore- and hind limb (Ruff, 2009) that suggest a strong shift in morphology within the genus *Homo* related to acquisition of fully human locomotor patterns in *Homo erectus* but not earlier species. The extreme morphology of Gombore IB-7594 may be reflective of strong selection on distal humeral traits concomitant with this major behavioral change.

7 Conclusion

A holistic understanding of morphological variation is important for drawing reliable conclusions about form-function relationships during hominin evolution. Many factors underlie variation in skeletal form, including phylogeny, development, and allometry. Failure to consider any one of these factors can inappropriately skew interpretations of fossil hominin anatomy. The analyses in the preceding chapters attempt to account for the functional underpinnings of distal humeral morphological variation by clarifying responsiveness to mechanical loading, overall shape differences between hominid taxa, and the effect of size-scaling on conclusions drawn from morphological comparisons.

Bilateral asymmetry in humeral morphological characteristics is used as an index of their developmental plasticity, assessed from both the degree of asymmetry present and the correlation of asymmetry in more distal features with that in the midshaft region, which is known to respond to mechanical loadings of the arm. The results of these analyses show significant asymmetry at all levels of the human distal humerus, indicating bone modeling/remodeling in response to loading for all regions. There is a general proximo-distal decline in asymmetry and correlation with midshaft asymmetry that reflects either a decline in bending moments and/or greater genetic constraints on more distal segments. Results do, however, show significant asymmetry of centroid size of the articular surface, which may be in response to factors not at play at midshaft (i.e.,

physiological factors specific to joint loading). The trochlea and capitulum show different directions of asymmetry, with the capitulum the only humeral feature exhibiting left-dominant asymmetry, indicating further complexities in articular development.

Morphological differences between humans and apes, assessed through 3D geometric morphometric analyses, are present in all regions of the distal humerus (shaft, distal 10%, articular and periarticular-only) to at least some extent. These differences are least clear in the shaft region, where humans and nonhuman great apes overlap broadly. This is consistent with evidence in humans that shaft properties are significantly developmentally plastic, but poses potential problems for use of shaft contours for taxonomic assignments (Susman et al., 2001; Lague, 2015). However, the present results largely mirror those reported earlier for a single distal shaft location, i.e., a generally more triangular cross section in humans and a rounder and mediolaterally broader cross section in great apes. Fossil specimens for which the shaft is available (A.L. 288-1, StW 431, KNM-ER 739) fall clearly within the great ape rather than human range. To the extent to which this reflects differences in locomotor behavior, these results may indicate continued significant use of the upper limb in the context of arboreal behavior, and are consistent with analyses of relative humeral diaphyseal strength in australopiths (Ruff et al., 2016).

The periarticular region shows a distinction between humans and great apes on the basis of anteroposterior flattening (greater in apes) as well as an apparent

terrestrial-arboreal gradient among great apes driven by retroversion of the medial epicondyle, which is highest in *G. beringei*. Most fossil specimens are ape-like in their periarticular morphology, including all *Australopithecus* specimens (KNM-KP 271, A.L. 288-1, StW 431), both *P. boisei* specimens (KNM-ER 739, KNM-ER 1504), and one *P. robustus* specimen (SXK 10924), further supporting claims of maintenance of at least some component of arboreal behavior late into hominin evolution. These individuals fall into the *Pan* range on the arboreal-terrestrial gradient among great apes, with most near the border with *Pongo*, suggesting arboreal behavior rather than knuckle-walking. However, this association is somewhat variable, with TM 1517, the type specimen of *P. robustus*, falling closer to humans. SK 24600, which has been assigned to *P. robustus* in some previous studies (Susman et al., 2001) but which the current results agree may be more consistent with assignment to *Homo* (Lague, 2014), and Gombore IB-7594 (*H. erectus*) are human-like, which may reflect freeing of the upper limb in these taxa from a locomotor role.

Articular differences between humans and great apes depend primarily on degree of articular relief, particularly weakening of the lateral trochlear crest in humans, and relative anteroposterior dimensions, which are larger in humans, compared to mediolateral dimensions, which are larger in great apes except along the posterior trochlea. Though the traits seen in great apes likely serve to improve stability when the upper limb is used in locomotion and are most extreme in *Gorilla*, no clear locomotor divisions are observable among great apes in articular morphology. Fossil hominins are

generally intermediate in their articular morphology, falling in the overlap of the *Pan* and human ranges, but significant introgression of SK 24600 into the human range supports assignment of this specimen to *Homo* rather than *P. robustus*, which appears to have more intermediate morphology. Positioning of Gombore IB-7594 at the extreme end of the human range may suggest strong selection on articular morphology in the evolution of the genus *Homo*.

Distal humeral centroid sizes and biepicondylar and articular breadths are strongly correlated with body mass in all taxa, but scaling relationships differ between species. Measures of distal humeral size in great apes are close to isometric, but very positively allometric in humans, which affects analyses that use distal humeral properties rather than body mass as a scaling factor. The relationship of taxa to each other in size-scaled analyses changes depending on these scaling factors because apes of lesser body mass have distal humeri equivalent in size to relatively larger humans. The PCs on which determinations of human-ape differences are based show size-related changes for all regions except the periarticular surface when scaled to body mass and centroid size, with larger humans showing more 'ape-like' traits. Accounting for allometry has significant impact on interpretation of fossil hominin distal humeri. Only one of the three fossils for which body mass is available (A.L. 288-1) shows a scaling relationship between centroid size and body mass that is clearly consistent with the relationship seen in modern humans. However, scaled morphology of A.L. 288-1 is distinctly ape-like in all regions. This is consistently true for fossil hominins as a group

(with the exception of Gombore IB-7594), which are far more ape-like in size-scaled analyses than in unscaled analyses.

Contrary to some previous assertions (Straus, 1948; Lovejoy et al., 2016), distal humeral morphology does include useful information for reconstructing phylogenetic relationships and past behavior. Geometric morphometric analyses show clear taxonomic differences among extant hominid species, likely related in part to freeing of the upper limb from locomotor demands in humans, and significant variation among fossil hominin taxa. The analyses included here have shown that the distal humerus is developmentally plastic in response to mechanical loads, supporting interpretation of at least some distal humeral traits as indicative of living behavior. Some regions (i.e., the shaft and periarticular surface) both appear more responsive to variability in loading environment in modern humans, and differentiate fossil hominin taxa from modern humans and from each other. The sum total of evidence presented here suggests maintenance of arboreality as a significant component of behavior in many fossil hominin taxa, while also providing evidence for species-level differences in morphology useful for testing phylogenetic hypotheses.

REFERENCES

Acsádi G, Nemeskéri J. 1970. History of human life span and mortality. Akadémiai Kiadó.

Aguilar MA, Aguilar FJ, Negreiros J. 2009. Off-the-shelf laser scanning and close-range digital photogrammetry for measuring agricultural soils microrelief. Biosyst Eng 103:504–517.

Aiello L, Dean C. 1990. An Introduction to Human Evolutionary Anatomy. Academic Press.

Aiello LC. 1992. Allometry and the analysis of size and shape in human evolution. J Hum Evol 22:127–147.

Alexander RM. 1980. Forces in Animal Joints. Eng Med 9:93–97.

Anon. ScanStudio.

Arias-Martorell J, Tallman M, Potau JM, Bello-Hellegouarch G, Pérez-Pérez A. 2015. Shape analysis of the proximal humerus in orthograde and semi-orthograde primates: Correlates of suspensory behavior. Am J Primatol 77:1–19.

Auerbach BM, Ruff CB. 2006. Limb bone bilateral asymmetry: variability and commonality among modern humans. J Hum Evol 50:203–218.

Bacon AM. 2000. Principal components analysis of distal humeral shape in Pliocene to recent African hominids: the contribution of geometric morphometrics. Am J Phys Anthropol 111:479–87.

Bass SL, Saxon L, Daly RM, Turner CH, Robling AG, Seeman E, Stuckey S. 2002. The Effect of Mechanical Loading on the Size and Shape of Bone in Pre-, Peri-, and Postpubertal Girls: A Study in Tennis Players. J Bone Miner Res 17:2274–2280.

Bertram JEA, Biewener AA. 1988. Bone curvature: Sacrificing strength for load predictability? J Theor Biol 131:75–92.

Biewener A. 1983. Allometry of quadrupedal locomotion: the scaling of duty factor, bone curvature and limb orientation to body size. J Exp Biol 105:147–171.

Birkbeck DP, Failla JM, Hoshaw SJ, Fyhrie DP, Schaffler M. 1997. The interosseous membrane affects load distribution in the forearm. J Hand Surg Am 22:975–980.

Blackburn A. 2011. Bilateral asymmetry of the humerus during growth and development. Am J Phys Anthropol 145:639–646.

Blackburn A, Knüsel CJ. 2006. Hand Dominance and Bilateral Asymmetry of the Epicondylar Breadth of the Humerus A Test in a Living Sample. Curr Anthropol 47:377–382.

Blakely RL. 1971. Comparison of the mortality profiles of Archaic, Middle Woodland, and

Middle Mississippian skeletal populations. Am J Phys Anthropol 34:43–53.

Bookstein FL. 1991. Morphometric tools for landmark data: geometry and biology. Cambridge: Cambridge University Press.

Bouvier M, Hylander WL. 1982. The effect of dietary consistency on morphology of the mandibular condylar cartilage in young macaques (Macaca mulatta). Prog Clin Biol Res 101:569—579.

Bridges PS, Blitz JH, Solano MC. 2000. Changes in Long Bone Diaphyseal Strength With Horticultural Intensification in West-Central Illinois. J Phys Anthr 112:217–238.

Brooks S, Suchey JM. 1990. Skeletal age determination based on the os pubis: a comparison of the Acsádi-Nemeskéri and Suchey-Brooks methods. Hum Evol 5:227–238.

Broom PR. 1938a. Iii. paranthropus robustus.

Broom R. 1938b. Further Evidence on the Structure of the South African Pleistocene Anthropoids. Nature 142:897–899.

Brothwell DR. 1981. Digging up bones: the excavation, treatment, and study of human skeletal remains. Cornell University Press.

Burgess ML, McFarlin SC, Mudakikwa A, Cranfield MR, Ruff CB. 2017. Body mass estimation in hominoids: Age and locomotor effects. J Hum Evol.

Calder WA. 1996. Size, function, and life history. Courier Corporation.

Cant JGHH. 1987. Positional behavior of female bornean orangutans (Pongo pygmaeus). Am J Primatol 12:71–90.

Carlson KJ. 2005. Investigating the form-function interface in African apes: Relationships between principal moments of area and positional behaviors in femoral and humeral diaphyses. Am J Phys Anthropol 127:312–334.

Carretero JM, Haile-Selassie Y, Rodriguez L, Arsuaga JL. 2009. A partial distal humerus from the Middle Pleistocene deposits at Bodo, Middle Awash, Ethiopia. Anthropol Sci 117:19–31.

De Castro JMB, Carretero JM, García-González R, Rodríguez-García L, Martinón-Torres M, Rosell J, Blasco R, Martín-Francés L, Modesto M, Carbonell E. 2012. Early pleistocene human humeri from the gran dolina-TD6 site (sierra de atapuerca, spain). Am J Phys Anthropol 147:604–617.

Chadwick EKJ, Nicol AC. 2000. Elbow and wrist joint contact forces during occupational pick and place activities.

Chavaillon J, Chavaillon N, Coppens Y, Senut B. 1977. Presence d'hominide dans le site oldowayen de Gombore I a Melka Kunture, Ethiopie. CR Acad Sci Paris:961–963.

Churchill SE, Holliday TW, Carlson KJ, Jashashvili T, Ruiter DJ De, Berger LR, Macias ME,

Mathews S, Sparling TL, Schmid P, de Ruiter DJ, Berger LR. 2013. The Upper Limb of Australopithecus sediba. Science (80-) 340:1233476–1233477.

Clarke RJ, Tobias P V. 1995. Sterkfontein-Member-2 Foot Bones of the Oldest South-African Hominid. Science (80-) 269:521–524.

Coppens Y. 2004. The hominids of Melka Kunture. Some general reflections. In: Studies on the Early Paleolithic Site of Melka. . p 685–686.

Corruccini RS. 1975. Morphometric affinities in the forelimb of Anthropoid primates Morphometric affinities in the forelimb of Anthropoid primates With 3 figures and 2 tables in the text. 67:19–31.

Crompton RH, Vereecke EE, Thorpe SKS. 2008. Locomotion and posture from the common hominoid ancestor to fully modern hominins, with special reference to the last common panin/hominin ancestor. J Anat 212:501–543.

Dart RA. 1925. Australopithecus africanus: The man-ape of South Africa. Nature 115.

Darwin C. 1871. The descent of man and selection in relation to sex, in Charles Darwin, The origin of species and The descent of man (combined volume). J Anat Physiol.

Day MH. 1978. Functional interpretations of the morphology of postcranial remains of early African hominids. Early hominids of Africa:311–345.

Domínguez-Rodrigo M, Pickering TR, Baquedano E, Mabulla A, Mark DF, Musiba C, Bunn HT, Uribelarrea D, Smith V, Diez-Martin F, Pérez-González A, Sánchez P, Santonja M, Barboni D, Gidna A, Ashley G, Yravedra J, Heaton JL, Arriaza MC. 2013. First Partial Skeleton of a 1.34-Million-Year-Old Paranthropus boisei from Bed II, Olduvai Gorge, Tanzania. PLoS One 8:e80347.

Doran D. 1996. Comparative positional behavior of the African Apes. In: McGrew M, Marchant L, Nishida T, editors. Great ape societies. Cambridge: Cambridge University Press. p 213–224.

Doran DM. 1993. Sex differences in adult chimpanzee positional behavior: The influence of body size on locomotion and posture. Am J Phys Anthropol 91:99–115.

Drapeau MSM. 2008. Articular morphology of the proximal ulna in extant and fossil hominoids and hominins. J Hum Evol 55:86–102.

Feldesman MR. 1982. Morphometric analysis of the distal humerus of some Cenozoic Catarrhines: the Late Divergence Hypothesis revisited. Am J Phys Anthropol 59:73–95.

Ferretti J, Capozza R, Zanchetta J. 1996. Mechanical validation of a tomographic (pQCT) index for noninvasive estimation of rat femur bending strength. Bone.

Feuerriegel EM, Green DJ, Walker CS, Schmid P, Hawks J, Berger LR, Churchill SE. 2017. The upper limb of Homo naledi. J Hum Evol 104:155–173.

Fleagle JG. 2013. Primate adaptation and evolution. Academic Press.

Le Floch P. 1982. The distal humerus: A structure with two pillars. Anat Clin 4:235–244.

Frayer DW, Clarke RJ, Fiore I, Blumenschine RJ, Pérez-Pérez A, Martinez LM, Estebaranz F, Holloway R, Bondioli L. 2016. OH-65: The earliest evidence for right-handedness in the fossil record. J Hum Evol 100:65–72.

Frost HMMD. 1979. A Chondral Modeling Theory. Calcif Tissue Int 28:181–200.

Gebo DL. 1996. Climbing, brachiation, and terrestrial quadrupedalism: Historical precursors of hominid bipedalism. Am J Phys Anthropol 101:55–92.

Godde K. 2009. An examination of Nubian and Egyptian biological distances: Support for biological diffusion or in situ development? HOMO - J Comp Hum Biol 60:389–404.

Godfrey L, Sutherland M, Boy D, Gomberg N. 1991. Scaling of Limb Joint Surface-Areas in Anthropoid Primates and Other Mammals. J Zool 223:603–625.

Gould SJ, Vrba ES. 1982. Exaptation-A Missing Term in the Science of Form. Paleontol Soc 8:4–15.

Gower JC. 1975. Generalized procrustes analysis. Psychometrika 40:33–51.

Grajetzki W. 2012. Middle Kingdom, Egypt. In: The Encyclopedia of Ancient History. Hoboken, NJ, USA: John Wiley & Sons, Inc.

Gray H, Standring S. 2008. Gray's anatomy. Arcturus Publishing.

Green DJ. 2013. Ontogeny of the hominoid scapula: The influence of locomotion on morphology. Am J Phys Anthropol 152:239–60.

Green DJ, Alemseged Z. 2012. Australopithecus afarensis scapular ontogeny, function, and the role of climbing in human evolution. Science 338:514–7.

Grine FE, Susman RL. 1991. Radius of Paranthropus robustus From Member 1, Swartkrans Formation, South Africa. Am J Phys Anthropol 248:229–248.

Le Gros Clark WE. 1947a. The Importance of the Fossil Australopithecinæ in the Study of Human Evolution. Sci Prog 35:377–395.

Le Gros Clark WE. 1947b. Observations on the anatomy of the fossil Australopithecinae. J Anat 81:300–33.

Fleagle, J.G. 2013. *Primate adaptation and evolution*. Academic Press.

Groves, C., 2001. Primate taxonomy. *The International Encyclopedia of Biological Anthropology*, p 1-6.

Guidi G, Remondino F, Morlando G, Del Mastio A, Uccheddu F, Pelagotti A. 2007. Performances Evaluation of a Low Cost Active Sensor for Cultural Heritage Documentation. Sensors Peterbrgh NH 2:59–69.

Gunz P, Mitteroecker P, Bookstein FL. 2005. Semilandmarks in Three Dimensions. In: Slice DE, editor. Modern Morphometrics in Physical Anthropology. New York: Kluwer Academic/Plenum Publishers. p 73–98.

Haapasalo H, Kontulainen S, Sievänen H, Kannus P, Järvinen M, Vuori I. 2000. Exercise-induced bone gain is due to enlargement in bone size without a change in volumetric bone density: a peripheral quantitative computed tomography study of the upper arms of male tennis players. Bone 27:351–357.

Halenar, L. B. 2011. Reconstructing the locomotor repertoire of Protopithecus brasiliensis. I. Body size. *The Anatomical Record: Advances in Integrative Anatomy and Evolutionary Biology 294*(12):2024-2047.

Hammond AS, Plavcan JM, Ward C V. 2013. Precision and accuracy of acetabular size measures in fragmentary hominin pelves obtained using sphere-fitting techniques. Am J Phys Anthropol 150:565–578.

Hammond AS, Plavcan JM, Ward C V. 2016. A validated method for modeling anthropoid hip abduction in silico. Am J Phys Anthropol 160:529–548.

Hamrick MW. 1996. Articular size and curvature as determinants of carpal joint mobility and stability in strepsirhine primates. J Morphol 230:113–27.

Hamrick MW. 1999. A chondral modeling theory revisited. J Theor Biol 201:201–8.

Hartwig-Scherer S, Martin RD. 1991. Was “Lucy” more human than her “child”? Observations on early hominid postcranial skeletons. J Hum Evol 21:439–449.

Hill A, Ward S. 1988. Origin of the hominidae: The record of african large hominoid evolution between 14 my and 4 my. Am J Phys Anthropol 31:49–83.

Hofman MA. 1988. Allometric scaling in palaeontology: a critical survey. Hum Evol 3:177–188.

Holliday TW, Friedl L. 2013. Hominoid humeral morphology: 3D morphometric analysis. Am J Phys Anthropol 152:506–515.

Hopkins WD, Morris RD. 1993. Handedness in great apes: A review of findings. Int J Primatol 14:1–25.

Hopkins WD, Phillips KA, Bania A, Calcutt SE, Gardner M, Russell J, Schaeffer J, Lonsdorf E V., Ross SR, Schapiro SJ. 2011. Hand preferences for coordinated bimanual actions in 777 great apes: Implications for the evolution of handedness in Hominins. J Hum Evol 60:605–611.

Hsieh YF, Robling AG, Ambrosius WT, Burr DB, Turner CH. 2001. Mechanical loading of diaphyseal bone in vivo: The strain threshold for an osteogenic response varies with location. J Bone Miner Res 16:2291–2297.

Hunt DR, Albanese J. 2005. History and demographic composition of the Robert J. Terry

anatomical collection. Am J Phys Anthropol 127:406–417.

Hunt KD. 1991. Mechanical implications of chimpanzee positional behavior. Am J Phys Anthropol 86:521–536.

Hunt KD. 1992. Positional behavior ofPan troglodytes in the Mahale Mountains and Gombe Stream National Parks, Tanzania. Am J Phys Anthropol 87:83–105.

Hunt KD. 1994. The evolution of human bipedality: ecology and functional morphology. J Hum Evol 26:183–202.

Hunt KD, Cant JGH, Gebo DL, Rose MD, Walker SE, Youlatos D. 1996. Standardized descriptions of primate locomotor and postural modes. Primates 37:363–387.

Ibáñez-Gimeno P, De Esteban-Trivigno S, Jordana X, Manyosa J, Malgosa AA, Galtés I. 2013a. Functional plasticity of the human humerus: Shape, rigidity, and muscular entheses. Am J Phys Anthropol 150:609–617.

Ibáñez-Gimeno P, Galtés I, Jordana X, Fiorin E, Manyosa J, Malgosa A. 2013b. Entheseal Changes and Functional Implications of the Humeral Medial Epicondyle. Int J Osteoarchaeol 23:211–220.

Ibáñez-Gimeno P, Galtés I, Manyosa J, Malgosa A, Jordana X. 2014. Analysis of the forearm rotational efficiency in extant hominoids: New insights into the functional implications of upper limb skeletal structure. J Hum Evol 76:165–176.

Jenkins FA. 1973. The functional anatomy and evolution of the mammalian humero-ulnar articulation. Am J Anat 137:281–297.

Johanson DC, Lovejoy CO, Kimbel WH, White TD, Ward SC, Bush ME, Latimer BM, Coppens Y. 1982. Morphology of the Pliocene partial hominid skeleton (A.L. 288-1) from the Hadar formation, Ethiopia. Am J Phys Anthropol 57:403–451.

Johanson DC, Taieb M. 1976. Plio—Pleistocene hominid discoveries in Hadar, Ethiopia. Nature 260:293–297.

Johnston FE, Snow CE. 1961. The reassessment of the age and sex of the Indian Knoll skeletal population: Demographic and methodological aspects. Am J Phys Anthropol 19:237–244.

Jolly CJ. 1970. The Seed-Eaters: A New Model of Hominid Differentiation Based on a Baboon Analogy. Man 5:5.

Jones HH, Priest JD, Hayes WC, Tichenor CC, Nagel DA. 1977. Humeral hypertrophy in response to exercise. J Bone Joint Surg Am 59:204–8.

Jungers W. 1984. Aspects of size and scaling in primate biology with special reference to the locomotor skeleton. Am J Phys Anthropol.

Jungers WL. 1982. Lucy's limbs: Skeletal allometry and locomotion in Australopithecus afarensis. Nature 297:676–678.

Jungers WL. 1985. Body size and scaling of limb proportions in primates. In: Size and scaling in primate biology. Springer. p 345–381.

Jungers WL. 1988. Relative joint size and hominoid locomotor adaptations with implications for the evolution of hominid bipedalism. J Hum Evol 17:247–265.

Jungers WL. 1990. Problems and methods in reconstructing body size in fossil primates. Body size Mamm Paleobiol Estim Biol Implic Cambridge Univ Press Cambridge:103–118.

Jungers WL, Godfrey LR, Simons EL, Wunderlich RE, Richmond BG, Chatrath PS. 2002. Ecomorphology and Behavior of Giant Extinct Lemurs from Madagascar. In: Reconstructing Behavior in the Primate Fossil Record. Boston, MA: Springer US. p 371–411.

Jungers WL, Susman RL. 1984. Body Size and Skeletal Allometry in African Apes BT - The Pygmy Chimpanzee: Evolutionary Biology and Behavior. In: Susman RL, editor. Boston, MA: Springer US. p 131–177.

Kivell TL, Deane AS, Tocheri MW, Orr CM, Schmid P, Hawks J, Berger LR, Churchill SE. 2015. The hand of Homo naledi. Nat Commun 6:1–9.

Kivell TL, Kibii JM, Churchill SE, Schmid P, Berger LR. 2011. Australopithecus sediba Hand Demonstrates Moasaic Evolution of Locomotor and Manipulative Abilities. Science (80-) 333:1411–1417.

Klingenberg CP. 2016. Size, shape, and form: concepts of allometry in geometric morphometrics. Dev Genes Evol 226:113–137.

Knussman R. 1967. Humerus, Ulna and Radius der simiae. In: Bibl.Primatol. Vol. 5. Basel: S. Karger.

Kubicka AM, Myszka A, Piontek J. 2015. Geometric Morphometrics: Does the Appearance of the Septal Aperture Depend on the Shape of Ulnar Processes? Anat Rec 298:2030–2038.

Kubicka AM, Nowaczewska W, Balzeau A, Piontek J. 2018. Bilateral asymmetry of the humerus in Neandertals , Australian aborigines and medieval humans. :1–15.

Lague M, Jungers W. 1996. Morphometric variation in Plio-Pleistocene hominid distal humeri. Am J Phys Anthropol.

Lague MR. 2014. The pattern of hominin postcranial evolution reconsidered in light of size-related shape variation of the distal humerus. J Hum Evol 75:90–109.

Lague MR. 2015. Taxonomic identification of Lower Pleistocene fossil hominins based on distal humeral diaphyseal cross-sectional shape. PeerJ 3:e1084.

Lamarck JB. 1809. Philosophie Zoologique,.

Larson SG. 2007. Evolutionary transformation of the hominin shoulder. Evol Anthropol

16:172–187.

Latimer B. 1991. Locomotor adaptations in Australopithecus afarensis: the issue of arboreality. Orig la Bipédie chez les Hominidés:169–176.

Latimer B, Lovejoy CO. 1989. Calcaneus of *Australopithecus afarensis* and its implications for the evolution of bipedality. Am J Phys Anthropol 78:369–386.

Latimer B, Ward C V. 1993. The thoracic and lumbar vertebrae. In: Walker A, Leakey R, editors. The Nariokotome Homo Erectus Skeleton. Cambridge: Harvard University Press. p 266–293.

Leakey MG, Feibel CS, McDougall I, Walker A. 1995. New four-million-year-old hominid species from Kanapoi and Allia Bay, Kenya. Nature 376:565–571.

Leakey MG, Leakey RE. 1978. Koobi Fora Research Project Vol. 1 The Fossil Hominids and an Introduction to their Context 1968--1974. Clarendon, Oxford.

Leakey REF. 1971. Further Evidence of Lower Pleistocene Hominids from East Rudolf, North Kenya. Nature 231:241–245.

Leakey REF. 1973. Further Evidence of Lower Pleistocene Hominids from East Rudolf, North Kenya, 1972. Nature 242:170–173.

Leakey REF, Walker AC. 1985. Further hominids from the Plio-Pleistocene of Koobi Fora, Kenya. Am J Phys Anthropol 67:135–163.

Lieberman DE, Devlin MJ, Pearson OM. 2001. Articular area responses to mechanical loading: effects of exercise, age, and skeletal location. Am J Phys Anthropol.

Lovejoy CO. 2010. The Great Divides : Ardipithecus ramidus Reveals the Postcrania of Our Last Common Ancestors with African Apes. 73.

Lovejoy CO, Latimer BM, Spurlock L, Haile-Selassie Y. 2016. The Pelvic Girdle and Limb Bones of KSD-VP-1/1. In: Haile-Selassie Y, Su DF, editors. The Postcranial Anatomy of Australopithecus afarensis: New Insights from KSD-VP-1/1. Dordrecht: Springer Netherlands. p 155–178.

Lovejoy CO, Meindul RS, Pryzback TR, Mensforth P. 1985. Chronological metamorphosis of the auricular surgace of the ilium. A new method for the determination of adult skeletal age at death. Am J Phys Antrhropol 68:15–28.

Mace A. 1921. The Egyptian Expedition 1920-1921: I. Excavations at Lisht. Metrop Museum Art Bull.

Mays SA. 2002. Asymmetry in metacarpal cortical bone in a collection of British post-mediaeval human skeletons. J Archaeol Sci 29:435–441.

McHenry H. 1976. Multivariate analysis of early hominid humeri. Meas Man.

McHenry H, Berger LR. 1998a. Limb lengths in Australopithecus and the origin of the genus Homo. S Afr J Sci 94:447–1450.

McHenry HM. 1992. Body size and proportions in early hominids. Am J Phys Anthropol 87:407–431.

McHenry HM, Berger LR. 1998b. Body proportions in Australopithecus afarensis and A. africanus and the origin of the genusHomo. J Hum Evol 35:1–22.

McHenry HM, Brown CC. 2008. Side steps: the erratic pattern of hominin postcranial change through time. J Hum Evol 55:639–51.

McHenry HM, Corruccini RS. 1975. Distal Humerus in Hominoid Evolution. Folia Primatol 23:227–244.

Van der Meulen MCH, Ashford MW, Kiratli BJ, Bachrach LK, Carter DR. 1996. Determinants of femoral geometry and structure during adolescent growth. J Orthop Res 14:22–29.

Miller RA. 1932. Evolution of the pectoral girdle and fore limb in the Primates. Am J Phys Anthropol 17:1–56.

Milner GR. 1992. Determination of skeletal age and sex: a manual prepared for the Dickson Mounds Reburial Team. Ms file, Dickson Mounds Museum.

Nadell JA, Shaw CN. 2016. Phenotypic plasticity and constraint along the upper and lower limb diaphyses of Homo sapiens. Am J Phys Anthropol 159:410–422.

Nakatsukasa M. 1994. Morphology of the Humerus and Femur in African Mangabeys and Guenons: Functional Adaptation and Implications for the Evolution of Positional Behavior. Afr Study Monogr 21:1–61.

Napier JR, Davis PR. 1959. The Fore-limb Skeleton and Associated Remains of Proconsul africanus. Foss Mamm Africa 16:1–69.

O'Higgens P, Jones N. 1998. Facial growth in Cercocebus torquatus : an application of three-dimensional geometric morphometric techniques to the study of morphological variation. J Anat:251–272.

Ohman JC, Krochta TJ, Lovejoy CO, Mensforth RF, Latimer B. 1997. Cortical Bone Distribution in the Femoral Neck of Hominiods: Implications for the Locomotion of Australopithecus afarensis. Am J Phys Anthropol 104:117–131.

Owen Lovejoy C, Simpson SW, White TD, Asfaw B, Suwa G. 2009. Careful climbing in the miocene: the forelimbs of ardipithecus ramidus and humans are primitive. Science (80-) 326.

Patterson B, Howells WW. 1967. Hominid humeral fragment from early Pleistocene of northwestern Kenya. Science 156:64–66.

Perino G. 1968. The Pete Klunk Mound Group. Illinois Archaeol Surv Bull 6:9–24.

Perry JMG, Cooke SB, Runestad Connour JA, Burgess ML, Ruff CB. 2018. Articular scaling and body mass estimation in platyrrhines and catarrhines: Modern variation and

application to fossil anthropoids. J Hum Evol 115:20–35.

Pfaeffle HJ, Fischer KJ, Manson TT, Tomaino MM, Woo SLY, Herndon JH. 2000. Role of the forearm interosseous ligament: Is it more than just longitudinal load transfer? J Hand Surg Am 25:683–688.

Phenice TW. 1969. A Newly Developed Visual Method of Sexing the Os Pubis. Am J Phys Anthropol 30:397–302.

Plochocki JH. 2004. Bilateral variation in limb articular surface dimensions. Am J Hum Biol 16:328–333.

Radin EL, Orr RB, Kelman JL, Paul IL, Rose RM. 1982. Effect of prolonged walking on concrete on the knees of sheep. J Biomech 15:487–492.

Rafferty KL, Ruff CB. 1994. Articular structure and function in Hylobates, Colobus, and Papio. Am J Phys Anthropol 94:395–408.

Ramons GL. 2014. Positional behavior of Pan paniscus at Lui Kotale, Democratic Republic of Congo. :176.

Rayner JMV. 1985. Linear relations in biomechanics: the statistics of scaling functions. J Zool 206:415–439.

Rein TR, Harrison T, Carlson KJ, Harvati K. 2017a. Adaptation to suspensory locomotion in Australopithecus sediba. J Hum Evol 104:1–12.

Rein TR, Harrison T, Carlson KJ, Harvati K. 2017b. Adaptation to suspensory locomotion in Australopithecus sediba. J Hum Evol 104:1–12.

Remis M. 1995. Effects of Body Size and Social Context on the Arboreal Activities of Lowland Gorillas in the Central African Republic. 433:413–433.

Richmond BG, Strait DS. 2000. Evidence that humans evolved from a knuckle-walking ancestor. Nature 404:382–5.

Robling AG, Hinant FM, Burr DB, Turner CH. 2002. Improved Bone Structure and Strength After Long-Term Mechanical Loading Is Greatest if Loading Is Separated Into Short Bouts - Robling - 2002 - Journal of Bone and Mineral Research - Wiley Online Library. 17:1545–1554.

Rosas A, Pérez-Criado L, Bastir M, Estalrrich A, Huguet R, García-Tabernero A, Pastor JF, de la Rasilla M. 2015. A geometric morphometrics comparative analysis of Neandertal humeri (epiphyses-fused) from the El Sidrón cave site (Asturias, Spain). J Hum Evol 82:51–66.

Rose M. 1993. Functional anatomy of the elbow and forearm in primates. In: Gebo D, editor. Postcranial adaptation in nonhuman primates. DeKalb, IL: Northern Illinois University Press. p 70–95.

Rose MD. 1988. Another look at the anthropoid elbow. J Hum Evol 17:193–224.

Roy TA, Ruff CB, Plato CC. 1994. Hand dominance and bilateral asymmetry in the structure of the second metacarpal. Am J Phys Anthropol 94:203–211.

Ruff C. 2003a. Ontogenetic adaptation to bipedalism: Age changes in femoral to humeral length and strength proportions in humans, with a comparison to baboons. J Hum Evol 45:317–349.

Ruff C. 2003b. Growth in bone strength, body size, and muscle size in a juvenile longitudinal sample. Bone 33:317–329.

Ruff C. 2008. Femoral/humeral strength in early African Homo erectus. J Hum Evol 54:383–390.

Ruff C. 2009. Relative limb strength and locomotion in Homo habilis. Am J Phys Anthropol 138:90–100.

Ruff C, Holt B, Trinkaus E. 2006. Who's afraid of the big bad Wolff?: "Wolff's law" and bone functional adaptation. Am J Phys Anthropol 129:484–498.

Ruff CB. 2000a. Body size, body shape, and long bone strength in modern humans. J Hum Evol 38:269–290.

Ruff CB. 2000b. Body mass prediction from skeletal frame size in elite athletes. Am J Phys Anthropol 113:507–517.

Ruff CB. 2002. Long bone articular and diaphyseal structure in old world monkeys and apes. I: locomotor effects. Am J Phys Anthropol 119:305–42.

Ruff CB, Burgess ML, Bromage TG, Mudakikwa A, McFarlin SC. 2013. Ontogenetic changes in limb bone structural proportions in mountain gorillas (Gorilla beringei beringei). J Hum Evol 65:693–703.

Ruff CB, Burgess ML, Junno JA, Mudakikwa A, Zollikofer CPE, Ponce de León MS, Mcfarlin SC. 2018a. Phylogenetic and environmental effects on limb bone structure in gorillas. Am J Phys Anthropol:353–372.

Ruff CB, Burgess ML, Ketcham RA, Kappelman J. 2016. Limb Bone Structural Proportions and Locomotor Behavior in A.L. 288-1 ("Lucy"). PLoS One 11:1–26.

Ruff CB, Burgess ML, Squyres N, Junno J-A, Trinkaus E. 2018b. Lower limb articular scaling and body mass estimation in Pliocene and Pleistocene hominins. J Hum Evol.

Ruff CB, Holt BM, Niskanen M, Sladék V, Berner M, Garofalo E, Garvin HM, Hora M, Maijanen H, Niinimäki S, Salo K, Schuplerová E, Tompkins D. 2012. Stature and body mass estimation from skeletal remains in the European Holocene. Am J Phys Anthropol 148:601–617.

Ruff CB, Scott WW, Liu AY-C. 1991. Articular and diaphyseal remodeling of the proximal femur with changes in body mass in adults. Am J Phys Anthropol 86:397–413.

Sarmiento EE. 1988. Anatomy of the hominoid wrist joint: Its evolutionary and functional implications. Int J Primatol 9:281–345.

Sarringhaus LA, Stock JT, Marchant LF, McGrew WC. 2005. Bilateral asymmetry in the limb bones of the chimpanzee (Pan troglodytes). Am J Phys Anthropol 128:840–845.

Shepers R, Broom GWH 1946. Paranthropus robustus Broom. *Transvaal Museum Memoirs* 2:84–122.

Schmidt-Nielsen K. 1984. Scaling: why is animal size so important? Cambridge University Press.

Selby MS, Lovejoy CO. 2017. Evolution of the hominoid scapula and its implications for earliest hominid locomotion. Am J Phys Anthropol 162:682–700.

Senut B. 1978. Etude comparative des piliers de la palette humérale (Premiere partie). Cah d'Anthropologie Paris:1–20.

Senut B. 1980. New data on the humerus and its joints in Plio-Pleistocene hominids. Coll Anthropol.

Senut B. 1981a. Humeral outlines in some hominoid primates and in plio-pleistocene hominids. Am J Phys Anthropol 56:275–83.

Senut B. 1981b. Outlines of the Distal Humerus in Hominoid Primates: Application to Some Plio-Pleistocene Hominids BT - Primate Evolutionary Biology. In: Chiarelli AB, Corruccini RS, editors. Berlin, Heidelberg, Heidelberg: Springer Berlin Heidelberg. p 81–92.

Senut B, Tardieu C. 1985. Functional Aspects of Plio-Pleistocene Hominid Limb Bones: Implications for Taxonomy and Phylogeny. In: Delson E, editor. Ancestors: The Hard Evidence. Alan R. Liss, Inc. p 193–201.

Shaw CN. 2011. Is 'hand preference' coded in the hominin skeleton? An in-vivo study of bilateral morphological variation. J Hum Evol 61:480–487.

Shaw CN, Stock JT. 2009. Habitual throwing and swimming correspond with upper limb diaphyseal strength and shape in modern human athletes. Am J Phys Anthropol 140:160–172.

Shea BT. 1984. An allometric perspective on the morphological and evolutionary relationships between pygmy (Pan paniscus) and common (Pan troglodytes) chimpanzees. In: The pygmy chimpanzee. Springer. p 89–130.

Sholts SB, W??rml??nder SKTS, Flores LM, Miller KWP, Walker PL. 2010. Variation in the measurement of cranial volume and surface area using 3d laser scanning technology. J Forensic Sci 55:871–876.

Singleton M. 2002. Patterns of cranial shape variation in the Papionini (Primates :

Cercopithecinae). p 547–578.

Sladék V, Berner M, Sosna D, Sailer R. 2007. Human Manipulative Behavior in the Central European Late Eneolithic and Early Bronze Age: Humeral Bilateral Asymmetry. Am J Phys Anthropol:669=681.

Sládek V, Ruff CB, Berner M, Holt B, Niskanen M, Schuplerová E, Hora M. 2016. The impact of subsistence changes on humeral bilateral asymmetry in Terminal Pleistocene and Holocene Europe. J Hum Evol 92:37–49.

Smith RJ. 1984. Allometric scaling in comparative biology: Problems of concept and method. Am J Phys Anthropol 246:R152–R160.

Soengas B. 2009. Preliminary Ethnographic Research on the Bakoya in Gabon. Afr Study Monogr 30:187–208.

Sokal RR, Rohlf FJ. 1995. Biometry. New York: W.H. Freeman and Company.

Squyres N, Ruff CB. 2015. Body mass estimation from knee breadth, with application to early hominins. Am J Phys Anthropol 158:198–208.

Steele J, Mays S. 1995. Handedness and directional asymmetry in the long bones of the human upper limb. Int J Osteoarchaeol 5:39–49.

Stern JT. 2000. Climbing to the top: A personal memoir ofAustralopithecus afarensis. Evol Anthropol Issues, News, Rev 9:113–133.

Stern JT, Susman R. 1983. The locomotor anatomy of Australopithecus afarensis. Am J Phys 60:279–317.

Straus WL. 1948. The humerus of Paranthropus robustus. Am J Phys Anthropol 6:285–313.

Sugardjito J. 1982. Locomotor behavior of the Sumatran orangutan Pongo pygmaeus abelii at Ketambe, Gunung Leuser National Park. Malay Nat J 35:57–64.

Susman RL, de Ruiter D, Brain CK. 2001. Recently identified postcranial remains of Paranthropus and early Homo from Swartkrans Cave, South Africa. J Hum Evol 41:607–629.

Susman RL, Stern JT, Jungers WL. 1984a. Arboreality and Bipedality in the Hadar Hominids. Folia Primatol 43:113–156.

Susman RL, Stern JT, Jungers WL. 1984b. Arboreality and bipedality in the Hadar hominids. Folia Primatol (Basel) 43:113–56.

Swartz SM. 1989. The functional morphology of weight bearing: limb joint surface area allometry in anthropoid primates. J Zool 218:441–460.

Sylvester AD. 2013. A geometric morphometric analysis of the medial tibial condyle of african hominids. Anat Rec 296:1518–1525.

Tallman M. 2010. Postcranial variation in Plio-Pleistocene hominins of Africa. City University of New York Doctoral Dissertation.

Tallman, M. 2013. Forelimb to hindlimb shape covariance in extant hominoids and fossil hominins. *The Anatomical Record*, *296*(2), 290-304.

Tallman M. 2015. Phenetic and Functional Analyses of the Distal Ulna of Australopithecus afarensis and Australopithecus africanus. Anat Rec 298:195–211.

Thorpe SKS, Crompton RH. 2006. Orangutan Positional Behavior and the Nature of Arboreal Locomotion in Hominoidea. Am J Phys Anthropol:384–401.

Thorpe SKS, Holder RL, Crompton RH. 2007. Origin of human bipedalism as an adaptation for locomotion on flexible branches. Science 316:1328–31.

Toussaint M, Macho GA, Tobias P V, Partridge TC, Hughes AR. 2003. The third partial skeleton of a late pliocene hominin. S Afr J Sci 99:215–223.

Trinkaus E, Churchill SE, Ruff CB. 1994. Postcranial robusticity in Homo II: Humeral bilateral asymmetry and bone plasticity. Am J Phys Anthropol 93:1–34.

Trujillo-Ortiz. 2014. gmregress.

Tuttle R, Basmajian J V. 1974. Electromyography of brachial muscles in Pan gorilla and hominoid evolution. Am J Phys Anthropol 41:71–90.

Tuttle RH, Watts DP. 1985. The positional behavior and adaptive complexes of Pan gorilla. Primate Morphophysiology, Locomot Anal Hum Bipedalism.

Ubelaker DH, Buikstra JE. 1994. Standards for data collection from human skeletal remains. Arkansas Archaeol Surv Res 44:206.

Di Vincenzo F, Rodriguez L, Carretero JM, Collina C, Geraads D, Piperno M, Manzi G. 2015. The massive fossil humerus from the Oldowan horizon of Gombore I, Melka Kunture. Quat Sci Rev 122:207–221.

Ward C V. 2002. Interpreting the posture and locomotion of Australopithecus afarensis: Where do we stand? Yearb Phys Anthropol 45:185–215.

Ward C V. 2013. Postural and Locomotor Adaptations of Australopithecus Species. In: Reed KE, Fleagle JG, Leakey RE, editors. The Paleobiology of Australopithecus. Dordrecht: Springer Netherlands. p 235–245.

Ward C V., Leakey MG, Walker A. 2001. Morphology of Australopithecus anamensis from Kanapoi and Allia Bay, Kenya. J Hum Evol 41:255–368.

Warden SJ, Mantila Roosa SM, Kersh ME, Hurd AL, Fleisig GS, Pandy MG, Fuchs RK. 2014. Physical activity when young provides lifelong benefits to cortical bone size and strength in men. Proc Natl Acad Sci 111:5337–5342.

Warton DI, Duursma RA, Falster DS, Taskinen S. 2012. smatr 3 - an R package for estimation and inference about allometric lines. Methods Ecol Evol 3:257–259.

Webb W, Winters H. 2001. Indian Knoll. University of Tennessee Press.

Yokley T, Churchill S. 2006. Archaic and modern human distal humeral morphology. J Hum Evol.

Young NM, Wagner GP, Hallgrimsson B. 2010. Development and the evolvability of human limbs. Proc Natl Acad Sci 107:3400–3405.

Zelditch ML, Swiderski DL, Sheets HD. 2012. Geometric morphometrics for biologists: a primer. Academic Press.

Zihlman AL, McFarland RK, Underwood CE. 2011. Functional anatomy and adaptation of male gorillas (Gorilla gorilla gorilla) With Comparison to Male Orangutans (Pongo pygmaeus). Anat Rec 294:1842–1855.

Zipfel B, DeSilva J, Kidd R, Carlson K. 2011. The foot and ankle of Australopithecus sediba. Science (80-).

Zollikofer CPE, Leo MSP De. 2002. Visualizing patterns of craniofacial shape variation in Homo sapiens. p 801–807.

CURRICULUM VITAE

The Johns Hopkins University School of Medicine

Kaya Gallagher Zelazny 1/3/2019
Birthplace: Princeton, NJ 1989

Educational History:

Ph.D. Candidate	2019	Center for Functional Anatomy and Evolution	Johns Hopkins University School of Medicine
		Mentors: Christopher B. Ruff, PhD and Adam D. Sylvester, PhD	
B.A.	2011	Ecology and Evolutionary Biology	Princeton University

Conference Presentations:

Zelazny KG, Sylvester AD, Ruff CB. 2018. Differences between Human and Great Ape Distal Humeral Articular Axes. *The FASEB Journal* 32(1):364-5.

Zelazny KG, Sylvester AD, Ruff CB. 2018. Morphological Variation in the Distal Humerus of Modern Humans, Apes and Fossil Hominins. *Am J Phys Anthropol* S66:310

Zelazny KG, Ruff CB. 2017. Bilateral Asymmetry in Cross-Sectional Properties Indicates Periarticular Plasticity in the Distal Humerus of Modern Humans. *Am J Phys Anthropol* S63:421

Teaching Experience:

Johns Hopkins University

Human Anatomy, School of Medicine, *Substitute and grader*	2017
Human Anatomy, School of Medicine, *Substitute and grader*	2016
Physical Medicine and Rehabilitation, *Prosector*	
Human Origins (290), *Teaching Assistant*	
Human Anatomy, School of Medicine, *Instructor*	2015
Introduction to the Human Body, *Teaching Assistant*	
Human Anatomy, School of Medicine, *Prosector*	2014
Introduction to the Human Body, *Teaching Assistant*	
Human Gross Anatomy (375), *Teaching Assistant*	

Guest Lectures:

Fossil Hominin Diversity: *Australopithecus* and *Paranthropus*	Johns Hopkins University	2016
Anatomy and Function of the Eye	Johns Hopkins University	2014

Professional Service:

Career Representative – Johns Hopkins School of Medicine Graduate Student Association	2016-2017
Vice President of Events – Johns Hopkins School of Medicine Graduate Student Association	2014-2015